Ultrastructural Analysis of Proteins Implicated in Synaptic Vesicle Docking and Priming in *C. elegans*

BY

Seema Sheoran
B.S., University of Delhi, India, 2010
M.S., National Centre for Biological Sciences, Tata Institute of Fundamental Research, 2013

THESIS

Submitted as partial fulfillment of the requirements for the degree of Doctor of Philosophy in Biological Sciences in the Graduate College of the University of Illinois at Chicago, 2020

Chicago, Illinois

Defense Committee:

Thomas J. Park, Biological Sciences, Chair
Janet E. Richmond, Biological Sciences, Advisor
Liang-Wei Gong, Biological Sciences
Simon T. Alford, Anatomy and Cell Biology
Hong Zhan, University of Wisconsin-Madison

Dedication

To my family, for their unconditional love and unwavering support

CONTRIBUTION OF AUTHORS

Seema Sheoran contributed to experimental conception and design of electron microscopy experiments for all the projects described in this thesis, performed those experiments, analyzed and interpreted the data, contributed to the writing of manuscripts, critically revised submitted manuscripts, approved final versions for publication, and wrote this thesis.

Additional contributions to Chapter 2A
Mia Krout contributed written sections for C2A and C2C domains.

Additional contributions to Chapter 2B
Haowen Liu and Lei Li contributed to project conception and design, acquisition of data, analysis and interpretation of data. Yi Yu contributed unpublished essential data or reagents. Zhitao Hu contributed to project conception and design, analysis and interpretation of data, drafting the manuscript. Janet E. Richmond contributed to interpretation of data and revising the manuscript.

Additional contributions to Chapter 3
Melinda Moseley-Alldredge conducted major portion of the experiments for this manuscript including suppressor screen identifying ksr-1, locomotion assays, generation of conditional sax-7 allele and related experiments, rescue experiment, aldicarb assay. Hayoung Yoo assisted with locomotion and aldicarb assays, quantification of SNB-1::GFP punctal intensity. Calvin O'keefe assisted with Matlab code for radial displacement graph. Lihsia Chen contributed to project conception and design, analysis and interpretation of data, drafting the manuscript. Janet E. Richmond contributed to acquisition of electrophysiology data and analysis, interpretation of data and revising the manuscript.

Additional contributions to Chapter 4
Susan Klosterman contributed to project conception and design, all the genetic characterization of *vps-39*, analysis and interpretation of data. Janet E. Richmond contributed to project conception and design, acquisition of electrophysiology data, analysis and interpretation of data.

Additional contribution to Appendix A
Kelly H. Oh and Hongkyun Kim performed research, analyzed the data and wrote the manuscript. Janet E. Richmond revised the manuscript and approved the final version for publication.

TABLE OF CONTENTS

LIST OF ABBREVIATIONS

ACh	Acetylcholine
ACR	Acetylcholine receptor
AP	Adaptor protein
APP	Amyloid precursor protein
AZ	Active zone
Ca^{2+}	Calcium
CaM	Calmodulin
CaMb	Calmodulin binding
CHCR	Clathrin Heavy Chain Repeat
Cre	site-specific DNA recombinase
DAG	Diacylglycerol
DKO	Double knock out
DMA-1	Dendrite morphology abnormal
DP	Dense projection
Dunc-13	*Drosophila unc-13*
EM	Electron microscopy
EPSC	Excitatory postsynaptic currents
Erk	Extracellular signal-regulated kinase
FGFR	Fibroblast Growth Factor Receptor
GABA	g-aminobutyric acid
GFP	Green fluorescent protein
GTP/GDP	Guanosine-5'-triphosphate/diphosphate
HOPS	Homotypic fusion and vacuole protein sorting
HPF-FS	High-pressure freeze fixation and freeze substitution
IgSF	Immunoglobulin superfamily proteins
IPSC	Inhibitory postsynaptic currents
Is	Integrated strain
kb	kilobase
kDa	kilo Dalton

KO	Knock out
KSR-1	Kinase suppressor of Ras 1
L1CAM	L1 cell adhesion molecule
MAPK	Mitogen activated protein kinase
MHD	Munc13 homology domain
MLD	Membrane Localization Domain
mM	millimolar
MNR-1	MeNoRin, dendritic branching protein
Munc-13	mammalian *unc-13*
NGM	Nematode growth medium
NMJ	Neuromuscular junctions
nmJ	nanometer
PD	Presynaptic density
PDZ	Post synaptic density protein (PSD95), Drosophila disc large tumor suppressor (Dlg1), and zonula occludens-1 protein (zo-1)
PE	Phorbol ester
PIP	Phosphatidylinositol phosphate
PIP$_2$	Phosphatidylinositol bisphosphate
PKC	Protein Kinase C
PLEKHM-1	pleckstrin homology domain-containing family M member 1
Rab	Ras related in brain
RBD	Rab binding domain
RIC	resistance to inhibitors of cholinesterase
RIM	RAB-3 interacting molecule
RIM-BP	RIM-binding protein
RRP	Readily releasable pool
SAX-7	Sensory axon guidance
SCI	Single copy insertion
SNAP-25	Synaptosome-associated protein of 25 kDa
SNARE	Soluble *N*-ethylmaleimide-sensitive factor attachment receptor
SNB	Synaptobrevin

SV	Synaptic vesicle
TEM	Transmission electron microscopy
TOM-1	Tomosyn-1
um	micrometer
UNC-13	Uncoordinated
VGCC	Voltage gated calcium channels
VPS	Vacuolar protein sorting
WES	whole exome sequencing
WT	Wild type
ZF	Zinc finger

SUMMARY

Neurotransmitter release at synapses is mediated by the fusion of neurotransmitter containing synaptic vesicles (SV) with the presynaptic membrane. As neurotransmitter release is critical for integrating sensory inputs and for the subsequent cognitive and behavioral outcomes, it is highly regulated at every stage by cellular and molecular players. Research over the years have established SNARE (soluble-N-ethylmaleimide-sensitive factor attachment receptor) complex as the core synaptic vesicle fusion machinery. There are several other neuronal proteins that regulate SV fusion by directly or indirectly affecting SNARE complex assembly and its function. My thesis focuses on understanding the role of three such neuronal proteins: UNC-13 (Uncoordinated), SAX-7 (Sensory Axon Guidance), and VPS-39 (Vacuolar Protein Sorting). By studying the ultrastructural changes at the synapses, I contributed to the understanding of the function of these regulators in the critical SV fusion stage of neurotransmission.

CHAPTER I: INTRODUCTION

Effective communication between neurons requires the precise control of neurotransmitter release at synapses to ensure proper cognitive and behavioral outcomes. Neurotransmitter release involves multiple steps summarized in Figure 1.1.A (Richmond 2005). Neurotransmitter-filled synaptic vesicles (SV) must be mobilized from a reserve pool to the site of neurotransmitter release, known functionally as the active zone. Here, SVs become morphologically docked with the presynaptic membrane near the presynaptic density, as observed by electron microscopy. Live imaging experiments suggest that this docking phase can be transient and reversible. Prior to exocytosis, SVs undergo a priming reaction during which they become fusion competent. In the final step Ca^{2+} triggers fusion of primed SVs with the presynaptic membrane releasing neurotransmitter into the synaptic cleft.

During priming SVs become stably associated with the plasma membrane as a result of SNARE complex assembly (Fig. 1.1.B) (Söllner et al. 1993; Poirier et al. 1998; Sutton et al. 1998; Hanson et al. 1997), named for the fact that they are soluble-NSF-attachment protein (SNAP) receptors. The neuronal SNARE complex consists of two plasma membrane SNAREs (t-SNAREs or Q-SNAREs), syntaxin-1 and SNAP-25, and the integral vesicle membrane SNARE (v-SNARE or R-SNARE) synaptobrevin-2. The SNAREs form a tight four-alpha helical bundle that zippers the SNARE complex toward the C-terminal transmembrane domains of syntaxin and synaptobrevin. Upon Ca^{2+} binding, the Ca^{2+}-sensor Synaptotagmin acts in association with the assembled SNARE complex to lower the energy barrier for SV fusion with the plasma membrane, triggering evoked release. Disruption of any of the SNARE proteins by

clostridial toxins or mutations abolishes evoked release, establishing that the SNARE complex is the core fusion machinery. Given the essential role of SNARE proteins in exocytosis, it is not surprising that multiple synaptic proteins have been shown to regulate synaptic transmission by either directly or indirectly impacting SNARE complex assembly. The following chapters will describe my contributions to understanding the role of several regulators implicated in this critical stage of neurotransmission.
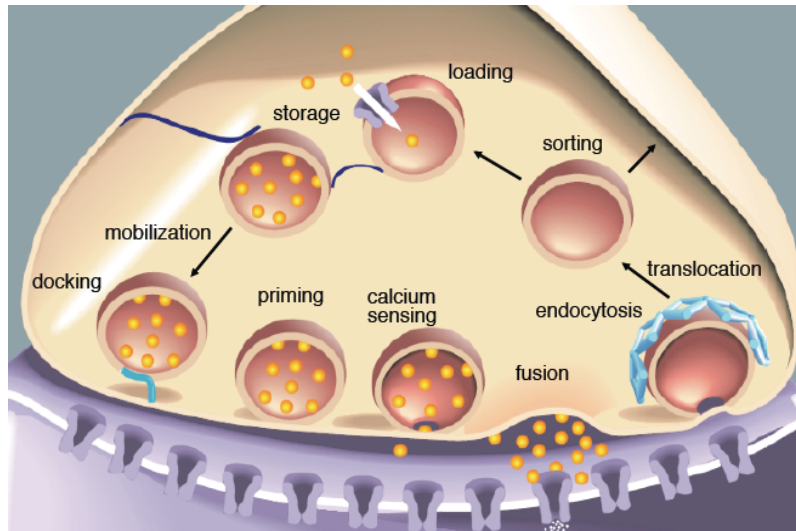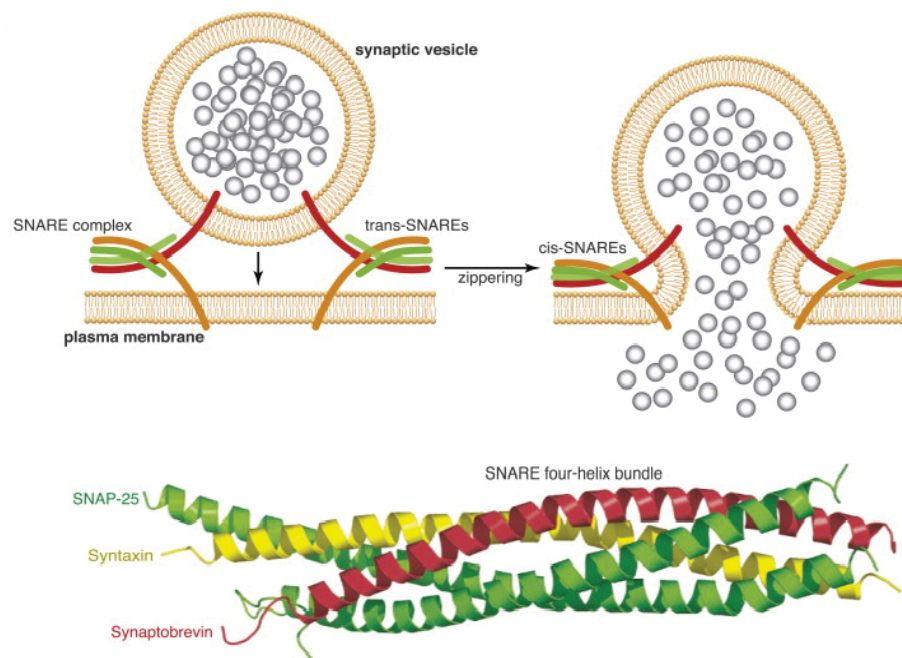
Figure 1. 1. Molecular mechanism underlying neurotransmitter release. (A) Steps involved in the synaptic vesicle cycle. Reproduced from (Richmond 2005). (B) Fusion of synaptic vesicles is mediated by SNARE complex consisting of four coiled-coil domains contributed by synaptobrevin (on vesicles), SNAP-25 and syntaxin (on plasma membrane). Reproduced from Zucker et al., 2014.

1.1. Regulators of neurotransmitter release

1.1.1. UNC-13/Munc13

unc-13, also known as Munc13 (mammalian *unc-13*) was first identified in 1974 in a genetic screen for *C. elegans* mutants showing uncoordinated (unc) movements by the Nobel Laureate Sydney Brenner, with the aim of identifying genes required for synaptic transmission at neuromuscular junctions (Brenner 1974). The 13th "unc" mutant isolated, *unc-13* was almost completely paralyzed and exhibited resistance to the lethal effects of an acetylcholine esterase inhibitor (aldicarb), while still showing sensitivity to the muscle acetylcholine receptor agonist (levamisole). These observations suggested that *unc-13* mutants were defective in presynaptic release rather than postsynaptic excitation/contraction coupling (Hosono, Sassa, and Kuno 1987; Nguyen et al. 1995). In *Drosophila*, null mutants of the *unc-13* homolog, D*unc13* were also found to be severely compromised and died in late embryogenesis. Similarly, Mice lacking Munc13-1 do not feed, have breathing problems, and die within a few hours of birth. The worm and fly phenotypes could not be attributed to defects in neuronal architecture, suggesting the underlying cause was a functional defect in synaptic transmission.

Subsequently, recordings from synapses in all three model systems confirmed that UNC-13/Munc13 proteins regulate release. For example, at *C. elegans* neuromuscular junctions (NMJs) evoked and spontaneous release were almost completely abolished in *unc-13* null mutants (Richmond, Davis, and Jorgensen 1999). Similar findings were reported for embryos from *Drosophila* Dunc13 mutants and for a mouse Munc13-1 knock-out (Aravamudan et al. 1999; Augustin, Betz, et al. 1999a). Furthermore in all three model organisms, loss of UNC-13/Munc13 eliminated hyperosmotic responses, a treatment that induces the fusion of the entire

readily releasable primed vesicle pool (Augustin, Rosenmund, et al. 1999; Richmond, Davis, and

Jorgensen 1999; Aravamudan et al. 1999). The SV priming function of Munc13 in most synapses

of hippocampal neurons is mediated solely by Munc13-1 and only a small subpopulation of

synapses (~10%) use bMunc13-2 or ubMunc13-2 (Augustin, Rosenmund, et al. 1999;

Varoqueaux et al. 2002). While initial EM analyses suggested that these priming defects were

downstream of SV docking, based on specimens prepared by classical chemical fixation, re-

examination first in *C. elegans* and later mouse synapses using high-pressure freeze (HPF)

fixation showed substantial defects in the morphological docking of SVs. Given that similar

electrophysiological and docking defects have been observed when SNARE proteins are

disrupted, the current consensus is that in the absence of priming a large fraction of docked SVs

are absent, in keeping with the hypothesis that UNC-13/Munc13 plays an essential role in

priming (Hammarlund et al. 2007; Imig et al. 2014).

In *C. elegans* UNC-13 proteins are encoded by a single gene locus giving rise to two

isoforms categorized as UNC-13-long (L or LR) and -short (S or MR) (Kohn et al. 2000),

whereas in *Drosophila*, the Dunc13 gene encodes for three isoforms. As is often the case in

vertebrates, mice exhibit gene duplications giving rise to multiple Munc13 isoforms: Munc13-1,

ubMunc13-2, bMunc13-2, and Munc13-3 encoded by three genes (*Unc13A/B/C*) (Fig. 1.2A). As

expected for a protein impacting synaptic transmission, UNC-13/Munc13 isoforms are highly

enriched at presynaptic terminals and have been identified in nearly every organism examined

that contains a nervous system. In *C. elegans* UNC-13 is expressed pan-neuronally, UNC-13L

closely associating with the presynaptic density, whereas UNC-13S is peri-synaptic (Hu, Tong,

and Kaplan 2013). In *Drosophila*, Dunc-13 isoforms also co-localize

A

C2A   C1 C2B   MUN   C2C

ce-unc-13L (or LR)

L   R

ce-unc-13S (or MR)

M

r-Munc13-1

r-ubMunc13-2

r-bMunc13-2

r-Munc13-3

dr-unc-13

B

SNARE complex   MUN

C₁   C₂B   C₂C

Ca²⁺

C₂C
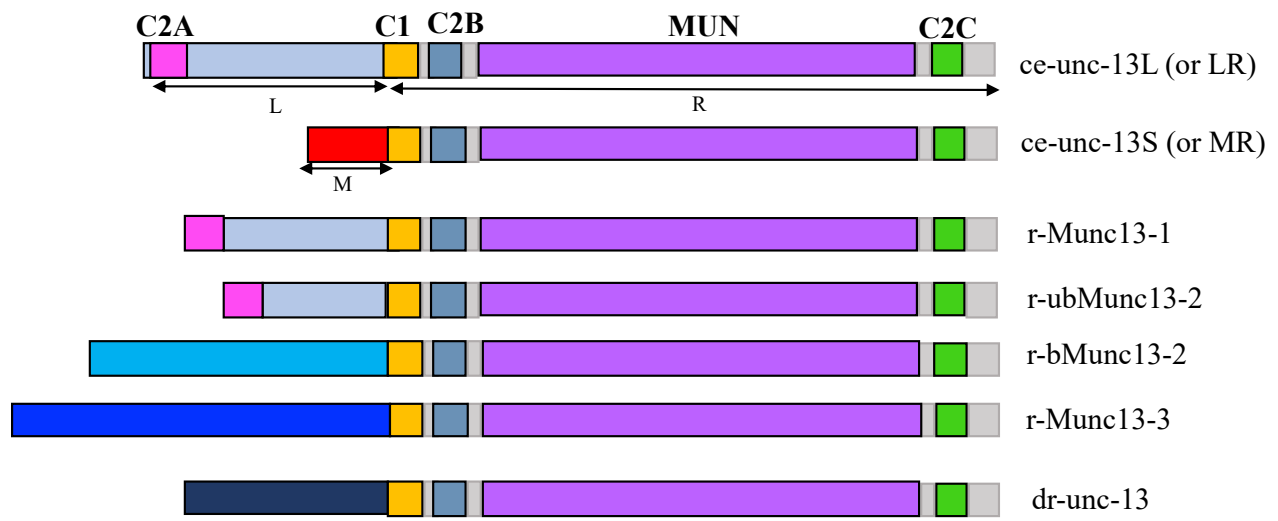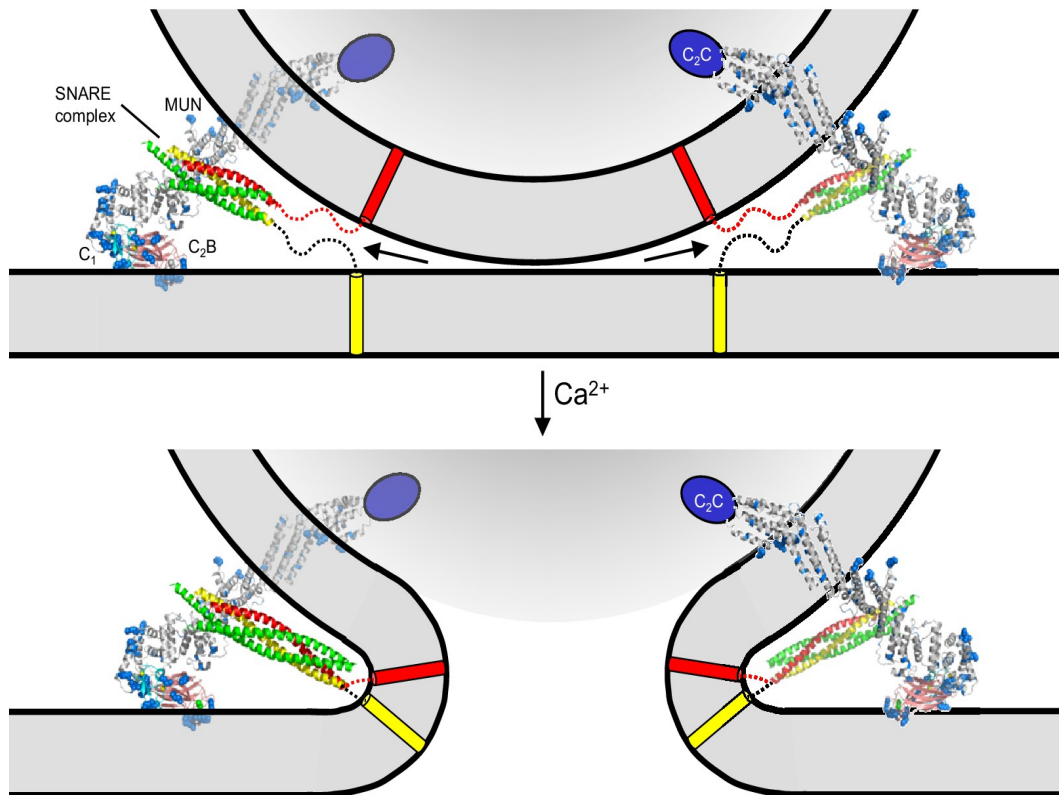
Figure 1. 2. Domain structure of Munc13/UNC-13 is conserved among different species (ce, C. elegans; r, rat; dr, D. melanogaster). (A) All Munc13/UNC-13 proteins have a highly conserved C-terminal (grey), containing PE/DAG binding C1 domain, two C2 domains, and *the MUN domain*. In C. elegans UNC-13 proteins (ce-unc-13) are encoded by a single gene locus giving rise to two isoforms categorized as UNC-13-long (L or LR) and -short (S or MR). Mammalian homologs (r-Munc13) Munc13-1 and ubMunc13-2 share homology with the N-terminal of C. elegans UNC-13L (red). The N-termini of bMunc13-2, Munc13-3, and Drosophila isoform dr-unc-13 (or Dunc-13) are not related (orange, purple, blue). Adapted from (Koch, Hofmann, and Brose 2000). (B) Illustration showing UNC-13 mediated SV fusion. Reproduced from [*(Xu et al. 2017b)*. eLife 2017;6:e22567. Fig. 9B].

with presynaptic markers (Aravamudan et al. 1999), Dunc13A and Dunc13B, showing similar subsynaptic distributions to those in *C. elegans* (Böhme et al. 2016). In mammals, Munc13-1 is expressed throughout the brain, whereas expression of Munc13-2 is confined to neocortical/hippocampal region and Munc13-3 is primarily expressed in cerebellar neurons (Augustin, Betz, et al. 1999a; Augustin et al. 2001).

UNC-13/Munc-13 proteins have multiple conserved domains including two or three C2 domains, a CAM domain, C1 domain and a MUN domain (named for the minimal MUNC13 domain required for functional rescue) (Fig. 1.2A and Fig. 2A.2) (Koch, Hofmann, and Brose 2000; Xu et al. 2017b). Early biochemical data determined that the MUN domain of Munc13 interacts with the N-terminal of the plasma membrane SNARE syntaxin (Fig. 1.2B). Furthermore, Dulubova et al, demonstrated that in solution syntaxin adopts a closed confirmation dependent on intramolecular interactions involving the N-terminal, that occludes the SNARE interacting domain (Dulubova et al. 1999). This information lead to the hypothesis that Munc13's role in priming could be to transition syntaxin to an open confirmation, through a MUN/syntaxin N-terminal interaction, thereby promoting SNARE complex assembly (Richmond, Weimer, and Jorgensen 2001; Betz et al. 1997). This was first tested in *C. elegans* by overexpressing a constitutively open syntaxin protein (UNC-64LE) in the *unc-13* mutant background, which was able to partially bypass the requirement of UNC-13 in locomotion and neurotransmitter release. Subsequent HPF EM analysis of *unc-13* mutants expressing constitutively open syntaxin was also shown to rescue SV docking, consistent with data showing docking defects in the absence of syntaxin (Weimer et al. 2006; Hammarlund et al. 2007; Imig et al. 2014). Similarly, loss of another SNARE protein, SNAP-25, resulted in a docked vesicle deficit in cultured neurons from SNAP-25 knock out mice 18-20].

As will be further discussed in Chapter 2, recent studies have shown that UNC-13/Munc13 is not only required to transition syntaxin from the closed to open configuration but it is also critical for the proper alignment of the SNARE coiled-coil domains in an N-C parallel configuration within the SNARE complex that is required to ensure fusion between the SV and plasma membrane (Lai et al. 2017).

Apart from interacting with SNARE complex, Munc13 also interacts with another active zone protein, RIM. RIM is a Rab-3 interacting protein that is required for synaptic vesicle priming and proper neurotransmitter release (Koushika et al. 2001; Schoch et al. 2002; Gracheva et al. 2008; Weimer et al. 2006). The interaction between Munc13 and RIM is essential for normal vesicle fusion (Betz et al. 2001; Dulubova et al. 2005; Deng et al. 2011; Lu et al. 2006). Interruption of this interaction leads to a significant reduction in the number of primed vesicles and the size of the readily releasable pool (RRP), resulting in a reduced evoked response (Betz et al. 2001; Dulubova et al. 2005; Deng et al. 2011). The Munc13/RIM heterodimer also acts as a modulator of the probability of SV release and the RRP and is necessary for synaptic efficacy and plasticity (Betz et al. 2001; Camacho et al. 2017a; Dulubova et al. 2005; Lu et al. 2006). RIM binding to the N-terminal region of Munc13-1 and ubMunc13-2 also regulates recruitment of Munc13 to the active zones (Andrews-Zwilling et al. 2006; Hu, Tong, and Kaplan 2013). However, the N-terminal of bMunc13-2 does not contain a RIM binding region, instead it binds to ELKS1 (another RIM binding protein) which regulates its recruitment to the active zones in a small subset of hippocampal neurons (Kawabe et al. 2017). Recently it has been shown that Munc13 also interacts with RIM- binding protein 2 (RBP2), an active zone protein that is required for recruitment of Ca^{2+} channels at the presynaptic membrane. This interaction is required for the SV priming activity of Munc13 and is independent of engagement of RBP2 with

Ca^{2+} channels (Brockmann et al. 2020; Böhme et al. 2016). Munc13 is known to participate in homodimerization and heterodimerization. The full priming activity of Munc13 and RBP-2 is only achieved when Munc-13 is in its monomeric form indicating that binding of Munc13 with RBP-2 occurs after Munc13/RIM heterodimer step. RIM and RAB-2 are indispensable cofactors for the priming activity of Munc13.

In summary, Munc13 are multidomain proteins containing a variable N-terminal region that in some isoforms includes a C2 domain (the C2A domain), a CaM binding domain, and a highly conserved C-terminal region containing C1, C2B, MUN, and C2C domains (further discussed Chapter 2A). Over the years we have learned three major functions of Munc13 (a) MUN domain mediated transition of syntaxin from closed to open complex (b) MUN domain mediated proper alignment of the SNARE components within the SNARE complex. (c) C1-C2B-C2C domains acting to target and regulate the Munc13 priming function. Despite enormous progress in our understanding of the UNC-13/Munc-13 function, the interplay between the established domains within these proteins is been actively studied. My thesis Chapter 2B presents a novel function of *C. elegans* UNC-13 N-terminal M domain.

Clinical Significance

Synaptic activity not only transmits information but also determines synaptic strength through modifications which are essential for information processing, learning, and memory. Over the years UNC-13/Munc13 has been identified as an important presynaptic regulator of short-term and long-term synaptic plasticity as it determines the size of the readily releasable pool of fusion competent synaptic vesicles and regulates the probability of vesicle release (Junge et al. 2004; Basu et al. 2007; Shin, Lu, Rhee, Tomchick, Pang, Wojcik, Camacho-Perez, Brose,

Machius, Rizo, Rosenmund, and Südhof 2010; Breustedt et al. 2010; Yang and Calakos 2011).

Large scale whole exome sequencing (WES) studies have identified variants of neuronal

Munc13s as risk factors in autism spectrum disorders and schizophrenia (Fromer et al. 2014;

Purcell et al. 2014; Egawa et al. 2016). A heterozygous variation in the MUN domain of human

Munc13-1 paralog UNC-13A (Met1269Ile) on chromosome 19 was identified in a schizophrenia

patient (Fromer et al. 2014). Though expression of this variant in mouse hippocampal neurons

resulted in no changes in the functional parameters of synaptic transmission, it may still act with

other genetic or epigenetic factors to produce schizophrenia related behavioral outputs (Lipstein

et al. 2017). In another case study, a patient's condition characterized by a dyskinetic movement

disorder, development delay and autism was associated with a rare, *de novo* C>T nucleotide

exchange (Pro814Leu) in the UNC13A gene (Lipstein et al. 2017). Rescue of Munc13-1 and

Munc13-2 double knockout neurons with this variant Munc13-1^{P827L} resulted in larger EPSC

amplitudes in comparison to neurons rescued with Munc13-1^{WT}. This increase was a

consequence of an increase in the probability of vesicle release due to increased vesicle

fusogenicity. In *C. elegans*, expression of a mutated UNC-13L carrying this mutation (P/L) in

unc-13 null mutants as well as UNC-13 (WT) resulted in an increased sensitivity to aldicarb

induced paralysis, indicating that this mutation has a dominant gain-of-function effect. Another

homozygous nonsense mutation resulting in truncation of the Munc13-1 (UNC-13A) was

identified in a patient suffering from a fatal syndrome exhibiting microcephaly, cortical

hyperexcitability, and myasthenia (Engel et al. 2016). This mutation eliminates all functionally

important Munc13-1 domains except for the RIM-binding C2A domain and causes depletion of

the RRP without having an effect on the probability of vesicle release. EM images of the

glutaraldehyde-fixed synapses of this patient showed docking of synaptic vesicles, but this is

inconclusive as aldehyde fixation is known to cause SV docking artifacts. Experiments involving transfection of Munc13-1 knock out mice and human neuroblastoma cells with mutant and wild type Munc13-1 constructs demonstrated that Munc13 modulates amyloid precursor protein (APP) metabolism, independently of and in parallel with protein kinase C (Rossner 2004). APP results in ß-amyloid peptides which are the major constituents of plaques in the brains of Alzheimer's patients. Munc13 also plays a role in drug addiction as self-administration of cocaine in rats enhances synaptic transmission efficiency by increasing protein levels of Munc-13 and RIM in the nucleus accumbens (Smaga et al. 2020).

The complexity of functional phenotypes caused by different Munc13 mutants in cultured neurons and in mouse models, along with the extensive expression of Munc13 in the nervous system, explains the role of Munc13 in multiple clinical phenotypes. These patient phenotypes highlight the critical role of Munc13 in the human brain. It is expected that the increased use of whole exome sequencing as a diagnostic tool will further help in identifying Munc13-related disorders.

1.1.2. SAX-7 (Sensory AXon guidance)/ L1CAMs (L1 Cell Adhesion Molecule)

L1CAMs are conserved cell adhesion molecules that are crucial for nervous system development and function. These are transmembrane proteins with a core of six immunoglobulin-like domains and an extracellular domain containing five fibronectin type III repeats, a single transmembrane domain and a highly conserved cytoplasmic tail (Fig. 1.3). These domains interact with various proteins to facilitate cell adhesion and regulate signal transduction in cellular processes including axon guidance, myelination, formation and maintenance of synapses and overall neuronal architecture (Chen and Zhou 2010; Sakurai 2012).

In mammals, L1CAMs are encoded by four genes that are highly expressed in the nervous system: L1, NrCAM, CHL1, and neurofascin (Hortsch, Nagaraj, and Mualla 2014; Chen and Zhou 2010). L1, NrCAM, CHL1 has been shown to function in axon guidance mediated by a semaphorin signaling pathway. Neurofascin promotes axon myelination during neuronal development and both NrCAM and neurofascin control the assembly of the nodes of Ranvier.

L1CAMs mediate axon guidance by forming a complex with the axonal receptor neuropilins (Nrp) and class 3 semaphorins (Sema3s) (Castellani, Falk, and Rougon 2004; Bechara et al. 2008). Semaphorins are a family of membrane attached and diffuse guidance cues that from heterocomplexes with neuropilins and prevent neuronal projections from invading inappropriate targets. L1 associates with Nrp1 and mediates the recruitment and activation of a Sema3A induced Focal Adhesion Kinase (FAK)- mitogen activated protein kinase cascade. This signaling downstream of L1 is essential for the disassembly of adherence junctions formed in growth cones and subsequent growth cone collapse in response to Sema3A. L1CAMs role in axonal development is partially dependent on its interaction with the adaptor protein, ankyrin, for the recruitment and maintenance of voltage gated sodium channels at the nodes of Ranvier (Lustig et al. 2001). L1 has also been implicated in promoting neurite outgrowth through the MAPK cascade which becomes activated only upon endocytosis of L1 (Schaefer et al. 1999; Schmid, Pruitt, and Maness 2000).

In *C. elegans*, L1CAMs are encoded by two genes, *sax-7* (aka *lad-1*) which encodes for the canonical L1CAM, and *lad-2*. In contrast to the four L1CAM genes in mammals that can compensate for one another hence complicating L1CAM analysis, *sax-7* and *lad-2* have distinct, non-overlapping functions (Chen and Zhou 2010; Wang et al. 2008). While *lad-2* is expressed
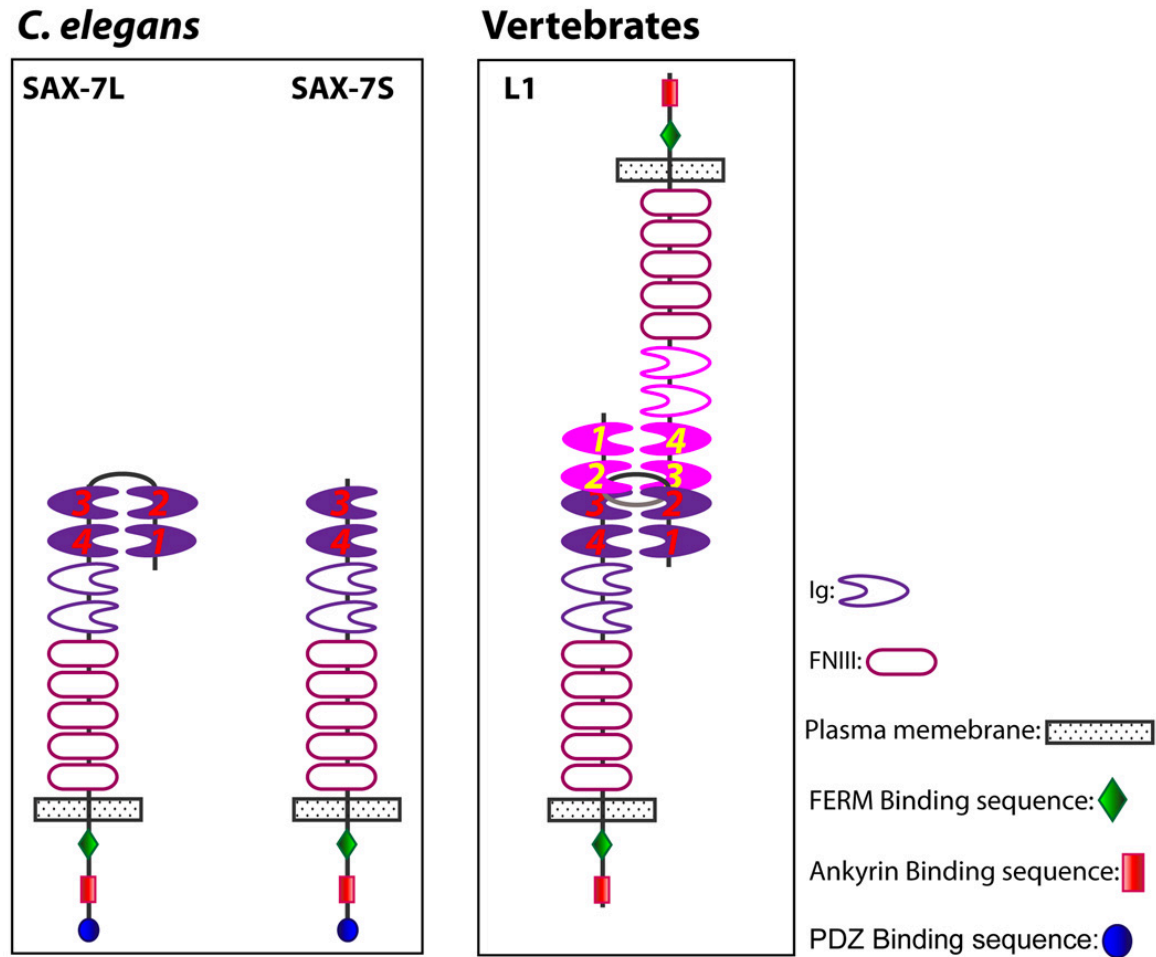
Figure 1. 3. Proposed protein conformations adopted by SAX-7L and SAX-7S on the basis of structural data from mammalian L1. The first four immunoglobulin (Ig) motifs fold into a horseshoe configuration and are essential for L1 mediated homophilic adhesion. Reproduced from (Chen and Zhou 2010).

only in a subset of neurons, *sax-7* is expressed in almost all cells as early as the two-cell-stage embryo (Chen, Ong, and Bennett 2001; Aurelio, Hall, and Hobert 2002). Similar to vertebrate L1CAMs, the extracellular domain of SAX-7 participates in homophilic and heterophilic interactions (Sasakura et al. 2005; Pocock et al. 2008; Wang et al. 2005; Aurelio, Hall, and Hobert 2002; Bénard et al. 2006; Bénard et al. 2009). SAX-7 has also been shown to function in maintaining neuronal positioning as mutations in *sax-7* result in displacement of neuronal cell bodies and axons (Zallen, Kirch, and Bargmann 1999; Sasakura et al. 2005; Wang et al. 2005; Pocock et al. 2008). This neuron displacement phenotype can be partially suppressed by paralyzing *sax-7* mutant animals showing that SAX-7 helps in maintaining neuronal integrity by countering the effects of mechanical force (Sasakura et al. 2005; Pocock et al. 2008). SAX-7 has also been shown to act as a guidance cue in the hypodermis to guide the outgrowth, branching and stability of dendrites in the sensory neuron PVD (Dong et al. 2013; Salzberg, Díaz-Balzac, et al. 2013). This function is attributed to the tripartite complex formed by SAX-7 and MNR-1 (MeNoRin, dendritic branching protein) in the hypodermis and the DMA-1 (Dendrite Morphology Abnormal) receptor on the dendrites.

There are two alternatively spliced isoforms of SAX-7, SAX-7 long (SAX-7L) and SAX-7 short (SAX-7S) (Fig. 1.3.) (Chen, Ong, and Bennett 2001). SAX-7L contains all six Ig motifs whereas SAX-7S lacks the first two Ig motifs. These structural differences have been proposed to confer different adhesive activity to these isoforms. *In vivo* expression of SAX-7 in adjacent neurons, that normally do not physically interact with each other, results in aberrant adhesion of the two neurons via SAX-7 homophilic interactions (Sasakura et al. 2005; Pocock et al. 2008).

SAX-7 also participates in heterophilic interactions though other immunoglobulin superfamily (IgSF) proteins including DIG-1, ZIG-3, and ZIG-4 (Aurelio, Hall, and Hobert

2002; Bénard et al. 2009; Bénard et al. 2006), and EGL-15/Fibroblast Growth Factor Receptor

(FGFR) (Bülow, Boulin, and Hobert 2004; Kulahin et al. 2008). The cytoplasmic tail of SAX-7

contains binding sites for cytoskeletal linking adaptor proteins FERM (protein 4.1, Ezrin,

Radixin, Moesin) proteins, ankyrin, and PDZ (PSD95, DlgA, ZO-1) (Pocock et al. 2008; Zhou et

al. 2008). These SAX-7 interacting proteins are conserved in vertebrate L1CAMs. These

intracellular interactions of SAX-7 are suggested to regulate SAX-7 activity by anchoring it to

the cortical actin cytoskeleton (Davis and Bennett 1994).

   sax-7 has also been shown to genetically interact with proteins that regulate

neurotransmitter release, specifically *unc-13* and *rab-3,* resulting in synthetic locomotion defects

and enhanced resistance to inhibitors of cholinesterase (Ric) in *rab-3; sax-7* mutants (Opperman

et al. 2015). These phenotypes can be suppressed by transient expression of *sax-7* in mature

animals showing its novel non-developmental role that impinges on synaptic function. Chapter 3

provides further synapse focused assessment of how SAX-7 promotes coordinated locomotion.

Clinical Significance

   As L1CAMs mediate protein-protein interactions they regulate various molecular

functions and are crucial for formation and maintenance of nervous system. In humans,

mutations in the L1 genes result in the X-linked neurological L1 syndrome. The symptoms of L1

syndrome are represented by CRASH for Corpus callosum hypoplasia, mental Retardation (or

intellectual disability), Adducted thumbs, Spastic paraplegia, and Hydrocephalus (Fransen et al.

1995; Chen and Zhou 2010). These symptoms have a varied range from mild mental retardation

to pre- or perinatal death due to severe hydrocephalus. Other L1CAM genes are associated with

autism (NrCAM), schizophrenia, and non-specific mental retardation linked with the 3p

syndrome (CHL1) (Marui et al. 2009; Sakurai et al. 2002; Frints et al. 2003). L1 is also linked to Hirschsprung disease, a neuro developmental defect associated with lack of intramural ganglion cells along the gastrointestinal tract (Fernández et al. 2012). These syndromes accentuate the need to further understand the roles of L1CAMs at the level of synapses.

1.1.3. VPS-39 (Vacuolar Protein Sorting)

Vacuolar protein sorting (Vps) proteins regulate the transport of vacuolar proteins such as hydrolases from the trans-Golgi network to endosomal compartments that eventually fuse with the vacuole in yeast (Vida, Huyer, and Emr 1993). *Vps* mutants have been divided into six major classes (A-F) on the basis of morphology of vacuoles, distinct hydrolase mis-sorting and growth phenotypes (Raymond et al. 1992). VPS39 is a class B *vps* gene and its deletion causes cytoplasmic accumulation of endoplasmic reticulum and vesicles which are incompetent to fuse with the vacuole, causing vacuolar fragmentation, and significant mis-sorting of hydrolases (Raymond et al. 1992; Wada, Ohsumi, and Anraku 1992). Overexpression of a human homologue of yeast vps-39 (hVam6p) in the HeLa cells induces massive clustering and fusion of lysosomes, without any impact on early endosomes and other organelles of the endocytic and secretory pathway (Caplan et al. 2001). vps-39 is also a part of homotypic fusion and vacuole protein sorting (HOPS) complex, which consists of six functionally conserved vps family proteins (Vps 18, 11, 16, 33, 41, and 39). Initially the yeast HOPS complex was shown to consist of a 'seahorse' shaped structure with Vps39 and Vps41 on opposite ends whereas a more recent study proposed an open spaghetti-dancer structure for the HOPS complex (Fig. 1.4.) (Bröcker et al. 2012; Chou et al. 2016). These two different structures could represent two different conformations of HOPS complex (Lürick, Kümmel, and Ungermann 2018). Within the HOPS
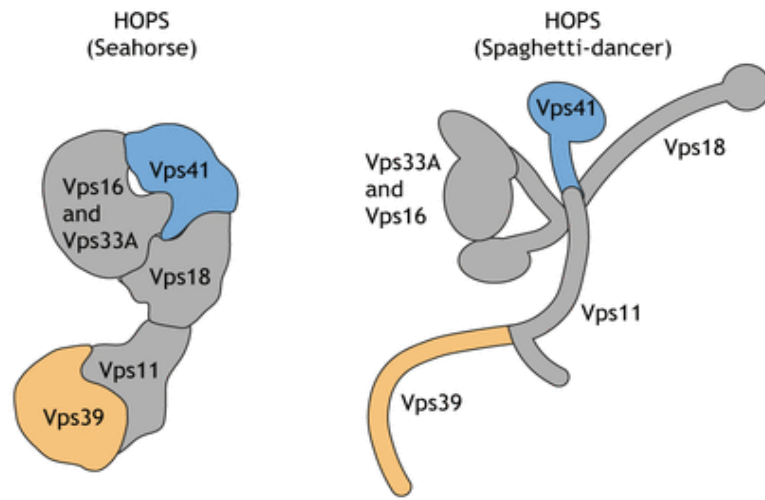
Figure 1. 4. Proposed structures of the HOPS complex. Reproduced from [(van der Beek et al. 2019). 10.1242/jcs.189134 Box 1.]

complex, Vps39 and Vps41 form two Rab binding sites which mediate HOPS complex binding

to the Rab7 GTPase and promotes fusion of late endosomes, adaptor protein AP-3 associated

vesicles, and autophagosomes with vacuoles (Nickerson, Brett, and Merz 2009; Bröcker et al.

2012; Plemel et al. 2011). The HOPS complex is recruited to the lysosomes by binding of a

small GTPase present on lysosomes to Vps41 (Garg et al. 2011). HOPS complexes present on

lysosomes are recruited to autophagosomes by interactions with the Rab7 effector and LC3-

binding protein pleckstrin homology domain-containing family M member 1 (PLEKHM-1) via

its interaction with HOPS components, Vps11, Vps39, and Vps41 (McEwan et al. 2015). HOPS

mediated close proximity of lysosomes and autophagosomes leads to SNARE mediated fusion of

the two organelles (Jiang et al. 2014; Takáts et al. 2014).

hVps39 knockdown in A431 human cell lines leads to greatly reduced kinetics of

conversion from Rab5-positive early endosomes to Rab7-positive late endosomes implicating

Vps39/HOPS complex in the Rab5 dependent recruitment of Rab7 onto endosomes (Rink et al.

2005). Independent of its function as a component of the HOPS complex, Vps39 binds to Rab7

on lysosomes and Tom40 on mitochondria resulting in lysosome-mitochondria contact sites

which are critical for yeast survival during starvation or stress (Elbaz-Alon et al. 2014; Hönscher

et al. 2014; González Montoro et al. 2018).

Pertinent to the focus of this thesis, the HOPS complex also interacts with the yeast

syntaxin homolog Vam 3. Vam3 forms a SNARE complex with the SNAP-25 homolog Vam7

that mediates vesicle docking/fusion in yeast (Sato et al. 2000). The mammalian HOPS complex

members (hVps11, hVPS18, hVPS16) are highly enriched in the nervous system and specifically

interact with Munc18 and Syntaxin 1A, both crucial proteins for neurotransmitter release (Kim et

al. 2006). Overexpression of these HOPS complex members leads to asynchronous discharges in

cultured hippocampal neurons suggesting a regulatory function for the HOPS complex in synaptic transmission. In *Drosophila*, HOPS complex mediated endo-lysosomal trafficking has been shown to regulate turnover of SV associated protein, synaptobrevin, facilitating neurotransmitter release (Fernandes et al. 2014). Chapter 4 in my thesis describes data characterizing the role of *C. elegans* VPS-39 specifically in neurotransmitter release.

Clinical Significance

A full knockout of components of HOPS complex is mostly lethal. Homozygous *vps39* deletion results in embryonic lethality in mice showing that VPS39 plays nonredundant functions for early embryonic development (Messler et al. 2011). As the HOPS complex regulates autophagy, defects in its components are expected to result in clinical disorders (van der Beek et al. 2019). Autophagy impairment is a common factor for various neuronal disorders such as Alzheimer's, Parkinson's, and Huntington's disease. Mutations in HOPS components have been shown to cause neurological defects in *C. elegans*, *D. melanogaster*, zebrafish, and mouse animal models. Patients carrying mutations in the HOPS components, Vps11, Vps16 or Vps33A exhibit dystonia, demyelination, and psychomotor retardation. Mutations in *vps39* results in hypopigmentation of skin melanocytes and the retinal pigment epithelium which causes visual defects in zebrafish (Schonthaler et al. 2008). Electron microscopy of the livers of *vps* mutants shows hepatocytes filled with large vesicles (likely swollen endosomes) leading to hepatomegaly in zebrafish. Rab2a-GTP, an interactor of Vps39, is elevated in human breast cancers and acts as an independent predictor of reoccurrence of breast cancer in patients (Kajiho et al. 2016). Lysosomal hydrolases that are secreted into the extracellular matrix act together with matrix metalloproteinases to remodel the connective tissue that allows cancer cells to migrate. Rab2a in

combination with Vps39 is required for the release of metalloproteinases by lysosomal exocytosis, and depletion of Vps39 significantly hampers the capability of cells to degrade extracellular matrix. This wide variety of disorders caused by components of the HOPS complex including VPS-39 require a more detailed understanding of its mechanism of action at the cellular and molecular levels.

1.2. *C. elegans* as a model system

In 1974, *Caenorhabditis elegans* was introduced as a model system by Sydney Brenner to explore the molecular nature of the nervous system (Brenner 1974). *C. elegans* have a simple nervous system which is composed of 302 neurons, reducing the challenges faced in other model systems with a complex nervous system (Fig. 1.5.). A nearly complete map of all axons and synapses in *C. elegans* is available due to serial EM reconstruction conducted by John White (White et al. 1986). Optical transparency of *C. elegans* allows visualization of florescent reporters *in vivo*. In addition, availability of fluorescent reporters for each of the 302 neurons allows visualization of neurons at a single cell resolution. Short life cycle of *C. elegans* allows faster generation of worms with different genetic backgrounds and relatively quicker acquisition of data. It is a tractable genetic model system to identify, characterize and investigate the interaction of genes involved in biological processes. Due to its short life cycle, large scale genetic screens for identifying genes involved in neurotransmitter release can be carried out in a short period of time. Moreover, *C. elegans* was the first multicellular organism to have the complete genome sequenced and this resulted in several databases and resources that are currently available online for the scientific community (*C. elegans* Sequencing Consortium, 1998). There are a significant number of proteins that are evolutionary conserved between *C. elegans* and human, with a high possibility that what is identified in worms will be applicable to humans.
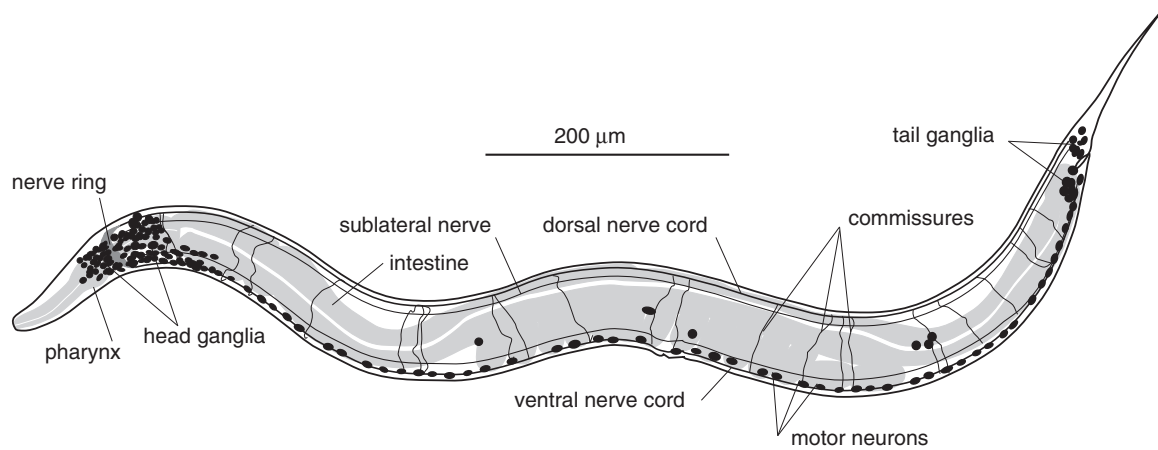
Figure 1. 5. The adult nervous system architecture of C. elegans. Most of the neuronal cell bodies are located in the head ganglia, in the ventral nerve cord, or in the tail ganglia. This image does not include all axon bundles. Reproduced from [(Hobson et al. 2017) doi:10.1016/B978-0-12-809633-8.06787-X. Fig 1]

1.3. High Pressure Freeze and Freeze Substitution (HPF/FS) Electron Microscopy (EM)

C. elegans are ~1 mm in length and 65 µm in diameter, with synapses ~500 nm in diameter and SVs ~30 nm in diameter. Though there have been some significant advances in light microscopy, it still does not have sufficient resolution to analyze changes in the SV parameters such as size, localization to the presynaptic membrane and distribution with respect to the active zone. Therefore, electron microscopy (EM) has been used to analyze the SV alterations for my thesis research. EM uses a beam of electrons with a wavelength 100,000 times shorter than the photons which provides higher resolution. In transmission electron microscopy, a beam of electrons is transmitted through a specimen to form an image. Electrons passing through the samples can be detected by a charge-coupled device (CCD) camera and appear as light spots whereas electrons that get scattered appear as dark spots. Heavy metals such as lead citrate and uranyl acetate are used to provide better contrast to biological samples that generally exhibit lower contrast. As the samples need to be less than ~200 nm and water-free, usage of EM requires a special sample preparation.

Traditional chemical fixation of worms required disruption of its tough cuticle in order for fixatives to penetrate. Animals are then kept in hyperosmotic fixatives for hours to immobilize the internal structures. Disruption of hydrostatic pressure and slower fixation of organelles results in many structural artifacts such as disruption of the integrity of nearby tissue, distortion of synaptic membrane, and shrinkage of extracellular space (Weimer 2006). In addition, aldehyde fixatives can lead to accumulation of SVs closer to the synaptic membrane and have resulted in inaccurate results with respect to the number of docked vesicles [(Broadie et al. 1995) Vs (Hammarlund et al. 2007) (Imig et al. 2014); and (Richmond, Davis, and Jorgensen

1999) Vs (Weimer et al. 2006)](Smith and Reese 1980). The development of high-pressure freeze (HPF) has become a valuable tool to overcome these issues (Moor 1987). Under high pressure (2100 bar), freezing point of water is lowered resulting in formation of amorphous ice while slowing down ice crystal nucleation and growth. As samples up to 600 μm in thickness can be frozen using HPF, this makes *C. elegans* an apt system for using this technique. HPF allows freezing of intact worms within milliseconds in their nearest physiological state, allowing significant improvement in the preservation of its ultrastructure in comparison to chemical fixation (Fig. 1.6.) (Rostaing et al. 2004). Up to 30 adult *C. elegans* can be simultaneously frozen in a specimen holder under high pressure and low temperature (2100 bar, -180 °C) using HPF machine. After that, samples are thawed gradually (7 days) in a controlled manner using automated freeze substitution machine (AFS). During this time worms are incubated with fixatives such as osmium tetroxide and tannic acid. Fixed worms are then embedded in epoxy resin and cut in thin sections for imaging.

I used HPF-FS EM to analyze various synaptic parameters including total number of SVs, number of docked vesicles, distribution of docked vesicles from the dense projection, diameter of SVs, size of presynaptic density, synaptic terminal area. My findings contribute to a better understanding of the genes involved in docking and priming of SVs, as described in the following chapters.
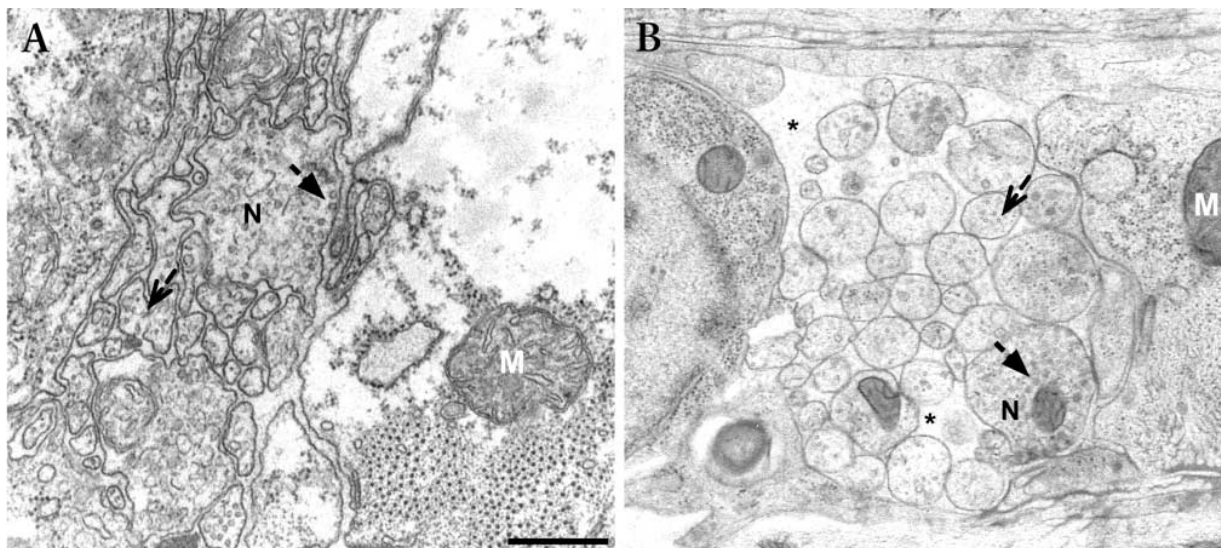
Figure 1. 6. Morphology of C. elegans tissues: Classical fixation Vs high pressure freeze method. (A) Classical fixation often results in morphological alternations such as distortion of membranes and shrinkage of the extracellular space whereas (B) HPF results in well preserved structures. M, muscle mitochondria; N, neuronal processes within the nerve cord. Reproduced from (Rostaing et al. 2004)

CHAPTER IIA: MUNC13 AND ITS MULTIPLE MODULATORY DOMAINS

This chapter is a modified version of an invited review (*in preparation*) for the

International Journal of Molecular Sciences

Seema Sheoran, Mia Krout, Zhitao Hu, and Janet E. Richmond

As mentioned in the Chapter 1, Munc13/UNC-13 is required at various intermediate steps leading to SV fusion. Over the years, studies have provided more details into the structure and functions of each of the Munc13 domains (Fig. 2A.1.). This chapter (2A) summarizes these findings on C1, C2A, C2B, MUN, C2C, and CaM-binding domains of Munc13. In the next chapter (2B) we report a novel function of the N-terminal M domain of the short isoform of UNC-13 in *C. elegans*.

2A.1. The MUN domain

Identification: In 2005, the MUN domain was identified as the **m**inimal **UN**C-13/Munc13 domain required for the SV priming function of Munc13 (Basu et al. 2005; Madison, Nurrish, and Kaplan 2005; Stevens et al. 2005). Mice lacking Munc13-1 and Munc13-2 have essentially no release-competent synaptic vesicles (Varoqueaux et al. 2002) and exhibit a severe vesicle docking defect (Imig et al. 2014). Overexpression of the MUN domain in cultured excitatory and inhibitory neurons from these double-knockout mice partially rescued neurotransmitter release (Basu et al. 2005). In *C. elegans*, mutants lacking UNC-13 are characterized by a nearly complete abolition of neurotransmitter release and severe locomotion defects. Similarly, expression of a truncated UNC-13 protein containing the MUNC homology (MUN domain +C2C) domains partially rescued both the behavioral and secretion defects of *unc-13* mutants

Figure 2A. 1. Model of Munc13 mediated SV priming. Munc13 contains multiple conserved

domains. First, UNC-13/Munc13 mediates the transition of syntaxin from a closed conformation

to an open conformation. Second, UNC-13 in collaboration with UNC-18 aligns syntaxin and
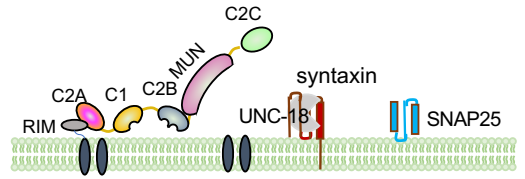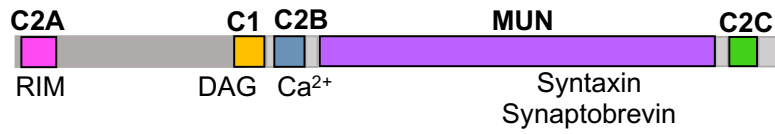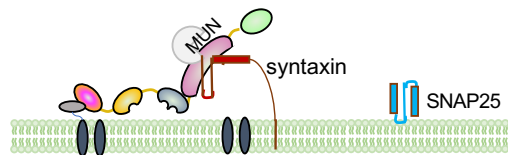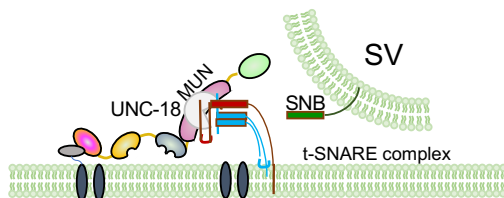
SNAP-25 in proper conformation. Third, UNC-13 alone aligns synaptobrevin to the

syntaxin/SNAP-25 dimer. At this step, SV is in a primed state. Fourth, DAG and Ca^{2+} binding to

the C1 and C2B domain respectively disinhibits the MUN domain and increases the sensitivity of

primed SVs for Ca^{2+}. Adapted from (Palfreyman and Jorgensen 2017) and (Li et al. 2019a).

(Madison, Nurrish, and Kaplan 2005). These experiments highlighted the MUN domain of

Munc13 as the primary regulator of SV priming activity.

Structure and Function: In 2015, the crystal structure of the rat MUN domain revealed

that it exhibits an elongated arch-shape consisting of helices packed against each other in mixed

parallel or antiparallel manner connected by flexible loops, stabilized by interhelical interactions

(Yang et al. 2015). In *C. elegans*, a constitutively open configuration of syntaxin can partially

bypass the requirement of UNC-13 in synaptic priming suggesting that UNC-13 is involved in

the transition of syntaxin from its closed to open configuration (Richmond, Weimer, and

Jorgensen 2001). This was further supported by NMR and fluorescence spectroscopy showing

that the Munc13-1 MUN domain markedly expedites the transition from the syntaxin-1-Munc18-

1 complex (syntaxin-closed) to the assembled SNARE complex (syntaxin-open) (Ma et al.

2011). The MUN domain consists of four subdomains (A-D) aligned accordingly from the N-

terminal to C-terminal of MUN^{933} (Fig. 2A.2). Subdomains B and C have been identified as the

core regions for MUN activity to stimulate the opening of syntaxin (Yang et al. 2015). Double

mutation of the highly conserved residues Asn-1128 and Phe-1131 (referred to as NF) within a

hydrophobic pocket created by subdomains B-C completely disrupted MUN activity *in vitro*. In

addition, mutation in the NF residues of UNC-13S in *C. elegans* failed to rescue both

endogenous and evoked EPSCs, showing the functional importance of these two residues *in vivo*.

The Syntaxin-1 linker region undergoes a conformational change from a defined secondary

structure to a random coiled coil conformation while becoming a part of the SNARE complex

(Misura, Scheller, and Weis 2000; Margittai et al. 2003). The NF residues in the MUN domain

induce this conformational change in syntaxin-1 by interacting with two conserved residues
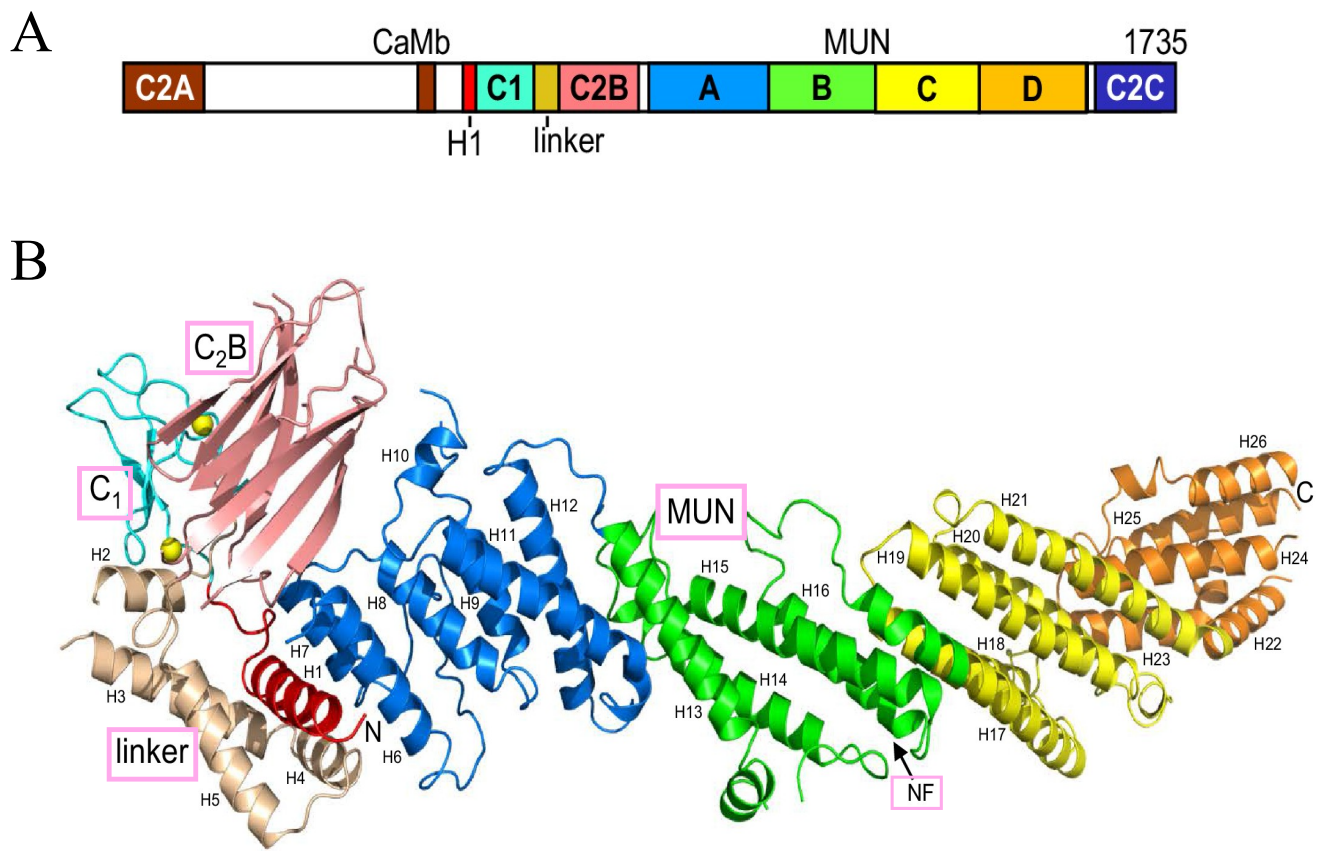
Figure 2A. 2. **The crystal structure of Munc13-1 C1-C2B-MUN domains**. (A) Diagram

representing different domains of rat Munc13-1: C2A, CaMb (CaM binding domain), C1, C2B,

MUN (subdomains A-D), and C2C. (B) Structure of C1-C2B-MUN color coded similar to part A

with helices labeled. The position of the NF sequence within the MUN domain which is involved

in opening synatxin-1 is indicated. Zn^{2+} bound to the C1 domain are shown as yellow spheres.

Reproduced from [*(Xu et al. 2017b)*. eLife 2017;6:e22567. Fig 1 A, B]

R151 and I155 (referred to as RI) in the syntaxin linker region (Wang et al. 2017). The MUN-mediated opening of the syntaxin-1 linker region leads to extension of Munc18 3a domain which in turn forms an activated Munc-18/syntaxin complex that is accessible for binding to synaptobrevin-2 (Wang et al. 2020; Magdziarek et al. 2020). The MUN domain also interacts with the linker region of synaptobrevin-2 and recruits synaptobrevin-2 embedded vesicles to the plasma membrane, increasing the accessibility of Munc18 to synaptobrevin-2 (Wang, Li, et al. 2019). Further the MUN domain stabilizes the Munc-18/syntaxin-1/synaptobrevin-2 complex and enhances binding of SNAP-25 to this complex for subsequent full SNARE assembly (Shu et al. 2020).

Recently it has been shown that the MUN domain also promotes the proper arrangement of SNARE components within the SNARE complex (Lai et al. 2017; Palfreyman and Jorgensen 2017). The SNARE complex consists of syntaxin, synaptobrevin, and SNAP25, structurally arranged in a parallel four helix bundle (Sutton et al. 1998). When the ternary SNARE complex is assembled *in vitro* starting from a syntaxin/SNAP25 assembled docking platform , the MUN domain promotes the proper N to C terminal parallel configuration between syntaxin and synaptobrevin (Lai et al. 2017). This ability of the MUN domain to produce the proper syntaxin/synaptobrevin subconfiguration significantly increases the Ca^{2+}-triggered amplitude and vesicle fusion ratio, emphasizing its indirect role in Ca^{2+} mediated vesicle fusion. In addition to this autonomous function of the MUN domain in mediating proper alignment of the syntaxin/synaptobrevin helices, prior to this, it also cooperates with Munc18 to mediate the proper syntaxin/SNAP-25 configuration within the SNARE complex such that the two helices of SNAP-25 orient along syntaxin in the N to C direction. These recent findings have expanded our

understanding of the MUN domain from not only required at the initial step but also throughout the assembly of the SNARE assembly.

2A.2. The C1 domain

Identification: In 1995, *C. elegans* UNC-13 was identified as a novel member of the phorbol ester receptor family, having a high binding affinity for phorbol esters (PE) and diacylglycerol (DAG) to its C1 domain (Kazanietz et al. 1995). PE binding to the C1 domain of protein kinase C (PKCs) has been shown to act as a hydrophobic anchor for association of PKC with the plasma membrane and to increase its accessibility to second messengers. Similar to the PKCs, binding of PE to the Munc13 C1 domain promotes recruitment of Munc13 to the plasma membrane in human embryonic kidney cells (HEK293) (Betz et al. 1998). Hippocampal neurons from mice expressing a PE binding-deficient Munc13-1^{H567K} variant show normal spontaneous and evoked release, but exhibit increased probability of vesicle release (Rhee et al. 2002). It is important to note that though the C1 domain is not essential for basal neurotransmitter release activity it is required for the survival of these mice indicating its indispensable role. In *C. elegans,* introduction of a point mutation at a conserved histamine within the C1 domain of UNC-13 (H173K), which was also predicted to disrupt PE binding, eliminates PE induced enhancement of cholinergic signaling (Lackner, Nurrish, and Kaplan 1999). Later it was suggested that Munc13-1^{H173K} might be a gain of function mutation as the Munc13-1^{H173K} PE binding deficient mutant synapses show neurotransmitter release properties similar to PE potentiated wild type synapses, mirroring the PE activated state of Munc13-1 (Basu et al. 2007). Various studies have speculated that the C1 domain may have an inhibitory function on neurotransmitter release (Lipstein et al. 2013; Liu et al. 2016; Rhee et al. 2002; Xu et al.

2017b). A recent study showed that complete deletion of the UNC-13 C1 domain enhances calcium-triggered neurotransmitter release, further suggesting its role in stabilizing UNC-13 in an autoinhibited state in absence of Ca^{2+} (discussed more in next sections) (Michelassi et al. 2017b).

Structure and Function: Resembling the C1 domain structure of PKCs, the Munc13 C1 domain contains two beta sheets, a short C-terminal alpha helix and two Zn^{2+} binding sites (Fig. 2A.2. B) (Shen, Guryev, and Rizo 2005). Unlike the PKC C1 domain, a conserved tryptophan side chain occludes the PE/DAG binding site of the Munc-13 C1 domain requiring a considerable conformational change for ligand binding. This unique structural characteristic is thought to decrease DAG activity so that neurotransmitter release is activated only at higher DAG concentrations and hence uncoupling enhancement of vesicle release from other signaling processes mediated by DAG. As PE binding increases spontaneous and Ca^{2+} evoked neurotransmitter release rates without impacting the size of the readily releasable vesicle pool, activation of the C1 domain has been suggested to lower the energy barrier for vesicle fusion (Basu et al. 2007).

The crystal structure of a Munc13-1 fragment including C1C2BMUN domain shows that the C1 and C2B domains are packed at the N-terminal of Munc13-1 (Fig. 2A.2.B) (Xu et al. 2017b). DAG and Ca^{2+}-binding sites of the C1 and C2B domains are in similar orientation, suggesting that these two domains cooperate in binding to the synaptic membrane and that activation of Munc13-1 by Ca^{2+} and DAG are closely inter-connected. In *C. elegans*, removal of the C1 domain enhances Ca^{2+} triggered synaptic transmission (Michelassi et al. 2017b). This increase is similar to the effect of deletion of the C2B domain on synaptic transmission.

Moreover, deletion of the C1 domain almost completely reverses C2B inhibition (discussed in the next section) observed by behavioral assays and electrophysiological recordings in *C. elegans,* suggesting that C1 is required to stabilize C2B inhibition in the calcium-free state. These recent studies refine our understanding of the C1 domain and demonstrate that under resting conditions it inhibits a post-priming function, and DAG/PE mediated activation relieves this autoinhibition and thereby facilitates neurotransmitter release.

Ethanol has been well known to have effects on neuronal presynaptic activity. Flies with reduced activity of the Dunc-13 (*Drosophila unc-13*) ortholog exhibit significantly higher preference for ethanol in comparison to wild type (Das et al. 2013). This phenotype is rescued by expression of rat Munc-13 in the mutant flies showing that Munc13 is a conserved presynaptic regulator of ethanol related behaviors. The C1 domain of Munc13 has been shown to be a target site for ethanol *in vitro*, mutation of Glu-582 within the C1 domain affecting ethanol binding. Additionally, ethanol interaction with Glu-582 stabilizes interactions of the ternary SNARE complex, C1 domain-(phorbol-13-acetate)- lipid membrane (You and Das 2020). Intoxicating levels of ethanol exposure does not impact Ca^{2+} influx or membrane depolarization, but it dramatically inhibits SV fusion in olfactory sensory neurons of *Drosophila* (Xu et al. 2018). Ethanol binding to the C1 domain at concentrations comparable with binge exposure reduces binding of DAG and has been proposed to reduce neuronal activity by impacting DAG mediated localization of Munc13 to the synaptic membrane. These studies highlight the importance of the Munc-13 C1 domain in alcohol induced changes in neuronal activity and cognitive outputs.

2A.3. The C2B domain

Identification: The C2B domain of Munc13 is a Ca^{2+}-binding motif that binds to phospholipids in a Ca^{2+}-dependent manner, with a predisposition for phosphatidylinositol phosphate (PIP) and phosphatidylinositol bisphosphate (PIP_2) (Shin, Lu, Rhee, Tomchick, Pang, Wojcik, Camacho-Perez, Brose, Machius, Rizo, Rosenmund, and Südhof 2010; Rizo and Südhof 1998). Ca^{2+} binding to the Munc13-1 C2B domain leads to more efficient bridging of synaptobrevin liposomes (vesicle SNARE) to syntaxin-1-SNAP-25 liposomes (plasma membrane SNAREs) (Liu et al. 2016). Abolishing Ca^{2+} binding to the Munc13-2 C2B domain in mouse neuronal cultures did not alter SV exocytosis caused by isolated action potentials, but impaired facilitation of SV exocytosis induced by repeated action potentials. This indicates that the C2B domain acts as a Ca^{2+} regulator of short-term synaptic plasticity. In *C. elegans,* deletion of the UNC-13 C2B domain enhances Ca^{2+}-dependent exocytosis downstream of SV priming, revealing a novel autoinhibitory function of the C2B domain (Michelassi et al. 2017b).

Structure and Function: The crystal structure of the C2B domain in the presence or absence of Ca^{2+} consists of a typical C2 domain β-sandwich fold with top loops containing Ca^{2+} binding sites (Fig. 2A.2.B) (Shin, Lu, Rhee, Tomchick, Pang, Wojcik, Camacho-Perez, Brose, Machius, Rizo, Rosenmund, and Südhof 2010; Rizo and Südhof 1998). In the case of Munc13 C2B domain, Ca^{2+}-dependent phospholipid binding occurs at relatively high concentrations of PIP and PIP_2 in comparison to other C2 domains. This unusual biochemical property specific to the Munc13 C2B domain is partially attributed to its Ca^{2+}-binding loop 3 containing a unique protruding α-helix. The crystal structure of C1-C2B-MUN incorporating the Ca^{2+}-binding loops of the C2B domain, reveals that these loops are in close proximity to the DAG/PE -binding region of the C1 domain (Xu et al. 2017b). This arrangement likely promotes

cooperation between the C1 and C2B domains in membrane binding. A mutation in the Ca^{2+} binding loop of Munc13-2 C2B results in an increase in the release probability (Shin, Lu, Rhee, Tomchick, Pang, Wojcik, Camacho-Perez, Brose, Machius, Rizo, Rosenmund, and Südhof 2010). In *C. elegans*, deletion of the C2B domain enhances Ca^{2+}-dependent synaptic vesicle release downstream of SV priming (Michelassi et al. 2017b). This suggested an auto-inhibitory state of C2B which is relieved upon Ca^{2+} binding. A highly conserved linker region between the C2B and MUN domains plays a crucial role in maintaining the C1-C2B autoinhibition. Disruption of this linker enhances acetylcholine secretion to a similar degree as deleting the entire C2B domain. Deletion of the C1 domain, C2B domain, and the sequence between C2A and C1 results in an hyperactive form of UNC-13 which results in dramatically increased neurotransmitter release, Ca^{2+} sensitivity, and probability of SV release (Li et al. 2019a). Similarly, in mouse hippocampal neuronal cultures, a double mutation designed to disrupt the hydrophobic packing of helix H1 (at the N terminal of the C1 domain) against the linker region (between C1 and C2B domains) and against the MUN domain led to an increase in mEPSC frequency, whereas the mEPSC charge and amplitude were unaltered (Xu et al. 2017b). Further in *C. elegans*, removal of either the C1 or C2B domain enhanced Ca^{2+}-triggered synaptic transmission (Michelassi et al. 2017b). Mimicking the constitutively Ca^{2+}-bound C2B domain resulted in a phenotype similar to the deletion of the C2B domain, hence Ca^{2+}-binding appears to relieve a basal inhibitory state of the C2B domain. Whereas a Ca^{2+}-binding-deficient C2B domain seems to be locked into its autoinhibitory mode. These recent studies suggest that C1 and C2B domains act together to stabilize an inhibited state of Munc13 when the membrane recruitment signals such as Ca^{2+}, PIPs, and DAG are not available.

The spatial proximity of Voltage-Gated Ca^{2+} Channels (VGCC) with respect to the SV release machinery at the active zones is a critical determinant of synaptic fidelity. Munc13 is an important regulator for the localization and proper functioning of VGCC (Kusch et al. 2018; Calloway et al. 2015). Munc13 interacts with the VGCC, $Ca_V2.2$, via its C2B domain (Calloway et al. 2015). Knock down of Munc13-1/2 resulted in a 34% reduction in the Ca^{2+} influx following a single action potential in comparison to wild type. Re-expression of Munc13-1 in these Munc13 KD neurons resulted in complete rescue of Ca^{2+} influx from a single AP. Whereas re-expression of Munc13 containing point mutations within the C2B domain that prevent interaction with VGCC (Munc13 KR/AA) restored SV exocytosis but failed to rescue Ca^{2+} influx. As C2B domains of synaptotagmin-1 and RIM1 also interact with the synaptic protein interaction region (synprint) on $Ca_V2.2$ (Sheng, Yokoyama, and Catterall 1997; Chapman et al. 1998; Coppola et al. 2001) and as Munc13 is known to interact with RIM1, in future, it would be interesting to learn about the interplay between these AZ proteins to understand the underlying mechanism regulating the VGCC functions.

2A.4. The C2C domain

Identification: The C2C domain is part of the highly conserved C-terminal of Munc13/UNC-13. A study from 2005 showed Munc13-1 constructs containing C2C were able to increase the size of the readily releasable pool in chromaffin cells, whereas C-terminal domains lacking C2C showed no difference as compared to WT (Stevens et al. 2005). Additionally, an *in vivo* study that same year in *C. elegans*, showed the C2C domain, in conjunction with the MHD1 and MHD2 domains (Munc13 Homology Domains 1 and 2), were necessary for full rescue of *unc-13* null mutant locomotion defects and could partially restore priming function to UNC-13S

levels (Madison, Nurrish, and Kaplan 2005). More recent work in neuronal autaptic cultures from Munc13-1/2 DKO mice shows the C-terminal region, including the C1, C2B, MUN, and C2C, can partially rescue the RRP and evoked transmission, whereas a construct missing the C2C domain failed to rescue (Liu et al. 2016).

Structure and Function: Multiple attempts have been made to determine the structure and properties of the C2C domain, all have failed to produce soluble protein, though fragments including the MUN domain are possible, suggesting that the MUN domain is necessary for proper folding of the C2C (Quade et al. 2019). Recent work in *C. elegans* shows one or two alpha helices of the MUN domain that precede the C2C and the predicted alpha helices of the last 60 residues (MCT) are necessary for folding and stability (Narayanappa et al. 2020). Deletion of C2C or MCT impairs synaptic transmission, decreases SV priming, and disrupts nervous system function (Narayanappa et al. 2020). Additionally, ^{1}H-^{13}C heteronuclear multiple quantum coherence (HMQC) spectra of the MUNC2C fragments show that the C2C domain is structured and supports the idea that there are interactions between the two domains (Quade et al. 2019). C2C structural models based on sequence homology to the synaptotagmin-1 and RIM1 C2B domains suggested that C2C, like other C2 domains that participate in membrane may contain exposed basic and hydrophobic residues, and a polybasic region, in its predicted membrane-binding loops and ß-sandwich, respectively (Quade et al. 2019). Studies using bacterially expressed versions of Munc13-1 C1C2BMUNC2C with single R1598E and F1658E mutations or the double R1598E/F1658E mutations in the predicted loop, as well as a K1613A/K1616A double residue substitutions in the polybasic region, were used to disrupt binding of MUNC2C to membranes (Quade et al. 2019). Cryo-electron tomography (cryo-ET)

was used to image reconstitution reactions with T- and V-liposomes combined with Munc13-1 C1C2BMUNC2C, Munc18-1, NSF and SNAP and showed that clusters were typically formed with each liposome pair bridged by one or more C1C2BMUNC2C molecules (Quade et al. 2019). Disruption of C2C binding by R1598E/F1658E mutations in C1C2BMUNC2C with intact C1-C2B regions showed more dispersed liposomes as compared to specimens with WT C1C2BMUNC2C (Quade et al. 2019). Dynamic light scattering (DLS), used to assay clustering between SV- and PM-liposomes, showed single R1598E and F1658E mutations disrupted vesicle clustering, as did the K1613A/K1616A substitution, although to a lesser degree, while clustering was completely eliminated by the R1598E/F1658E mutation (Quade et al. 2019). Knowledge regarding membrane binding to C2 domains, predicts that F1658 is a key residue involved in insertion into a lipid bilayer (Chapman and Davis 1998; Rhee et al. 2005) while the polybasic region is expected to moderately contribute to membrane binding (Li et al. 2006). In neuronal autaptic cultures from Munc13-1/2 DKO mice the R1598E, F1658E and R1598E/F1658E mutations severely inhibited spontaneous, evoked and hyperosmotic induced release, with evoked release almost completely abolished by the F1658E and R1598E/F1658E mutations (Quade et al. 2019). There was no difference in the release probability or paired-pulse ratios measured for rescue with WT or K1613A/K1616A substituted Munc13-1, however the K1613A/K1616A showed less depression upon repetitive stimulation than WT Munc13-1 (Quade et al. 2019). Together these results show the role of the C2C domain in bridging the membrane.

2A.5. The C2A domain

Identification: The C-terminal region of MUNC13, from the C1 to the C2C domains, are highly conserved from *C. elegans* to humans. In contrast, whereas the N-terminal C2A domain is present in mammals and *C. elegans*, it is absent in *Drosophila.* C2A, present in the L region of *C. elegans* UNC-13 Long and in Munc13-1 and ubMunc13-2 mammalian isoforms, was first found to bind the zinc finger of RIM to form a heterodimer (Betz et al. 2001). Disruption of this heterodimer led to a reduction in the readily releasable pool in cultured hippocampal neurons (Betz et al. 2001). However, Munc13-1 lacking the N-terminal C2A domain in chromaffin cells was able to prime vesicles (Deng et al. 2011); likewise, removal of the C2A of UNC-13L in *C. elegans* showed no change in the readily releasable pool (Liu et al. 2019).

Structure and Function: The C2A domain of Munc13–1 spans residues 3–130, with additional residues in the C-terminus necessary for tight binding, forms heterodimers with RIM ZF and C2A homodimers (Fig. 2A.3.) (Lu et al. 2006). The crystal structure of the Munc13-1 C2A domain homodimer shows that the C2A domain adopts a ß-sandwich structure with a four-stranded concave side that when homodimerized leads to the formation of an eight-stranded ß-barrel; whereas the crystal structure of the Munc13-1 C2A/ RIM ZF heterodimer engages the bottom tip of the C2A-domain ß-sandwich and a C-terminal α-helical extension, which then wrap around the RIM ZF domain (Fig. 2A.3.) (Hu, Tong, and Kaplan 2013). Homodimerization of C2A is thought to compete with the formation of the Munc13-1 C2A/RIM ZF heterodimer.

A

1. Munc13–1/Munc13–1 homodimer   2. Munc13–1 monomer   3. Munc13–1/RIM heterodimer

B

Munc13-1 fragment

RIM ZF

E128

E137
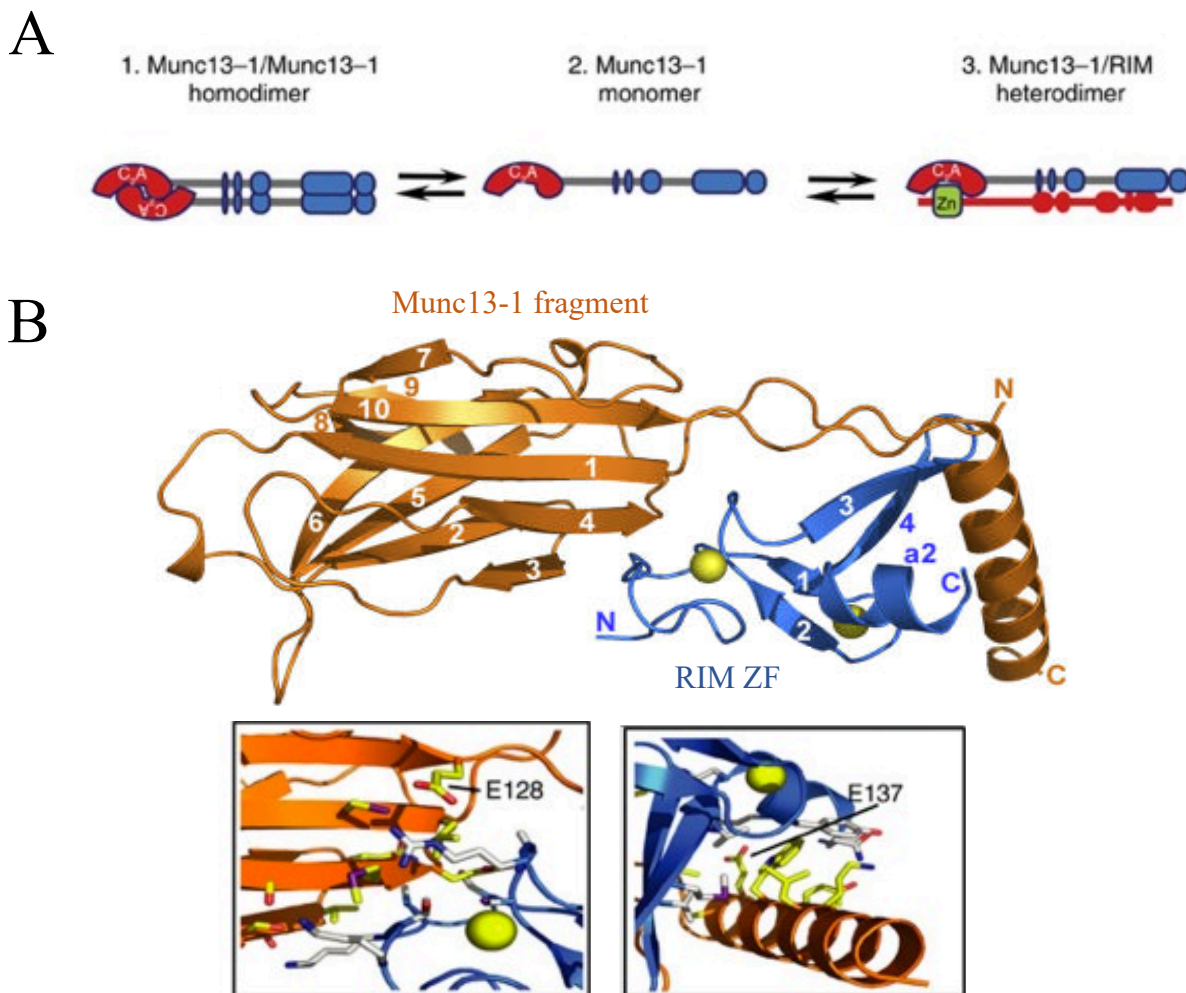
Figure 2A. 3. Munc13 heterodimerizes with RIM through its C2A domain.

(A) Schematic representation of Munc13 homodimerization and heterodimerization with RIM

(B) Overall structure of the Munc13-1/RIM2α heterodimer. Munc13-1 fragment containing C2A

domain is shown in orange and the RIM ZF domain in blue with Zinc atoms as yellow spheres.

The β-strands are labeled with numbers, the α-helix at the C-terminal of RIM ZF domain is

labeled a2. Bottom two panels show the heterodimerization interface of the RIM2α ZF with the

Munc13-1 C2A domain and C-terminal α-helix respectively. Mutated side chains (E128 and

E137) are labelled. Reproduced and modified from (Lu et al. 2006) and [(Camacho et al. 2017b).

https://doi.org/10.1038/ncomms15293. Fig 3b]

Experiments in cultured hippocampal DKO of Munc13-1/2 neurons rescued with Munc13-1 mutants that lacked the C2A domain (del 1–150) and mutants with a truncated N-terminus (del 1–520) including the C2A, domain showed a reduction of docked vesicles by TEM, implying the C2A domain is necessary to maintain normal SV docking (Camacho et al. 2017a). Synapses that expressed the Munc13-1 a point mutation (K32E) that disrupts homodimerization, showed docking activity comparable to Munc13-1 WT rescued synapses. In contrast Munc13-1 (E128K, E137K), which favors homodimerization and (K32E, E128K, E137K) which impairs both homo- and heterodimerization showed a reduction in docked SVs (Fig. 2A.3B). Rescue of Munc13-1/2 DKO neurons with the Munc13-1 (K32E) rescued priming and evoked release; while Munc13-1 (E128K, E137K), impaired both vesicle priming and evoked responses (Camacho et al. 2017a). Expression of the triple point mutant Munc13-1 (K32E, E128K, E137K), promoting monomeric Munc13-1 led to a reduced RRP size and evoked release with no effect on release probability (Camacho et al. 2017a). The Munc13-1 (E128K, E137K) mutant, unable to interact with RIM to disrupt homodimerization, also exhibited a reduction of primed vesicles; whereas the Munc13-1 (K32E) mutant had no reduction of priming or evoked release (Camacho et al. 2017a). Taken together the data from the monomeric Munc13-1 (K32E, E128K, E137K) and the heterodimeric Munc13-1 (K32E) mutant show that Munc13 monomers are not efficient in priming and neurotransmitter release when compared to Munc13-1 in the heterodimerized state (Camacho et al. 2017a). In *C. elegans*, though the C2A/RIM interaction is conserved, priming of SVs does not require the heterodimerization of UNC-13/RIM or rely on the C2A domain of UNC-13 as animals lacking the C2A domain of UNC-13L restored primed vesicle levels to that of WT animals although vesicle docking was not examined (Liu et al. 2019). The monomeric C2A domain is functional for tonic release, though evoked release is impaired when C2A/RIM

heterodimerization is prohibited (Liu et al. 2019). However, this disruption of heterodimerization has no effect on synaptic depression or recovery. Differing results in these studies lead to the possibility of distinct priming mechanisms between mouse and worms.

2A.6. The Calmodulin (CaM) binding domain

Identification: The CaM domain was first identified in Dunc-13 as a N-terminal Calmodulin binding motif in a screen for retinal calmodulin-binding proteins in *Drosophila* (Xu et al. 1998). It was subsequently shown that Calmodulin binds to the Munc13 CaM binding domain in a Ca^{2+} dependent manner (Junge et al. 2004; Dimova et al. 2006). Unlike the C2B domain of Munc13 that is directly activated by Ca^{2+} influx during action potentials, the CaM binding domain is activated indirectly by binding of accumulating residual Ca^{2+} to calmodulin. The Munc13 CaM binding region has significant sequence homology with Dunc-13/UNC-13/huUnc-13 showing that this domain is evolutionary conserved.

Structure and Function: Calmodulin (CaM) is a 148 amino acid protein arranged in two globular domains each containing two EF-hand binding sites for Ca^{2+} (Babu, Bugg, and Cook 1988). The high-resolution NMR structure of Ca^{2+}_4–CaM in complex with the CaM binding domain of Munc13-1$^{459-492}$ features a novel 1-5-8-26 CaM binding motif with two independent modules; a C-module and N-module, connected by flexible linkers (Fig. 2A.4.) (Rodríguez-Castañeda et al. 2010). The C-module consists of an amphiphilic α-helix of Munc13-1 anchored to the C-terminal CaM domain by the hydrophobic residues in positions 1-5-8, whereas the N-module contains a tryptophan at position 26 embedded in the hydrophobic cleft of the N-terminal CaM domain.
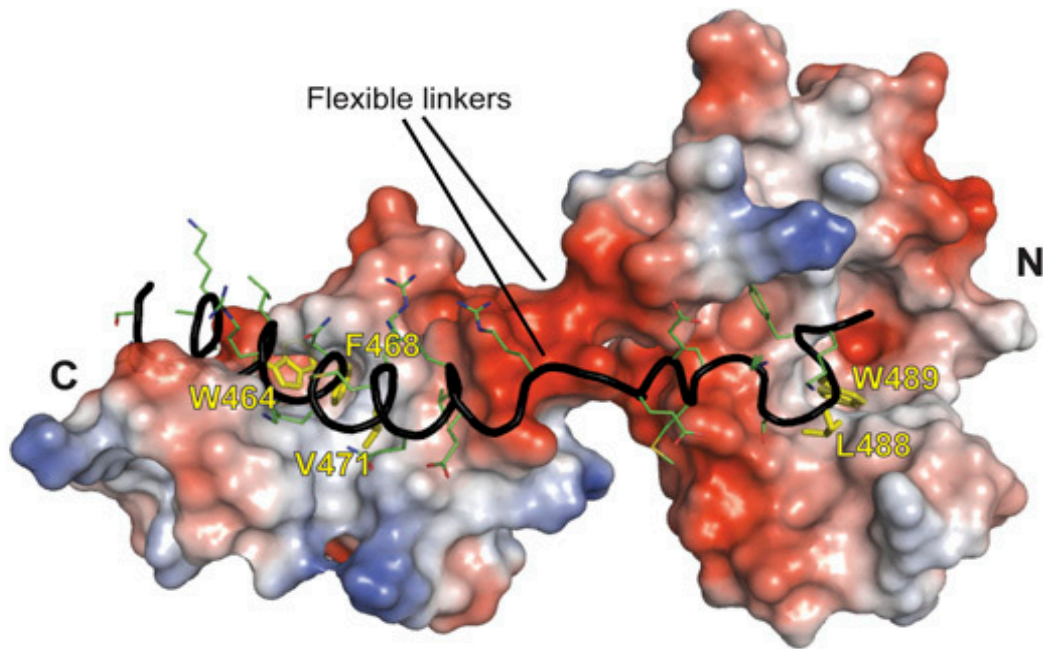
Figure 2A. 4. Structure of Ca²⁺₄–CaM in complex with the CaM binding domain of Munc13-1.

Munc13-1 is represented as a black ribbon and its side chains are shown as black sticks. Ca^{2+}_4–CaM is shown as electrostatic potential surface. The complex highlights two modules: an amphiphilic α-helical 1-5-8 motif bound to the CaM C-terminal domain and the Trp in position 26 attached to the CaM N-terminal domain. The side chains of the anchoring residues are highlighted as yellow sticks. Reproduced from (Rodríguez-Castañeda et al. 2010).

The C-terminal CaM domain shows a high affinity binding with the helical segment at the N-terminal of Munc13-1$^{459-492}$ whereas the N-terminal CaM domain shows lower affinity for binding with the C-terminal of Munc13-1$^{459-492}$. This kind of structure allows sequential formation of an intermediate Munc13/Ca^{2+}_2-CaM (two Ca^{2+}) state and then the fully loaded Munc13/Ca^{2+}_4-CaM (four Ca^{2+}) complex. The rapid interconversion between these two states helps the Munc13-CaM complexes to act as an efficient Ca^{2+} sensor at micromolar Ca^{2+} concentrations (5mm) consistent with a role in short-term synaptic plasticity.

In mice, arginine substitution of a conserved tryptophan residue in the calmodulin-binding motif of both Munc13-1(W464R) and ubMunc13-2(W387R) completely abolished CaM binding (Junge et al. 2004). Cultured autaptic hippocampal neurons expressing these CaM-binding deficient Munc13 variants showed normal evoked synaptic transmission and SV priming, indicating that basal SV priming and release is not dependent on CaM binding to Munc13. However, absence of CaM binding results in striking differences in Munc13-dependent synaptic plasticity. Specifically, high-frequency stimulation-induced synaptic depression observed in wild-type Munc13-1 became more prominent in the presence of Munc13-1(W464R) and the moderate augmentation normally observed following the stimulation train was reduced. These results suggested a deficiency in refilling the primed pool of SVs. Similarly, calyces of Held in knockin mice expressing the Ca^{2+}-CaM insensitive Munc13-1 (W464R) variant show a slower rate of SV replenishment, abnormal short-term depression and reduced recovery from synaptic depression after high-frequency stimulation (Lipstein et al. 2013). In *C. elegans*, rescue with a chimeric UNC-13 protein containing the predicted CaM binding domain fused with the R domain (UNC-13 region containing C1, C2B, MUN, and C2C domains) showed evoked responses with significantly faster activation kinetics and more EGTA-resistance than in

UNC13R rescued animals (Hu, Tong, and Kaplan 2013). This shows that the CaM bining domain expedites release kinetics and reinforces Ca^{2+} coupling. These studies place Ca^{2+}-CaM-Munc13-1 as a core complex in facilitating short term plasticity.

2A.7. Summary

As reviewed in this chapter, Munc13 plays multifaceted roles in SV release, that can be attributed to its specific and highly conserved domains (2A.5). The MUN domain mediates transition of syntaxin from closed to open complex which leads to the formation of activated Munc-18/syntaxin complex that is accessible for binding to SV associated synaptobrevin-2. In addition, the MUN domain also interacts with synaptobrevin-2 and recruits synaptobrevin-2 embedded vesicles to the plasma membrane, increasing the accessibility of Munc18 to synaptobrevin-2. Further the MUN domain stabilizes the Munc-18/syntaxin-1/synaptobrevin-2 complex and enhances binding of SNAP-25 to this complex for subsequent full SNARE assembly, and ensures proper alignment of the SNARE components within the SNARE complex. The DAG binding C1 domain and Ca^{2+}/ PIP_2 binding C2B domain act together to stabilize the autoinhibitory state of Munc13 when the membrane recruitment signals- Ca^{2+}, PIPs, and DAG are unavailable, thereby acting as a check point for proper vesicle fusion. The C2C domain along with C1 and C2B domains helps in bridging the SV membrane to the synaptic plasma membrane. The C2A domain interacts with RIM (Rab3 interacting molecule) and leads to formation of Munc13/RIM heterodimer which acts as a modulator of the probability of SV release and the RRP (readily releasable pool) and is necessary for synaptic efficacy and plasticity. The CaM binding domain expedites release kinetics by reinforcing Ca^{2+} coupling.

These studies have helped in advancing our understanding of the roles of conserved domains of Munc-13/UNC-13, prompting the examination of remaining regions of the Munc13 that have yet to be characterized. In the following section we examined the role of the N-terminal region of the UNC-13 short isoform.

2A.8. References

Babu, Y. S., C. E. Bugg, and W. J. Cook. 1988. 'Structure of calmodulin refined at 2.2 A resolution', *J Mol Biol*, 204: 191-204.

Basu, J., A. Betz, N. Brose, and C. Rosenmund. 2007. 'Munc13-1 C1 domain activation lowers the energy barrier for synaptic vesicle fusion', *J Neurosci*, 27: 1200-10.

Basu, J., N. Shen, I. Dulubova, J. Lu, R. Guan, O. Guryev, N. V. Grishin, C. Rosenmund, and J. Rizo. 2005. 'A minimal domain responsible for Munc13 activity', *Nat Struct Mol Biol*, 12: 1017-8.

Betz, A., U. Ashery, M. Rickmann, I. Augustin, E. Neher, T. C. Südhof, J. Rettig, and N. Brose. 1998. 'Munc13-1 is a presynaptic phorbol ester receptor that enhances neurotransmitter release', *Neuron*, 21: 123-36.

Betz, A., P. Thakur, H. J. Junge, U. Ashery, J. S. Rhee, V. Scheuss, C. Rosenmund, J. Rettig, and N. Brose. 2001. 'Functional interaction of the active zone proteins Munc13-1 and RIM1 in synaptic vesicle priming', *Neuron*, 30: 183-96.

Calloway, N., G. Gouzer, M. Xue, and T. A. Ryan. 2015. 'The active-zone protein Munc13 controls the use-dependence of presynaptic voltage-gated calcium channels', *Elife*, 4.

Camacho, M., J. Basu, T. Trimbuch, S. Chang, C. Pulido-Lozano, S. S. Chang, I. Duluvova, M. Abo-Rady, J. Rizo, and C. Rosenmund. 2017a. 'Heterodimerization of Munc13 C2A domain with RIM regulates synaptic vesicle docking and priming', *Nat Commun*, 8: 15293.

———. 2017b. 'Heterodimerization of Munc13 C(2)A domain with RIM regulates synaptic vesicle docking and priming', *Nat Commun*, 8: 15293.

Chapman, E. R., and A. F. Davis. 1998. 'Direct interaction of a Ca2+-binding loop of synaptotagmin with lipid bilayers', *J Biol Chem*, 273: 13995-4001.

Chapman, E. R., R. C. Desai, A. F. Davis, and C. K. Tornehl. 1998. 'Delineation of the oligomerization, AP-2 binding, and synprint binding region of the C2B domain of synaptotagmin', *J Biol Chem*, 273: 32966-72.

Coppola, T., S. Magnin-Luthi, V. Perret-Menoud, S. Gattesco, G. Schiavo, and R. Regazzi. 2001. 'Direct interaction of the Rab3 effector RIM with Ca2+ channels, SNAP-25, and synaptotagmin', *J Biol Chem*, 276: 32756-62.

Das, J., S. Xu, S. Pany, A. Guillory, V. Shah, and G. W. Roman. 2013. 'The pre-synaptic Munc13-1 binds alcohol and modulates alcohol self-administration in Drosophila', *J Neurochem*, 126: 715-26.

Deng, L., P. S. Kaeser, W. Xu, and T. C. Südhof. 2011. 'RIM proteins activate vesicle priming by reversing autoinhibitory homodimerization of Munc13', *Neuron*, 69: 317-31.

Dimova, K., H. Kawabe, A. Betz, N. Brose, and O. Jahn. 2006. 'Characterization of the Munc13-calmodulin interaction by photoaffinity labeling', *Biochim Biophys Acta*, 1763: 1256-65.

Hu, Z., X. J. Tong, and J. M. Kaplan. 2013. 'UNC-13L, UNC-13S, and Tomosyn form a protein code for fast and slow neurotransmitter release in Caenorhabditis elegans', *Elife*, 2: e00967.

Imig, C., S. W. Min, S. Krinner, M. Arancillo, C. Rosenmund, T. C. Südhof, J. Rhee, N. Brose, and B. H. Cooper. 2014. 'The morphological and molecular nature of synaptic vesicle priming at presynaptic active zones', *Neuron*, 84: 416-31.

Junge, H. J., J. S. Rhee, O. Jahn, F. Varoqueaux, J. Spiess, M. N. Waxham, C. Rosenmund, and N. Brose. 2004. 'Calmodulin and Munc13 form a Ca2+ sensor/effector complex that controls short-term synaptic plasticity', *Cell*, 118: 389-401.

Kazanietz, M. G., N. E. Lewin, J. D. Bruns, and P. M. Blumberg. 1995. 'Characterization of the cysteine-rich region of the Caenorhabditis elegans protein Unc-13 as a high affinity phorbol ester receptor. Analysis of ligand-binding interactions, lipid cofactor requirements, and inhibitor sensitivity', *J Biol Chem*, 270: 10777-83.

Kusch, V., G. Bornschein, D. Loreth, J. Bank, J. Jordan, D. Baur, M. Watanabe, A. Kulik, M. Heckmann, J. Eilers, and H. Schmidt. 2018. 'Munc13-3 Is Required for the Developmental Localization of Ca(2+) Channels to Active Zones and the Nanopositioning of Ca(v)2.1 Near Release Sensors', *Cell Rep*, 22: 1965-73.

Lackner, M. R., S. J. Nurrish, and J. M. Kaplan. 1999. 'Facilitation of synaptic transmission by EGL-30 Gqalpha and EGL-8 PLCbeta: DAG binding to UNC-13 is required to stimulate acetylcholine release', *Neuron*, 24: 335-46.

Lai, Y., U. B. Choi, J. Leitz, H. J. Rhee, C. Lee, B. Altas, M. Zhao, R. A. Pfuetzner, A. L. Wang, N. Brose, J. Rhee, and A. T. Brunger. 2017. 'Molecular Mechanisms of Synaptic Vesicle Priming by Munc13 and Munc18', *Neuron*, 95: 591-607.e10.

Li, L., H. Liu, Q. Hall, W. Wang, Y. Yu, J. M. Kaplan, and Z. Hu. 2019. 'A Hyperactive Form of unc-13 Enhances Ca(2+) Sensitivity and Synaptic Vesicle Release Probability in C. elegans', *Cell Rep*, 28: 2979-95.e4.

Li, L., O. H. Shin, J. S. Rhee, D. Arac, J. C. Rah, J. Rizo, T. Sudhof, and C. Rosenmund. 2006. 'Phosphatidylinositol phosphates as co-activators of Ca2+ binding to C2 domains of synaptotagmin 1', *J Biol Chem*, 281: 15845-52.

Lipstein, N., T. Sakaba, B. H. Cooper, K. H. Lin, N. Strenzke, U. Ashery, J. S. Rhee, H. Taschenberger, E. Neher, and N. Brose. 2013. 'Dynamic control of synaptic vesicle replenishment and short-term plasticity by Ca(2+)-calmodulin-Munc13-1 signaling', *Neuron*, 79: 82-96.

Liu, H., L. Li, D. Nedelcu, Q. Hall, L. Zhou, W. Wang, Y. Yu, J. M. Kaplan, and Z. Hu. 2019. 'Heterodimerization of UNC-13/RIM regulates synaptic vesicle release probability but not priming in C. elegans', *Elife*, 8.

Liu, X., A. B. Seven, M. Camacho, V. Esser, J. Xu, T. Trimbuch, B. Quade, L. Su, C. Ma, C. Rosenmund, and J. Rizo. 2016. 'Functional synergy between the Munc13 C-terminal C1 and C2 domains', *Elife*, 5.

Lu, J., M. Machius, I. Dulubova, H. Dai, T. C. Südhof, D. R. Tomchick, and J. Rizo. 2006. 'Structural basis for a Munc13-1 homodimer to Munc13-1/RIM heterodimer switch', *PLoS Biol*, 4: e192.

Ma, C., W. Li, Y. Xu, and J. Rizo. 2011. 'Munc13 mediates the transition from the closed syntaxin-Munc18 complex to the SNARE complex', *Nat Struct Mol Biol*, 18: 542-9.

Madison, J. M., S. Nurrish, and J. M. Kaplan. 2005. 'UNC-13 interaction with syntaxin is required for synaptic transmission', *Curr Biol*, 15: 2236-42.

Magdziarek, M., A. A. Bolembach, K. P. Stepien, B. Quade, X. Liu, and J. Rizo. 2020. 'Re-examining how Munc13-1 facilitates opening of syntaxin-1', *Protein Sci*, 29: 1440-58.

Margittai, M., D. Fasshauer, R. Jahn, and R. Langen. 2003. 'The Habc domain and the SNARE core complex are connected by a highly flexible linker', *Biochemistry*, 42: 4009-14.

Michelassi, F., H. Liu, Z. Hu, and J. S. Dittman. 2017. 'A C1-C2 Module in Munc13 Inhibits Calcium-Dependent Neurotransmitter Release', *Neuron*, 95: 577-90.e5.

Misura, K. M., R. H. Scheller, and W. I. Weis. 2000. 'Three-dimensional structure of the neuronal-Sec1-syntaxin 1a complex', *Nature*, 404: 355-62.

Narayanappa, M., H. W. Liu, L. Li, F. Michelassi, Z. T. Hu, and J. Dittman. 2020. 'The C2C-MCT Domain of Munc13 is Essential for Priming Synaptic Vesicles', *Biophysical Journal*, 118: 401a-01a.

Palfreyman, M. T., and E. M. Jorgensen. 2017. 'Unc13 Aligns SNAREs and Superprimes Synaptic Vesicles', *Neuron*, 95: 473-75.

Quade, B., M. Camacho, X. Zhao, M. Orlando, T. Trimbuch, J. Xu, W. Li, D. Nicastro, C. Rosenmund, and J. Rizo. 2019. 'Membrane bridging by Munc13-1 is crucial for neurotransmitter release', *Elife*, 8.

Rhee, J. S., A. Betz, S. Pyott, K. Reim, F. Varoqueaux, I. Augustin, D. Hesse, T. C. Südhof, M. Takahashi, C. Rosenmund, and N. Brose. 2002. 'Beta phorbol ester- and diacylglycerol-induced augmentation of transmitter release is mediated by Munc13s and not by PKCs', *Cell*, 108: 121-33.

Rhee, J. S., L. Y. Li, O. H. Shin, J. C. Rah, J. Rizo, T. C. Sudhof, and C. Rosenmund. 2005. 'Augmenting neurotransmitter release by enhancing the apparent Ca2+ affinity of synaptotagmin 1', *Proc Natl Acad Sci U S A*, 102: 18664-9.

Richmond, J. E., R. M. Weimer, and E. M. Jorgensen. 2001. 'An open form of syntaxin bypasses the requirement for UNC-13 in vesicle priming', *Nature*, 412: 338-41.

Rizo, J., and T. C. Südhof. 1998. 'C2-domains, structure and function of a universal Ca2+-binding domain', *J Biol Chem*, 273: 15879-82.

Rodríguez-Castañeda, F., M. Maestre-Martínez, N. Coudevylle, K. Dimova, H. Junge, N. Lipstein, D. Lee, S. Becker, N. Brose, O. Jahn, T. Carlomagno, and C. Griesinger. 2010. 'Modular architecture of Munc13/calmodulin complexes: dual regulation by Ca2+ and possible function in short-term synaptic plasticity', *Embo j*, 29: 680-91.

Shen, N., O. Guryev, and J. Rizo. 2005. 'Intramolecular occlusion of the diacylglycerol-binding site in the C1 domain of munc13-1', *Biochemistry*, 44: 1089-96.

Sheng, Z. H., C. T. Yokoyama, and W. A. Catterall. 1997. 'Interaction of the synprint site of N-type Ca2+ channels with the C2B domain of synaptotagmin I', *Proc Natl Acad Sci U S A*, 94: 5405-10.

Shin, O. H., J. Lu, J. S. Rhee, D. R. Tomchick, Z. P. Pang, S. M. Wojcik, M. Camacho-Perez, N. Brose, M. Machius, J. Rizo, C. Rosenmund, and T. C. Südhof. 2010. 'Munc13 C2B

domain is an activity-dependent Ca2+ regulator of synaptic exocytosis', *Nat Struct Mol Biol*, 17: 280-8.

Shu, T., H. Jin, J. E. Rothman, and Y. Zhang. 2020. 'Munc13-1 MUN domain and Munc18-1 cooperatively chaperone SNARE assembly through a tetrameric complex', *Proc Natl Acad Sci U S A*, 117: 1036-41.

Stevens, D. R., Z. X. Wu, U. Matti, H. J. Junge, C. Schirra, U. Becherer, S. M. Wojcik, N. Brose, and J. Rettig. 2005. 'Identification of the minimal protein domain required for priming activity of Munc13-1', *Curr Biol*, 15: 2243-8.

Sutton, R. B., D. Fasshauer, R. Jahn, and A. T. Brunger. 1998. 'Crystal structure of a SNARE complex involved in synaptic exocytosis at 2.4 A resolution', *Nature*, 395: 347-53.

Varoqueaux, F., A. Sigler, J. S. Rhee, N. Brose, C. Enk, K. Reim, and C. Rosenmund. 2002. 'Total arrest of spontaneous and evoked synaptic transmission but normal synaptogenesis in the absence of Munc13-mediated vesicle priming', *Proc Natl Acad Sci U S A*, 99: 9037-42.

Wang, S., U. B. Choi, J. Gong, X. Yang, Y. Li, A. L. Wang, X. Yang, A. T. Brunger, and C. Ma. 2017. 'Conformational change of syntaxin linker region induced by Munc13s initiates SNARE complex formation in synaptic exocytosis', *Embo j*, 36: 816-29.

Wang, S., Y. Li, J. Gong, S. Ye, X. Yang, R. Zhang, and C. Ma. 2019. 'Munc18 and Munc13 serve as a functional template to orchestrate neuronal SNARE complex assembly', *Nat Commun*, 10: 69.

Wang, X., J. Gong, L. Zhu, S. Wang, X. Yang, Y. Xu, X. Yang, and C. Ma. 2020. 'Munc13 activates the Munc18-1/syntaxin-1 complex and enables Munc18-1 to prime SNARE assembly', *Embo j*, 39: e103631.

Xu, J., M. Camacho, Y. Xu, V. Esser, X. Liu, T. Trimbuch, Y. Z. Pan, C. Ma, D. R. Tomchick, C. Rosenmund, and J. Rizo. 2017. 'Mechanistic insights into neurotransmitter release and presynaptic plasticity from the crystal structure of Munc13-1 C(1)C(2)BMUN', *Elife*, 6.

Xu, S., S. Pany, K. Benny, K. Tarique, O. Al-Hatem, K. Gajewski, J. L. Leasure, J. Das, and G. Roman. 2018. 'Ethanol Regulates Presynaptic Activity and Sedation through Presynaptic Unc13 Proteins in Drosophila', *eNeuro*, 5.

Xu, X. Z., P. D. Wes, H. Chen, H. S. Li, M. Yu, S. Morgan, Y. Liu, and C. Montell. 1998. 'Retinal targets for calmodulin include proteins implicated in synaptic transmission', *J Biol Chem*, 273: 31297-307.

Yang, X., S. Wang, Y. Sheng, M. Zhang, W. Zou, L. Wu, L. Kang, J. Rizo, R. Zhang, T. Xu, and C. Ma. 2015. 'Syntaxin opening by the MUN domain underlies the function of Munc13 in synaptic-vesicle priming', *Nat Struct Mol Biol*, 22: 547-54.

You, Y., and J. Das. 2020. 'Effect of ethanol on Munc13-1 C1 in Membrane: A Molecular Dynamics Simulation Study', *Alcohol Clin Exp Res*.

Chapter IIB: UNC-13 REGULATES THE HETEROGENEITY OF RELEASE PROBABILITY IN C. ELEGANS

Haowen Liu[1][§], Lei Li[1][§], Seema Sheoran[2], Yi Yu[1], Janet Richmond[2], Zhitao Hu[1*]

[1]Queensland Brain Institute, Clem Jones Centre for Ageing Dementia Research (CJCADR), The University of Queensland, Brisbane, 4072, Australia

[2]Department of Biological Sciences, University of Illinois at Chicago, Chicago, Illinois 60607, USA

[§]These authors contributed equally to this work

*Correspondence to: z.hu1@uq.edu.au

Lead Contact: Zhitao Hu, z.hu1@uq.edu.au

2B.1. Abstract

Synapses exhibit multiple forms of short-term plasticity which have been attributed to the heterogeneity of neurotransmitter release probability. However, the molecular mechanisms that underlie differential release states remain to be fully elucidated. The Unc-13 family of proteins appears to play key roles in synaptic function through multiple regulatory domains. Here we report a novel role for the N-terminal M domain of the short UNC-13 isoform in *C. elegans* UNC-13MR. Deleting the M domain led to a significant increase in release probability, revealing an inhibitory function of this domain. The inhibitory effect of this domain was eliminated when the adjacent C1 and C2B domains were absent or activated, suggesting that the M domain inhibits synaptic transmission and release probability by suppressing the activity of C1 and C2B domains. When fused directly to the MUNC2C fragment of UNC-13, the M domain greatly enhanced release probability. The N terminus of rat Munc13-2 exhibited similar regulatory roles when replacing the M domain in UNC-13MR, or fused to *C. elegans* MUNC2C, indicating that these functions are conserved. Thus, our findings reveal a novel mechanism by which the UNC-13 M domain regulates release probability, and provides molecular insights into the heterogeneity of short-term plasticity.

2B.2. Introduction

Synaptic strength is altered in response to changes in neuronal activity, thereby producing multiple forms of short-term plasticity (Atwood and Karunanithi 2002). Presynaptic mechanisms that affect the probability of synaptic vesicle (SV) release are believed to play important roles in regulating synaptic strength. The presynaptic fusion machinery, including the SNARE complex, Munc13s, RIMs and synaptotagmins, are involved in the regulation of release probability in many synapse types (Sudhof and Rizo 2011; Jahn and Fasshauer 2012). However, the mechanisms by which these proteins function to control synaptic release and plasticity remain to be fully elucidated.

Of the known synaptic proteins that form the fusion machinery, the Unc13 family of proteins are particularly important as they are involved in almost all steps of the exocytic process, including docking, priming, and fusion (Aravamudan et al. 1999; Augustin, Rosenmund, et al. 1999; Richmond, Davis, and Jorgensen 1999; Madison, Nurrish, and Kaplan 2005), as well as short-term plasticity (Junge et al. 2004; Chen et al. 2013; Calloway et al. 2015; Xu et al. 2017a). Four Munc13 isoforms have been identified in the mammalian nervous system (Munc13-1, ubMunc13-2, Munc13-2, and Munc13-3), with Munc13-1 and ubMunc13-2 playing prominent roles in synaptic transmission at many synapses. Both of these isoforms possess an N-terminal C2A domain, which localizes the proteins at the active zone, close to Ca^{2+} entry sites, thereby mediating fast SV exocytosis (Brose et al. 1995; Song, Ailenberg, and Silverman 1998; Betz et al. 2001). In contrast, Munc13-2 (also called bMunc13-2) and Munc13-3 lack an N-terminal C2A domain, leading to more diffuse expression relative to active zone proteins (Chen et al. 2013). Synaptic transmission is completely arrested in Munc13-1/2 double knockout hippocampal neurons, in which only these two Munc13 isoforms are expressed (Rosenmund et

al. 2002; Varoqueaux et al. 2002). Munc13-3 is exclusively expressed in the cerebellum where its deletion also causes a synaptic transmission defect (Augustin, Betz, et al. 1999b; Augustin et al. 2001).

The importance of Unc13 proteins in synaptic transmission was first demonstrated in the fruit fly, *Drosophila melanogaster* and the soil nematode, *Caenorhabditis. elegans* (Aravamudan et al. 1999; Richmond, Davis, and Jorgensen 1999; Madison, Nurrish, and Kaplan 2005). *C. elegans* expresses two UNC-13 isoforms: a long isoform UNC-13L, which contains an N-terminal C2A domain, and a short isoform UNC-13MR (also called UNC-13S; Figure 1A) which has a unique N-terminal M domain lacking the C2A motif. At the *C. elegans* neuromuscular junction (NMJ), UNC-13L colocalizes with the active zone protein UNC-10/RIM and mediates a fast SV release component, analogous to Munc13-1 (Hu, Tong, and Kaplan 2013). In contrast, UNC-13MR exhibits a more diffuse synaptic distribution and mediates a slow component of SV release (Hu, Tong, and Kaplan 2013), indicating the two UNC-13 isoforms have differential roles in synaptic transmission. We have shown that UNC-13L regulates release probability through several distinct functional domains within the N-terminal (Michelassi et al. 2017a; Liu et al. 2019; Li et al. 2019b). The C2A domain promotes SV release by binding to the active zone protein *unc-10*/RIM, and the X, C1, and C2B domains inhibit SV release by multiple mechanisms, revealing two opposing functions of UNC-13L in regulating synaptic transmission. Similar effects have also been observed in studies of Munc13-1 (Liu et al. 2016; Camacho et al. 2017a; Basu et al. 2007; Lou et al. 2008; Shin, Lu, Rhee, Tomchick, Pang, Wojcik, Camacho-Perez, Brose, Machius, Rizo, Rosenmund, and Sudhof 2010), demonstrating a conserved functionality of this protein. These results provide significant evidence that the C2A-containing

UNC-13/Munc13 functions as one of the major substrates that regulates the heterogeneity of synaptic release probability and short-term plasticity.

The role of the N-terminal region of Unc-13 proteins that lack the C2A domain remains unknown. In this study, we report novel functions of the N-terminal M domain in the worm UNC-13MR isoform. Our data suggest that the M domain inhibits release probability by regulating C1 and C2B. We further demonstrate that the M domain promotes release when fused directly to the C-terminal MUNC2C fragment in UNC-13. Furthermore, we demonstrate that the N-terminal of rat Munc13-2 exhibits similar regulatory functions with the worm M domain, despite poor sequence homology. Thus, our findings indicate that the M domain has important and conserved functions in controlling UNC-13MR-mediated synaptic transmission, thereby providing significant mechanistic advances in our understanding of how UNC-13s/Munc13s regulate synaptic release probability and plasticity.

2B.3. Results

The M domain inhibits tonic and evoked neurotransmitter release

To determine the role of the M domain in UNC-13MR, we generated a construct lacking the M domain (termed UNC-13R) (Figure 1A). Single copy expression of UNC-13MR or UNC-13R in the nervous system in *unc-13* null mutants (*s69*) partially restored locomotion (Figure 1B, C) indicating both proteins could support neuronal function. To directly assess the role of the M domain in synaptic transmission we first examined tonic neurotransmitter release at the neuromuscular junctions (NMJs) of UNC-13MR or UNC-13R rescued animals. Since *C. elegans* NMJs are innervated by both cholinergic excitatory neurons and GABAergic inhibitory neurons,

the frequencies of miniature excitatory (mEPSCs) and inhibitory postsynaptic currents (mIPSCs) were analyzed separately. The frequencies of both mEPSCs and mIPSPs were significantly higher in UNC-13R rescued animals compared to UNC-13MR, over a range of Ca^{2+} concentrations (0mM, 0.25mM, 0.5mM, and 1mM). These data indicate that the M domain inhibits tonic release in UNC-13MR even in nominally Ca^{2+}-free medium (Figure 1D-F). The enhanced tonic release frequency in UNC-13R relative to UNC-13MR was more pronounced at inhibitory synapses, particularly in $0Ca^{2+}$ saline, in which the UNC-13R rescued animal mIPSPs were increased 15-fold but only 2-fold in 1mM Ca^{2+}. In previous studies we have shown that the ACh current amplitude in body wall muscles is 50% reduced in the absence of Ca^{2+}, therefore we speculate that the lower mEPSC frequencies in $0Ca^{2+}$ saline may partially reflect a detection limitation.

To determine whether the M domain also regulates evoked release, ventral nerve cord stimulation anterior to the voltage-clamped muscle was recorded. UNC-13R rescued animals exhibited significantly larger amplitude evoked EPSCs and evoked charge integrals compared to UNC-13MR rescued animals at all Ca^{2+} concentrations tested (0.25mM, 0.5mM, and 1mM) (Figure 1G-J). These results reveal a previously unknown inhibitory function of the M domain in both Ca^{2+}-independent and Ca^{2+}-dependent neurotransmitter release mediated by UNC-13MR.

The inhibitory effects of the M domain were also observed when multicopy UNC-13MR and UNC-13R extrachromosomal arrays were examined (Figure 1 supplemental 1, Table S1, Table S2), indicating that the difference between UNC-13MR and UNC-13R is unlikely to reflect differences in expression levels.

Compared to the UNC-13MR rescued animals the charge transfer of the evoked EPSCs was increased 6-fold in 0.25mM Ca^{2+}, and only 1.5-fold in 1mM Ca^{2+} (Figure 1K). Both tonic

and evoked EPSCs rescued by UNC-13MR and UNC-13R displayed an obvious Ca^{2+}

concentration dependence, whereas the steepness of the concentration-effect relationship in

UNC-13MR rescued animals was lower than that in UNC-13R rescued animals (Figure 1L-N),

indicating that the M domain regulates the Ca^{2+} dependence of SV release.

It has previously been reported that the evoked EPSCs mediated by UNC-13MR display

slower kinetics relative to UNC-13L (Hu, Tong, and Kaplan 2013). To determine whether the M-

domain of UNC-13MR regulates release kinetics we analyzed the risetime and decay of the

evoked EPSCs (in 1mM Ca^{2+}). These parameters were indistinguishable between UNC-13MR

and UNC-13R rescued animals (Figure 1O), indicating that the M domain does not affect release

kinetics. Taken together, these findings demonstrate a novel inhibitory function of the M domain

in the short *unc-13* isoform in the regulation of synaptic transmission.

The probability of SV release is enhanced by the removal of the M domain

The increase in Ca^{2+}-triggered neurotransmitter release in the UNC-13R rescued animals

may arise from a larger primed vesicle pool. To test this, we assessed SV priming in UNC-13MR

and UNC-13R rescued animals. SV priming was measured by the pulsed application of

hypertonic sucrose solution (1M, 2s) onto the ventral nerve cord. The size of the readily

releasable vesicle pool (RRP) was calculated by integrating the sucrose-evoked current (Liu et al.

2019; Li et al. 2019b; Rosenmund and Stevens 1996). As shown in Figure 2A, the sucrose

current was nearly eliminated in *unc-13* mutants, but was fully restored by single copy

expression of UNC-13MR, indicating that UNC-13MR is sufficient to maintain SV priming.

Compared to UNC-13MR, the charge integral of UNC-13R rescued animals was slightly

increased (Figure 2B). However, the mEPSC charge integral of UNC-13R rescued animals was

also increased (Figure 2C), as a result the quantal content calculated by dividing the hyperosmotic charge integral by that of the mEPSCs was unchanged in UNC-13R relative to UNC-13MR rescued animals (Figure 2D). These data suggest that the primed vesicle pool is unaltered in UNC-13R.

Previous data have shown that *unc-13* mutant defects in SV priming correlate with reduced morphologically docked SVs at *C. elegans* NMJs in specimens prepared by high-pressure freeze fixation and freeze substitution (HPF/FS) (Weimer et al., 2006). Based on the hyperosmotic data above we would expect a similar number of docked SV in UNC-13MR and UNC-13R rescued animals. Morphometric analysis of synaptic profiles imaged by serial section electron microscopy (EM) confirmed that the number of docked SVs was significantly reduced in *unc-13* null mutants compared to the wild-type (Figure 2E, F). Both UNC-13MR and UNC-13R restored the SV docking defect of *unc-13* mutants to the same extent (Figure 2E, F), indicating that the M domain does not affect overall SV docking, a result that is consistent with the similar RRP sizes determined electrophysiologically. Other parameters, such as the total number of SVs, the terminal area, and the SV distribution in each synaptic profile, were also indistinguishable between UNC-13MR and UNC-13R rescued animals (Figure 2 supplemental 2). Taken together, these results suggest that the M domain inhibits neurotransmitter release through a post-priming regulatory mechanism.

We next analyzed the probability of SV release in UNC-13MR and UNC-13R rescued worms. Release probability was first assessed at the single SV level by calculating the ratio of the mEPSC frequency to the quantal content of the RRP (termed tonic release rate). Tonic release rate was markedly increased by UNC-13R compared to UNC-13MR (Figure 2G). Similarly, at the whole synapse level, the probability of release (P_{vr}), which was determined as

the ratio of the evoked charge transfer to the RRP (P_{vr}) (Gerber et al. 2008) was also significantly enhanced in UNC-13R relative to UNC-13MR at all Ca^{2+} concentrations (0.25, 0.5, and 1mM Ca^{2+}) as shown in Figure 2H. These results suggest that the M domain of UNC-13MR inhibits the overall probability of SV release through molecular mechanisms that act downstream of vesicle priming.

M domain inhibition of SV release acts through the C1 and C2B domains

How might the M domain regulate release probability? Recent studies have shown that the neighboring diacylglycerol-activated C1 domain and the Ca^{2+}/phospholipid activated C2B domain common to all UNC-13/Munc13 isoforms are involved in the regulation of synaptic release probability and plasticity (Basu et al. 2007; Shin, Lu, Rhee, Tomchick, Pang, Wojcik, Camacho-Perez, Brose, Machius, Rizo, Rosenmund, and Sudhof 2010). Evidence suggests that C1 and C2B are autoinhibitory, disinhibition upon Ca^{2+} or DAG binding allowing a superpriming function of UNC-13/Munc13. Consistent with this model, deletion of the C1 or C2B domain in *C. elegans* UNC-13L causes an increase in both synaptic transmission and release probability (Michelassi et al. 2017a; Li et al. 2019b).

Given that the M domain-mediated inhibition of UNC-13MR is relieved in high Ca^{2+} conditions known to activate C1 and C2B we hypothesized that the M domain exerts an inhibitory effect on release probability by regulating the activity of the C1 and C2B domains. If true, we would expect to see a change in the M domain inhibition in the absence of the C1 and C2B domains.

Because both the C1 and C2B domains inhibit synaptic transmission mediated by UNC-13L, we first examined whether these two domains have similar functions in UNC-13MR. As shown in Figure 3 supplemental 3, deleting the C1 or the C2B domain in UNC-13MR

significantly enhanced the frequency of mEPSCs and mIPSCs in the absence of Ca^{2+}, consistent with the results observed in UNC-13L (Li et al. 2019b). These results indicate that these two domains are functionally conserved in both UNC-13 isoforms. We next investigated M domain inhibition in the absence of C1, C2B, or both (Figure 3A). Our results revealed that deleting either the C1 or the C2B domain almost abolished the inhibitory effect of the M domain on the mEPSCs (MRΔC1 vs RΔC1, MRΔC2B vs RΔC2B; Figure 3B-E). The inhibition of mIPSCs was decreased in MRΔC1 and MRΔC2B in the absence of Ca^{2+}, but was unaltered in 1mM Ca^{2+} (Figure 3B-E). Furthermore, removing C1 and C2B simultaneously in UNC-13MR completely eliminated M domain inhibition (MRΔC1ΔC2B vs RΔC1ΔC2B) of tonic release (Figure 3B-E). This disinhibition was confirmed over a range of Ca^{2+} concentrations (0.25, 0.5, and 1mM) (Figure 3F, G). These results indicate that the inhibitory effects of the M domain on tonic release rely on the presence of the C1 and C2B domains. Similarly, the inhibitory effect of the M domain on stimulus-evoked release was removed in the absence of the C1, C2B, or C1 and C2B domains (Figure 3H, I), a finding which was confirmed by comparing the evoked EPSCs in UNC-13MRΔC1ΔC2B and UNC-13RΔC1ΔC2B at various Ca^{2+} concentrations (0.25, 0.5, and 1mM) (Figure 3J). Strikingly, removal of both C1 and C2B increased the evoked EPSC, suggesting that C1 and C2B inhibitory regulation of in the short UNC-13MR isoform is additive. Collectively, these results demonstrate that the M domain in UNC-13MR inhibits SV release by regulating the neighboring C1 and C2B domains.

C1 and C2B domain activation eliminates M domain inhibition

How does the M domain regulate the C1 and the C2B domains to inhibit SV release? It is known that the C1 domain binds phorbol ester/diacylglycerol (DAG), and that the C2B domain

interacts with the plasma membrane in the presence of Ca^{2+} (Shin, Lu, Rhee, Tomchick, Pang, Wojcik, Camacho-Perez, Brose, Machius, Rizo, Rosenmund, and Sudhof 2010; Maruyama and Brenner 1991). Functional studies in UNC-13L have shown mutations in the C1 (H696K) and C2B (D3,4N) domains that mimic DAG and Ca^{2+} binding, repectively, increase synaptic transmission and release probability by relieving autoinhibition of the MUN domain (Michelassi et al. 2017a; Li et al. 2019b). This raises the question of whether M domain-mediated inhibition is still observed in UNC-13MR when C1 and C2B are activated.

To address this question, we first examined whether these C1 and C2B activating mutations increase synaptic transmission in UNC-13MR, as found in UNC-13L. Our results showed that UNC-13MR carrying the H348K mutation (MR^{H348K}) or the D3,4N mutations ($MR^{D3,4N}$) produced significantly higher mEPSC and mIPSC frequencies than observed with wild-type UNC-13MR (Figure 3 supplemental 3). These results suggest that the C1 and C2B domains are activated by these mutations in UNC-13MR, consistent with previous findings (Basu et al. 2007; Lou et al. 2008; Michelassi et al. 2017a; Li et al. 2019b) and indicate that the C1 and C2B domains function is conserved in the two UNC-13 isoforms.

We next examined the impact of introducing HK and DN mutations into UNC-13MR and UNC-13R (termed $MR^{HK,DN}$ and $R^{HK,DN}$) on M domain functions (Figure 4A). We found that the mEPSC and mIPSC frequencies (in 0mM and 1mM Ca^{2+}), as well as the evoked EPSC amplitude and charge transfer (in 1mM Ca^{2+}), were indistinguishable between $MR^{HK,DN}$ and $R^{HK,DN}$ rescued worms (Figure 4B-E), demonstrating that the inhibitory effects of the M domain are diminished by activity of the C1 and C2B domains, and eliminated upon the activation of both domains, simultaneously.

It should be noted that the C1 domain DAG and the C2B domain plasma membrane interaction are both Ca^{2+}-dependent (Shin, Lu, Rhee, Tomchick, Pang, Wojcik, Camacho-Perez, Brose, Machius, Rizo, Rosenmund, and Sudhof 2010; Maruyama and Brenner 1991; Betz et al. 1998). It is therefore likely that these two domains are more active at higher Ca^{2+} levels, and that the M domain should produce relatively weak inhibition in high Ca^{2+} and strong inhibition in low Ca^{2+}, a notion which is well supported by our findings. Compared to UNC-13MR rescued animals, the ratio of increase in evoked charge in UNC-13R rescued animals was markedly decreased in high Ca^{2+} (Figure 1K). Taken together, our results indicate that the M domain inhibits synaptic transmission by suppressing the activity of the C1 and C2B domains, and that Ca^{2+}-induced activation of the C1 and C2B domains weakens M domain inhibition.

The M domain facilitates SV release when fused to the MUNC2C fragment

Compared to UNC-13MR, the evoked EPSCs rescued by UNC-13MRΔC1ΔC2B were dramatically increased (charge transfer, 13pC vs 60pC; Figure 1H, Figure 3I). The N terminus of MRΔC1ΔC2B contains only the M domain and three linkers (Figure 4A), a sequential structure that is similar to that of a previously studied hyperactive truncated form of UNC-13L (i.e., super UNC-13 or sUNC-13, produced by deleting the X, C1, and C2B domains of UNC-13L), leaving the C2A domain and the same three linkers in its N terminus (Li et al. 2019b). The evoked EPSCs rescued by sUNC-13 were increased 6-fold compared to UNC-13L (20pC vs 120pC) (Li et al. 2019b). Moreover, the C2A domain in sUNC-13 produced strong facilitation of SV release.

Prompted by these results, we hypothesized that the M domain in MRΔC1ΔC2B might also facilitate SV release. However, such effect may be masked by the presence of the linker domains (Figure 4A), which can enhance synaptic transmission via an unknown mechanism

(Figure 3H, I; see discussion) (Li et al. 2019b). Given that the MUNC2C fragment has been proposed to be the minimal region for SV priming and Ca^{2+}-triggered fusion, we tested the possibility that the M domain promotes SV release by directly fusing it to the MUNC2C fragment (termed M-MUNC2C, Figure 5A). We first assessed the role of the MUNC2C fragment in rescuing tonic and evoked release in *unc-13* mutants. Overexpression of MUNC2C in *unc-13* mutants partially restored mEPSCs and almost fully restored mIPSCs (Figure 5B-E), indicating that this fragment is still functional for tonic release. The evoked EPSCs, however, were only slightly restored by MUNC2C overexpression (Figure 5F, G), consistent with previous findings (Madison, Nurrish, and Kaplan 2005; Liu et al. 2016). These results indicate that MUNC2C is likely to be the minimal fragment responsible for tonic and evoked release. We did not see a further increase of mEPSCs or mIPSCs in M-MUNC2C rescued animals (Figure 5B-E), suggesting that the M domain does not facilitate tonic release. However, compared to MUNC2C rescued animals, the evoked EPSCs in the M-MUNC2C chimera were dramatically increased (Figure 5F, G). The increase in evoked EPSCs was also observed at a lower Ca^{2+} concentration (Figure 5H). These results suggest that the M domain has an intrinsic facilitatory capability that promotes evoked neurotransmitter release in this chimeric construct. The sucrose-evoked currents rescued by MUNC2C and M-MUNC2C were comparable (Figure 5I, J), suggesting that the M domain does not affect SV priming. Instead, the low release probability of MUNC2C was significantly enhanced by the inclusion of the M domain (P_{vr}; Figure 5 J). Taken together, these results reveal a facilitatory function of the M domain in evoked neurotransmitter release.

As the inhibitory effects of the M domain do not rely on the expression level of UNC-13MR (Figure 1, Figure 1 supplemental 1), we next examined whether the facilitatory function of the M domain depends on the expression level of M-MUNC2C. To do this, we constructed

MUNC2C and M-MUNC2C single copy insertion (SCI) rescue in *unc-13* mutants. Unlike

MUNC2C overexpression, we found that MUNC2C SCI failed to restore locomotion (data not

shown) and synaptic transmission (Figure 6K-N). Both tonic and evoked EPSCs (in 1mM Ca^{2+})

in the MUNC2C SCI rescued animals were nearly the same as those in the *unc-13* mutants.

These results indicate that the rescue ability of MUNC2C is expression level dependent.

Similarly, M-MUNC2C SCI did not restore synaptic transmission to the same level as that

obtained with M-MUNC2C overexpression. However, the rescue of both tonic and evoked

release by M-MUNC2C SCI was significantly increased compared to that observed following

rescue of MUNC2C SCI (Figure 5K-N). These results further demonstrate that the M domain is

capable of enhancing Ca^{2+}-dependent neurotransmitter release and release probability, despite

the expression level of the UNC-13 fragment.

Expression level of the UNC-13 proteins is not regulated by the M domain

The inhibitory and facilitatory functions of the M domain may arise from its roles in

regulating the abundance of UNC-13 proteins. To investigate this, we made fusion proteins of

UNC-13MR, UNC-13R, MUNC2C and M-MUNC2C, tagged with mApple in their C terminus.

The expression levels of UNC-13 proteins were measured based on the mApple fluorescence

intensity. As shown in Figure 6, UNC-13MR::mApple and UNC-13R::mApple displayed

comparable fluorescence intensity, suggesting that they were expressed at similar levels.

Similarly, the fluorescence intensities of MUNC2C::mApple and M-MUNC2C::mApple were

also indistinguishable. These results demonstrate that the inhibition and facilitation in synaptic

transmission and release probability mediated by the M domain do not result from changes in the

abundance of UNC-13 proteins.

The Munc13-2 N terminus inhibits synaptic transmission

The above experiments revealed novel functions of the N-terminal M domain in UNC-13MR in regulating release probability. Both Munc13-2 and Munc13-3 also lack a C2A domain in their N terminus, and have been found to regulate the kinetics of the priming pool in some synapses (Chen et al. 2013). UNC-13MR in the worm also plays essential roles in regulating the kinetics of SV fusion (Hu, Tong, and Kaplan 2013), suggesting that the UNC-13 and Munc13 proteins lacking a C2A domain may function similarly. However, sequence analysis of the N terminus in Munc13-2 and Munc13-3, revealed no similarity with the M domain in UNC-13MR (Figure 7 supplemental 4). In fact, these N-terminal sequences have no homology to any known proteins (Augustin, Betz, et al. 1999b; Kohn et al. 2000). Despite the lack of sequence similarity, we examined whether mammalian N-terminal domain could exert similar functions to the UNC-13 M domain in regulating synaptic transmission.

We focused on Munc13-2 as it is the only Munc13 isoform to be coexpressed with Munc13-1 in some synapses, such as those in the hippocampus (Varoqueaux et al. 2002). Moreover, Munc13-2 can functionally replace Munc13-1 to mediate SV release in inhibitory hippocampal neurons (Varoqueaux et al. 2002), demonstrating the importance of this isoform. We therefore constructed chimeric UNC-13 proteins containing the N terminus of Munc13-2 (0-765aa) fused to the worm UNC-13R (termed $N^{Munc13-2}R$) to examine whether it inhibits SV release, and to the worm MUNC2C (termed $N^{Munc13-2}MUNC2C$) to determine whether it is capable of facilitating *C. elegans* MUNC2C function (Figure 7A). The Munc13-2 N terminus did not appear to inhibit tonic release, as both mEPSCs and mIPSCs were unaltered in $N^{Munc13-2}R$ rescued animals compared to those in UNC-13R rescued animals (Figure 7B, C; Table S1).

However, we found strong inhibition by the Munc13-2 N terminus on evoked EPSCs in $N^{Munc13-2}$R rescued animals (Figure 7D, E; Table S2), consistent with the results in UNC-13MR rescue worms. These results indicate that the Munc13-2 N terminus also inhibits Ca^{2+}-dependent neurotransmitter release, similar to the M domain of UNC-13MR. Compared to MUNC2C, evoked EPSCs were significantly increased in $N^{Munc13-2}$MUNC2C rescued animals (Figure 7D, E; Table S1; Table S2), whereas tonic EPSCs were unchanged (Figure 7B, C; Table S1), demonstrating that the Munc13-2 N terminus is able to facilitate SV release. Taken together, these results revealed that the N terminus of Munc13-2 exhibits similar inhibitory and facilitatory functions to that involving the M domain of UNC-13MR in regulating Ca^{2+}-dependent neurotransmitter release, likely via conserved mechanisms.

2B.4. Discussion

Although the functional importance of UNC-13/Munc13 proteins lacking a C2A domain has been reported, the detailed mechanisms by which they regulate neurotransmitter release and release probability are poorly understood. By conducting a structure-function analysis of the worm UNC-13MR isoform, we show that the N-terminal M domain strongly inhibits neurotransmitter release and release probability. This inhibitory function appears to be conserved as the N-terminal sequence of Munc13-2 can substitute for the M domain of UNC-13MR. We further demonstrate that M domain-mediated inhibition requires the presence of the C1 and the C2B domains, with activation of both C1 and C2B mitigating M-domain inhibition. Furthermore, we demonstrate that the M domain has an intrinsic facilitatory ability and strongly promotes neurotransmitter release and release probability when fused to the N terminus of the MUNC2C fragment, suggesting multiple effects of the M domain in UNC-13MR. This study is the first

report regarding the function of the M domain and reveals novel regulatory functions, thereby providing mechanistic insights by which UNC-13/Munc13 regulate synaptic transmission and release probability.

Sequences and functions of the N terminus in UNC-13s/Munc13s

Based on their N-terminal sequences, UNC-13/Munc13 isoforms can be divided into two groups based on the presence or absence of the C2A domain. The C-terminal sequences (spanning from the C1 to the C2C domain) in all isoforms share high sequence similarity in domain structure. Amongst the UNC-13/Munc13 isoforms that have an N-terminal C2A domain, sequence similarity in this region is also apparent. In contrast the M domain of worm UNC-13MR has no sequence homology to other proteins (Kohn et al. 2000) including the N-terminal sequences of Munc13-2 and Munc13-3 (Figure 7 supplemental 4) that also lack a C2A domain. Furthermore, the N-terminal sequences of Munc13-2 and Munc13-3 only share a small stretch of similarity spanning 54 residues (Figure 7 supplemental 4, blue) (Augustin, Betz, et al. 1999b) that does not exist in the worm UNC-13 M domain. Although UNC-13MR, Munc13-2 and the Munc13-3 have all been shown to be important in synaptic transmission (Augustin et al. 2001; Rosenmund et al. 2002; Varoqueaux et al. 2002), the function of their N termini are completely unknown. Does this region regulate synaptic transmission? Do the N-termini of these three UNC-13/Mun13 proteins have conserved functions and are these similar to the C2A domain? What is their physiological relevance? These questions motivated us to investigate the functional roles of the M domain in *C. elegans*.

Prior studies have shown that the N-terminal C2A domain in both UNC-13L and Munc13-1 form inhibitory homodimers that undergo a molecular switch upon C2A binding to the zinc finger domain of UNC-10/RIM forming UNC-10/UNC-13 heterodimers that promote release (Camacho et al. 2017a; Liu et al. 2019). By contrast, little is known about the biochemical characteristics of the N-terminal domains in UNC-13MR and Munc13-2/3. Nevertheless, our data show that the N-terminal domains in UNC-13MR and Munc13-2 exhibit conserved functions, inhibiting synaptic transmission mediated by UNC-13R. Furthermore, attaching the UNC-13 M domain or Munc-13-2 N-terminal is able to facilitate synaptic transmission mediated by the minimal fusion domain encompassing MUNC2C, indicating that the N-termini exhibit functional conservation.

The C2A domain exhibits additional regulatory abilities, including localizing UNC-13L and Munc13-1 at the active zones close to Ca^{2+} entry sites, and accelerating release kinetics (Hu, Tong, and Kaplan 2013). Neither of these functions, appear to be conserved in the M domain of UNC-13MR. No significant differences in the risetime or decay of evoked EPSCs were found between UNC-13MR and UNC-13R rescued animals (Figure 1O). In fact, we did not see changes in release kinetics in any of the rescued strains used in this study (i.e., MRΔC1 vs RΔC1, MRΔC2B vs RΔC2B, MRΔC1ΔC2B vs RΔC1ΔC2B, MUNC2C vs M-MUNC2C; data not shown), demonstrating that the M domain does not regulate the kinetics of SV fusion. We also did not observe apparent changes in the expression levels or distribution of UNC-13 proteins with or without the M domain (i.e., compare UNC-13MR vs UNC-13R, or MUNC2C vs M-MUNC2C; Figure 6), indicating that the M domain does not regulate the synaptic abundance or localization of UNC-13MR. Thus, our data demonstrate that M domain regulation of UNC-13MR differs in several aspects from that of C2A containing UNC-13/Munc13 proteins.

Given that UNC-13/Munc13 proteins have been implicated in multiple steps of the SV cycle, including docking, priming, and fusion (Aravamudan et al. 1999; Augustin, Rosenmund, et al. 1999; Richmond, Davis, and Jorgensen 1999; Varoqueaux et al. 2002; Madison, Nurrish, and Kaplan 2005; Weimer et al. 2006), we assessed the involvement of the M domain in each of these stages. Our EM data revealed that the number of docked vesicles in UNC-13R rescued animals is indistinguishable from that in UNC-13MR (Figure 2). Similarly, the SV numbers in the primed vesicle pool derived from hyperosmotic responses were also comparable between UNC-13MR and UNC-13R rescued animals (Figure 2). Furthermore, the sucrose-evoked currents in the M-MUNC2C chimera were unchanged compared to those of MUNC2C. Together, these results suggest that the M domain functions downstream of docking and priming to regulate release probability.

Possible model for the M domain inhibition

Unlike the N-terminal C2A domain in UNC-13L, which promotes the release of SVs, the N-terminal M domain inhibits synaptic transmission and release probability in UNC-13MR. Both tonic and evoked neurotransmitter release were significantly increased in UNC-13R rescued animals lacking the M domain (Figure 1). Notably, this M domain inhibition only occurred in the presence of the neighboring C1 and C2B domains. Deletion of C1, C2B or both, exhibited similar release properties in UNC-13MR and UNC-13R. Mutations that mimic the activation of C1 and C2B also abolished M domain inhibition (Figure 4). These results indicate that the M domain exerts an inhibitory function by suppressing the activation of the C1 and C2B domains. However, it is still unclear how this suppression occurs. Because the activity of C1 and C2B is Ca^{2+}-dependent (Shin, Lu, Rhee, Tomchick, Pang, Wojcik, Camacho-Perez, Brose, Machius,

Rizo, Rosenmund, and Sudhof 2010; Maruyama and Brenner 1991), it is possible that the M domain suppresses Ca^{2+} entry, thereby inhibiting Ca^{2+}-triggered neurotransmitter release. However, this would not explain why M domain inhibition was strongest in 0mM Ca^{2+}.

Analysis of the crystal structure of Munc13 C1C2BMUN suggests a "bridge model" in which the C2C domain interacts with the vesicle membrane, and the C1-C2B act as a module interacting with both the plasma membrane and the MUN domain (Liu et al. 2016; Xu et al. 2017a). The interaction between C2B and the MUN domain is not thought to interfere with the ability of the MUN domain to bind syntaxin, correctly orient SNARE complex assembly and prime vesicles for fusion. Instead evidence suggests that activation of the C1-C2B module by Ca^{2+} or DAG causes a conformational change at the membrane interface that also alleviates autoinhibition of the MUN domain by C2B allowing the MUN domain to increase release probability (superpriming) through an unspecified post-priming function (Michelassi et al. 2017a; Basu et al. 2007). It is therefore possible that the M domain stabilizes (or locks) the C1 and C2B in their inactive conformation. This would allow vesicle priming to occur but lead to lower release probabilities (Figure 8A). Sufficient Ca^{2+} influx may relieve M-domain inhibition (unlock) of C1 and C2B, allowing them to undergo conformational changes that allows the MUN domain to enhance release probability (Figure 8B). This would explain why M domain inhibition is strong in low Ca^{2+} but weak in high Ca^{2+}. In the complete absence of Ca^{2+}, the M domain stabilization or lock would be even tighter, and UNC-13MR would be unable to trigger Ca^{2+}-independent neurotransmitter release.

Facilitatory function of the M domain

The facilitatory effects of the N-terminal C2A domain in UNC-13L can also be observed in a chimera consisting of C2AMUNC2C that markedly increases tonic and evoked release and release probabilities compared to MUNC2C alone (Li et al. 2019b). Moreover, the C2A domain also increased tonic release in the absence of Ca^{2+}, indicating that its facilitatory function is Ca^{2+}-independent. By contrast, the M domain facilitated SV release in a Ca^{2+}-dependent manner. Increases in evoked EPSCs by the M-MUNC2C chimera were observed in 1mM and 0.5mM Ca^{2+}, but not in 0.25mM Ca^{2+} (Figure 5H), and no increase in tonic release was found in the presence or absence of Ca^{2+}. These results demonstrate that unlike the C2A domain, the facilitation of synaptic transmission by the M domain is Ca^{2+}-dependent.

How does the M domain promote release of SVs? Prior studies have shown that the MUNC2C fragment is the minimal domain responsible for UNC-13/Munc13 activity (Basu et al. 2005; Madison, Nurrish, and Kaplan 2005; Liu et al. 2016; Stevens et al. 2005). Overexpression of MUNC2C restored only 20% of the evoked EPSCs in *unc-13* mutants, demonstrating that this fragment is inefficient in triggering synaptic transmission, possibly due to the fact that this domain is not stable under physiological conditions. Another possibility is that the MUNC2C fragment is unable to efficiently connect the vesicle and the plasma membranes to establish the UNC-13 bridge (Figure 8C). It is therefore likely that the M domain directly or indirectly interacts with the plasma membrane, thereby bridging the two membranes (Figure 8D). In this way, the M domain could stabilize the MUN domain in a conformation and position to catalyze SNARE complex assembly and promote fusion. Compared to the evoked EPSCs, overexpression of MUNC2C led to a better rescue in tonic release in high Ca^{2+}, restoring 50% of mEPSCs and

80% of mIPSCs in 1mM Ca^{2+} (Figure 5D, E), probably because tonic release has a lower fusion threshold than stimulus-evoked release.

Unexpectedly, single copy expression of MUNC2C failed to restore tonic and evoked release in *unc-13* mutants, possibly because MUNC2C proteins are inefficient and require higher expression levels (Figure 5K-N). These comparisons provide additional evidence that MUNC2C is the minimal fragment in UNC-13 required for vesicular priming and fusion. The levels of tonic and evoked release rescued by insertion of a single copy of M-MUNC2C were also much lower than those rescued by overexpression of M-MUNC2C (Figure 5K-N). Nevertheless, we still observed a marked increase in synaptic transmission in M-MUNC2C SCI rescued animals compared to MUNC2C SCI. These results confirmed the facilitatory capability of the M domain.

Of note, the M domain did not enhance release when the three N-terminal linkers remained between the M domain and MUN domains (i.e., MRΔC1ΔC2B or MlinkerMUNC2C; Figure 3A). In this case, deleting the M domain did not produce any changes in transmission. This is mainly because the linkers themselves are also able to promote SV fusion. Although the mechanism is still unclear, it is likely that the linkers can also interact with the plasma membrane. In fact, the three linkers exhibited a much stronger ability to promote fusion than the C2A domain and or M domain (evoked charge: linkerMUNC2C, 60pC; C2AMUNC2C, 35pC; M-MUNC2C, 13pC; MUNC2C, 3pC) (Li et al. 2019b). Moreover, the M domain does not appear to be functional in the presence of the linkers (MlinkerMUNC2C or MRΔC1ΔC2B, evoked charge, 60pC), whereas the C2A domain still has a strong facilitatory role and promotes evoked release to a much higher level together with the linkers (i.e. C2AlinkerMUNC2C or sUNC-13, evoked charge, 120pC), suggesting differential mechanisms by which these two UNC-13 N termini facilitate transmission.

Functional diversity of UNC-13s/Munc13s in short-term plasticity

As important synaptic hub proteins, UNC-13s/Munc13s contain multiple functional domains, which have various binding partners such as UNC-10/RIM, DAG, Ca^{2+}/ phospholipids, and the SNARE proteins. Due to their binding properties, UNC-13/Munc13 proteins are involved in several cellular pathways by acting as essential substrates that regulate synaptic release (Lackner, Nurrish, and Kaplan 1999; Hu, Vashlishan-Murray, and Kaplan 2015; Betz et al. 1998). Previous studies, together with our recent work, have shown that distinct domains in UNC-13L/Munc13-1 have opposing regulatory functions in synaptic transmission and release probability. The C2A domain promotes SV release and enhances release probability (Camacho et al. 2017a; Liu et al. 2019), whereas the X, C1 and C2B domains inhibit synaptic transmission and release probability (Michelassi et al. 2017a; Li et al. 2019b). Thus, the net regulatory effect of UNC-13L/Munc13-1 on synaptic transmission reflects a balance of facilitation and inhibition. In this study, we further demonstrate that the C1 and C2B domains inhibit synaptic transmission in UNC-13MR, analogous to their functions in UNC-13L. The M domain also inhibits synaptic transmission and release probability through a mechanism that involves C1 and C2B. These findings therefore provide novel insights into the mechanisms that govern the function of UNC-13s/Munc13 isoforms lacking C2A domains in synaptic release probability and short-term plasticity. Future studies will focus on the biochemical characteristics and crystal structure of the M domain to further elucidate mechanistic details by which this occurs.

2B.5. Materials and Methods

Strains

Strain maintenance and genetic manipulation were performed as previously described (Brenner

1974). Animals were cultivated at room temperature on nematode growth medium (NGM) agar plates seeded with OP50 bacteria. On the day before experiments L4 larval stage animals were transferred to fresh plates seeded with OP50 bacteria for all the electrophysiological recordings. The following strains were used:

Wild type, N2 bristol

KP6901 *unc-13(s69)*

ZTH456 hztSi1 [P*snb-1*::UNC-13MR]; *unc-13(s69)*

CZ15872 juSi67 [P*rgef-1*::UNC-13R]; *unc-13(s69)*

ZTH11hztEx11 [P*snb-1*::UNC-13MR]; *unc-13(s69)*

ZTH99 hztEx20 [P*snb-1*::UNC-13R]; *unc-13(s69)*

ZTH498 hztEx53 [P*snb-1*::UNC-13MR(ΔC1)]; *unc-13(s69)*

ZTH521 hztEx68 [P*snb-1*::UNC-13R(ΔC1)]; *unc-13(s69)*

ZTH517 hztEx55 [P*snb-1*::MR(ΔC2B)]; *unc-13(s69)*

ZTH507 hztEx69 [P*snb-1*::UNC-13R(ΔC2B)]; *unc-13(s69)*

ZTH495 hztEx70 [P*snb-1*::MR(ΔC1ΔC2B)]; *unc-13(s69)*

ZTH696 hztEx109 [P*snb-1*::UNC-13R(ΔC1ΔC2B)]; *unc-13(s69)*

ZTH421 hztEx54 [P*snb-1*::UNC-13MR(H348K)]; *unc-13(s69)*

ZTH447 hztEx56 [P*snb-1*::UNC-13MR(C2B D3,4N)]; *unc-13(s69)*

ZTH451 hztEx72 [P*snb-1*::UNC-13MR(HK, C2B D3,4N)]; *unc-13(s69)*

ZTH448 hztEx71 [P*snb-1*::UNC-13R(HK, C2B D3,4N)]; *unc-13(s69)*

ZTH858 hztSi7 [P*rab-3*::UNC-13(MUNC2C)]; *unc-13(s69)*

ZTH752 hztSi5 [P*rab-3*::UNC-13(M-MUNC2C)]; *unc-13(s69)*

ZTH442 hztEx107 [P*snb-1*::UNC-13(MUNC2C)]; *unc-13(s69)*

ZTH577 hztEx108 [P*snb-1*::UNC-13(M-MUNC2C)]; *unc-13(s69)*

ZTH738 hztEx111 [P*snb-1*:: N$^{Munc13-2}$::UNC-13R]; *unc-13(s69)*

ZTH740 hztEx112 [P*snb-1*::N$^{Munc13-2}$:: UNC-13(MUNC2C)]; *unc-13(s69)*

ZTH686 hztEx79 [P*unc-129*::UNC-13(MR)::mApple]; NuIs165 [P*unc-129*::UNC-10::GFP]

ZTH711 hztEx80 [P*unc-129*::UNC-13(R)::mApple]; NuIs165 [P*unc-129*::UNC-10::GFP]

ZTH693 hztEx82 [P*unc-129*::UNC-13(MUNC2C)::mApple]; NuIs165 [P*unc-129*::UNC-10::GFP]

ZTH692 hztEx81 [P*unc-129*::UNC-13(M-MUNC2C)::mApple]; NuIs165 [P*unc-129*::UNC-10::GFP]

Constructs, transgenes and germline transformation

The *snb-1* promoter (3kb) and *unc-129* promoter (2.6kb) were inserted into JB6 vector between the SphI and BamHI sites, all the UNC-13 expression constructs were amplified by PCR and inserted into JB6 vector between the KpnI and NotI sites. Red fluorescent protein mApple was inserted between NotI and MluI sites in-frame with unc-13 genes for imaging experiments. The miniMos-based single-copy insertion plasmid KP3313 (modified from pCFJ910) was gift from Josh Kaplan Lab. The rab-3 promoter (1.2kb) was inserted into KP3313 between SbfI and XmaI, unc-13 genes were constructed using AscI and NotI.

Transgenic strains were isolated by microinjection of various plasmids using either Pmyo-2::NLS-GFP (KP#1106) or Pmyo-2::NLS-mCherry (KP#1480) as the co-injection marker. Single-copy insertions were generated using miniMos-based single copy insertion (minimosSCI) method, as previously described (Frokjaer-Jensen et al. 2014).

Electrophysiology

Electrophysiology was conducted on dissected *C. elegans* as previously described (Li et al. 2019b; Liu et al. 2019). Worms were superfused in an extracellular solution containing 127 mM NaCl, 5 mM KCl, 26 mM $NaHCO_3$, 1.25 mM NaH_2PO_4, 20 mM glucose, 1 mM $CaCl_2$, and 4 mM $MgCl_2$, bubbled with 5% CO_2, 95% O_2 at 22°C. The 1mM $CaCl_2$ was replaced by 1mM $MgCl_2$ to record mEPSCs and mIPSCs in 0mM of Ca^{2+}. Whole-cell recordings were carried out at -60mV for all EPSCs, including mEPSCs, evoked EPSCs, and sucrose-evoked responses. The holding potential was switched to 0mV to record mIPSCs. The internal solution contained 105 mM CH_3O_3SCs, 10 mM CsCl, 15 mM CsF, 4mM $MgCl_2$, 5mM EGTA, 0.25mM $CaCl_2$, 10mM HEPES, and 4mM Na_2ATP, adjusted to pH 7.2 using CsOH. Stimulus-evoked EPSCs were stimulated by placing a borosilicate pipette (5–10 μm) near the ventral nerve cord (one muscle distance from the recording pipette) and applying a 0.4 ms, 85 μA square pulse using a stimulus current generator (WPI). A pulsed application of sucrose (1M, 2s) was applied onto the ventral nerve cord using a Picospritzer III (Parker). The glass pipette containing sucrose was placed at the end of the patched muscle (around half muscle distance from the recording pipette).

Fluorescence imaging

Animals were immobilized on 2% agarose pads with 30 mM levamisole. Fluorescence imaging was performed on a spinning-disk confocal system (3i Yokogawa W1 SDC) controlled by Slidebook 6.0 software. Animals were imaged with an Olympus 100x 1.4 NA Plan-Apochromat objective. Z series of optical sections were acquired at 0.11 μm steps. Images were deconvolved with Huygens Professional version 16.10 (Scientific Volume Imaging, The Netherlands) and

then processed to yield maximum intensity projections using ImageJ 1.51n (Wayne Rasband, National Institutes of Health).

Electron microscopy

Samples were prepared using high-pressure freeze fixation (Weimer et al. 2006). ~30 young adult hermaphrodites were placed in each specimen chamber containing *E. coli* and were rapidly frozen at -180°C under high pressure (Leica HPM 100). Frozen specimens then underwent freeze substitution (Leica Reichert AFS) during which samples were held at −90°C for 107 hr in 0.1% tannic acid and 2% OsO4 in anhydrous acetone. The temperature was then increased at 5°C/hr to −20°C, kept at −20°C for 14 hr, and increased by 10°C/hr to 20°C. After fixation, samples were infiltrated with 50% Epon/acetone for 4 hr, 90% Epon/acetone for 18 hr, and 100% Epon for 5 hr. Finally, samples were embedded in Epon and incubated for 48 hr at 65°C. Ultrathin (40 nm) serial sections were cut using a Leica Ultracut 6 and collected on formvar-covered, carbon-coated copper grids (EMS, FCF2010-Cu). Poststaining was performed using 2.5% aqueous uranyl acetate for 4 min, followed by Reynolds lead citrate for 2 min. Images were acquired using a JEOL JEM-1220 transmission electron microscope operating at 80 kV using a Gatan digital camera at a magnification of 100k (1.8587 pixels/nm). Images were collected from the ventral nerve cord region anterior to the vulva for all genotypes. Serial micrographs were manually annotated using NIH ImageJ/Fiji software to quantify the number of SVs, number of plasma membrane docked SVs, and distance of docked SVs from the dense projection (DP) for each synaptic profile. Specimens were encrypted to ensure unbiased analysis. Cholinergic synapses were identified on the basis of their typical morphology (White et al. 1986). A synapse was defined as a series of sections (profiles) containing a dense projection as well as two

flanking sections on both sides without dense projections. SVs were identified as spherical, light grey structures with an average diameter of ~30 nm. A docked synaptic vesicle was defined as a synaptic vesicle whose membrane was morphologically contacting the plasma membrane. Image acquisition and analysis using NIH ImageJ/Fiji software were performed blinded for genotype.

Data acquisition and statistical analysis

All recordings were obtained using a HEKA EPC10 double amplifier (HEKA Elektronik) filtered at 2 kHz, and analyzed by built-in programs in Igor 7 software (WaveMetrics). All imaging data were analysed in ImageJ software. Each set of data represents the mean ± SEM of an indicated number (n) of animals. Statistical significance was determined using student's-t test or one-way ANOVA followed by Dunnett's test to control for multiple comparisons.

2B.6. Acknowledgements

through the IIN. Further, this work utilized instrumentation provided by the University of Illinois Research Resources Center, Electron Microscopy Core.

2B.7. Author contributions

2B.8. References

Aravamudan B, Fergestad T, Davis WS, Rodesch CK, Broadie K (1999) Drosophila UNC-13 is essential for synaptic transmission. Nature neuroscience 2:965-971.

Atwood HL, Karunanithi S (2002) Diversification of synaptic strength: presynaptic elements. Nature reviews Neuroscience 3:497-516.

Augustin I, Rosenmund C, Sudhof TC, Brose N (1999a) Munc13-1 is essential for fusion competence of glutamatergic synaptic vesicles. Nature 400:457-461.

Augustin I, Betz A, Herrmann C, Jo T, Brose N (1999b) Differential expression of two novel Munc13 proteins in rat brain. The Biochemical journal 337 (Pt 3):363-371.

Augustin I, Korte S, Rickmann M, Kretzschmar HA, Sudhof TC, Herms JW, Brose N (2001) The cerebellum-specific Munc13 isoform Munc13-3 regulates cerebellar synaptic transmission and motor learning in mice. The Journal of neuroscience : the official journal of the Society for Neuroscience 21:10-17.

Basu J, Betz A, Brose N, Rosenmund C (2007) Munc13-1 C1 domain activation lowers the energy barrier for synaptic vesicle fusion. The Journal of neuroscience : the official journal of the Society for Neuroscience 27:1200-1210.

Basu J, Shen N, Dulubova I, Lu J, Guan R, Guryev O, Grishin NV, Rosenmund C, Rizo J (2005) A minimal domain responsible for Munc13 activity. Nature structural & molecular biology 12:1017-1018.

Betz A, Ashery U, Rickmann M, Augustin I, Neher E, Sudhof TC, Rettig J, Brose N (1998) Munc13-1 is a presynaptic phorbol ester receptor that enhances neurotransmitter release. Neuron 21:123-136.

Betz A, Thakur P, Junge HJ, Ashery U, Rhee JS, Scheuss V, Rosenmund C, Rettig J, Brose N (2001) Functional interaction of the active zone proteins Munc13-1 and RIM1 in synaptic vesicle priming. Neuron 30:183-196.

Brenner S (1974) The genetics of Caenorhabditis elegans. Genetics 77:71-94.

Brose N, Hofmann K, Hata Y, Sudhof TC (1995) Mammalian homologues of Caenorhabditis elegans unc-13 gene define novel family of C2-domain proteins. The Journal of biological chemistry 270:25273-25280.

Calloway N, Gouzer G, Xue M, Ryan TA (2015) The active-zone protein Munc13 controls the use-dependence of presynaptic voltage-gated calcium channels. eLife 4.

Camacho M, Basu J, Trimbuch T, Chang S, Pulido-Lozano C, Chang SS, Duluvova I, Abo-Rady M, Rizo J, Rosenmund C (2017) Heterodimerization of Munc13 C2A domain with RIM regulates synaptic vesicle docking and priming. Nat Commun 8:15293.

Chen Z, Cooper B, Kalla S, Varoqueaux F, Young SM, Jr. (2013) The Munc13 proteins differentially regulate readily releasable pool dynamics and calcium-dependent recovery at a central synapse. The Journal of neuroscience : the official journal of the Society for Neuroscience 33:8336-8351.

Frokjaer-Jensen C, Davis MW, Sarov M, Taylor J, Flibotte S, LaBella M, Pozniakovsky A, Moerman DG, Jorgensen EM (2014) Random and targeted transgene insertion in Caenorhabditis elegans using a modified Mos1 transposon. Nature methods 11:529-534.

Gerber SH, Rah JC, Min SW, Liu X, de Wit H, Dulubova I, Meyer AC, Rizo J, Arancillo M, Hammer RE, Verhage M, Rosenmund C, Sudhof TC (2008) Conformational switch of syntaxin-1 controls synaptic vesicle fusion. Science 321:1507-1510.

Hu Z, Tong XJ, Kaplan JM (2013) UNC-13L, UNC-13S, and Tomosyn form a protein code for
fast and slow neurotransmitter release in Caenorhabditis elegans. eLife 2:e00967.

Hu Z, Vashlishan-Murray AB, Kaplan JM (2015) NLP-12 engages different UNC-13 proteins to
potentiate tonic and evoked release. The Journal of neuroscience : the official journal of
the Society for Neuroscience 35:1038-1042.

Jahn R, Fasshauer D (2012) Molecular machines governing exocytosis of synaptic vesicles.
Nature 490:201-207.

Junge HJ, Rhee JS, Jahn O, Varoqueaux F, Spiess J, Waxham MN, Rosenmund C, Brose N
(2004) Calmodulin and Munc13 form a Ca2+ sensor/effector complex that controls short-
term synaptic plasticity. Cell 118:389-401.

Kohn RE, Duerr JS, McManus JR, Duke A, Rakow TL, Maruyama H, Moulder G, Maruyama
IN, Barstead RJ, Rand JB (2000) Expression of multiple UNC-13 proteins in the
Caenorhabditis elegans nervous system. Molecular biology of the cell 11:3441-3452.

Lackner MR, Nurrish SJ, Kaplan JM (1999) Facilitation of synaptic transmission by EGL-30
Gqalpha and EGL-8 PLCbeta: DAG binding to UNC-13 is required to stimulate
acetylcholine release. Neuron 24:335-346.

Li L, Liu H, Hall Q, Wang W, Yu Y, Kaplan JM, Hu Z (2019) A Hyperactive Form of unc-13
Enhances Ca(2+) Sensitivity and Synaptic Vesicle Release Probability in C. elegans. Cell
Rep 28:2979-2995 e2974.

Liu H, Li L, Nedelcu D, Hall Q, Zhou L, Wang W, Yu Y, Kaplan JM, Hu Z (2019)
Heterodimerization of UNC-13/RIM regulates synaptic vesicle release probability but not
priming in C. elegans. eLife 8.

Liu X, Seven AB, Camacho M, Esser V, Xu J, Trimbuch T, Quade B, Su L, Ma C, Rosenmund C, Rizo J (2016) Functional synergy between the Munc13 C-terminal C1 and C2 domains. eLife 5.

Lou X, Korogod N, Brose N, Schneggenburger R (2008) Phorbol esters modulate spontaneous and Ca2+-evoked transmitter release via acting on both Munc13 and protein kinase C. The Journal of neuroscience : the official journal of the Society for Neuroscience 28:8257-8267.

Madison JM, Nurrish S, Kaplan JM (2005) UNC-13 interaction with syntaxin is required for synaptic transmission. Current biology : CB 15:2236-2242.

Maruyama IN, Brenner S (1991) A phorbol ester/diacylglycerol-binding protein encoded by the unc-13 gene of Caenorhabditis elegans. Proceedings of the National Academy of Sciences of the United States of America 88:5729-5733.

Michelassi F, Liu H, Hu Z, Dittman JS (2017) A C1-C2 Module in Munc13 Inhibits Calcium-Dependent Neurotransmitter Release. Neuron 95:577-590 e575.

Richmond JE, Davis WS, Jorgensen EM (1999) UNC-13 is required for synaptic vesicle fusion in C. elegans. Nature neuroscience 2:959-964.

Rosenmund C, Stevens CF (1996) Definition of the readily releasable pool of vesicles at hippocampal synapses. Neuron 16:1197-1207.

Rosenmund C, Sigler A, Augustin I, Reim K, Brose N, Rhee JS (2002) Differential control of vesicle priming and short-term plasticity by Munc13 isoforms. Neuron 33:411-424.

Shin OH, Lu J, Rhee JS, Tomchick DR, Pang ZP, Wojcik SM, Camacho-Perez M, Brose N, Machius M, Rizo J, Rosenmund C, Sudhof TC (2010) Munc13 C2B domain is an

activity-dependent Ca2+ regulator of synaptic exocytosis. Nature structural & molecular biology 17:280-288.

Song Y, Ailenberg M, Silverman M (1998) Cloning of a novel gene in the human kidney homologous to rat munc13s: its potential role in diabetic nephropathy. Kidney Int 53:1689-1695.

Stevens DR, Wu ZX, Matti U, Junge HJ, Schirra C, Becherer U, Wojcik SM, Brose N, Rettig J (2005) Identification of the minimal protein domain required for priming activity of Munc13-1. Current biology : CB 15:2243-2248.

Sudhof TC, Rizo J (2011) Synaptic vesicle exocytosis. Cold Spring Harbor perspectives in biology 3.

Varoqueaux F, Sigler A, Rhee JS, Brose N, Enk C, Reim K, Rosenmund C (2002) Total arrest of spontaneous and evoked synaptic transmission but normal synaptogenesis in the absence of Munc13-mediated vesicle priming. Proceedings of the National Academy of Sciences of the United States of America 99:9037-9042.

Weimer RM, Gracheva EO, Meyrignac O, Miller KG, Richmond JE, Bessereau JL (2006) UNC-13 and UNC-10/rim localize synaptic vesicles to specific membrane domains. The Journal of neuroscience : the official journal of the Society for Neuroscience 26:8040-8047.

White JG, Southgate E, Thomson JN, Brenner S (1986) The structure of the nervous system of the nematode Caenorhabditis elegans. Philosophical transactions of the Royal Society of London Series B, Biological sciences 314:1-340.

Xu J, Camacho M, Xu Y, Esser V, Liu X, Trimbuch T, Pan YZ, Ma C, Tomchick DR,
Rosenmund C, Rizo J (2017) Mechanistic insights into neurotransmitter release and
presynaptic plasticity from the crystal structure of Munc13-1 C1C2BMUN. eLife 6.

Figure 1
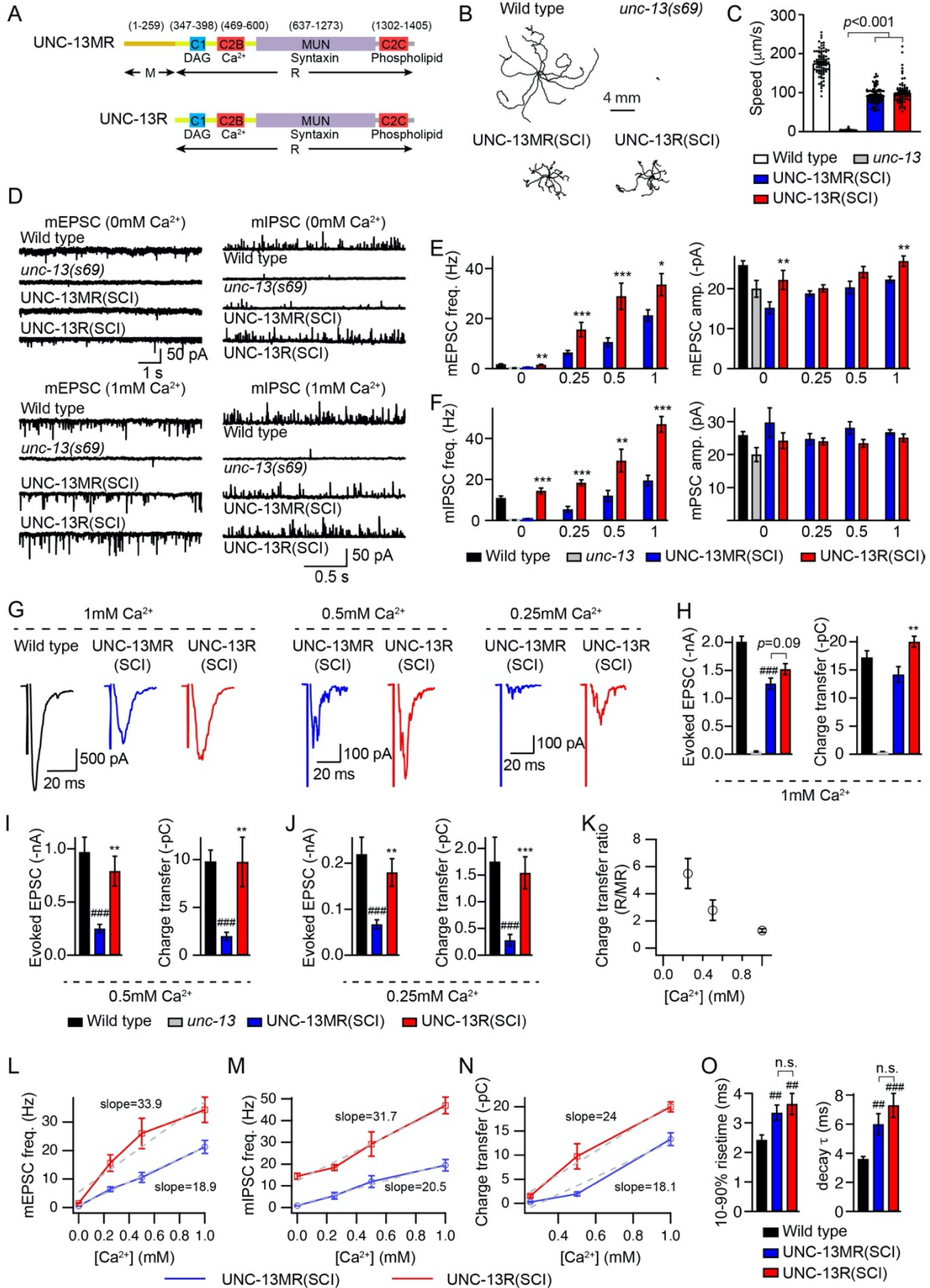
Figure 1. The M domain in UNC-13MR inhibits tonic and evoked neurotransmitter release.
Miniature EPSCs/IPSCs and stimulus-evoked EPSCs were recorded from body wall muscle of adult worms in various Ca^{2+} levels. (A) The domain structures of UNC-13MR and UNC-13R are illustrated. Ligands for each domain are indicated. (B) Representative locomotory trajectories of 10 animals for wild-type, *unc-13(s69)*, and *unc-13* rescued by single copy insertion of UNC-13MR and UNC-13R under the pan neuronal promoter. The starting points of each trajectory have been aligned for clarity. (C) Quantification of the average locomotion speed for the indicated genotypes or transgenes. (D) Representative mEPSC and mIPSC traces (recorded at 0mM and 1mM Ca^{2+}) from the indicated genotypes. (E, F) Quantification of the frequency and amplitude of the mEPSCs and mIPSCs under all tested Ca^{2+} levels (0, 0.25, 0.5, and 1mM) from the same genotypes as in D. (G) Example traces of stimulus-evoked EPSCs recorded in various Ca^{2+} levels (0.25, 0.5, 1mM) from wild-type (black), UNC-13MR rescued (blue), and UNC-13R rescued (red) animals. (H-J) Quantification of the evoked EPSC amplitude and charge transfer from the same genotypes and Ca^{2+} levels as in G. (I) Ratio of the charge transfer in UNC-13MR rescued worms to that in UNC-13MR rescued animals in different Ca^{2+} levels. (L-N) Comparison of the concentration effect for mEPSC frequency, mIPSC frequency, and evoked charge transfer versus extracellular Ca^{2+} concentration between the UNC-13MR and UNC-13R rescued animals. (M) Quantification of the 10-90% risetime and decay of the evoked EPSCs from the indicated genotypes. Data are mean ± SEM (##, $p < 0.01$, ###, $p < 0.001$ when compared to wild type, one-way ANOVA; *, $p < 0.05$, **, $p < 0.01$, ***, $p < 0.001$ when compared to UNC-13MR rescue animals, student's t-test; n.s., non-significant when compared to UNC-13MR rescue animals; one-way ANOVA). Data collected by Zhitao Hu lab.

Figure 1, supplemental 1
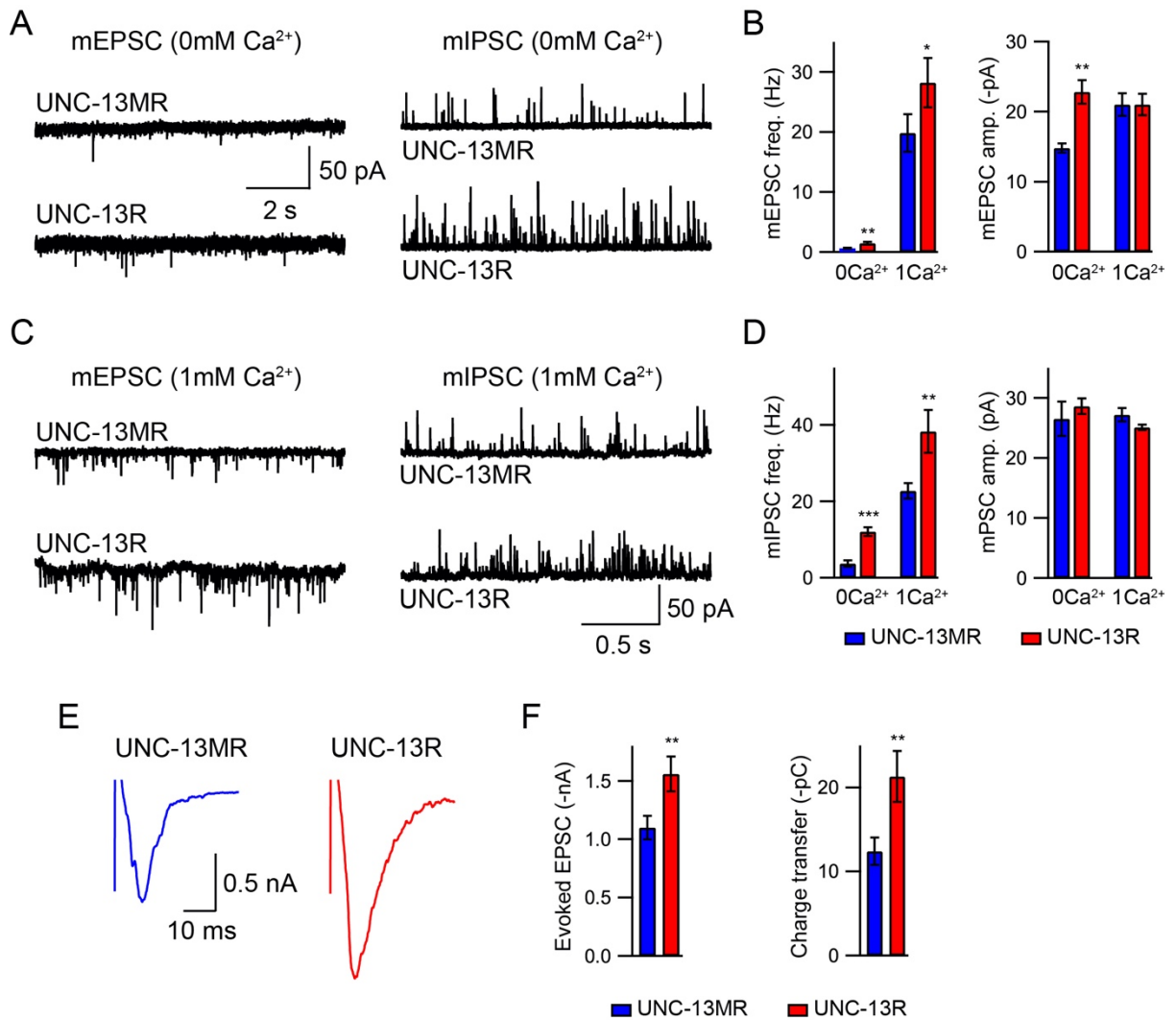
Figure 1, supplemental 1. The M domain inhibits synaptic transmission in UNC-13MR overexpression rescue worms.

(A, C) Representative mEPSC and mIPSC traces (recorded in 0mM and 1mM Ca^{2+}) from UNC-13MR and UNC-13R overexpression rescue animals. (B, D) Quantification of the frequency and amplitude of the mEPSCs and mIPSCs from the same genotypes as in A and C. (E) Example traces of stimulus-evoked EPSCs recorded from UNC-13MR and UNC-13R overexpression rescue animals. (F) Quantification of the evoked EPSC amplitude and charge transfer. Data are mean $\pm$ SEM (*, $p < 0.05$, **, $p < 0.01$, ***, $p < 0.001$ when compared to UNC-13MR rescue animals; student's t-test). Data collected by Zhitao Hu lab.

Figure 2
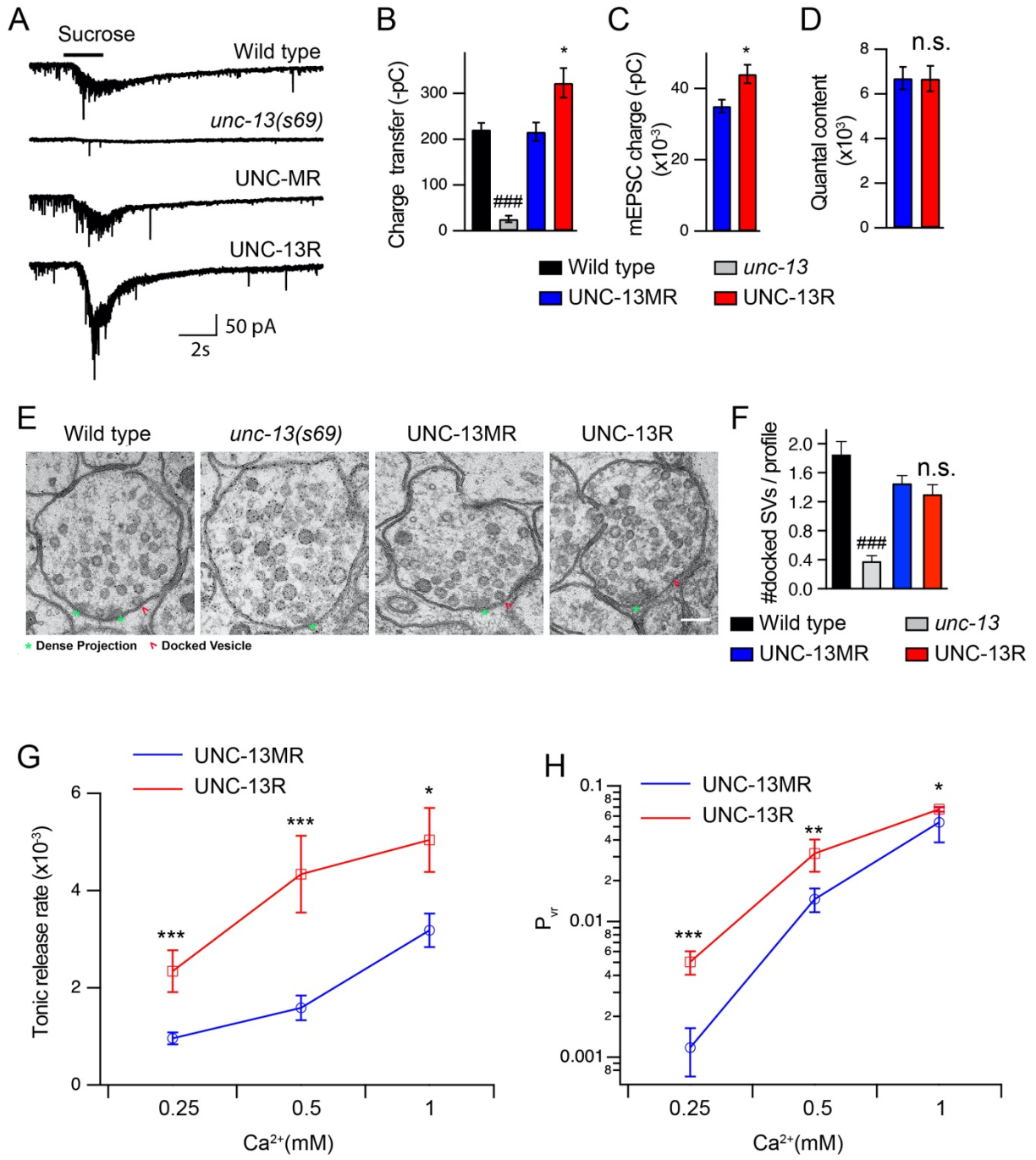
Figure 2. Deleting the M domain increases the fusogenicity of synaptic vesicles.

(A) Hypertonic sucrose-evoked current recorded from wild-type (black), *unc-13* null mutant (grey), UNC-13MR rescued (blue), and UNC-13R rescued (red) animals. (B) Averaged charge transfer from the sucrose-evoked currents in A. (C, D) Quantification of the charge transfer of the mEPSCs, and averaged quantal content in UNC-13MR and UNC-13R rescued animals. (E) Presynaptic ultrastructure of cholinergic motor neuron synapses in wild type, *unc-13* null mutant, UNC-13MR rescued, and UNC-13R rescued animals. Asterisks indicate Dense Projection (DP); arrowheads indicate synaptic vesicles docked at the plasma membrane. Scale bar = 100nm. (F) Quantification of the number of synaptic vesicles docked at the plasma membrane per synaptic profile. (G) Summary of the tonic vesicular release rate (mEPSC frequency divided by the number of vesicles in the RRP) in tested Ca^{2+} levels (0.25, 0.5, 1mM). (H) Quantification of the probability of synaptic vesicle release (P_{vr}) in various Ca^{2+} levels (0.25, 0.5, 1mM) from the indicated genotypes. Data are mean ± SEM (###, $p < 0.001$ when compared to wild type, one-way ANOVA; *, $p < 0.05$, **, $p < 0.01$, ***, $p < 0.001$ when compared to UNC-13MR rescue, student's t-test; n.s., non-significant when compared to UNC-13MR rescued animals, student's t-test;). Data collected by Zhitao Hu lab (A-D,G,H) and Seema Sheoran (E,F).
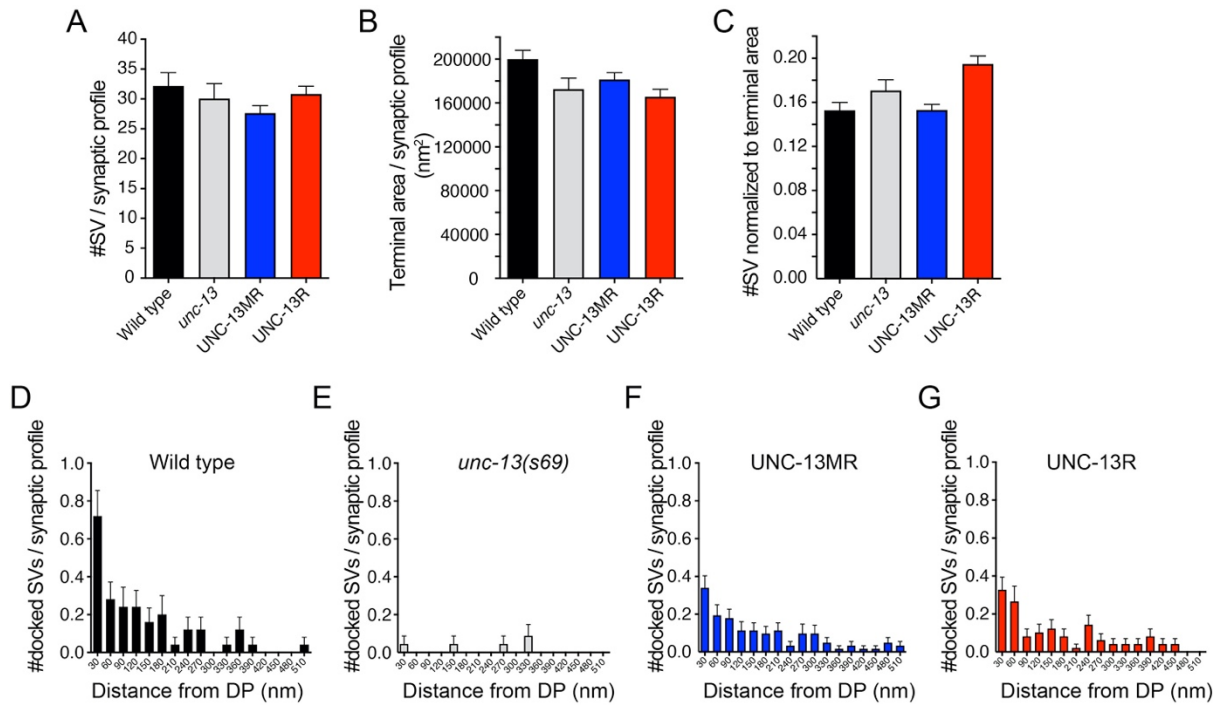
Figure 2, supplemental 2. The M domain is not required for SV docking.

Quantification of (A) number of synaptic vesicles (SVs) per synaptic profile (B) presynaptic terminal area per synaptic profile (C) number of SVs normalized to the presynaptic terminal area. (D-G) Distribution of docked SVs plotted as distance from the dense projection. Data are mean ± SEM. Data collected by Seema Sheoran.

Figure 3
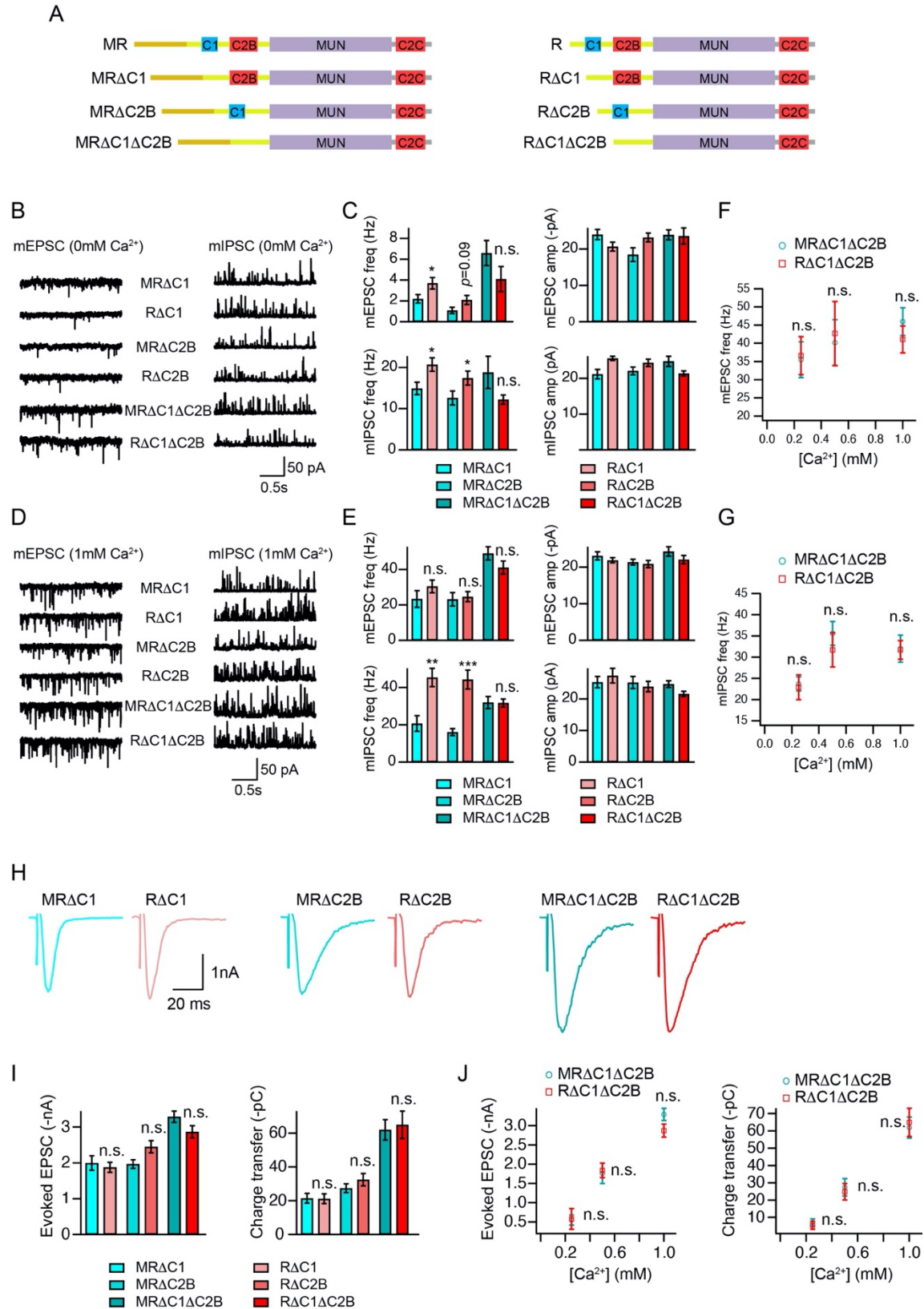
Figure 3. The inhibitory effects of the M domain are eliminated in the absence of the C1 and C2B domains.

(A) Cartoon depicting the domain structure of UNC-13MR and UNC-13R lacking their C1, C2B, or C1 and C2B domains. (B, D) Representative mEPSC and mIPSC traces (recorded at 0mM and 1mM Ca^{2+}) from the indicated genotypes. (C, E) Quantification of the frequency and amplitude of the mEPSCs and mIPSCs from the same genotypes as in B and D. (F, G) Comparison of the mEPSC and mIPSC frequency between MRΔC1ΔC2B and RΔC1ΔC2B rescue animals in various Ca^{2+} levels (0.25, 0.5, 1mM). (H) Example traces of stimulus-evoked EPSCs from the indicated genotypes. (I) Quantification of the evoked EPSC amplitude and charge transfer from the same genotypes as in H. (J) Comparison of the amplitude and charge transfer of the evoked EPSCs between MRΔC1ΔC2B and RΔC1ΔC2B rescue animals in various Ca^{2+} levels (0.25, 0.5, 1mM). Data are mean ± SEM (*, $p < 0.05$, **, $p < 0.01$, ***, $p < 0.001$ when compared to UNC-13MR rescue; n.s., non-significant when compared to UNC-13MR rescue; one-way ANOVA). Data collected by Zhitao Hu lab.
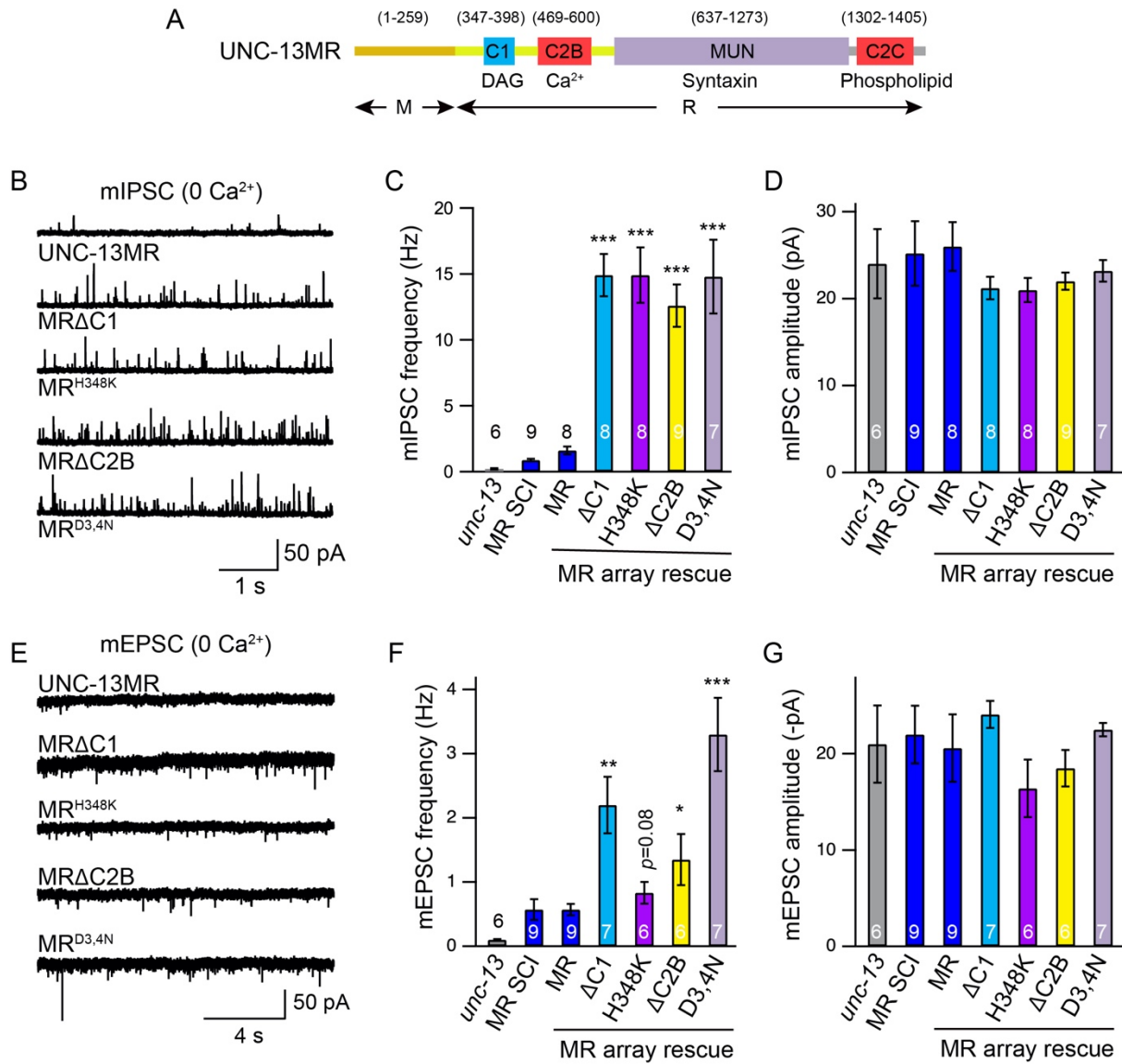
Figure 3, supplemental 3. The HK and DN mutations in the C1 and C2B domains in UNC-13MR cause a dramatic increase in tonic release.

(A) Cartoon depicting the HK and DN mutations in UNC-13MR. (B) Representative mIPSC traces (recorded in 0mM Ca^{2+}) from the indicated genotypes. (C, D) Quantification of the mIPSC frequency and amplitude from the same genotypes as in B. (E) Representative mEPSC traces (recorded in 0mM Ca^{2+}) from the indicated genotypes. (F, G) Quantification of the mEPSC frequency and amplitude from the same genotypes as in E. Data are mean ± SEM (*, $p < 0.05$, **, $p < 0.01$, ***, $p < 0.001$ when compared to UNC-13MR rescue; one-way ANOVA). The number of worms analyzed for each genotype is indicated in the bar graphs. Data collected by Zhitao Hu lab.

Figure 4
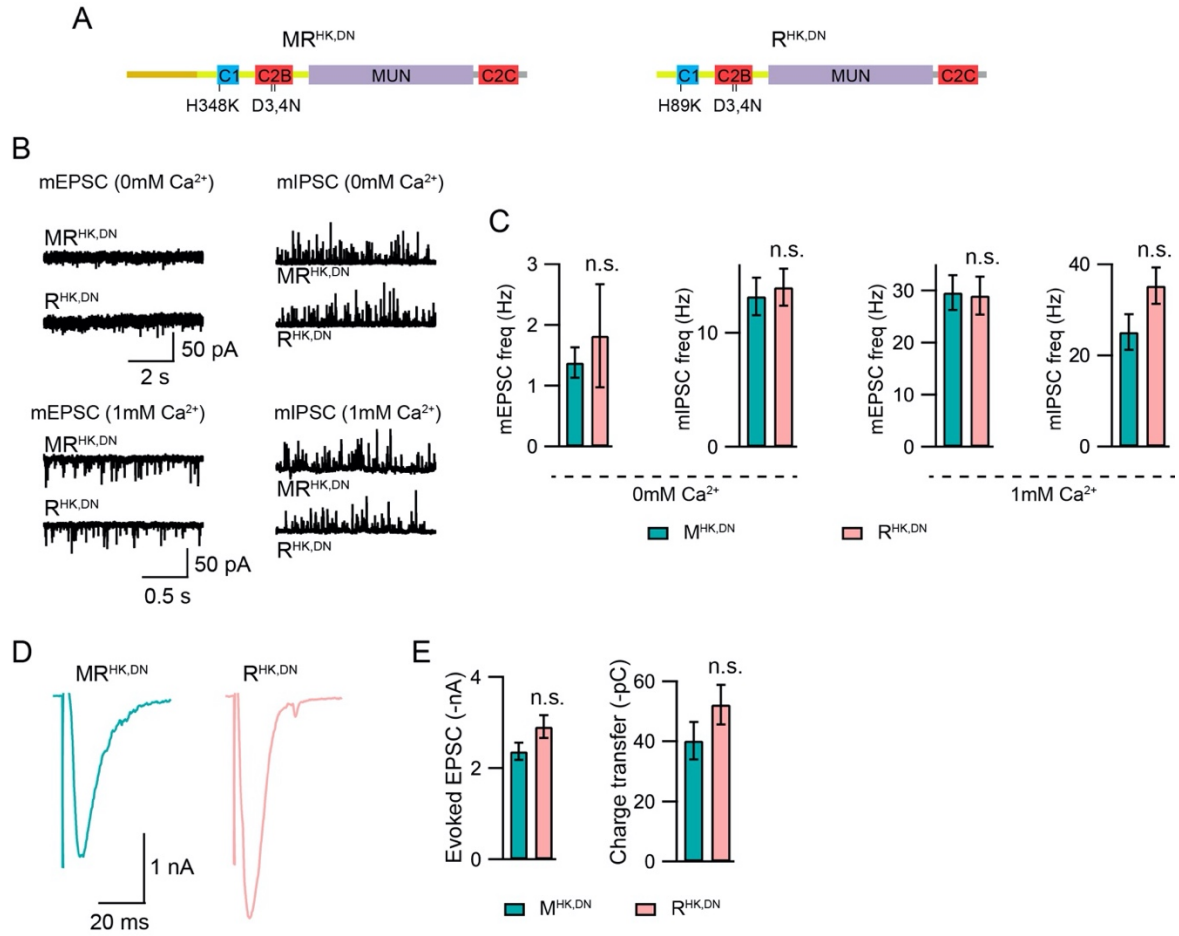
Figure 4. Activation of the C1 and C2B domains eliminates the M domain inhibition.

(A) Cartoon depicting the HK and DN mutations in UNC-13MR and UNC-13R. (B) Representative mEPSC and mIPSC traces (recorded in 0mM and 1mM Ca^{2+}) from the $MR^{HK,DN}$ and $R^{HK,DN}$ transgenic worms. (C) Quantification of the mEPSC and mIPSC frequencies from the same genotypes as in B. (D) Example traces of stimulus-evoked EPSCs from the $MR^{HK,DN}$ and $R^{HK,DN}$ transgenic worms (recorded in 1mM Ca^{2+}). (I) Quantification of the evoked EPSC amplitude and charge transfer from the same genotypes as in D. Data are mean ± SEM (n.s., non-significant when compared to UNC-13MR^{HK,DN} rescue; student's t-test). Data collected by Zhitao Hu lab.

Figure 5
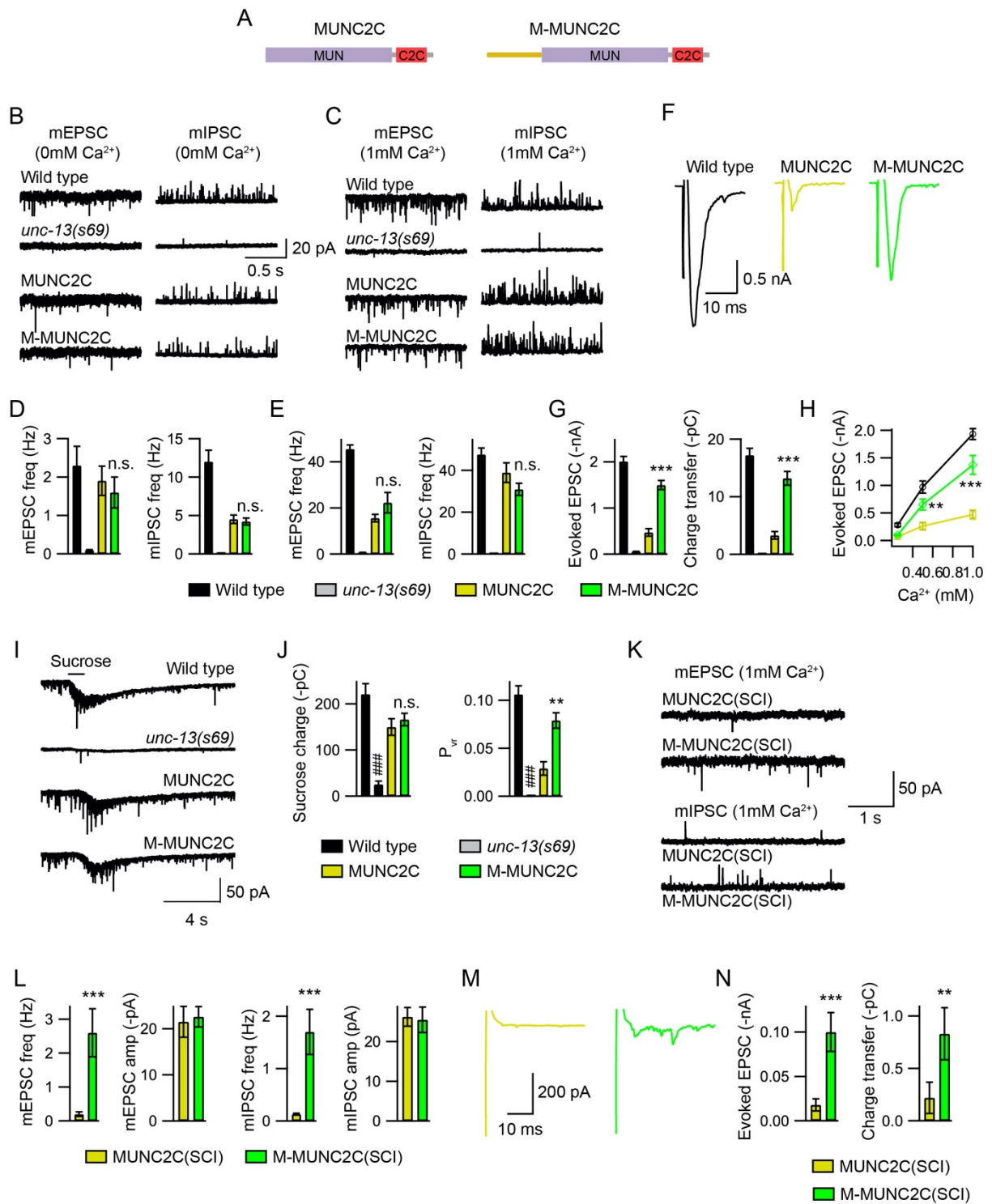
Figure 5. The M domain promotes evoked neurotransmitter release and enhances release probability.

(A) Cartoon depicting the domain structure of UNC-13 MUNC2C and M-MUNC2C. (B, C) Representative mEPSC and mIPSC traces (recorded in 0mM and 1mM Ca^{2+}) from wild-type (black), *unc-13* (grey), MUNC2C overexpression rescue (yellow) and M-MUNC2C overexpression rescue (green) animals. (D, E) Quantification of the frequency and amplitude of the mEPSCs and mIPSCs from the same genotypes as in B and C. (F) Example traces of stimulus-evoked EPSCs from wild-type (black), *unc-13* (grey), MUNC2C overexpression rescue (yellow) and M-MUNC2C overexpression rescue (green) animals (recorded in 1mM Ca^{2+}). (G) Quantification of the evoked EPSC amplitude and charge transfer from the same genotypes as in F. (H) Quantification of the evoked EPSCs amplitude in various Ca^{2+} concentrations (0.25mM, 0.5mM, and 1mM). (I) Hypertonic sucrose-evoked current recorded from wild-type (black), *unc-13* (grey), MUNC2C overexpression rescue (blue), and M-MUNC2C overexpression rescue (red) animals. (J) Averaged charge transfer from the sucrose-evoked currents in I, and quantification of the probability of synaptic vesicle release (P_{vr}) from the indicated genotypes. Data are mean ± SEM (###, $p < 0.001$ when compared to wild type; **, $p < 0.01$***, $p < 0.001$ when compared to the MUNC2C overexpression rescue; n.s., non-significant when compared to the MUNC2C overexpression rescue; one-way ANOVA). (K) Example traces of mEPSCs and mIPSCs from MUNC2C SCI rescue and M-MUNC2C SCI rescue animals (in 1mM Ca^{2+}). (L) Quantification of the mEPSC and mIPSC frequencies in K. (M, N) Representative traces of evoked EPSCs and quantification of the amplitude and charge transfer from the indicated genotypes. Data are mean ± SEM (**, $p < 0.01$, ***, $p < 0.001$ when compared to the MUNC2C SCI rescue; student's t-test). Data collected by Zhitao Hu lab.

Figure 6
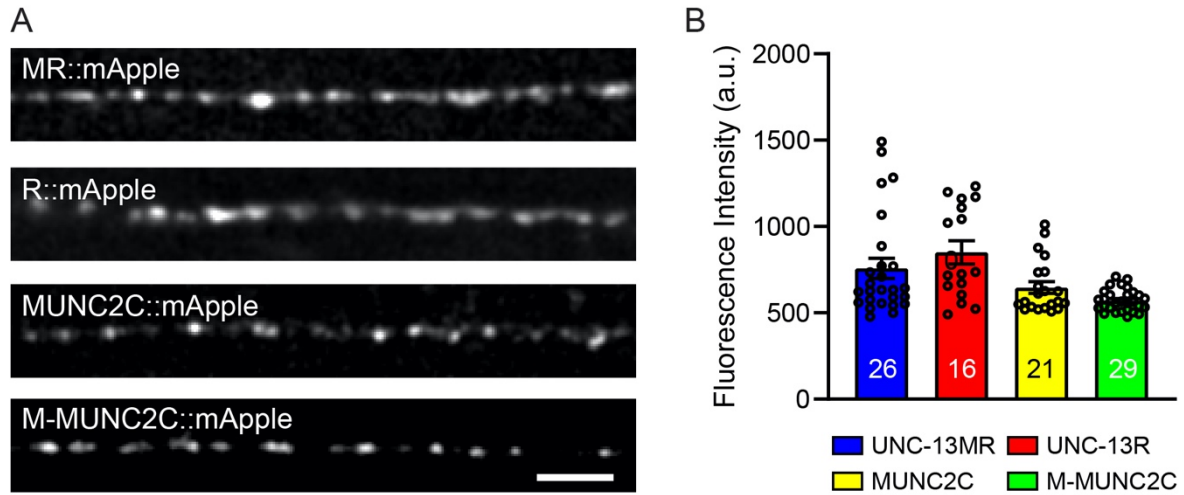
Figure 6. The M domain does not alter UNC-13 protein levels. (A) Representative confocal Z-stack images for mApple-tagged UNC-13MR, UNC-13R, MUNC2C, and M-MUNC2C (all driven by the unc-129 promoter). Scale bar, 5 m. (B) Quantification of the fluorescence intensity from the lines in A. Data are mean ± SEM. The number of worms analyzed for each genotype is indicated in the bar graphs. Data collected by Zhitao Hu lab.

Figure 7
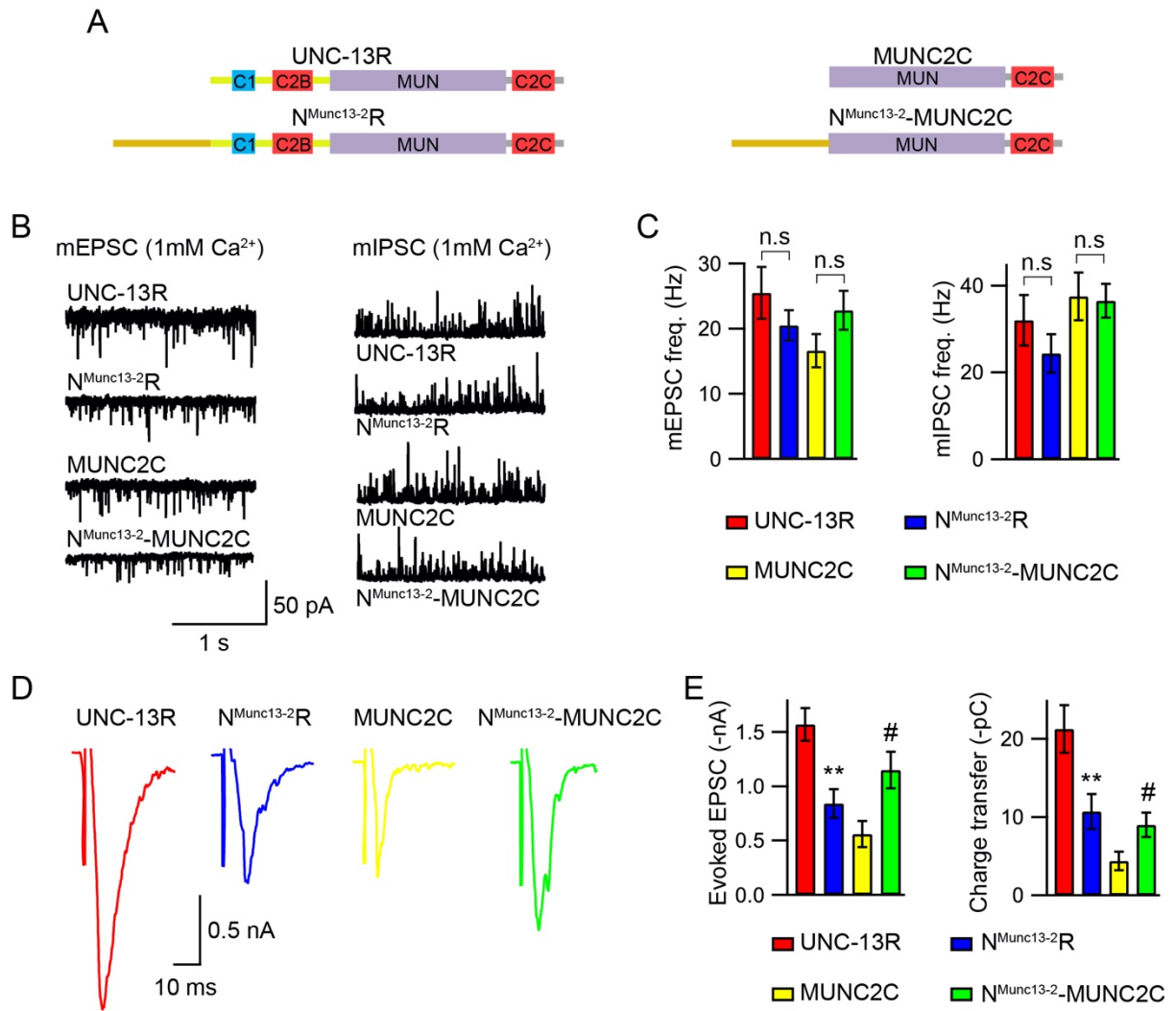
Figure 7. The N terminus in Munc13-2 exhibits both inhibition and facilitation in synaptic transmission.

(A) Cartoon depicting the domain structure of UNC-13R, $N^{Munc13-2}$-R, MUNC2C and $N^{Munc13-2}$-MUNC2C. (B) Representative mEPSC and mIPSC traces (recorded in 1mM Ca^{2+}) from the indicated genotypes (UNC-13R, $N^{Munc13-2}$-R, MUNC2C and $M^{Munc13-2}$-MUNC2C rescue animals). (C) Quantification of the frequency and amplitude of the mEPSCs and mIPSCs from the same genotypes as in B. (D) Example traces of stimulus-evoked EPSCs (recorded in 1mM Ca^{2+}) from indicated genotypes. (E) Quantification of the evoked EPSC amplitude and charge transfer from the same genotypes as in D. Data are mean ± SEM (#, $p < 0.05$ when compared to MUNC2C rescue; **, $p < 0.01$ when compared to UNC-13R rescue; n.s., non-significant; one-way ANOVA). Data collected by Zhitao Hu lab.

```
UNC-13MR  ------------------------------------------------------------
Munc13-2  MKRLLRESEEEIMLTLGPSSSLSPDQVRTETVCIVKGKSTGPTGSLPEDNFPPPCCESAD

UNC-13MR  -------------------MNPVPSLA----------------------------------
Munc13-2  STTSGERDRNLAQLGSFEQQASSQPSLACTACASGSDSRELSPASITSCSEPSERNKARP

UNC-13MR  -VPMSPGPYLNSDPPSPVSPNPQ-I----------KRSIYRIKESYEDRNGGRERIYTTN
Munc13-2  IFPRGPGQRCRHEHQEPLGDVVEYIIRELQGISRLQSEIAELQQHLNQVRGSVDEVSS--

UNC-13MR  LVSVYLEKMKPPDELEEGSS--GSMRETQN-------------EIKNGTQLHNAESNIF
Munc13-2  CVDSV---LSEIEGLHVGSSSLGKVRHGEKAQELHVERSREEAILYLYGLPEHDGESTVE

UNC-13MR  FPQDSVPKSISYNAGNLKNTSITTSKTSSAITNHSSLPPQPPSKPASRDSDPMKQLLTFS
Munc13-2  LVDNFLAKHLCVNGMQC-NRYV-----REAYRAGTAPAPRPTV---VKLVHPEHRDLILQ

UNC-13MR  KSFKKVRRVRSAMPRRRKRKRVKIKKSRSCPILWKTEKTPHPMKSKSMTCIRIPKKTV--
Munc13-2  KSIL-------------LQSVGVRVATREEPVWPEGCKNPP--KESLSCLQQFQDHSRN

UNC-13MR  ---------------------------------------------------IAPLRKE
Munc13-2  HQGKPALQLETGNRRQMSGPHQMRTQNQHRELQASEHQGLSFLPKDGSAKQSDVSKLQDE

UNC-13MR  IKIVR----------------------MKPPAARCE------SDSKAHKKKNL----
Munc13-2  VKGTSGAPQVISDPCGELSLLHQLEGSSPVLIPKEEDCGKLQIFKQDSQEHKACNVTKLQ

UNC-13MR  -------------------------------------------LDVYKDMGK------
Munc13-2  SDCNNAIKASSCLSLSGPLKAEKVNAEDRMLGGEDGLDILSPKQLEDLLADKSRRFATLN

UNC-13MR  ------------------------------------------------------------
Munc13-2  PDSAVEEVIIGPETFSNMVHIDLNEEETCTAQVLKNVFDKSSCVLGGSQEDEDVEIKFHT

UNC-13MR  ------------------------------------------------------------
Munc13-2  TKLSRAIHHFRLALQGVFQKLENNGSISPEDLESNESGSQSENSDRLLWTVSSGGAHDCS

UNC-13MR  ------------------------------------------------------------
Munc13-2  VESPASQGSESLLSVVSGGVGISVQGDQTPQAPSNFSLASNNSPLTNSLLSFPLAPGLGN

UNC-13MR  ------------------------------------------------------------
Munc13-2  ETCSRPDSPNQGKLSLEQVCAETIYLNKCINNFKNVLREKRLRQKKLLQELVQTASHLSV

UNC-13MR  --------------
Munc13-2  EDIPSEGKREALQIS
```

Figure 7, supplemental 4. Sequence alignment between the UNC-13 M domain and the Munc13-2 N terminus. The small stretch region in Munc13-2 is indicated by blue. Data collected by Zhitao Hu lab.

Figure 8
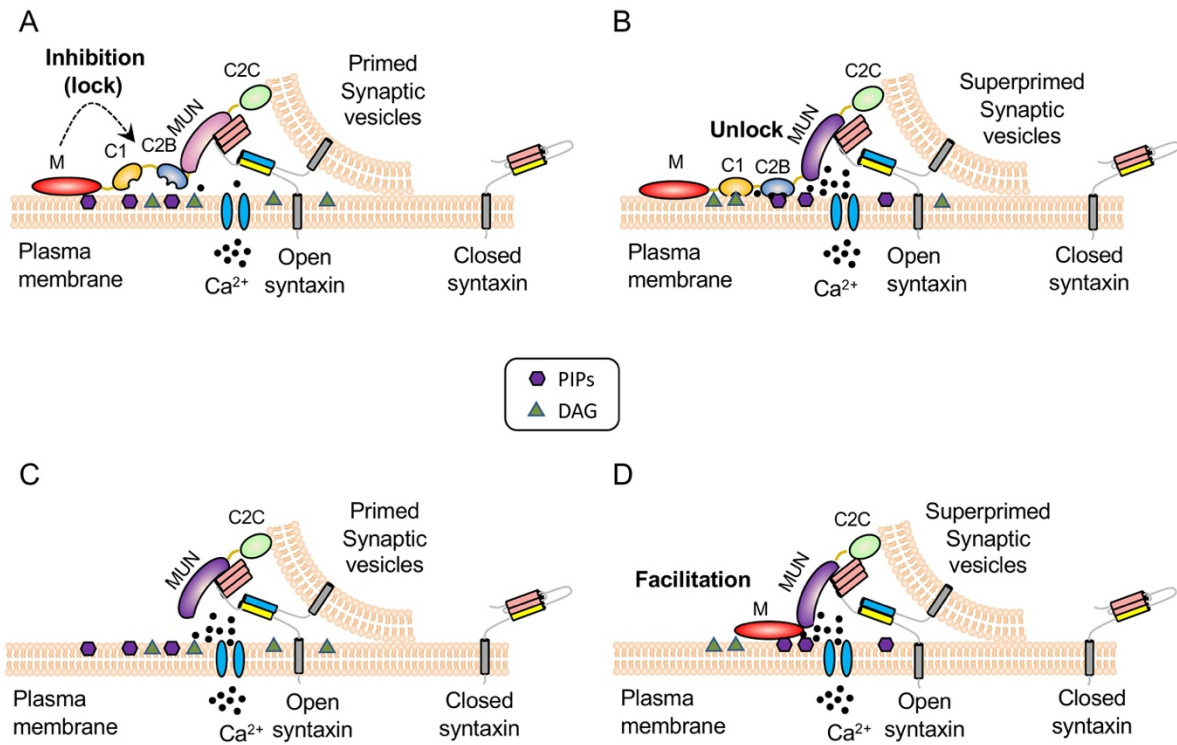
Figure 8. Models for the M domain function in UNC-13.

(A) The M domain locks the C1 and C2B domains in an autoinhibitory conformation under low Ca^{2+} conditions, limiting UNC-13MR triggered membrane fusion. (B) Ca^{2+} increase activates the C1 and C2B domains and unlocks from the M domain. The release of the C1 and C2B domains in turn bind to the plasma membrane and superprime synaptic vesicles. (C) The MUNC2C fragment is unable to form an effective bridge for membrane fusion. (D) The M domain potentially interacts with the plasma membrane establishing an UNC-13 bridge with the synaptic vesicle. This stabilizes the MUN domain and enhances SV fusion.

Table S1

Table S1. Summary of all tonic release

	0mM Ca²⁺						0.25mM Ca²⁺						0.5mM Ca²⁺						1mM Ca²⁺					
	mEPSC			mIPSC			mEPSC			mIPSC			mEPSC			mIPSC			mEPSC			mIPSC		
	Frequency (Hz)	Amplitude (-pA)	N	Frequency (Hz)	Amplitude (pA)	N	Frequency (Hz)	Amplitude (-pA)	N	Frequency (Hz)	Amplitude (pA)	N	Frequency (Hz)	Amplitude (-pA)	N	Frequency (Hz)	Amplitude (pA)	N	Frequency (Hz)	Amplitude (-pA)	N	Frequency (Hz)	Amplitude (pA)	N
Wild type	1.9±0.61	27.3±1.69	18	11±0.92	25.9±0.98	20	42±4.27	23±1.66	10	49.7±6.16	26.2±1.1	12	56.2±7.27	21.9±1.35	12	43.5±4.34	22.5±1.35	9	50.9±5.39	21.2±0.91	17	48±4.79	22.4±1	19
unc-13(s69)	0.57±0.1	15.2±0.67	9	0.9±0.11	27.7±2.57	9													0.5±0.09	16.8±1.75	14	0.1±0.05	26±2.51	5
UNC-13MR (SCI)	1.0±0.21	20.5±1.8	6	14.4±1.26	24.2±1.31	6	6.4±0.84	18.8±0.67	13	5.4±1.49	24.7±1.74	13	10.6±1.71	20.3±1.59	9	12±2.75	28.1±1.93	10	21.3±2.32	22.3±2.81	17	19.5±2.6	26.8±0.79	15
UNC-13R (SCI)	0.62±0.09	14.8±0.65	10	3.7±0.87	26.5±2.85	11	15.6±2.87	20.1±0.89	6	18.4±1.41	24±1	7	28.9±5.27	24.2±1.38	5	29.2±5.63	23.4±1.16	7	33.6±4.4	26.9±1.33	15	47±3.81	25.1±1.16	15
UNC-13MR	1.49±0.21	22.8±1.69	15	12.1±1.1	28.6±1.29	13													19.8±3.14	21±1.6	17	22.7±2.04	27.2±1.11	15
UNC-13R	2.2±0.44	24.1±1.35	7	14.9±1.56	21.2±1.26	8													28.2±4.1	21±1.54	7	38.3±5.63	25.1±0.45	6
MRΔC1	3.7±0.54	20.7±1.17	9	20.7±1.64	25.6±0.55	7													23.4±4.69	23.1±1.13	9	20.7±4.21	25.3±1.8	7
RΔC1	1.1±0.33	18.5±1.95	8	11.6±1.61	22.3±1	8													30.4±3.64	21.9±0.67	14	45.4±4.95	27.4±2.34	9
MRΔC2B	2.1±0.43	23.2±1.18	8	17.4±1.69	24.4±1	8													23.2±3.79	21.4±0.84	8	16.1±1.82	25.2±1.85	7
RΔC2B	6.6±1.16	23.9±1.42	10	18.8±3.97	24.8±1.49	8													24.7±2.83	20.9±0.98	7	44.3±5.14	23.9±1.65	7
MRΔC1ΔC2B	4.1±1.22	23.6±2.25	6	12.2±1.12	21.4±0.72	7	35.5±4.89	24.5±2.09	8	23.7±1.65	24.3±1.19	6	40.2±6.28	20.8±1.78	7	35.6±2.78	25.3±0.86	8	49±3.79	24.3±1.27	11	32±3.2	24.7±1.14	8
RΔC1ΔC2B							36.6±5.25	20.6±2.28	7	22.9±2.86	24.3±1.51	6	44.7±7.67	21.3±1.63	7	31.7±4.04	22.8±0.59	8	41.1±3.68	22.1±1.11	14	31.7±2.17	21.6±0.82	8
MUNC2C (SCI)																			0.2±0.065	21.5±3.37	8	0.13±0.056	26.2±2.34	8
M-MUNC2C (SCI)																			2.6±0.71	22.6±2.2	6	1.7±0.43	25.5±3.18	6
MUNC2C	1.9±0.38	19.8±1.36	11	4.5±0.55	25.2±1.11	13													16.6±2.54	21.2±1.46	16	37.5±5.48	30.4±1.65	10
M-MUNC2C	1.6±0.4	23.4±1.64	7	4.2±0.45	27.8±1.96	7													22.3±4.37	22.7±1.21	10	30.9±2.87	33.5±2.02	8
N^Munc13-2_R	0.9±0.19	23.8±2.38	12	9.9±1.42	25.9±1.48	12													22.5±2.33	20.5±0.85	12	24.4±4.44	25.7±1.51	8
N^Munc13-2-MUNC2C	1.4±0.35	23.4±1.9	7	4.5±1.2	24.1±1.3	8													22.8±3.1	22±1.55	16	36.5±3.9	26.8±2.34	10

SCI, single copy insertion; If not indicated, all other strains represent overexpression rescue; N, number of worms analyzed

Table S2

Table S2. Summary of evoked EPSCs and sucrose charge

| | Evoked EPSCs | | | | | | | | | Sucrose | |
| | 0.25mM Ca^{2+} | | | 0.5mM Ca^{2+} | | | 1mM Ca^{2+} | | | | |
	Amplitude (-nA)	Charge (-pC)	N	Amplitude (-nA)	Charge (-pC)	N	Amplitude (-nA)	Charge (-pC)	N	Charge (-pC)	N
Wild type	0.28±0.029	2.75±0.61	6	0.97±0.14	9.8±1.21	7	2.01±0.1	17.2±1.19	14	221±14.6	20
unc-13(s69)							0.026±0.007	0.15±0.008	5	25.5±7.06	7
UNC-13MR (SCI)	0.067±0.013	0.28±0.1	10	0.25±0.045	1.98±0.41	8	1.26±0.1	14.2±1.4	15	216±20.2	17
UNC-13R (SCI)	0.18±0.032	1.54±0.3	9	0.79±0.15	9.75±2.6	9	1.52±0.1	20±1	14	323±32.2	11
UNC-13MR							1.1±0.1	12.4±1.62	9		
UNC-13R							1.56±0.15	21.3±3.04	9		
MRΔC1							2±0.2	21.4±2.86	8		
RΔC1							1.88±0.14	21.2±2.88	10		
MRΔC2B							1.97±0.12	27.4±2.63	7		
RΔC2B							2.45±0.17	32.5±3.63	15		
MRΔC1ΔC2B	0.55±0.14	7.1±2.1	6	1.76±0.26	27.4±4.95	6	3.29±0.16	62±6.09	13		
RΔC1ΔC2B	0.58±0.25	5.4±2.1	6	1.84±0.19	24.8±4.76	8	2.87±0.17	65±8.14	10		
MUNC2C (SCI)							0.018±0.0068	0.22±0.15	6		
M-MUNC2C (SCI)							0.1±0.022	0.83±0.25	6		
MUNC2C	0.074±0.016	0.33±0.14	9	0.26±0.068	1.83±0.47	9	0.56±0.12	4.4±1.19	15	150±17.8	15
M-MUNC2C	0.1±0.016	0.74±0.2	12	0.65±0.1	5.8±1.1	9	1.5±0.11	13.2±1.18	8	153±13.1	9
N$^{Munc13-2}$R							0.84±0.13	10.7±2.21	8		
N$^{Munc13-2}$-MUNC2C							1.15±0.17	9.0±1.58	13		

SCI, single copy insertion; If not indicated, all other strains represent overexpression rescue; N, number of worms analyzed

CHAPTER III: SAX-7/L1CAM GENETICALLY INTERACT WITH MPK-1/ERK TO COORDINATE LOCOMOTION

Presented as *in preparation* manuscript with permission from the authors

Melinda Moseley-Alldredge[1], Seema Sheoran[2], Hayoung Yoo[1], Calvin O'Keefe[1],

Janet E. Richmond[2] and Lihsia Chen[1]

[1]Department of Genetics, Cell Biology and Development, University of Minnesota, Minneapolis, MN, USA

[2]Department of Biological Sciences, University of Illinois at Chicago, Chicago, IL, USA

3.1. Introduction

L1CAMs are highly conserved single-pass transmembrane immunoglobulin-like cell adhesion molecules essential for nervous system development and function in vertebrates, *Drosophila*, and *C. elegans*. Studies have established conserved roles for L1CAMs that include axon guidance, myelination, and fasciculation, dendrite morphogenesis, and synaptogenesis. Consistent with these neurodevelopmental roles, mutations in human L1CAM-encoding genes, L1, NrCAM, CHL1, and neurofascin, are strongly implicated in a variety of neurological disorders. For example, mutations in the L1 gene are directly linked to the congenital X-linked L1 syndrome that encompasses a range of neurological conditions, including hydrocephalus, spastic paraplegia, intellectual disability, and corpus callosum hypoplasia. Interestingly, the severity or manifestation of these conditions can vary even among family members carrying the same L1 mutation, suggesting the presence of other genetic variants that can interact with L1 to modify disease expressivity or penetrance. Subsequent genome-wide association studies as well as individual patient analyses also strongly implicated L1CAMs in behavioral conditions, with NrCAM associated with the autism spectrum disorder and susceptibility to addiction and CHL1 linked to schizophrenia. Consistent with this association of L1CAMs to behavioral disorders, L1, NrCAM, and CHL1 knockout mice exhibit altered social and exploratory behaviors.

The heterogeneous nature of behavioral disorders makes it challenging to define the mechanisms underlying these behavioral conditions or determine how altered L1CAM function contributes to them. Because most identified variants in behavioral disorders have mild effects, the current hypothesis is that it requires two or more variants that genetically interact to promote the manifestation of behavioral conditions. Identifying such genetic interactions will help uncover how L1CAMs and associated genetic networks govern behavior.

We previously identified several genetic interactions with the *C. elegans* canonical L1CAM encoded by the *sax-7* gene (Opperman et al. 2015). These genetic interactions uncovered a non-developmental role for *sax-7* in directing coordinated locomotion. Despite established roles in dendrite extension and morphogenesis, axon branching and fasciculation, and neural architecture maintenance, *sax-7* null animals do not have obvious locomotory defects. But in genetic backgrounds such as loss of *rab-3* GTPase or reduction of *unc-13* gene function, sax-7 null animals exhibit synthetic or synergistic uncoordinated (Unc) locomotion and neuronal dysfunction. Intriguingly, these synthetic phenotypes can be suppressed with late-onset, transient SAX-7 expression. Taken together with the fact that *rab-3* and *unc-13* have roles in neurotransmission, these findings suggest a role for *sax-7* in synaptic regulation. In this study, we use genetics, electrophysiology, and image analysis of synapses to assess how sax-7 promotes coordinated locomotion.

3.2. Results

sax-7 interacts with SV cycle genes, resulting in a coiling behavior

We previously identified a genetic interaction between *sax-7* and *rab-3*, which encodes a monomeric G-protein that is associated with synaptic vesicles in its GTP-bound state (Opperman et al. 2015). *rab-3; sax-7* double null animals display synthetic uncoordinated (Unc), loopy locomotion with a tendency to coil that is not observed in either *rab-3* or *sax-7* single null animals (Fig 1A, Suppl video). *rab-3; sax-7* double null animals, although not paralyzed, tend to meander locally, exhibiting apparent non-vectorial locomotion. As a result, *rab-3; sax-7* animals show limited radial displacement within a one minute period (Fig 1Bi, C). In contrast, *rab-3* or *sax-7* single mutant animals display robust dispersal behaviors with greater radial displacement within the one minute time frame.

114

The RAB-3 protein functions in the synaptic vesicle (SV) cycle for proper neurotransmission with roles that include the trafficking of synaptic vesicles to the active zone of synapses (Gracheva et al. 2008; Nonet et al. 1997). This interaction with *rab-3* suggests that *sax-7* may interact with additional genes that function in SV exocytosis. While most genetic mutants of SV cycle genes exhibit severely Unc phenotypes that preclude enhancement, we were nonetheless able to test for an interaction with *unc-10,* which encodes for the RAB-3-interacting molecule (RIM), a SV-recruiting active zone protein and *unc-13*, which forms a tripartite complex with RAB-3 and RIM, and functions in SV docking and priming at the synaptic active zone (Opperman et al. 2015; Richmond and Broadie 2002; Richmond, Weimer, and Jorgensen 2001; Dulubova et al. 2005). In combination with a loss of *sax-7*, we observed synthetic coiling behaviors and poor dispersal behaviors in the *unc-13* hypomorphic and *unc-10* null animals (Fig 1Bii, C). These results are consistent with the notion that *sax-7* interacts with SV cycle genes. In contrast, we did not observe an interaction between *sax-7* and genes with roles in synaptogenesis, such as *rpm-1* and *syd-1* (Cherra and Jin 2015; Schaefer, Hadwiger, and Nonet 2000; Zhen et al. 2000; Hallam et al. 2002; Patel et al. 2006). Loss of either *rpm-1* or *syd-1* in the *sax-7* null animals does not produce the coiling and poor dispersal behavior exhibited by *rab-3; sax-7* animals (Fig 1Biii, C). These results indicate that the *sax-7* interaction with SV cycle genes is specific.

The abnormal locomotory behaviors in double mutants of *sax-7* and SV cycle genes suggest underlying neuronal dysfunction. To test this notion, we measured the ability for *rab-3; sax-7* animals to swim in liquid and crawl on agar medium. The mean *rab-3; sax-7* swim rate is 20% that of Wild-type (Fig 2A). By comparison, the *rab-3* and *sax-7* average swim rates are 85% and 53% that of Wild-type, respectively. *rab-3; sax-7* double mutants also show a

synergistic decrease in crawl rates at 44% that of Wild-type; in contrast the *rab-3* and *sax-7* crawl rates are 116% and 82% that of Wild-type, respectively (Fig 2B). This synergistic reduction in swim and crawl rates is also observed in *sax-7* animals with impaired function of the SV genes *unc-13,* unc-*10*, or synaptobrevin-encoding *snb-1* (Nonet et al. 1998) (Fig 2). In contrast, *sax-7* double mutants with synaptogenesis genes, *rpm-1* and *syd-1,* do not exhibit such synergism (Fig 2). Not only are these results consistent with neuronal dysfunction contributing to the synthetic Unc and locomotion behaviors, but they also underscore the specificity of the *sax-7* interaction with SV cycle genes.

Sax-7 is required in the nervous system to promote coordinated locomotion

   sax-7 is expressed both in the nervous system and non-neuronal tissues, including body-wall muscles and the hypodermis (Chen, Ong, and Bennett 2001). Based on the Unc and locomotory deficiencies observed in *sax-7* double mutants with SV cycle genes, we predict that *sax-7* expression in the nervous system would suppress *rab-3; sax-7* phenotypes. However, non-neuronal *sax-7* expression has previously been shown to impact neural architecture maintenance, dendrite morphogenesis, and axon branching (Zhu et al. 2017; Diaz-Balzac et al. 2016; Salzberg, Diaz-Balzac, et al. 2013; Dong et al. 2013; Wang et al. 2005). To determine where *sax-7* is required for coordinated locomotion, we first established a conditional *sax-7* knock-in system using the Crispr-Cas9-engineered *sax-7(eq22)* allele. *eq22* is a DNA insertion in the penultimate exon of the *sax-7* gene that comprises coding sequence encoding mCherry interrupted by a gene-disrupting dual marker cassette comprising *Pmyo-3::GFP::unc-54 3'UTR* and *Prps-27::neoR::unc-54 3'UTR* sequences (Fig 3A) (Norris et al. 2015). As such, we expect disrupted *sax-7* function in *sax-7(eq22)* animals, which can be identified as neomycin-resistant animals

that express GFP in pharyngeal muscles. Indeed, *sax-7(eq22)* animals resemble *sax-7(eq1)* null animals, showing comparable reduced thrash rates (Fig 3B). Importantly, *eq22* also interacts with *rab-3*, producing similar synthetic coiling and Unc locomotion (data not shown) with similar synergistically-low thrash rates observed in *rab-3; sax-7(eq1)* animals (Fig 3B). Not only are these results consistent with *eq22* disrupting *sax-7* function, but they also demonstrate that the *sax-7* genetic interaction we observed with *rab-3* is not allele-specific.

In addition to the gene-disrupting cassette, the *eq22* DNA insertion also contains loxP sites flanking the gene-disrupting cassette (Fig 3Aii). The *loxP* sites provide the ability to direct the excision of the gene-disrupting cassette with tissue-specific Cre-recombinase expression for a targeted restoration of SAX-7 as a mCherry fusion protein (Fig 3A). Using germline Cre-recombinase expression, we successfully excised the gene-disrupting cassette in the *sax-7(eq22)* germline to generate the *eq23* allele. *sax-7(eq23)* animals are not neomycin-resistant and do not express GFP in the pharynx. Instead, they show SAX-7::mCherry expression and localization similar to that of endogenous SAX-7 (Fig S1A) (Chen, Ong, and Bennett 2001). Importantly, *sax-7(eq22)* phenotypes are suppressed in *sax-7(eq23)* animals. For example, *sax-7(eq23)* animals display a much higher thrash rate. Moreover, *eq23* does not interact with *rab-3*. *rab-3; sax-7(eq23)* do not display the *rab-3; sax-7(eq22)* Unc locomotion (data not shown) nor the synergistically-low thrash rate (Fig 3B). These results indicate that the SAX-7::mCherry protein expressed in *sax-7(eq23)* animals is functional.

To assess whether SAX-7 is required in the nervous system for proper locomotion in a *rab-3* background, we crossed into *rab-3; sax-7(eq22)* animals the *eqIs7* transgene, which drives neuronal Cre expression behind the *rgef-1* promoter. In *rab-3; sax-7(eq22); eqIs7* animals, neuronal *sax-7* expression is recovered with mCherry fluorescence present just in the nervous

system (Fig S1B). Importantly, *eqIs7* suppresses the *rab-3; sax-7(eq22)* Unc behavior (data not shown) and low thrash rates (Fig 3B), as does another neuronal-expressing Cre transgene, *tmIs778* (Kage-Nakadai et al. 2014). In contrast, body-wall muscle or hyp7 restoration of SAX-7 does not effectively suppress the *rab-3; sax-7*(*eq22)* phenotypes (Fig 3B). These results indicate a requirement for SAX-7 in the nervous system for coordinated locomotion in a *rab-3* null background.

A role for Erk signaling in locomotory behavior and function

One approach we took to determine the basis of the abnormal *rab-3; sax-7* locomotion and neuronal function was to perform a forward genetic screen for suppressors of the *rab-3; sax-7* Unc and coiling behavior. We isolated a strong suppressor, *eq7*, which we determined is a C-to-T transition resulting in a nonsense mutation in codon 546 of the *ksr-1* gene (kinase suppressor of Ras 1) that is consistent with a strong loss-of-function allele (see materials and methods). *rab-3; sax-7; ksr-1(eq7)* triple animals display similar locomotory and dispersal behavior as wild-type animals (Fig 4 A-C, video). In addition, their thrash and crawl rates are dramatically higher than those of *rab-3; sax-7* animals (Fig 5).   The *ksr-1* deletion allele, *ok786* ('large-scale screening for targeted knockouts in the Caenorhabditis elegans genome' 2012; Moerman and Barstead 2008), similarly suppresses *rab-3; sax-7* phenotypes (Fig 4, 5), confirming that loss of *ksr-1* function suppress *rab-3; sax-7* abnormal locomotion and neuronal defects. *ksr-1* single mutants do not have apparent locomotion deficiencies, displaying thrash and crawl rates that are similar to those of wild-type animals.

In addition to *rab-3; sax-7* phenotypes, *ksr-1(eq7)* also suppresses *unc-13; sax-7* defects, including their low swim and crawl rates (Fig 5). This suppression in the double mutants by loss

118

of *ksr-1* may be impacting the SV cycle, the SAX-7 pathway, or a third parallel pathway

regulating locomotion. Interestingly, the rescued swim and crawl rates in both *rab-3; sax-7; ksr-1* and *unc-13; sax-7; ksr-1* animals are more similar to those of *rab-3* and *unc-13*, respectively,

suggesting that loss of *ksr-1* may be impinging on the *sax-7* pathway rather than the SV cycle. If

this hypothesis is correct, loss of *ksr-1* should suppress *sax-7* phenotypes but not *rab-3* or *unc-13*

phenotypes. We chose to test this hypothesis using the thrashing assay since the *sax-7* phenotype

is robust in liquid and more modest on solid media (Fig 2A). In liquid, the *sax-7* swim rate of 86

thrashes/minute is 51% that of Wild-type while the *sax-7; ksr-1* swim rate of 154

thrashes/minute is 94% that of wild-type animals, showing almost complete suppression by loss

of *ksr-1*. By comparison, the impact of the loss of *ksr-1* on *unc-13* or *rab-3* swim rates is modest

(Fig 5A).

KSR-1 is a molecule that interacts with core components of the Mitogen-Activated

Protein Kinase (MAPK) cascade to facilitate the activation of the MAPK signaling pathway.

Because both putative loss-of-function *ksr-1* alleles suppressed *rab-3; sax-7* phenotypes, we

predicted that reducing the function of the MAPK, Erk, would similarly suppress *rab-3; sax-7*

phenotypes. To test this prediction, we crossed into *rab-3; sax-7* animals a null allele of Erk,

encoded by the *mpk-1* gene (Lackner et al. 1994)*.* Consistent with our hypothesis, *rab-3; mpk-1; sax-7* triple mutant animals display locomotory behavior and ability to swim that are similar to

that of wild-type animals (Fig 4, 5, video), revealing a role for MAPK signaling in regulating

locomotion and neuronal function. Interestingly, both *ksr-1* and *mpk-1* single mutant animals do

not display apparent locomotory deficiencies, suggesting that the role the MAPK signaling

pathway plays in coordinating locomotion is likely modulatory.

SAX-7 and KSR-1 do not affect SV release in ventral cord cholinergic motor neurons

A delayed response to the paralytic effects of the cholinesterase inhibitor, aldicarb, is often observed in animals with impaired SV exocytosis due to a slower build-up of acetylcholine in the synaptic cleft as compared to animals with wild-type SV exocytosis (Miller et al. 1996). Consistent with the role of *rab-3* in SV trafficking and recruitment to the active zone, *rab-3* mutant animals are mildly **r**esistant to **i**nhibitors of **c**holinesterase (RIC) (Gracheva et al. 2008; Nonet et al. 1997). Indeed, we observed ~10% of *rab-3* animals are still mobile after 180 minutes of exposure to 1mM aldicarb; at this time point, 100% of wild-type animals are paralyzed (Fig 6A). Although *sax-7* animals are not RIC, loss of *sax-7* synergistically enhances the RIC phenotype in *rab-3* animals (Fig 6), as previously reported (Opperman et al. 2015). Importantly, this robust *rab-3; sax-7* RIC phenotype can be dramatically suppressed by the loss of *ksr-1*, which by itself, responds to aldicarb similarly as wild-type animals (Fig 6). The *rab-3; sax-7* RIC phenotype, taken together with the accompanying Unc behavior and reduced swim and crawl rates, suggests *rab-3; sax-7* animals may have SV exocytosis defects.

To resolve potential SV abnormalities underlying *rab-3; sax-7* phenotypes, we performed synaptic electrophysiological analysis to determine functional consequences in *rab-3; sax-7* as compared to *rab-3; sax-7; ksr-1* and *rab-3, sax-7,* and *ksr-1* single mutant animals. Whole-cell voltage-clamped body recordings from medial ventral body wall muscles were directly assayed after stimulation of the ventral nerve cord. First, the average miniature event amplitude observed in each strain is similar to that of wild-type, suggesting that postsynaptic function in muscle does not account for the phenotypes observed in *rab-3; sax-7* animals (Fig 7). This finding is consistent with the poor ability of *sax-7* expression in muscle to rescue *rab-3; sax-7* phenotypes

(Fig 3B). Second, we examined the evoked responses in each strain. As expected, *rab-3* null animals exhibit reduced evoked responses, consistent with previous studies (Gracheva et al. 2008; Nonet et al. 1997), while *sax-7* and *ksr-1* animals showed wild-type evoked responses. Surprisingly and contrary to our prediction, *rab-3; sax-7* evoked responses were not significantly lower than that of *rab-3* animals (Fig 7). In fact, there was no significant difference among the evoked responses of *rab-3, rab-3; sax-7,* and *rab-3; sax-7; ksr-1.*

We also examined *rab-3; sax-7* synapses at the ultrastructural level using high pressure freeze electron microscopy (HPF-EM). As control, we first analyzed *rab-3* cholinergic presynaptic terminals. Consistent with published studies, we observed reduced numbers of docked SVs within 100nm of the presynaptic density in *rab-3* synapses (Fig 8B) (Gracheva et al. 2008). Interestingly, *rab-3; sax-7* synapses showed similar number of docked SVs within 100nm of the presynaptic density as *rab-3* synapses while *sax-7* synapses showed wild-type number of docked SVs. Moreover, *rab-3; sax-7; ksr-1* triple mutant animals showed a similar docking deficit as *rab-3* and *rab-3; sax-7* animals (Fig 8B). Surprisingly, *ksr-1* synapses also show a deficit in vesicle docking that is not consistent with the suppression of *rab-3; sax-7* neuronal phenotypes. These results are consistent with our findings in examining the synapses under light microscopy (Fig S2). Taken together, these data indicate that presynaptic dysfunction in the ventral cord cholinergic motor neurons is unlikely a contributing cause for the *rab-3; sax-7* Unc locomotion, RIC, swimming, and crawling phenotypes.

ksr-1 functions in a subset of cholinergic neurons in the head for coordinated locomotion.

A recent study uncovered a neuronal role for *ksr-1* (Coleman, Topalidou, and Ailion 2018). Specifically, loss-of-function *ksr-1* alleles were identified in a genetic screen for

suppressors of the hyperactive and loopy locomotion exhibited by activated Gq/EGL-30 animals. In addition, *ksr-1* expression in a subset of cholinergic neurons in the head of *egl-30; ksr-1* animals is sufficient to reverse the suppression; in contrast, *ksr-1* expression in ventral nerve cord cholinergic neurons in the body does not. To determine whether *ksr-1* similarly acts in cholinergic neurons to regulate locomotion in *rab-3; sax-7* animals, we used the promoter for the UNC-17 acetylcholine transporter to drive *ksr-1* expression in *rab-3; sax-7; ksr-1* cholinergic neurons. If *ksr-1* functions in cholinergic neurons, we expect to see a reversal of the rescued neuronal phenotypes observed in *rab-3; sax-7; ksr-1* animals by re-expressing *ksr-1* in cholinergic neurons. Indeed, expression of *ksr-1* under an acetylcholine neuron promoter (P_{unc-17}) or under a head acetylcholine neuron promoter in *rab-3; sax-7; ksr-1* resulted in a reversal of the suppression, which was manifested as Unc, coiling locomotion and reduced thrash rates (Fig 9). Importantly, head expression of *ksr-1* ($P_{unc-17H}$) in wild-type animals does not cause Unc locomotion or decrease in swim rates. In contrast, we did not see reversal of the suppression when *ksr-1* is expressed in *rab-3; sax-7; ksr-1* in the body cholinergic neurons with the $P_{unc-17B}$ promoter. These results indicate that *ksr-1* function in locomotion is restricted to head cholinergic neurons. This finding likely accounts for the absence in neuronal dysfunction or abnormality in ventral nerve cord synapse assayed in our electrophysiology and EM analyses.

We next assessed whether *sax-7* functions in the same set of neurons as *ksr-1* in coordinating locomotion. Using the same set of promoters, we expressed Cre-recombinase in *rab-3; sax-7(eq22)* animals to restore *sax-7* expression in head vs body cholinergic neurons. In both cases, we did not observe rescue of *rab-3; sax-7(eq22)* locomotion and thrash rates. Similarly, restoring *sax-7* expression in all cholinergic neurons using the full-length P_{unc-17} promoter also failed to suppress *rab-3; sax-7(eq22)* phenotypes. These results indicate that *sax-7*

expression in cholinergic neurons alone is not sufficient to rescue *rab-3; sax-7* phenotypes, suggesting *sax-7* function is also required in additional non-cholinergic neurons.

3.3. Discussion

In this study, we examine a genetic interaction between *sax-7* and key players in the synaptic vesicle cycle that result in synergistic abnormalities in locomotion behavior and neuronal function. We show that *sax-7* specifically interacts with SV cycle genes, *rab-3*, *unc-10*, and *unc-13* to regulate locomotion behavior in *C. elegans*. As *sax-7* is expressed in the nervous system as well as non-neuronal tissues, including body-wall muscles and the hypodermis, we further specify that the locomotory function of *sax-7* is mediated by its expression in the nervous system.

To determine the basis of the abnormal *rab-3; sax-7* locomotion and neuronal function, we conducted a genetic screen for suppressors of the *rab-3; sax-7* Unc and coiling behavior and identified KSR-1 as a genetic target. KSR-1 is a Mitogen-Activated Protein Kinase (MAPK) scaffold protein interacting with core components of the cascade to facilitate the activation of the MAPK signaling pathway. In addition to KSR-1, its downstream target, Erk (MPK-1), also suppresses the *rab-3; sax-7* Unc and coiling behavior phenotypes. As *ksr-1* and *mpk-1* single mutant animals do not exhibit apparent locomotory deficiencies, this suggests that the role of the MAPK signaling pathway in coordinating locomotion is likely modulatory.

Although *sax-7* animals do not show resistance to inhibitors of cholinesterase (RIC), loss of *sax-7* synergistically enhances the RIC phenotype in *rab-3* animals, as previously reported (Opperman et al. 2015). Similar to the behavior phenotypes, this robust *rab-3; sax-7* RIC phenotype can be dramatically suppressed by the loss of *ksr-1*. The *rab-3; sax-7* RIC phenotype,

123

indicated that *rab-3; sax-7* animals might have defective SV release. Interestingly, we did not

observe any significant difference in the evoked responses at neuromuscular junctions (NMJs) of

rab-3, rab-3; sax-7, and *rab-3; sax-7; ksr-1.* Similarly, there was no difference in the

ultrastructure of the cholinergic synapses, including number and distribution of docked SVs,

among these genotypes. Our electrophysiology and EM data concluded that the cholinergic

synapses in the ventral body wall muscles are not responsible for the *sax-7* mediated locomotory

phenotype.

A recent study shows that the Erk signaling acts in head acetylcholine neurons to

modulate Gq-rho signaling in controlling locomotion behavior (COLEMAN *et al.* 2018). The Gq

pathway has been known to regulate various aspects of *C. elegans* locomotion behavior

including the rate of locomotion and waveform. Different pathways downstream of Gq are

known to contribute differntially to these locomotion behaviors (Lackner, Nurrish, and Kaplan

1999; Topalidou et al. 2017). Taking our data and these studies into account, we analyzed the

impact of head and body specific expression of *ksr-1*. Indeed, expression of *ksr-1* under a head

acetylcholine neuron promoter in *rab-3; sax-7; ksr-1* resulted in a reversal of the suppression

whereas expression in the body did not. Our data suggests that *sax-7* functions in the head

cholinergic neurons together with Erk signaling to potentially influence acetylcholine release in

ventral motor cord neurons indirectly.

The roles of *sax-7* and Erk signaling in regulating nervous system function are uncovered

only in sensitized genetic backgrounds pointing to their roles in fine-tuning neural activity.

Supporting this notion are studies implicating L1CAM function and increased Erk activity in a

variety of neuropsychiatric disorders as well as in learning and memory.

3.4. References

2012 large-scale screening for targeted knockouts in the Caenorhabditis elegans genome. G3 (Bethesda) 2**:** 1415-1425.

Chen, L., B. Ong and V. Bennett, 2001 LAD-1, the Caenorhabditis elegans L1CAM homologue, participates in embryonic and gonadal morphogenesis and is a substrate for fibroblast growth factor receptor pathway-dependent phosphotyrosine-based signaling. J Cell Biol 154**:** 841-855.

Cherra, S. J., 3rd, and Y. Jin, 2015 Advances in synapse formation: forging connections in the worm. Wiley Interdiscip Rev Dev Biol 4**:** 85-97.

Coleman, B., I. Topalidou and M. Ailion, 2018 Modulation of Gq-Rho Signaling by the ERK MAPK Pathway Controls Locomotion in Caenorhabditis elegans. Genetics 209**:** 523-535.

Diaz-Balzac, C. A., M. Rahman, M. I. Lazaro-Pena, L. A. Martin Hernandez, Y. Salzberg *et al.*, 2016 Muscle- and Skin-Derived Cues Jointly Orchestrate Patterning of Somatosensory Dendrites. Curr Biol 26**:** 2379-2387.

Dong, X., O. W. Liu, A. S. Howell and K. Shen, 2013 An extracellular adhesion molecule complex patterns dendritic branching and morphogenesis. Cell 155**:** 296-307.

Dulubova, I., X. Lou, J. Lu, I. Huryeva, A. Alam *et al.*, 2005 A Munc13/RIM/Rab3 tripartite complex: from priming to plasticity? Embo j 24**:** 2839-2850.

Gracheva, E. O., G. Hadwiger, M. L. Nonet and J. E. Richmond, 2008 Direct interactions between C. elegans RAB-3 and Rim provide a mechanism to target vesicles to the presynaptic density. Neurosci Lett 444**:** 137-142.

Hallam, S. J., A. Goncharov, J. McEwen, R. Baran and Y. Jin, 2002 SYD-1, a presynaptic protein with PDZ, C2 and rhoGAP-like domains, specifies axon identity in C. elegans. Nat Neurosci 5**:** 1137-1146.

Kage-Nakadai, E., R. Imae, Y. Suehiro, S. Yoshina, S. Hori *et al.*, 2014 A conditional knockout toolkit for Caenorhabditis elegans based on the Cre/loxP recombination. PLoS One 9**:** e114680.

Lackner, M. R., K. Kornfeld, L. M. Miller, H. R. Horvitz and S. K. Kim, 1994 A MAP kinase homolog, mpk-1, is involved in ras-mediated induction of vulval cell fates in Caenorhabditis elegans. Genes Dev 8**:** 160-173.

Lackner, M. R., S. J. Nurrish and J. M. Kaplan, 1999 Facilitation of synaptic transmission by EGL-30 Gqalpha and EGL-8 PLCbeta: DAG binding to UNC-13 is required to stimulate acetylcholine release. Neuron 24**:** 335-346.

Miller, K. G., A. Alfonso, M. Nguyen, J. A. Crowell, C. D. Johnson *et al.*, 1996 A genetic selection for Caenorhabditis elegans synaptic transmission mutants. Proc Natl Acad Sci U S A 93**:** 12593-12598.

Moerman, D. G., and R. J. Barstead, 2008 Towards a mutation in every gene in Caenorhabditis elegans. Brief Funct Genomic Proteomic 7**:** 195-204.

Nonet, M. L., O. Saifee, H. Zhao, J. B. Rand and L. Wei, 1998 Synaptic transmission deficits in Caenorhabditis elegans synaptobrevin mutants. J Neurosci 18**:** 70-80.

Nonet, M. L., J. E. Staunton, M. P. Kilgard, T. Fergestad, E. Hartwieg *et al.*, 1997 Caenorhabditis elegans rab-3 mutant synapses exhibit impaired function and are partially depleted of vesicles. J Neurosci 17**:** 8061-8073.

Norris, A. D., H. M. Kim, M. P. Colaiacovo and J. A. Calarco, 2015 Efficient Genome Editing in Caenorhabditis elegans with a Toolkit of Dual-Marker Selection Cassettes. Genetics 201**:** 449-458.

Opperman, K., M. Moseley-Alldredge, J. Yochem, L. Bell, T. Kanayinkal *et al.*, 2015 A novel nondevelopmental role of the sax-7/L1CAM cell adhesion molecule in synaptic regulation in Caenorhabditis elegans. Genetics 199**:** 497-509.

Patel, M. R., E. K. Lehrman, V. Y. Poon, J. G. Crump, M. Zhen *et al.*, 2006 Hierarchical assembly of presynaptic components in defined C. elegans synapses. Nat Neurosci 9**:** 1488-1498.

Richmond, J. E., and K. S. Broadie, 2002 The synaptic vesicle cycle: exocytosis and endocytosis in Drosophila and C. elegans. Curr Opin Neurobiol 12**:** 499-507.

Richmond, J. E., R. M. Weimer and E. M. Jorgensen, 2001 An open form of syntaxin bypasses the requirement for UNC-13 in vesicle priming. Nature 412**:** 338-341.

Salzberg, Y., C. A. Diaz-Balzac, N. J. Ramirez-Suarez, M. Attreed, E. Tecle *et al.*, 2013 Skin-derived cues control arborization of sensory dendrites in Caenorhabditis elegans. Cell 155**:** 308-320.

Schaefer, A. M., G. D. Hadwiger and M. L. Nonet, 2000 rpm-1, a conserved neuronal gene that regulates targeting and synaptogenesis in C. elegans. Neuron 26**:** 345-356.

Topalidou, I., P. A. Chen, K. Cooper, S. Watanabe, E. M. Jorgensen *et al.*, 2017 The NCA-1 and
NCA-2 Ion Channels Function Downstream of G(q) and Rho To Regulate Locomotion in
Caenorhabditis elegans. Genetics 206**:** 265-282.

Wang, X., J. Kweon, S. Larson and L. Chen, 2005 A role for the C. elegans L1CAM homologue
lad-1/sax-7 in maintaining tissue attachment. Dev Biol 284**:** 273-291.

Zhen, M., X. Huang, B. Bamber and Y. Jin, 2000 Regulation of presynaptic terminal
organization by C. elegans RPM-1, a putative guanine nucleotide exchanger with a
RING-H2 finger domain. Neuron 26**:** 331-343.

Zhu, T., X. Liang, X. M. Wang and K. Shen, 2017 Dynein and EFF-1 control dendrite
morphology by regulating the localization pattern of SAX-7 in epidermal cells. J Cell Sci
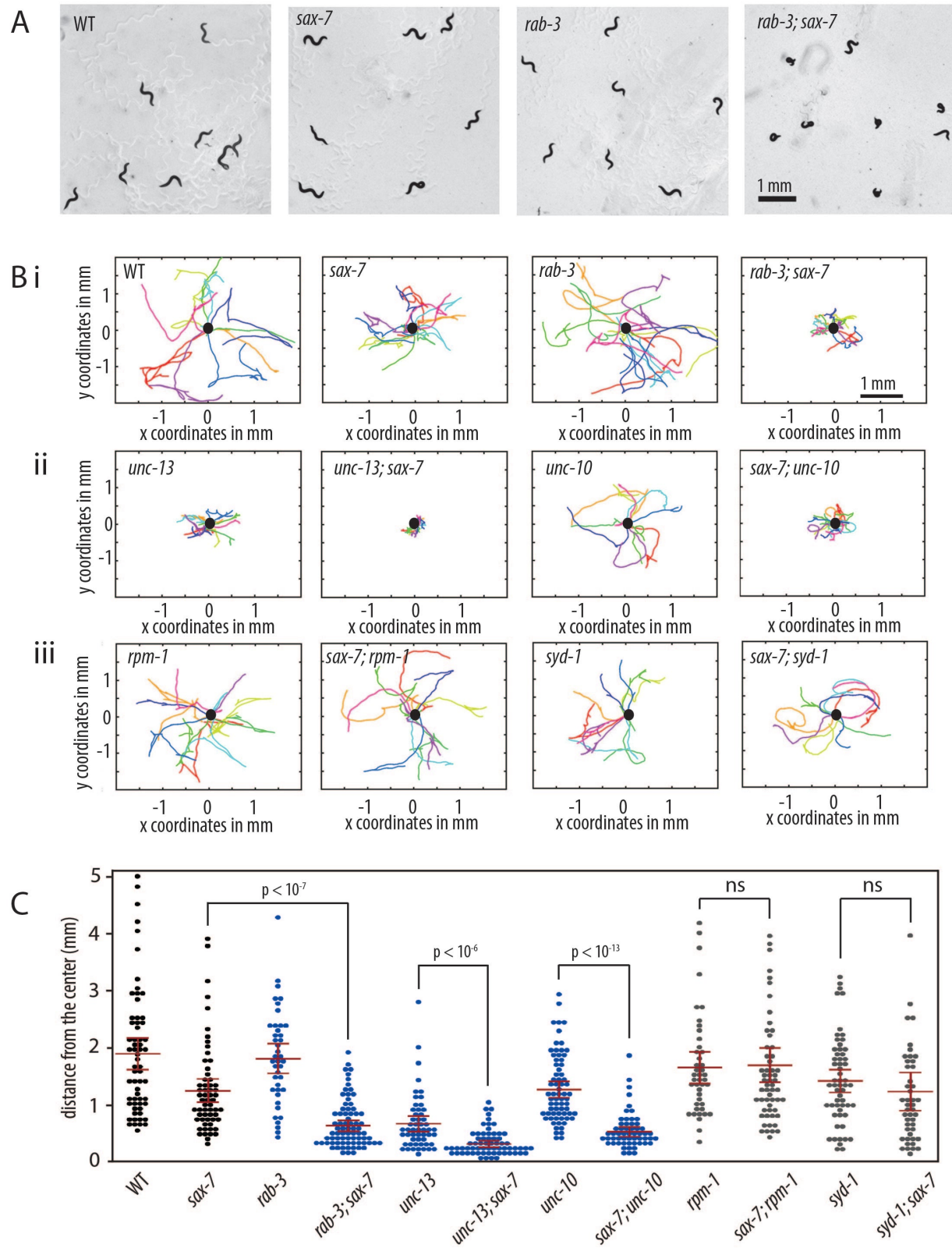130**:** 4063-4071.

Figure 1

Figure 1. sax-7 interacts with genes that function in the SV cycle but not in synaptogenesis.

(A) *rab-3; sax-7* mutant animals exhibit synthetic Unc locomotion with a tendency to coil, unlike either *rab-3* or *sax-7* single mutant animals. (B) Graphs tracing the movements of 10 random animals per strain over a span of one minute. Each colored line represents the tracks of an individual animal with the point of origin marked as a black circle in the center (0,0 coordinate). These graphs reveal that *sax-7* interacts with SV cycle genes, (i) *rab-3* as well as (ii) *unc-13* and *unc-10,* resulting in a synergistically-reduced ability to disperse. In contrast, *sax-7* does not interact with genes that function in synaptogenesis, (iii) *rpm-1* and *syd-1*. (C) The ability to disperse, quantified as the radial distance travelled by each animal over a span of one minute, is illustrated in a scatter plot where each point is a data point for a single animal; the mean with the 95% confidence interval are marked in red. The blue plots are data points for mutant strains of SV cycle genes while grey plots show data points for mutant strains of synaptogenesis genes. n = 50 – 75, p-values are shown, n.s., not significant, one-way ANOVA with Bonferroni's *post hoc* test. Data collected by Lihsia Chen lab.
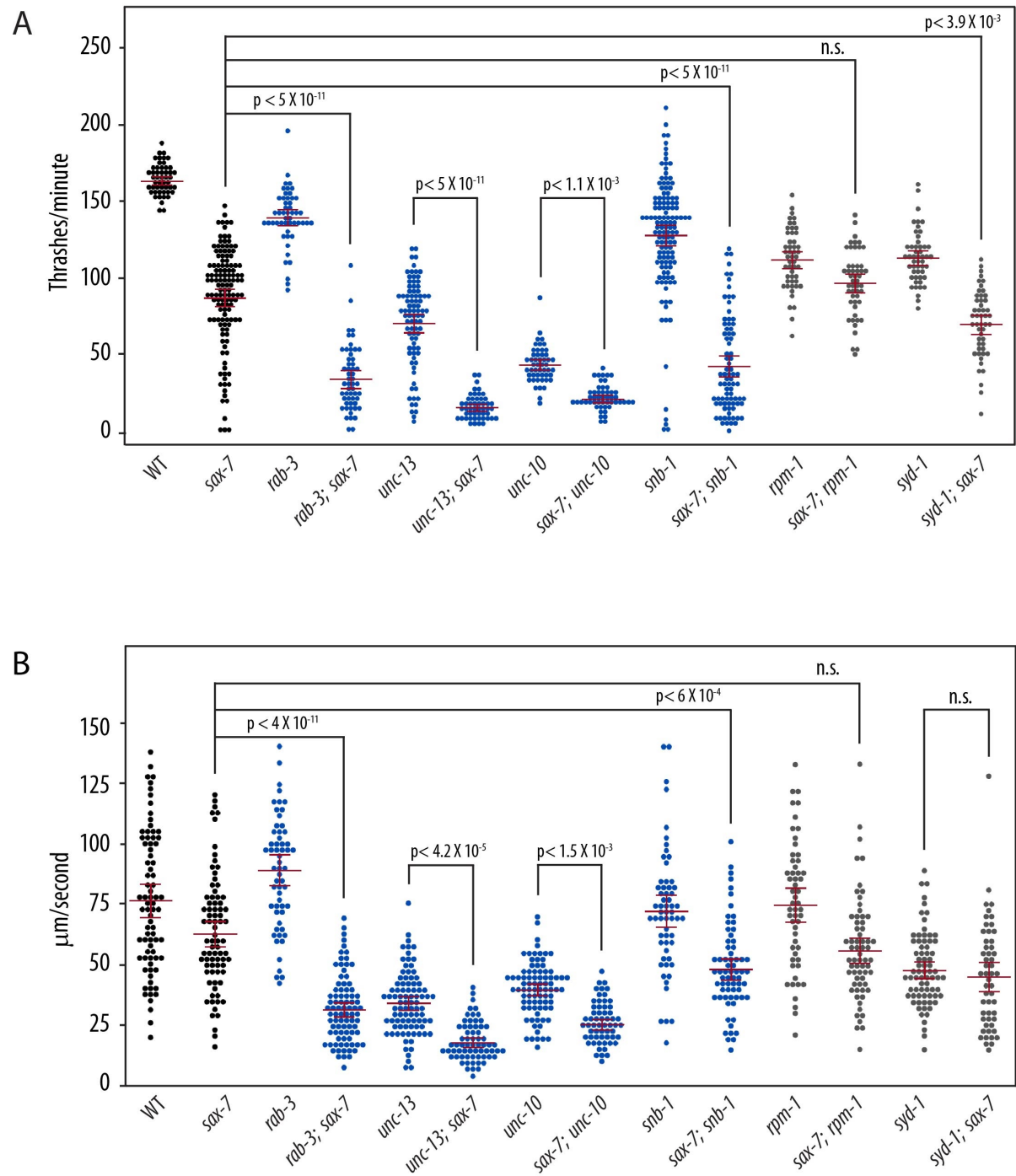
Figure 2

Figure 2. sax-7 double mutants with SV cycle genes display synergistic neuronal dysfunction

(A) sax-7 interacts with SV cycle but not synaptogenesis genes, showing synergistic reduction in thrash rates (number of thrashes per minute), which are represented as a percentage of the wild-type thrash rate at 163.3 ± 1.4 thrashes per minute. Error bars show 2X standard error of the proportion n = 50-75. n.s., not significant, one-way ANOVA with Bonferroni's *post hoc* test. (B) sax-7 interacts with SV cycle but not synaptogenesis genes, resulting in a synergistic reduction in crawl rates (mm per second). The crawl rate of each strain is shown in two ways: (i) a combined scatter and box-and-whisker plot where the ends of the box are the upper and lower quartiles and the line within the box is the median; (ii) a percentage of the wild-type crawl rate at 80.5 ± 4 mm per second. Error bars show 2X standard error of the proportion, n = 50-75. n.s., not significant, one-way ANOVA with Bonferroni's *post hoc* test. Data collected by Lihsia Chen lab.
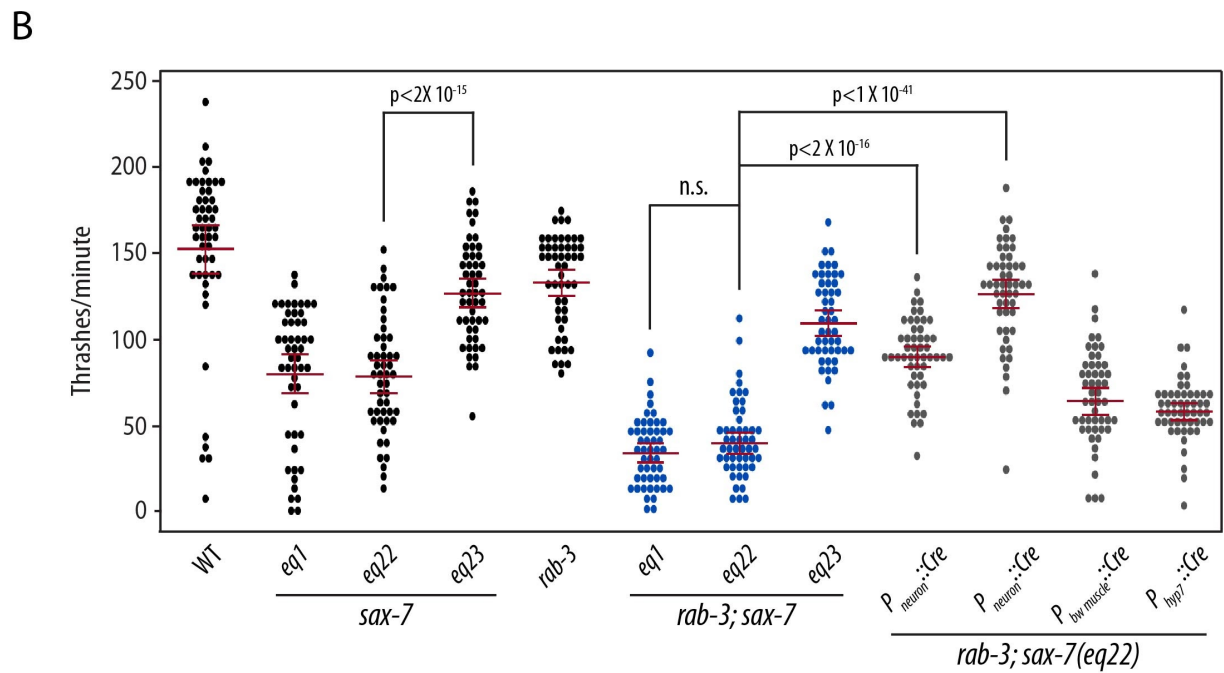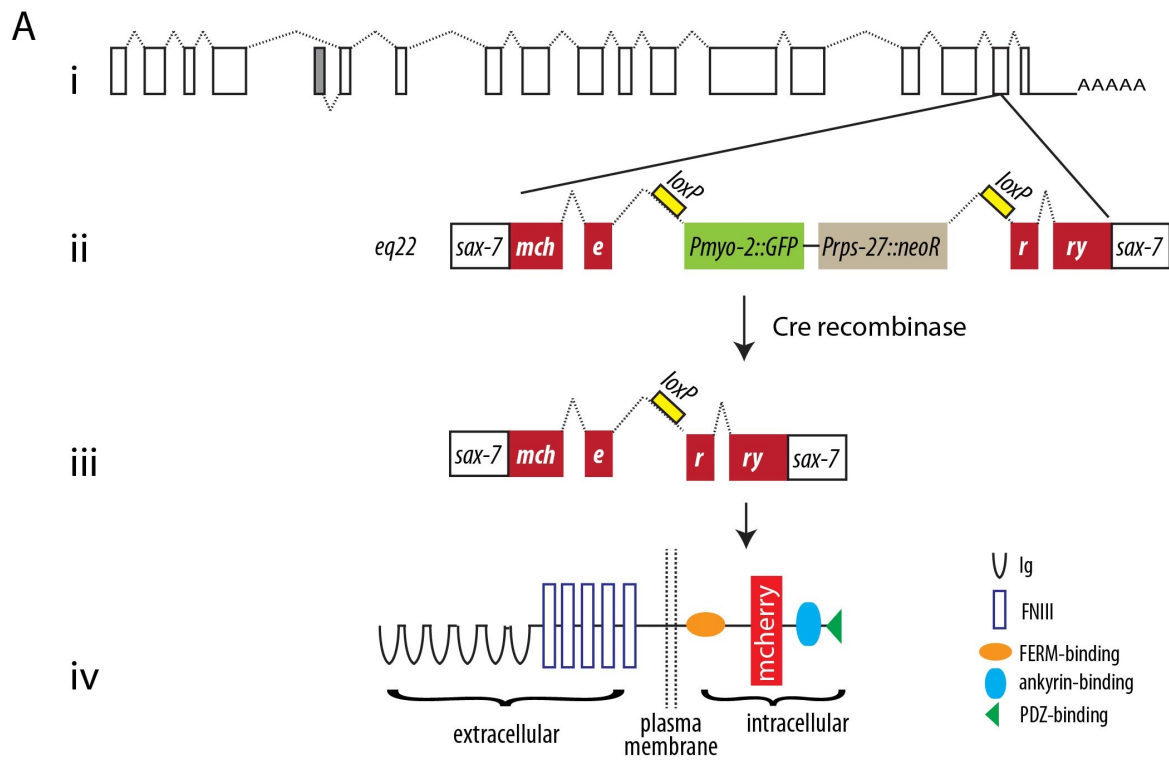
Figure 3

Figure 3. Neuronal expression of *sax-7* rescues *rab-3; sax-7* uncoordinated locomotion and neuronal dysfunction

(A) A schematic of the conditional *sax-7* knock-in allele, *eq22*. (i) Gene structure of the *sax-7* locus, with boxes representing exons and dotted lines representing introns; the grey box represents an exon used in alternatively-spliced isoform of *sax-7* (Chen, Ong, and Bennett 2001). *eq22* is an insertion into the penultimate *sax-7* exon of (ii) mCherry sequence and a gene-disrupting cassette (P*myo-2*::GFP and P*rps-27*::neoR) that interrupts the *sax-7* reading frame. This gene-disrupting cassette, which is flanked by loxP sites in intronic sequences, can be excised out with tissue-specific Cre-recombinase expression to restore *sax-7* expression as (iv) a full-length SAX-7::mCherry fusion protein. Cre-recombinase expression in the germline results in the *eq23* allele. (B) Quantitation of thrash rates reveal that *eq22* resembles the *eq1* null allele and similarly interacts with *rab-3* for a synergistically reduced thrash rate. On the contrary, *eq23* is more similar to Wild-type and does not interact with *rab-3*. Neuronal restoration of SAX-7 (using two independent neuronal CRE-expressing transgenes *eqIs* and *tmIs778*, repespectively) dramatically rescues the *rab-3; sax-7* thrash rate; in contrast, body-wall muscle or hypodermal restoration of SAX-7 shows poor rescue of *rab-3; sax-7* thrash rate. Error bars show 2X standard error of the proportion of at least 2 sample sets where n = 25 for each set. n.s., not significant, one-way ANOVA with Bonferroni's *post hoc* test. Data collected by Lihsia Chen lab.

Figure 4

A

B

C

134

Figure 4. Reducing Mitogen Activated Protein Kinase (MAPK) signaling suppresses *rab-3; sax-7* uncoordinated locomotion

(A) Null alleles of *ksr-1* or *mpk-1* suppress *rab-3; sax-7* uncoordinated locomotion yet *ksr-1* or *mpk-1* null animals themselves do not exhibit apparent locomotion abnormalities. (B) Graphs tracing the movements of 10 random animals per strain over a span of one minute. Each colored line represents the tracks of an individual animal with the point of origin marked as a black circle in the center (0,0 coordinate). These graphs reveal that loss of *ksr-1* or *mpk-1* effectively suppress *rab-3; sax-7* reduced ability to disperse. (C) The ability to disperse, quantified as the radial distance travelled by each animal over a span of one minute, is illustrated in a scatter plot where each point is a data point for a single animal; the mean with the 95% confidence interval are marked in red. The blue plots are data points for mutant strains of SV cycle genes while grey plots show data points for mutant strains of synaptogenesis genes. n = 50 – 75, p-values are shown, n.s., not significant, one-way ANOVA with Bonferroni's *post hoc* test. Data collected by Lihsia Chen lab.

Figure 5
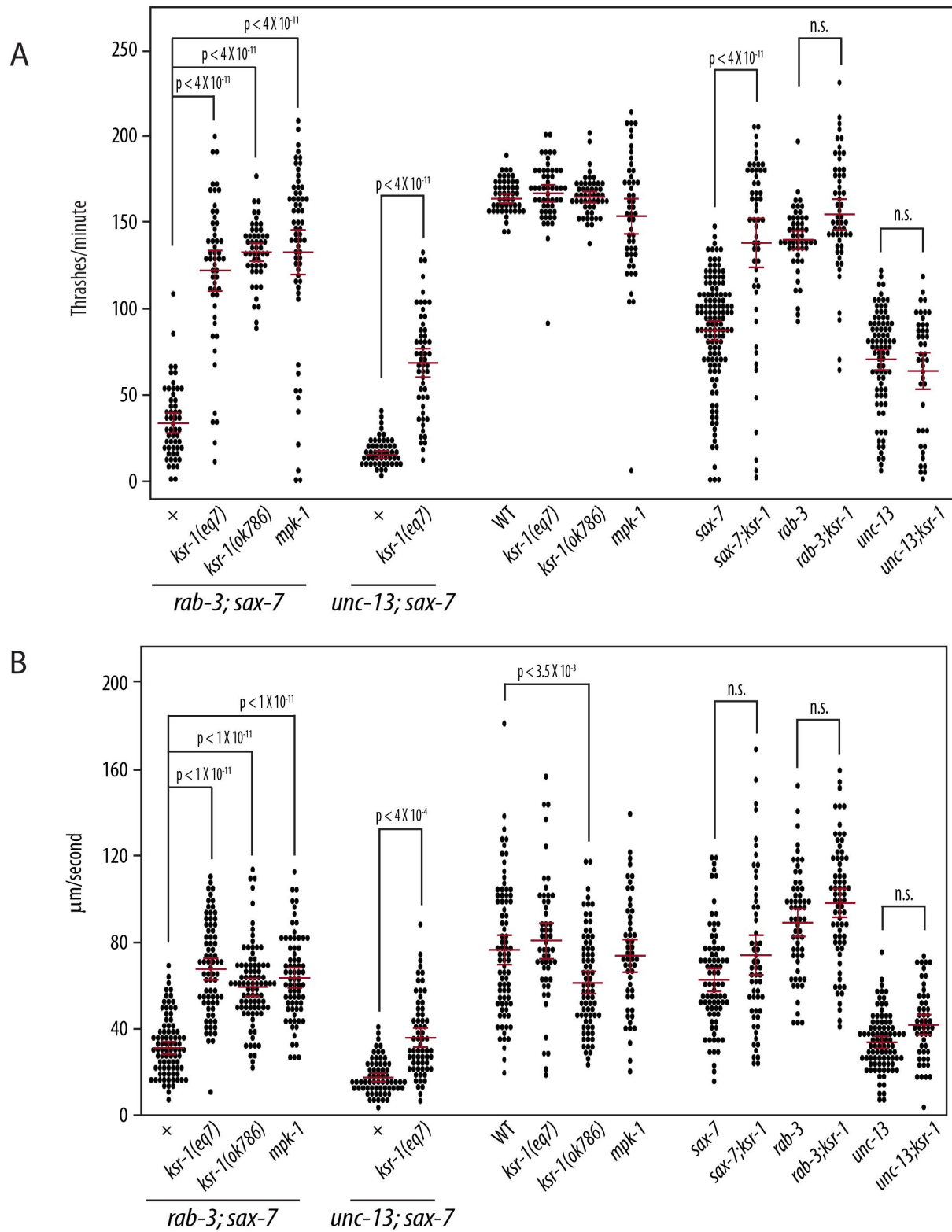
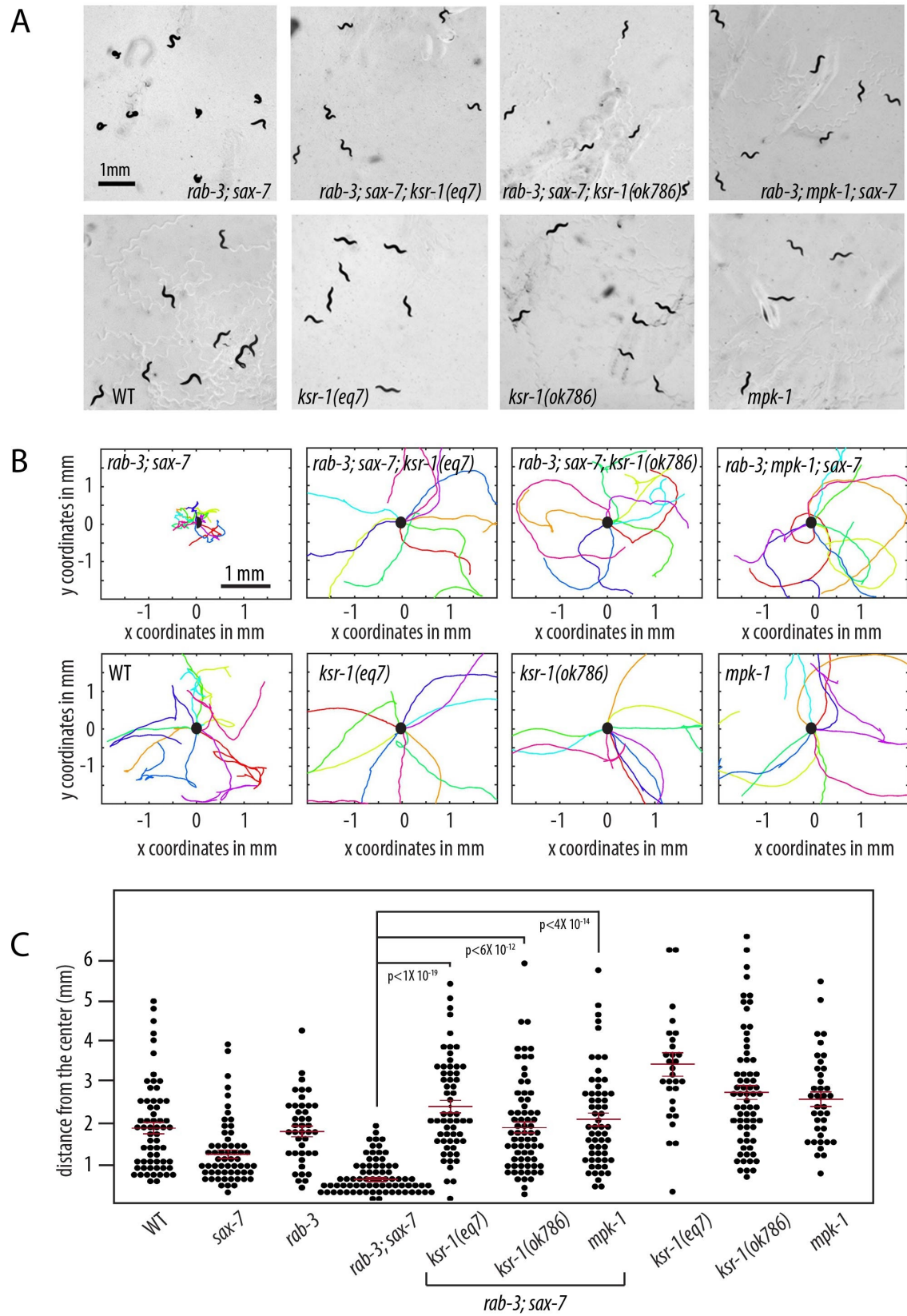**Figure 5. Reducing MAPK signaling suppresses neuronal dysfunction resulting from loss of sax-7 function**

Quantitation of neuronal dysfunction as assessed in (A) swim and (B) crawl assays reveals that while *ksr-1* or *mpk-1* null animals have similar swim and crawl rates as wild-type animals, *ksr-1* and *mpk-1* null alleles can suppress both *rab-3; sax-7* and *unc-13; sax-7* synergistically reduced swim and crawl rates. Moreover, loss of ksr-1 can suppress the reduced swim and crawl rates exhibited by *sax-7* null animals, but not of *rab-3* or *unc-13* animals, suggesting *ksr-1* interacts with *sax-7*. Error bars show 2X standard error of the proportion, n = 50-75. n.s., not significant, one-way ANOVA with Bonferroni's *post hoc* test. Data collected by Lihsia Chen lab.

Figure 6
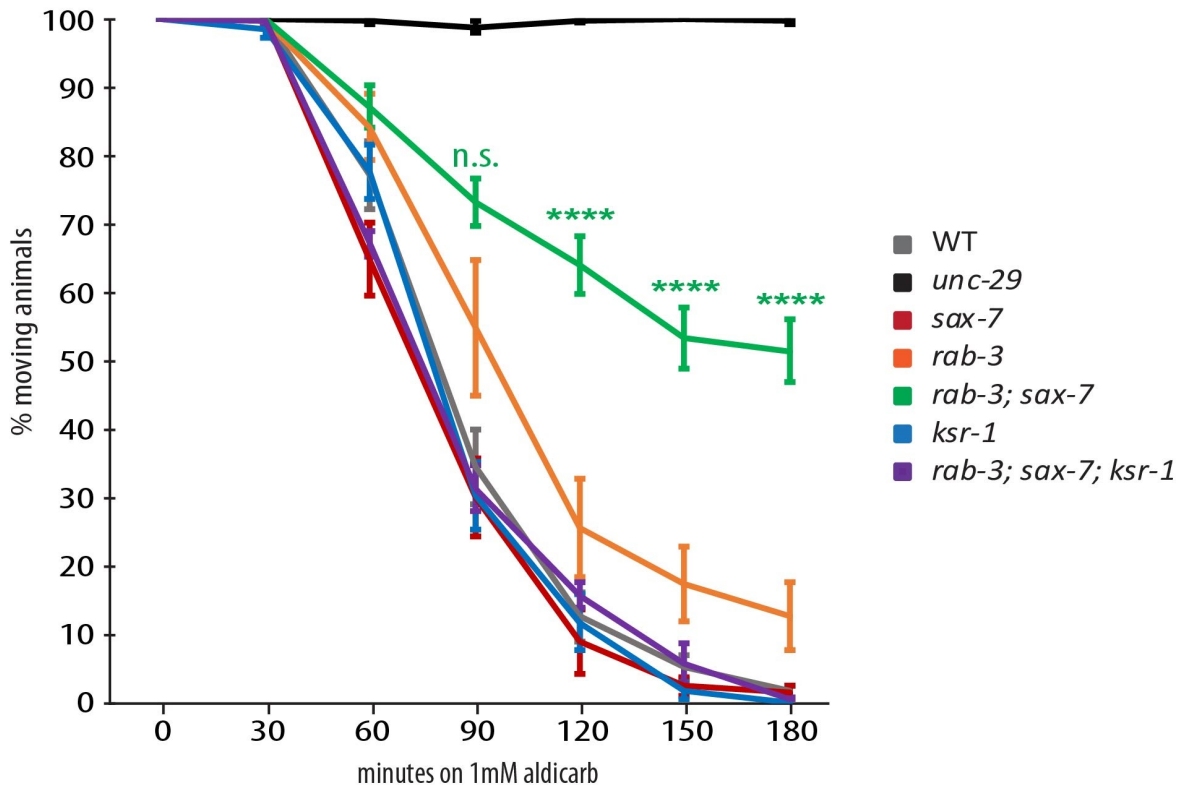
Figure 6. The synergistic resistance to aldicarb exhibited by *rab-3; sax-7* animals is suppressed by loss of *ksr-1* function

A graph showing a timed response of animals to exposure to the acetylcholinesterase inhibitor, aldicarb. Like Wild-type, both *sax-7* and *ksr-1* null animals become completely paralyzed after 180 minutes of aldicarb exposure. While *rab-3* null animals show modest aldicarb resistance with ~85% animals paralyzed at 180 minutes, *rab-3; sax-7* animals show synergistic aldicarb resistance with 50% animals paralyzed at the same time point. This synergistic aldicarb resistance can be significantly suppressed by loss of *ksr-1* function. Error bars show the S.E.M. of at least 12 sample sets, where n = 25 animals per set. **** P-value $< 1 \times 10^{-4}$, n.s., not significant, two-way ANOVA with Bonferroni's *post hoc* test. Data collected by Lihsia Chen lab.

Figure 7
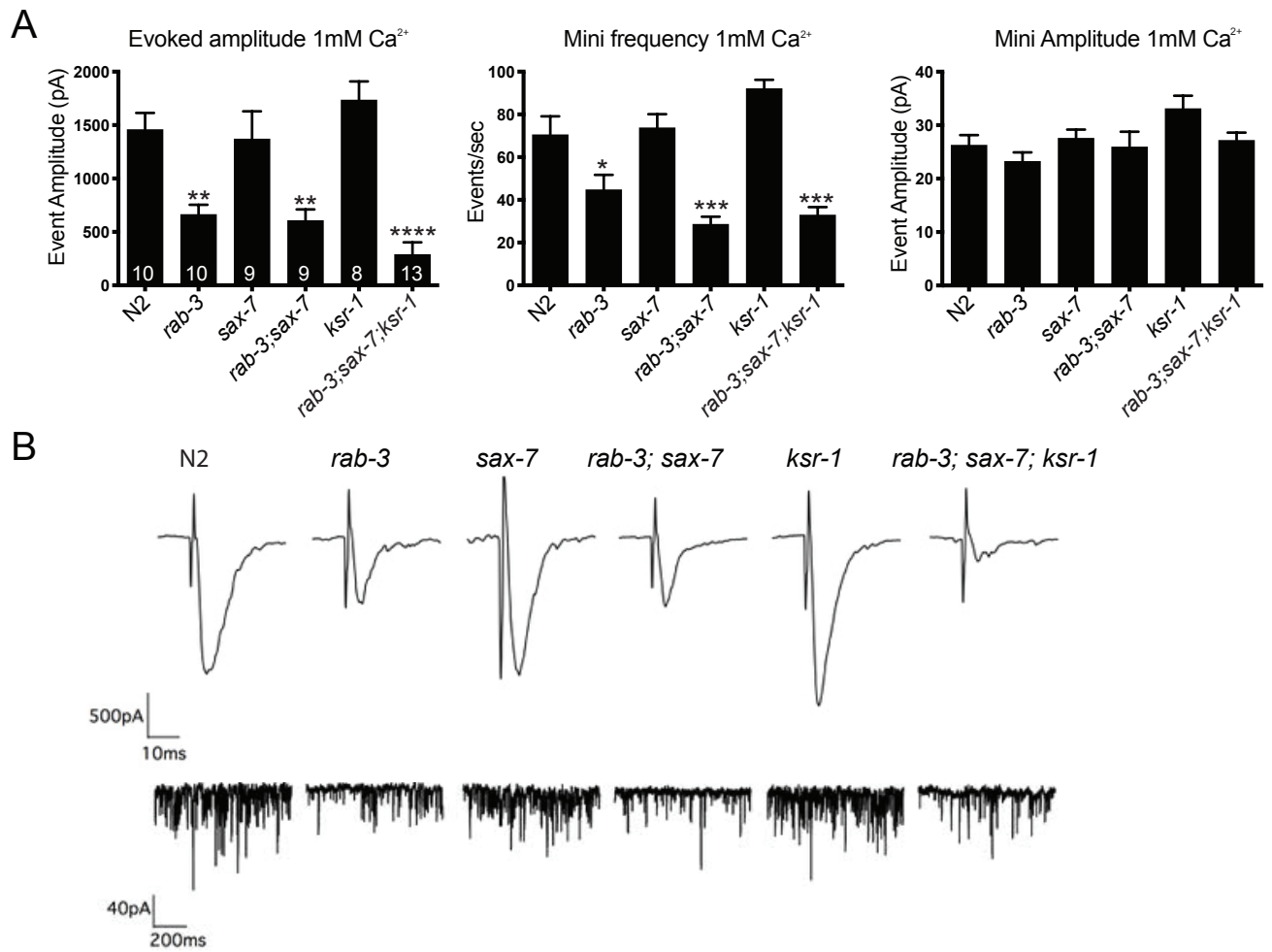
**Figure 7. SAX-7 and KSR-1 do not affect neurotransmitter release in ventral cord cholinergic motor neurons.**

(A) Whole-cell voltage-clamped body recordings from medial ventral body wall muscles (held at -60mV in 1mM Ca^{2+}) of dissected worms. The graphs show the average evoked amplitude, mini frequency, and mini amplitude at the NMJ of each strain. Number of animals analyzed per genotype are mentioned within the bars. Data shown as mean ± SEM (B) Representative evoked traces (top panel) and miniature traces (bottom panel) for genotypes labeled on the top. Data collected by Janet E. Richmond.

Figure 8

A
M=muscle N=neuron
∗Dense Projection ↑Docked vesicle

B

C
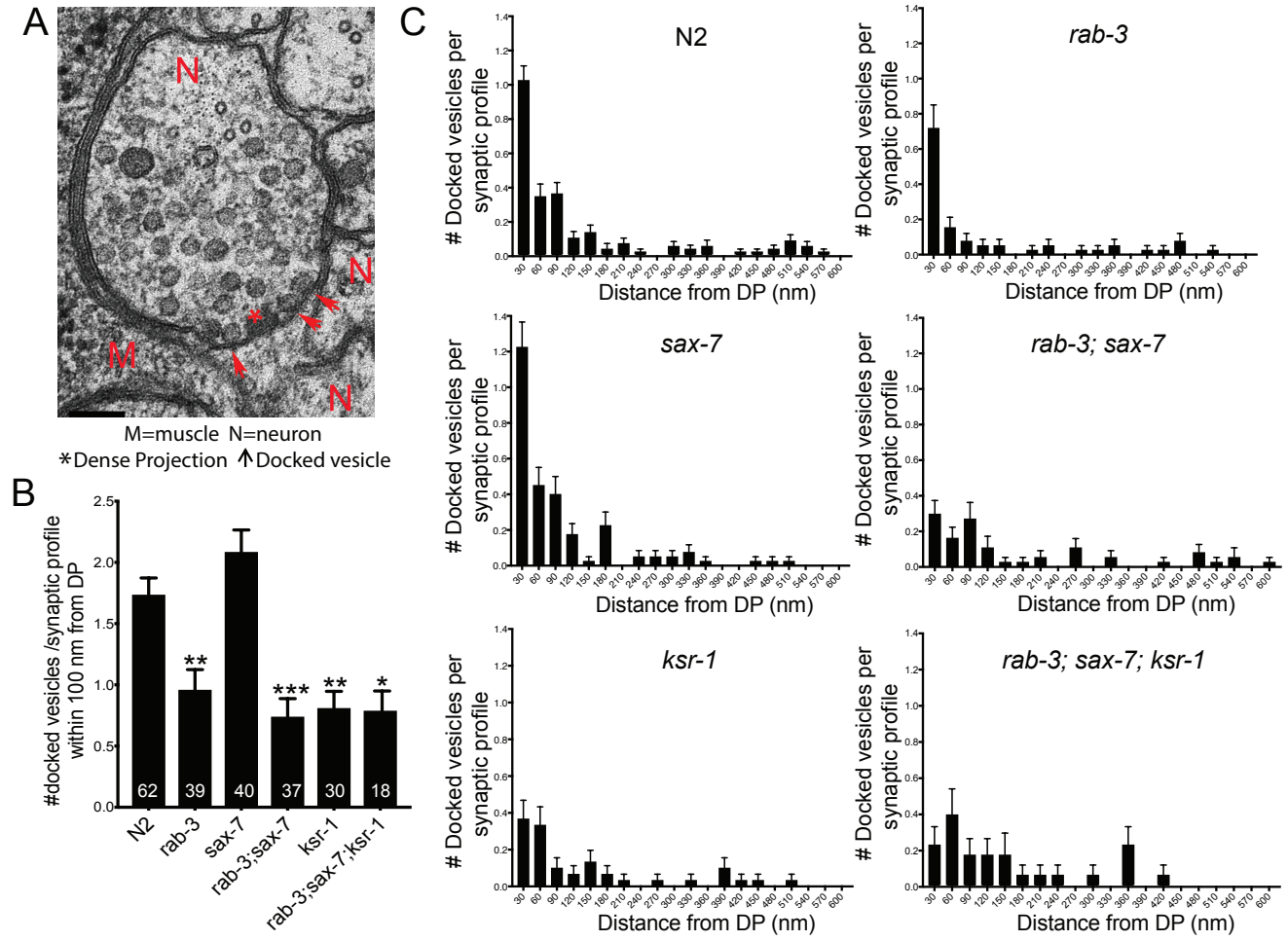
Figure 8. SAX-7 and KSR-1 do not affect number or distribution of docked SVs in ventral cord cholinergic motor neurons

(A) A representative electron micrograph of a cholinergic synaptic profile. (B) Average number of docked SVs per synaptic profile within 100 nm distance from dense projection (DP) or presynaptic density. Number of synaptic profiles analyzed per genotype are mentioned within the bars. (C) Distribution of docked SVs with respect to the dense projection. Data shown as mean ± SEM. Data collected by Seema Sheoran.

Figure 9
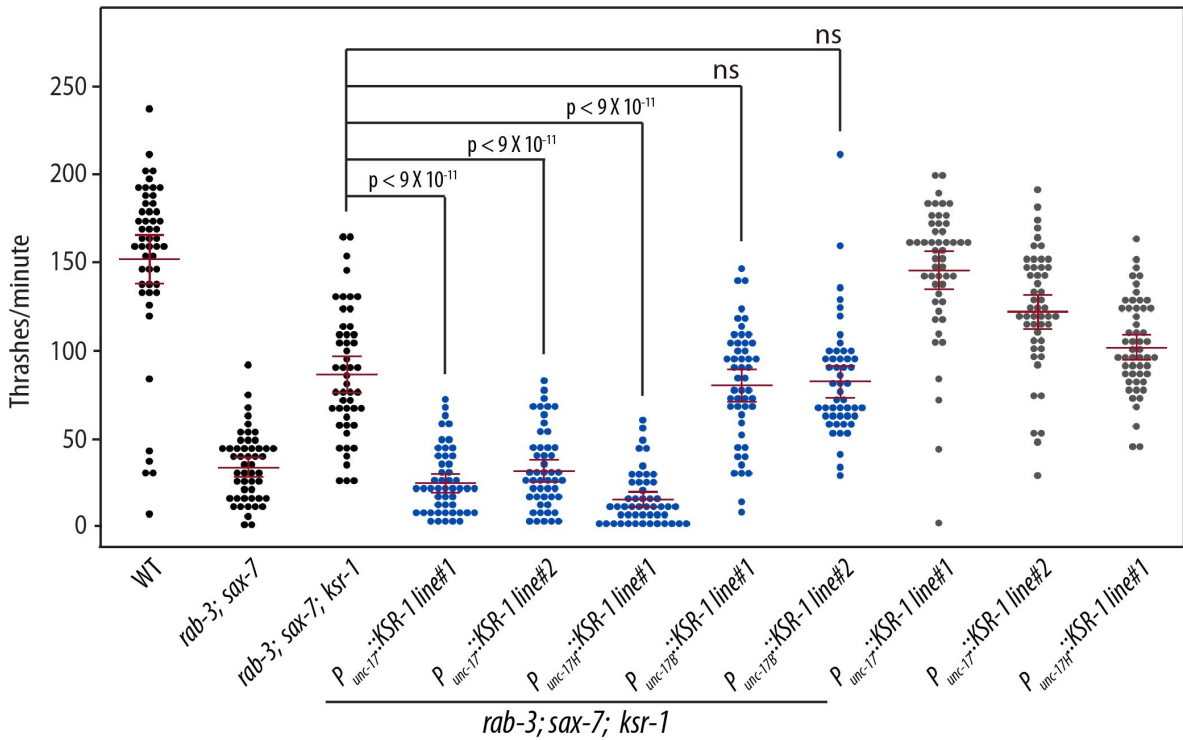
Figure 9. ksr-1 functions in a subset of cholinergic neurons in the head to modulate *rab-3; sax-7* neuronal function.

Loss of *ksr-1* suppresses *rab-3; sax-7* reduced swim rates, which are represented as a percentage of the wild-type thrash rate at 163.3 ± 1.4 thrashes per minute. This suppression is reversed to *rab-3; sax-7* levels by driving transgenic expression of *ksr-1* in all cholinergic neurons with the *unc-17* acetylcholine transporter promoter. This *rab-3; sax-7* swim rate is similarly restored when transgenic expression of *ksr-1* is restricted to a subset of *rab-3; sax-7; ksr-1* cholinergic neurons in the head using a partial *unc-17* promoter ($P_{unc-17H}$). In contrast, transgenic *ksr-1* expression confined to *rab-3; sax-7; ksr-1* cholinergic motor neurons in the body using a partial *unc-17* promoter ($P_{unc-17B}$) does not. Wild-type animals carrying each transgene exhibit normal swim rates. Error bars show 2X standard error of the proportion n = 50-75. n.s., not significant, two-way ANOVA with Bonferroni's *post hoc* test. Data collected by Lihsia Chen lab.

Figure Supplemental 1
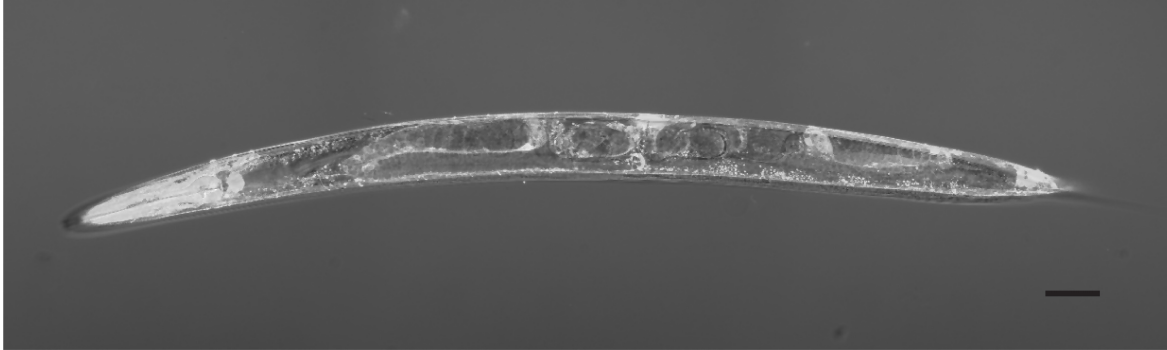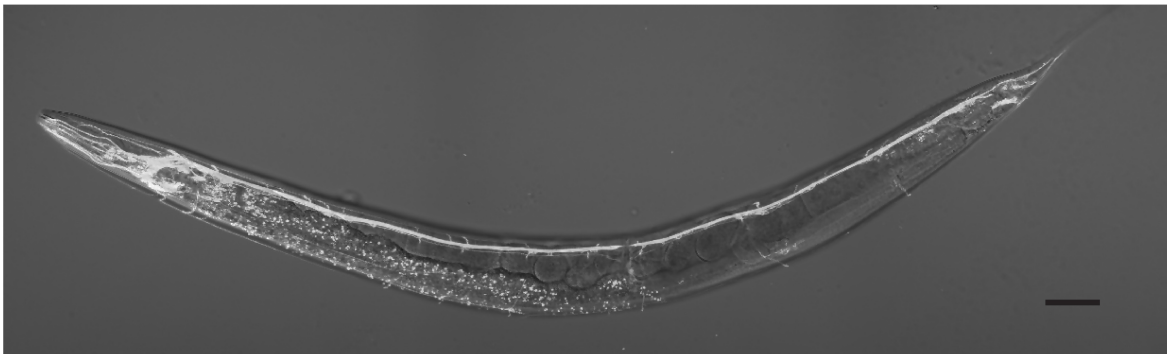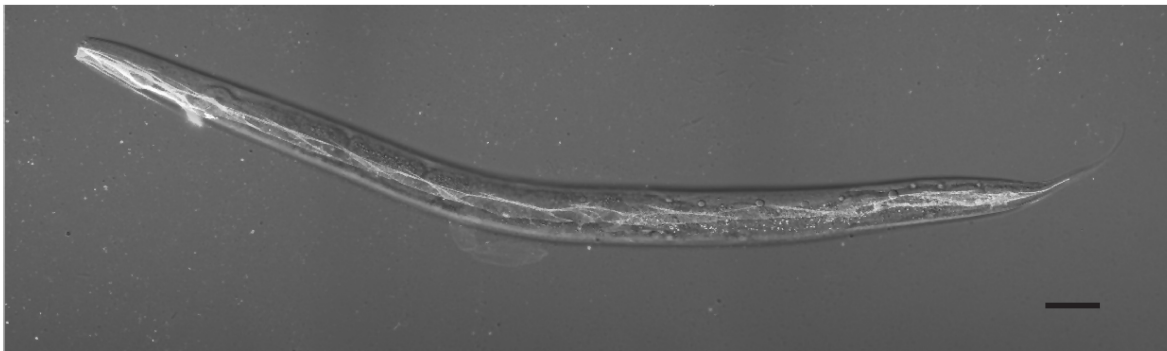
**Fig S1. An overlay over DIC images of *sax-7*(*eq22*) animal showing restored SAX-7::mCherry using tissue-specific Cre-recombinase expression.**

(A) Germline Cre-recombinase expression in sax-7(eq22) excises a gene-disrupting between loxP sites to generate sax-7(*eq23*) where endogenous SAX-7::mCherry is restored in all tissues. Tissue-specific Cre-recombinase expression in *sax*-7(eq22) was directed by crossing in pRab-3::Cre or Pmyo-3::Cre transgenes to restore endogenous SAX-7::mCherry expression (B) neurons and (C) body-wall muscles, respectively. Data collected by Lihsia Chen lab.

A. GABA neuron (P$_{unc-25}$::*snb-1*::*gfp*)
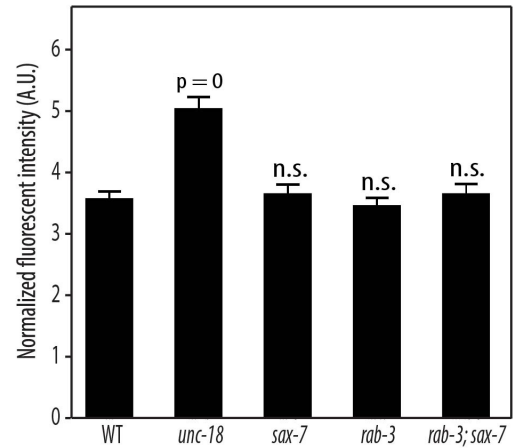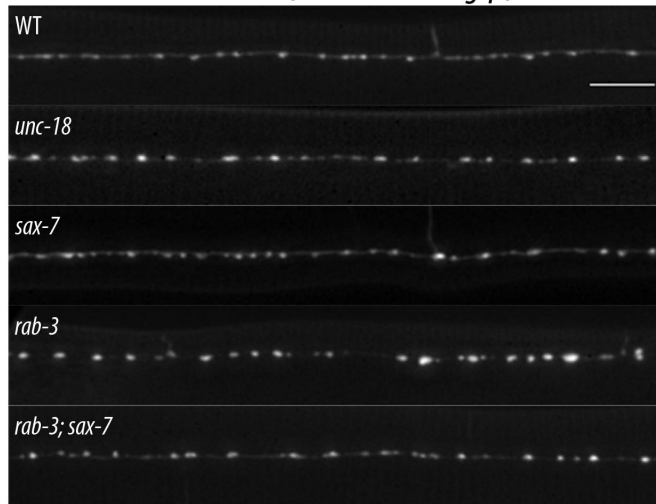
B. Cholinergic (P$_{unc-4}$::*snb-1*::*gfp*)
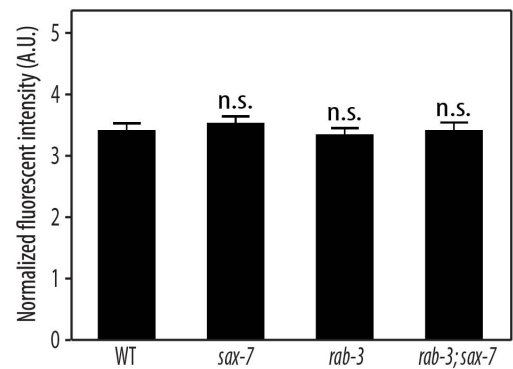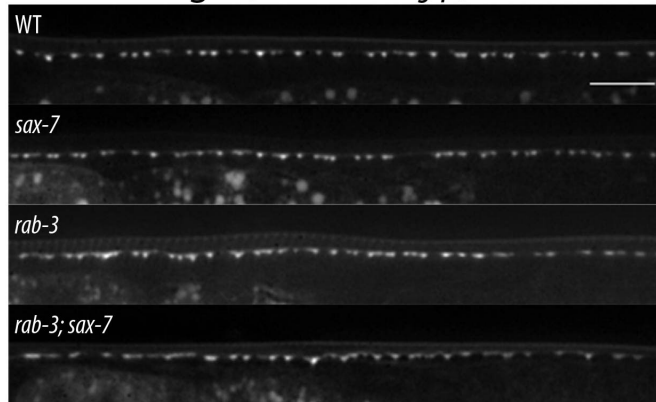
C. DA9 neuron (P$_{mig-13}$::*snb-1*::*yfp*)
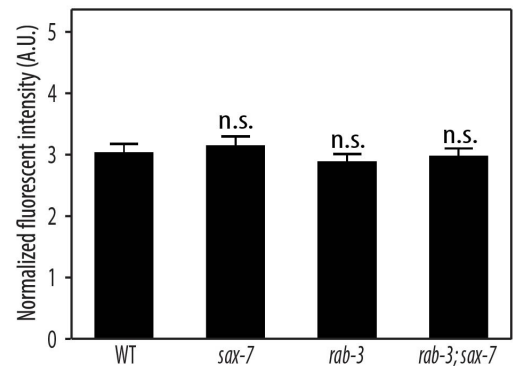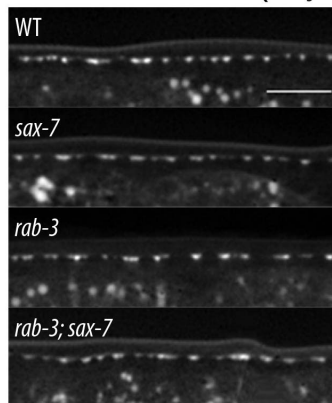
Fig S2. In vivo imaging and quantitation of the synaptic protein SNB-1::GFP reveals no apparent abnormalities in *rab-3; sax-7* synapses.

In vivo imaging and quantitation of SNB-1::GFP in reveal no apparent abnormalities in the number or intensity at *rab-3; sax-7* (A) GABA and cholinergic (B and C) synapses. In contrast, control *unc-18* animals (A) show the increased punctal intensity expected in animals with impaired synaptic vesicle release. Data collected by Lihsia Chen lab.

CHAPTER IV: CHARACTERIZATION OF VPS-39 IN THE CONTEXT OF SV RELEASE

4.1. Introduction

Recent studies have implicated the HOPS complex in nervous system function (see Chapter 1 for details). In yeast, the HOPS complex interacts with the yeast syntaxin homolog Vam 3 which in turn forms a SNARE complex with the SNAP-25 homolog Vam7 to mediate vesicle docking/fusion (Sato et al. 2000). The mammalian HOPS complex members (hVps11, hVPS18, hVPS16) are found to be highly enriched in the nervous system and specifically interact with the SNARE protein Syntaxin 1A, as well as Munc18 which regulates SNARE complex assembly required for neurotransmitter release (Kim et al. 2006). Overexpression of these HOPS complex members leads to asynchronous discharges in cultured hippocampal neurons suggesting a regulatory function for HOPS complex in synaptic transmission. In *Drosophila*, HOPS complex mediated endo-lysosomal trafficking has been shown to regulate turnover of SV associated protein, synaptobrevin, facilitating neurotransmitter release (Fernandes et al. 2014). These recent studies showing that the HOPS complex interacts with core components of the synaptic vesicle release machinery, specifically syntaxin and Munc18, encouraged us to explore the precise role of the HOPS complex in nervous system. This chapter presents a detailed characterization of one of the main components of the HOPS complex, VPS-39.

4.2. Materials and methods

Genetics

Strains were maintained at 20 °C on NGM agar plates seeded with OP50 bacteria (Brenner 1974). Genotypes used are as follows:

1. Bristol N2. Wild type/control strain.

2. *vps-39(tm2253)*. Loss of function allele balance with pF25B3.3::GFP to overcome maternal-effect sterility (SY1245).

3. VPS-39 rescue transgenic lines.

   Pvps-39::vps-39::mCherry::unc-54 3'UTR; vps-39(tm2253) [jaEx1056, SY1455]

   Pvps-39::vps-39::mCherry::unc-54 3'UTR; vps-39(tm2253), str-1::GFP [jaIs1096, SY1517]

   Pvps-39::vps-39::mCherry::unc-54 3'UTR; vps-39(tm2253), str-1::GFP [jaIs1099, SY1540]

Molecular Biology

Constructs expressing VPS-39 were generated using the MultiSite Gateway Three-Fragment Vector Construction Kit. 1.6 kb upstream of VPS-39 was amplified and cloned into pDONR P4-P1R (Invitrogen) using the following primers (homologous recombination sites compatible with the gateway vector are shown in red):

GGGGACAACTTTGTATAGAAAAGTTGCGCTTTCTTCAGCACAGGGTTCTTC and

GGGGACTGCTTTTTTGTACAAACTTGCCATTTTGCTTTGGTGGGTCGAAG

Genomic *vps-39*was amplified excluding its stop codon and cloned into pDONR 221 using following primers:

GGGGACAAGTTTGTACAAAAAAGCAGGCTCGATGTACGATGCATACACGCCTTGC

and GGGGACCACTTTGTACAAGAAAGCTGGGTCATTTCTGTTTCCTCCTTGAGAATC.

After final recombination into pDEST R4-R3 Vector II, all constructs were injected at concentration 10 ng/ml using STR-1::GFP as a co-injection marker. TMP mutagenesis was used

to integrate extrachromosomal transgenic lines. Integrated lines were then outcrossed four times to get rid of any background mutations.

Confocal Microscopy

Worms were mounted on 2% agarose pads with 10% sodium azide. All images were acquired using the Olympus Fluoview laser scanning confocal microscope. Images were analyzed using the ImageJ software. Fluorescent intensity was measured for region of interest spanning 10 mm long sections of the ventral nerve cord anterior to the vulva.

Dylox Assay

Worms were placed on dylox/trichlorfon treated plates (final concentration 5 mM) and examined every 10 min for 130 min. For each genotype, 10 worms at young adult stage were used per test. Each test was replicated at least three times. Worms were scored as paralyzed upon failure to respond to touch with a platinum wire. All tests were conducted after being blinded to the genotypes.

Electrophysiology

Electrophysiology was performed as published previously (Richmond 2009). Animals were immobilized using Histoacryl Blue glue. To expose NMJs, Incisions were made anterior to the vulva using a glass needle. Recordings were conducted in the whole-cell voltage-clamp mode at a holding potential of -60 mV using an EPC-10 HEKA amplifier, digitized at 1kHz. The 5 mM extracellular Ca^{2+} solution contained 5 mM $CaCl_2$, 150 mM NaCl, 5 mM KCl, 4 mM $MgCl_2$, 10 mM glucose, 5 mM sucrose, and 15 mM HEPES (~340 mOsm, pH 7.3). Ca^{2+} was replaced with

NaCl in the 0.5 mM extracellular Ca^{2+}. The patch pipette contained 5 mM (N

tris[Hydroxymethyl] methyl-2-aminoethane-sulfonic acid), 120 mM KCl, 20 mM KOH, 4 mM

MgCl2, , 0.25 mM CaCl2, 4 mM NaATP, 36 mM sucrose, and 5 mM EGTA (pH 7.4, ~315

mOsm). Data was collected using Pulse software (HEKA, Southbro, MA, US) and analyzed

using Pulsefit (HEKA), Mini analysis (Synaptosoft Inc., Decatur, GA, US) and Igor Pro

(Wavemetrics, Lake Oswego, OR, US).

Electron Microscopy

Samples were prepared using high-pressure freeze fixation (Weimer et al. 2006). ~30

young adult hermaphrodites were placed in each specimen chamber containing *E. coli* and were

rapidly frozen at -180°C under high pressure (Leica HPM 100). Frozen specimens then

underwent freeze substitution (Leica Reichert AFS) during which samples were held at −90°C

for 107 hr in 0.1% tannic acid and 2% OsO4 in anhydrous acetone. The temperature was then

increased at 5°C/hr to −20°C, kept at −20°C for 14 hr, and increased by 10°C/hr to 20°C. After

fixation, samples were infiltrated with 50% Epon/acetone for 4 hr, 90% Epon/acetone for 18 hr,

and 100% Epon for 5 hr. Finally, samples were embedded in Epon and incubated for 48 hr at

65°C. Ultrathin (40 nm) serial sections were cut using a Leica Ultracut 6 and collected on

formvar-covered, carbon-coated copper grids (EMS, FCF2010-Cu). Poststaining was performed

using 2.5% aqueous uranyl acetate for 4 min, followed by Reynolds lead citrate for 2 min.

Images were acquired using a JEOL JEM-1220 transmission electron microscope operating at 80

kV using a Gatan digital camera at a magnification of 100k (1.8587 pixels/nm). Images were

collected from the ventral nerve cord region anterior to the vulva for all genotypes. Serial

micrographs were manually annotated using NIH ImageJ/Fiji software to quantify the number of

SVs, number of plasma membrane docked SVs, and distance of docked SVs from the dense projection (DP) for each synaptic profile. Specimens were encrypted to ensure unbiased analysis. Cholinergic synapses were identified on the basis of their typical morphology (White et al. 1986). A synapse was defined as a series of sections (profiles) containing a dense projection as well as two flanking sections on both sides without dense projections. SVs were identified as spherical, light grey structures with an average diameter of ~30 nm. A docked synaptic vesicle was defined as a synaptic vesicle whose membrane was morphologically contacting the plasma membrane. Image acquisition and analysis using NIH ImageJ/Fiji software were performed blinded for genotype.

4.3. Results

Neuronal expression of VPS-39 is essential for embryonic development

With the aim of understanding the role of the HOPS complex in neuronal function, we conducted a detailed analysis of one of its main components, VPS-39, known to mediate interactions between Rab7 and the SNARE complex. VPS-39 is a highly conserved protein containing three known domains, a Rab Binding Domain (RBD), a Clathrin Heavy Chain Repeat (CHCR), and a Membrane Localization Domain (MLD) (Fig. 1A). *C. elegans* VPS-39 shares 30% identity and 50% homology with the human homolog, hVam6.

We used a *vps-39 (tm2253)* mutant strain obtained from the CGC to study the neuronal function of VPS39. *tm2253* allele contains a 1045 base pair (bp) deletion and a 4 bp insertion spanning exons 7-9 (Fig. 1B). *vps-39 (tm2253)* is a recessive mutation with maternal-effect embryonic lethality. As these mutants have hatching defect, the strain is maintained by balancing

over a GFP marker. *vps-39* mutants with the genetic balancer result in *vps-39 (tm2253)* one quarter homozygous progeny that survive to adulthood.

To determine the expression pattern of VPS-39, we generated transgenic animals containing an mCherry tag at the C-terminal of VPS-39. We observed expression of VPS-39 in multiple tissue types including muscles, coelomocytes (a type of phagocytes), and neurons (Fig. 2A). Interestingly, neuronal re-expression of VPS-39 under a pan-neuronal *rab-3* promoter (*Prab-3*) in *vps-39* mutants partially rescued the embryonic lethality, indicating that neuronal expression of VPS-39 is critical at the early developmental stage (Fig. 2B,C).

Axonal transport of VPS-39 is Kinesin-3 molecular motor dependent

SVs are transported from the cell body to the synapses using the microtubule associated molecular motor, Kinsein-3 (UNC-104). In order to determine if the synaptic localization of the VPS-39 is dependent on the SV transport mechanism, expression of the VPS-39::mCherry was observed in *unc-104* hypomorphic mutants (as the null is lethal) (Fig. 3). Impaired UNC-104 motor protein function results in accumulation of VPS-39::mCherry in the cell body of motor neurons with a concomitant reduction at the distal synapses. These results suggest that VPS-39 is transported from the neuronal cell body to the synapses via direct or indirect interaction with SV associated molecular motors.

VPS-39 promotes cholinergic synaptic transmission

Given that *C. elegans* VPS-39 is expressed in neurons and its neuronal expression is critical for early embryonic viability, we next assayed synaptic function in *vps-39* mutants.

Acetylcholine (ACh) release at the neuro-muscular junctions (NMJs) can be indirectly measured using an acetylcholinesterase inhibitor, trichlorfon (dylox). Exposure to dylox results in buildup of ACh in the synaptic cleft, leading to paralysis by hyper-contracting body wall muscles (Fig. 4A, B). Mutants with defective ACh release take longer to accumulate ACh in the synaptic cleft and for the resultant paralysis. When *vps-39* mutants were tested, we observed a dylox-resistant phenotype. We were able to reverse this phenotype through neuronal specific re-expression of VPS-39 in *vps-39* mutants (Fig. 4C). As one of the two different integrated lines used for the rescue of dylox sensitivity experiment contained the mCherry tag, our results confirm the functionality of the VPS-39::mCherry construct used in the previous expression pattern analysis (Fig. 4D). The dylox-resistant phenotype of *vps-39* mutants suggest an important function of VPS-39 in neurotransmitter release.

Mutant animals can also show resistance to dylox due to defects in synaptogenesis or overall defective neuronal outgrowth. To rule out this possibility we analyzed the neuronal architecture of *vps-39* mutants by labelling cholinergic motor neurons with pACR2::GFP (Fig. 5A). We found that the overall neuronal morphology including axon fasciculation and axon targeting in *vps-39* mutants was similar to wild type (Fig. 5B,C). We also analyzed the expression pattern of the post synaptic nicotinic receptor, ACR-16::GFP, and found no difference in the fluorescence intensity of the ACR-16 receptor in *vps-39* mutants in comparison to wild type (Fig. 5D,E). These data showing normal synaptogenesis and localization of post-synaptic receptors in *vps-39* mutants along with the neuronal recue of the dylox-resistant phenotype in *vps-39* mutants indicate that VPS-39 acts at the presynaptic level to regulate ACh release.

To understand the nature of the presynaptic defects in *vps-39* mutants, whole-cell voltage-clamped body wall muscle recordings from were made to assay muscle cholinergic

responses to stimulation of the ventral nerve cord. Under 5mM extracellular Ca^{2+} conditions,

vps-39 mutants show significantly reduced evoked responses to nerve stimulation in comparison

to wild type (Fig. 6A-D). On reducing the extracellular Ca^{2+} (0.5 mM), the extent of the

reduction in the evoked responses was similar to the reduction in 5 mM Ca^{2+} suggesting that

VPS-39 does not affect the Ca^{2+} dependence of release (Fig. 6E-H). In addition, neuronal

expression of VPS-39 completely rescued the evoked defect in *vps-39* mutants. These data show

that VPS-39 regulates cholinergic SV release in the ventral nerve cord.

 To further determine the role of VPS-39 at synapses, ultrastructural analysis of

cholinergic synapses in the ventral nerve cord was conducted using high pressure freeze (HPF)

electron-microscopy (Fig 7). The total number of SVs in vps-*39* mutants is similar to wild type

showing that changes in the overall size of the SV pool does not account for the defects in

neurotransmitter release in *vps-39* mutants (Fig. 7A). Although the total number of SVs are not

impacted, the number of SVs contacting the plasma membrane, also known as morphologically

docked SVs, are reduced in *vps-39* mutants in comparison to wild type (Fig. 7B. A reduced

number of fusion competent vesicles might account for the reduced neurotransmitter release

observed in *vps-39* mutants. Contrary to our expectations, re-expression of neuronal VPS-39 in

vps-39 mutants did not recue the SV docking defect. However, unlike the *vps-39* null, these

VPS-39 rescued synapses exhibit an overall reduction in total number of SVs as well as number

of docked SVs in comparison to wild type (Fig. 7A,B). Hence the rescue of neurotransmitter

release as observed by the dylox assay and electrophysiology in these rescued animals (*vps-39*;

Prab-3::VPS-39) might be a result of an increased probability of vesicle release.

 As we observed better rescue of neurotransmitter release on re-expression of neuronal

VPS-39 in *vps-39* mutants under lower Ca^{2+} conditions (0.5mM Vs 5mM Ca^{2+}) (Fig. 6), we

hypothesized that VPS-39 might be impacting the distribution of docked vesicles in addition to the number of docked vesicles (Fig. 8). Docked SVs represent two spatially and functionally different primed vesicle pools with (a) SVs docked closer to the dense projection (DP) or presynaptic density exhibiting fast, EGTA-resistant neurotransmitter release reflecting proximity to the voltage gated calcium channels and (b) vesicles docked farther away from DP showing slower, EGTA-sensitive vesicle release (Hu, Tong, and Kaplan 2013). After separating the distribution of docked vesicles in these two SV pools, we observed a reduction in the number of docked SVs in both of these SV pools (proximal pool <90 nm from the DP, and distal pool >90 nm from the DP) (Fig 8B). A similar reduction was observed in the VPS-39 rescued animals, suggesting that VPS-39 does not impact the distribution of docked vesicles at synapses. These data suggest that VPS-39 is an important determinant, directly or indirectly, for the docking and priming of SVs at the synaptic membrane.

4.4. Discussion

Recent studies demonstrating potential biochemical and functional interactions between the components of the HOPS complex and the SV release machinery, syntaxin and Munc18, prompted us to characterize the neuronal function of a crucial component of the HOPS complex, VPS-39. Our results show that VPS-39 is required for early development as the homozygous *vps-39(tm2253)* mutation results in embryonic lethality in *C. elegans*. Expression of VPS-39 under a pan neuronal promoter partially rescues the embryonic lethality in *vps-39* mutants suggesting that neuronal expression of VPS-39 is required for the viability at early stages. We further show that synaptogenesis and post synaptic receptor localization are normal in *vps-39* mutants excluding the possibility that limited viability is due to defective neuronal

cytoarchitecture. We report here that the *vps-39* mutants exhibit reduced evoked synaptic responses to nerve stimulation at NMJs showing that VPS-39 is required presynaptically. At the ultrastructural level, *vps-39* mutants show docking defects with reduced number of SVs docked to the plasma membrane in comparison to wild type. As the neuronal re-expression of VPS-39 in *vps-39* mutants rescued the evoked response but not the docking defect, it raises the possibility that VPS-39 might also be regulating the probability of vesicle release. As VPS-39 is an important component of endosomal machinery it might also have an indirect function in neurotransmitter release through endosomal or lysosomal sorting of synaptic components.

Our lab has also identified VPS-39 as a novel binding partner of the tomosyn-1 (TOM-1). TOM-1 is a cytosolic syntaxin (a SNARE protein)-binding protein that negatively regulates SV priming (Gracheva et al. 2006; Gracheva et al. 2007; Gracheva et al. 2010; Burdina et al. 2011). Synaptic enrichment of both VPS-39 and TOM-1 require Kinesin-3, a motor protein that exclusively transports SVs, suggesting that both proteins interact with SVs. Unpublished data from our lab further suggest that the interaction of TOM-1 with the SVs is dependent on VPS-39. As TOM-1 and VPS-39 have opposite effects on SV release with TOM-1 inhibiting neurotransmitter release and VPS-39 having a promoting effect, we hypothesize that VPS-39 negatively regulates TOM-1 levels (or function) at synapses and hence promotes SV release. We are currently conducting biochemistry and synaptic ultrastructural studies to further understand the importance of physical and functional interactions between VPS-39 and TOM-1 in SV release.
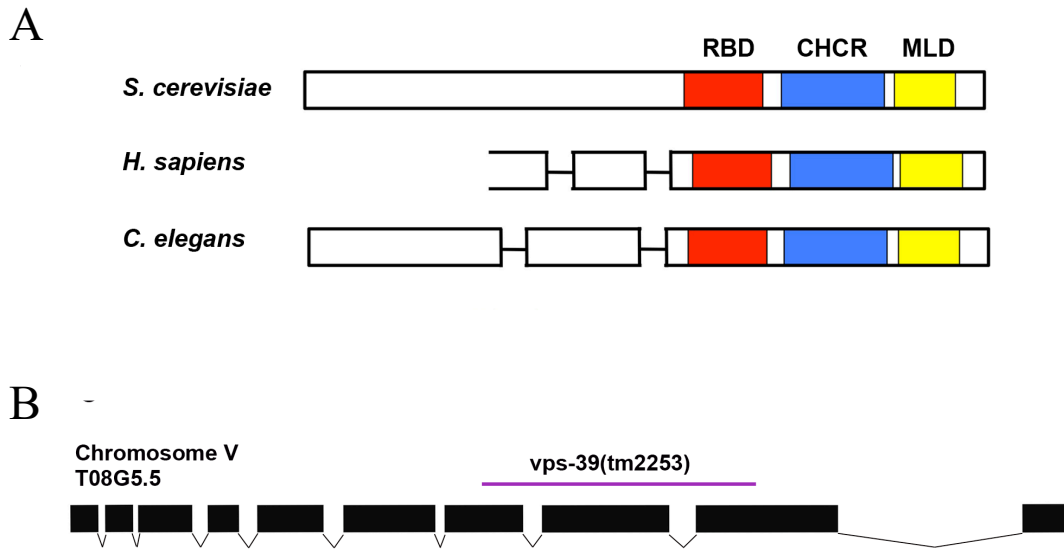
Figure 1. VPS-39 is a member of the HOPS complex.

(A) VPS-39 is conserved among species and contains three motifs: a Rab Binding Domain (RBD), a Clathrin Heavy Chain Repeat (CHCR), and a Membrane Localization Domain (MLD). (B) Gene structure of *vps-39*. It consists of 10 exons. *tm2253* allele contains a 1045 base pair (bp) deletion and a 4 bp insertion spanning exons 7-9. Data collected by Susan Klosterman.

44
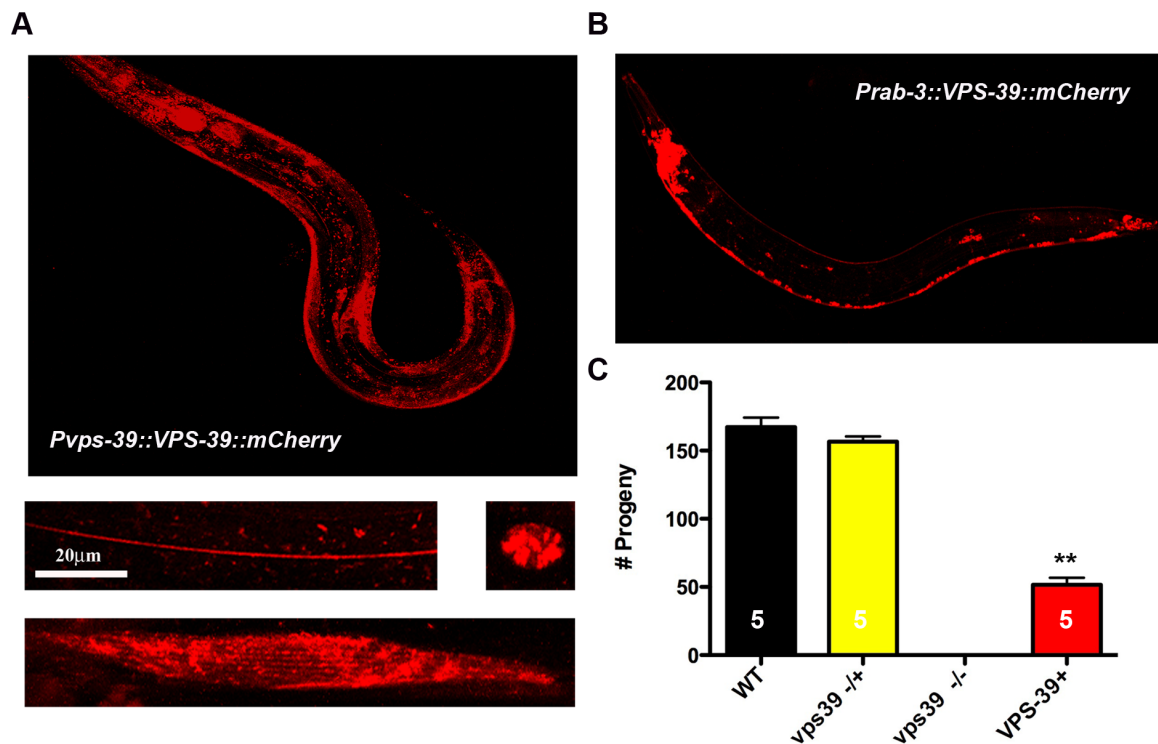
Figure 2. Expression pattern of VPS-39 and rescue of vps-39 mutant embryonic lethality.

(A) An extrachromosomal *VPS-39::mCherry* construct showing expression in many tissues. Lower enlarged images represent VPS-39::mCherry expression in neurons (left), a coelomocyte (right), and body wall muscle (bottom). (B) Neuronal expression of VPS-39 in *pRAB-3::VPS-39::mCherry* line. This was used for all neuronal recue experiments. (C) Graph showing the number of progenies after 4 days plating of individual worms. Sample size is indicated inside bars. Pan neuronal expression of VPS-39 partially recues the lethality in *vps-39* mutants. Data collected by Susan Klosterman.

46
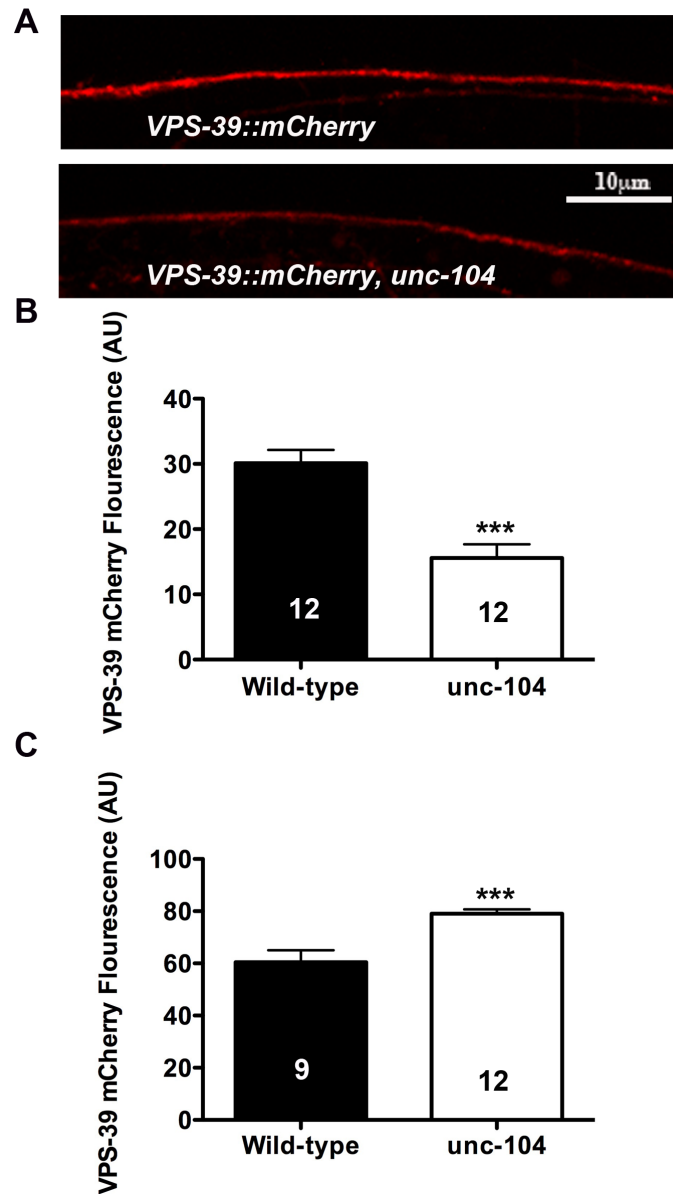
Figure 3. Axonal expression of VPS-39::mCherry is UNC-104/Kinesin-3 molecular motor dependent.

(A) Representative images of expression of VPS-39::mCherry in *unc-104* mutants in comparison to wild type. (B) Quantification of VPS-39::mCherry expression in the nerve cord and (C) cell body. Data collected by Susan Klosterman.

50
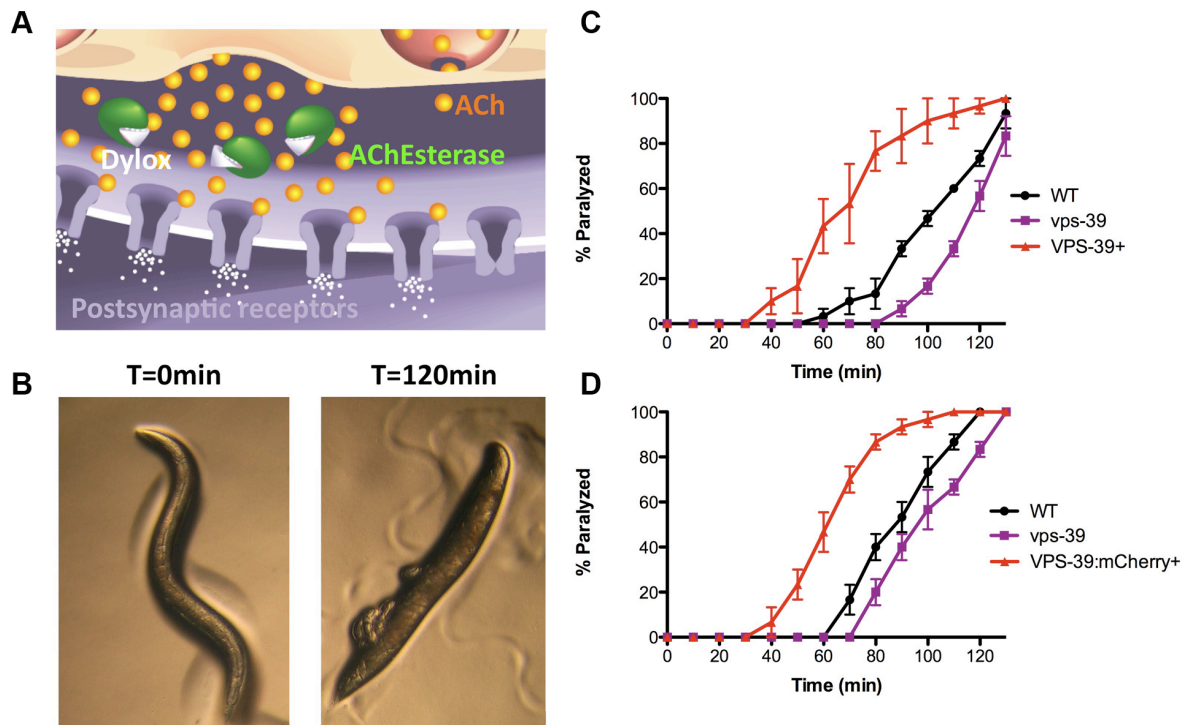
Figure 4. VPS-39 regulates ACh release in intact worms.

(A) Representative diagram showing inhibition of acetylcholinesterase activity by dylox resulting in accumulation of ACh in the synaptic cleft. (B) Exposure to dylox resulting in gradual onset of hypercontracted paralysis. (C) Graph showing percentage of animals paralyzed over time. Neuronal expression of VPS-39 and (D) VPS-39::mCherry rescues *vps-39* mutant phenotype. Data collected by Susan Klosterman.
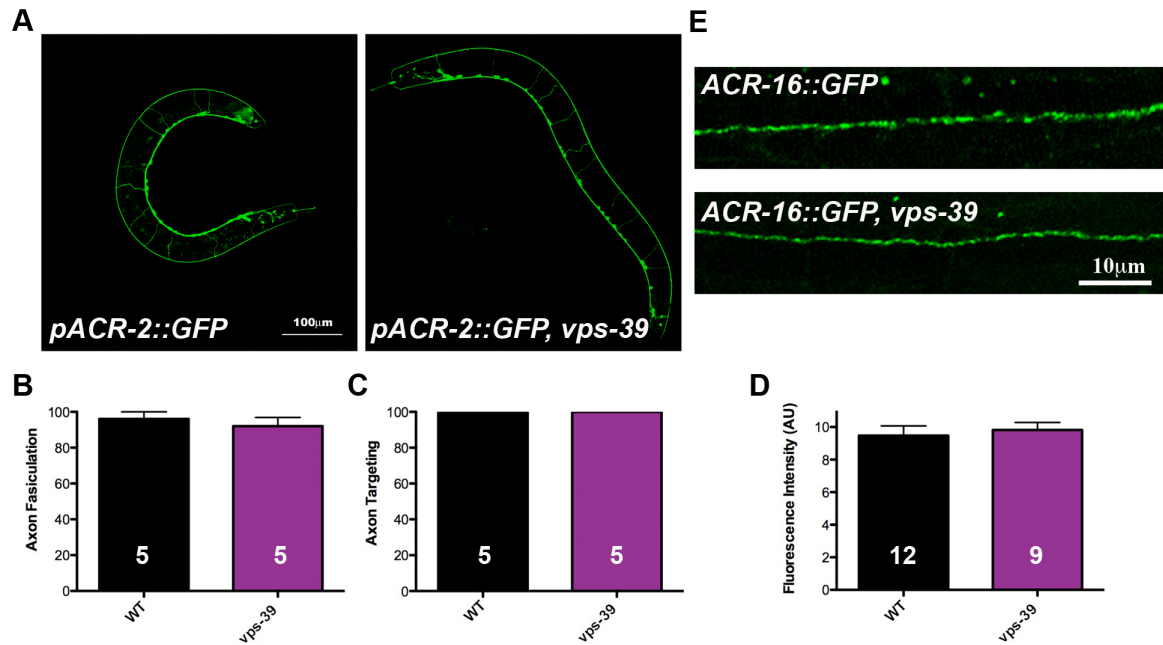
Figure 5. VPS-39 is not required for synaptic development.

(A) Representative images of pACR-2::GFP in wild type and *vps-39* mutant, with reciprocal
commissures extending between the ventral nerve cord (brighter) and the dorsal nerve cord.
Analysis of (B) axon fasciculation, (C) axon targeting. (D) Graph showing quantification ACR-
16 expression in the ventral nerve cord (E) Representative images of ACR-16 expression in the
ventral nerve cord in wild type and *vps-39* mutants. Data collected by Susan Klosterman.

54
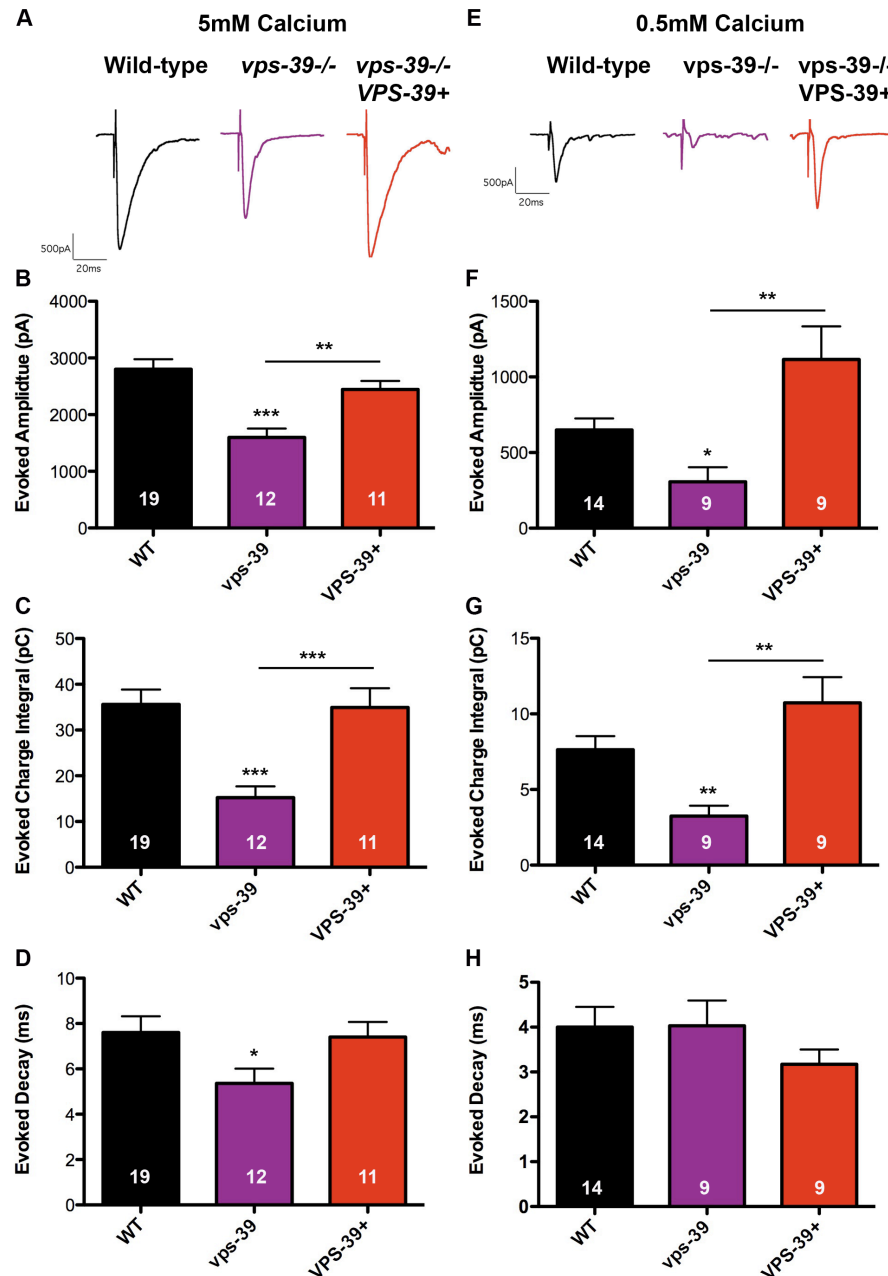
Figure 6. VPS-39 promotes evoked release at NMJs.

(A) Representative evoked traces in 5mM Ca^{2+}. Quantification of (B) Evoked amplitude (C) Evoked charge integral (D) Evoked decay in 5mM Ca^{2+}. (E) Representative evoked traces in 5mM Ca^{2+}. Quantification of (F) Evoked amplitude (G) Evoked charge integral (H) Evoked decay in 0.5mM Ca^{2+}. Sample size is indicated inside the bar. Data collected by Janet E. Richmond.

56
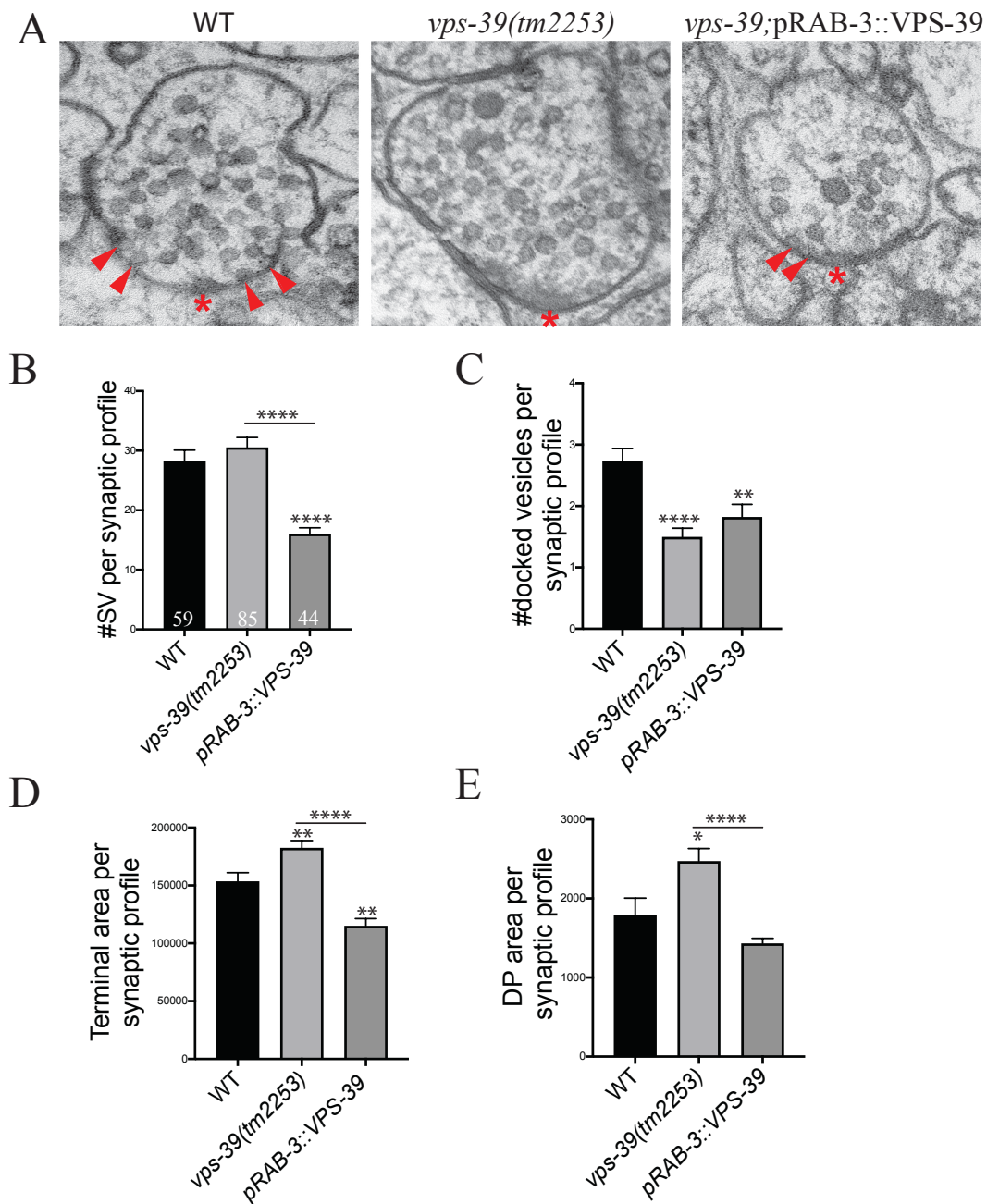
Figure 7. VPS-39 is required for SV docking/priming.

(A) Representative electron micrographs. Arrow, docked SVs; *Dense projection. Quantification of (B) total number of SVs (C) number of SVs docked to the synaptic membrane (D) area of synaptic terminals (E) area of dense projection. Data shown as mean ± SEM. Number of synaptic profiles analyzed are mentioned inside the bar. Data collected by Seema Sheoran.
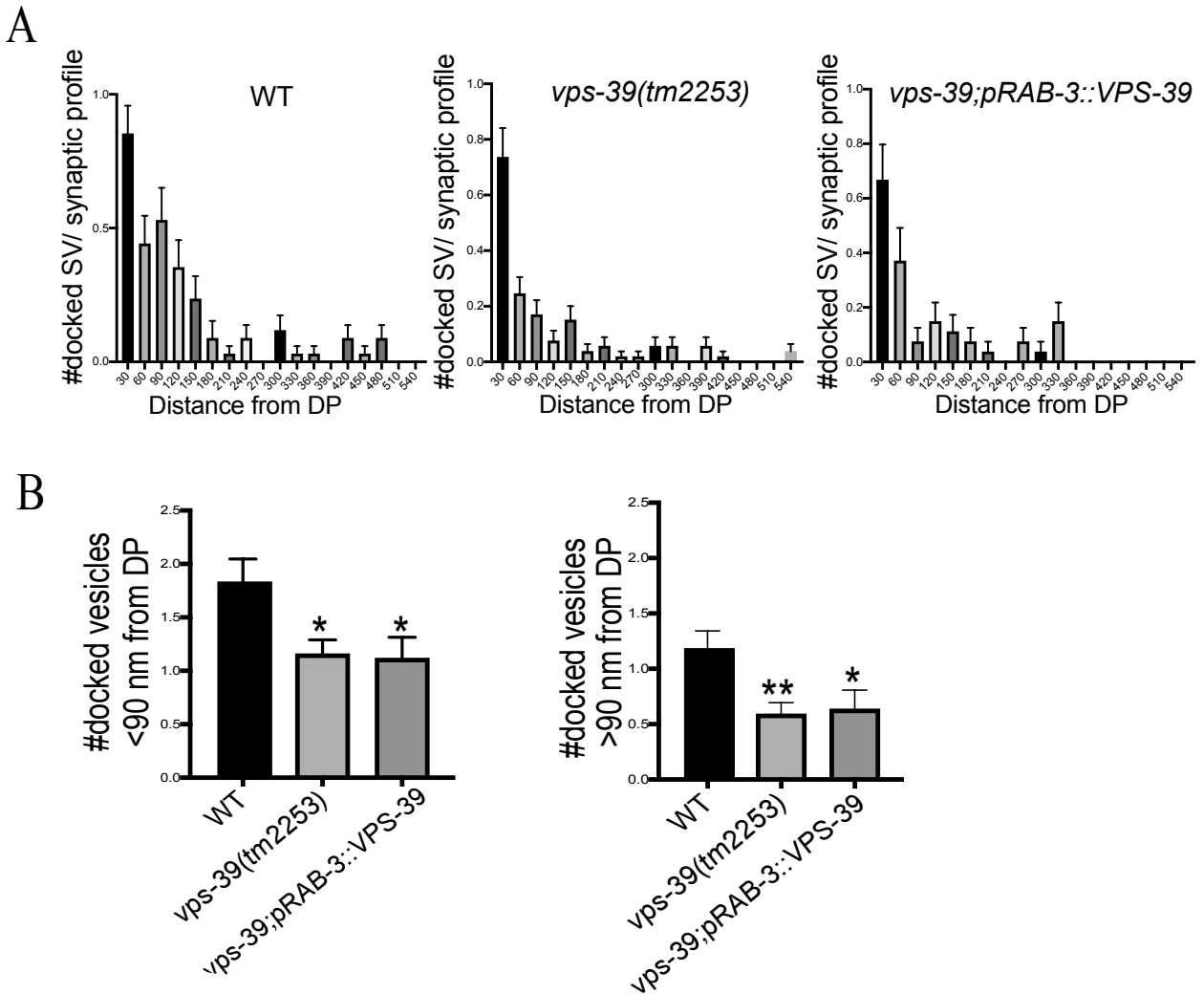
Figure 8. VPS-39 does not affect distribution of docked SVs.

(A) Graphs showing distribution of docked SVs in relation to the dense projection (DP). (B)

Graphs showing number of docked vesicles less than 90 nm distance from DP (left) and greater

than 90 nm distance from DP. Data shown as mean ± SEM. Data collected by Seema Sheoran.

4.5. References

Brenner, S. 1974. 'The genetics of Caenorhabditis elegans', *Genetics*, 77: 71-94.

Burdina, A. O., S. M. Klosterman, L. Shtessel, S. Ahmed, and J. E. Richmond. 2011. 'In vivo analysis of conserved C. elegans tomosyn domains', *PLoS One*, 6: e26185.

Fernandes, A. C., V. Uytterhoeven, S. Kuenen, Y. C. Wang, J. R. Slabbaert, J. Swerts, J. Kasprowicz, S. Aerts, and P. Verstreken. 2014. 'Reduced synaptic vesicle protein degradation at lysosomes curbs TBC1D24/sky-induced neurodegeneration', *J Cell Biol*, 207: 453-62.

Gracheva, E. O., A. O. Burdina, A. M. Holgado, M. Berthelot-Grosjean, B. D. Ackley, G. Hadwiger, M. L. Nonet, R. M. Weimer, and J. E. Richmond. 2006. 'Tomosyn inhibits synaptic vesicle priming in Caenorhabditis elegans', *PLoS Biol*, 4: e261.

Gracheva, E. O., A. O. Burdina, D. Touroutine, M. Berthelot-Grosjean, H. Parekh, and J. E. Richmond. 2007. 'Tomosyn negatively regulates both synaptic transmitter and neuropeptide release at the C. elegans neuromuscular junction', *J Physiol*, 585: 705-9.

Gracheva, E. O., E. B. Maryon, M. Berthelot-Grosjean, and J. E. Richmond. 2010. 'Differential Regulation of Synaptic Vesicle Tethering and Docking by UNC-18 and TOM-1', *Front Synaptic Neurosci*, 2: 141.

Hu, Z., X. J. Tong, and J. M. Kaplan. 2013. 'UNC-13L, UNC-13S, and Tomosyn form a protein code for fast and slow neurotransmitter release in Caenorhabditis elegans', *Elife*, 2: e00967.

Kim, B. Y., Y. Sahara, A. Yamamoto, E. Kominami, S. Kohsaka, and C. Akazawa. 2006. 'The interaction of mammalian Class C Vps with nSec-1/Munc18-a and syntaxin 1A regulates pre-synaptic release', *Biochem Biophys Res Commun*, 350: 691-7.

Richmond, J. 2009. 'Dissecting and recording from the C. Elegans neuromuscular junction', *J Vis Exp*.

Sato, T. K., P. Rehling, M. R. Peterson, and S. D. Emr. 2000. 'Class C Vps protein complex regulates vacuolar SNARE pairing and is required for vesicle docking/fusion', *Mol Cell*, 6: 661-71.

Weimer, R. M., E. O. Gracheva, O. Meyrignac, K. G. Miller, J. E. Richmond, and J. L. Bessereau. 2006. 'UNC-13 and UNC-10/rim localize synaptic vesicles to specific membrane domains', *J Neurosci*, 26: 8040-7.

White, J. G., E. Southgate, J. N. Thomson, and S. Brenner. 1986. 'The structure of the nervous system of the nematode Caenorhabditis elegans', *Philos Trans R Soc Lond B Biol Sci*, 314: 1-340.

APPENDIX A

Alcohol induces mitochondrial fragmentation and stress responses to maintain normal muscle function in Caenorhabditis elegans

Kelly H. Oh[1], Seema Sheoran[2], Janet E. Richmond[2], and Hongkyun Kim[1]

[1]Center for Cancer Cell Biology, Immunology, and Infection, Department of Cell Biology &

Anatomy, Chicago Medical School, School of Graduate and Postdoctoral Studies, Rosalind

Franklin University of Medicine and Science, North Chicago, Illinois 60064, USA

[2] Department of Biological Sciences, University of Illinois at Chicago, Chicago, Illinois 60607,

USA

Abstract

Chronic excessive ethanol consumption has distinct toxic and adverse effects on a variety of tissues. In skeletal muscle, ethanol causes alcoholic myopathy, which is characterized by myofiber atrophy and the loss of muscle strength. Alcoholic myopathy is more prevalent than all inherited muscle diseases combined. Current evidence indicates that ethanol directly impairs muscle organization and function. However, the underlying mechanism by which ethanol causes toxicity in muscle is poorly understood. Here, we show that the nematode *C. elegans* exhibits the key features of alcoholic myopathy when exposed to ethanol. As in mammals, ethanol exposure impairs muscle strength and induces the expression of protective genes, including oxidative stress response genes. In addition, ethanol exposure causes the fragmentation of mitochondrial networks aligned with myofibril lattices. This ethanol-induced mitochondrial fragmentation is dependent on the mitochondrial fission factor DRP-1 (dynamin-related protein 1) and its receptor proteins on the outer mitochondrial membrane. Our data indicate that this fragmentation contributes to the activation of the mitochondrial unfolded protein response (UPR). We also found that robust, perpetual mitochondrial UPR activation effectively reduces muscle weakness caused by ethanol exposure. Our results strongly suggest that the modulation of mitochondrial stress responses may provide a method to ameliorate alcohol toxicity and damage to muscle.

Introduction

Alcohol use disorder is a major health issue with enormous socioeconomic costs. The detrimental effects of acute and chronic alcohol consumption on liver, pancreas, and brain are well documented (Souza-Smith et al. 2016). Chronic alcohol consumption also causes the loss of skeletal muscle strength and cardiac contractile function (Urbano-Marquez et al. 1989; Kimball and Lang 2018). Alcoholic myopathy and cardiomyopathy, collectively called alcoholic striated muscle disease, are more prevalent than all inherited muscle disorders combined and have an incidence of 45-75% among chronic alcohol users (Preedy, Salisbury, and Peters 1994). While chronic alcoholic myopathy can be reversed by long-term abstinence from alcohol, alcoholic cardiomyopathy can be fatal, as it becomes irreversible at a certain point and leads to heart failure. Despite the significant health impacts of alcoholic muscle disease, we do not fully understand the pathogenic mechanism by which alcohol exerts its toxicity on striated muscles at the molecular and cellular levels.

Mitochondria are not only responsible for cellular energy production, but also central to cellular signaling and metabolism. These functions are closely linked to mitochondrial architecture, which is dynamically regulated by fission and fusion processes in response to stress and the metabolic state (Eisner, Picard, and Hajnoczky 2018). Mitochondrial fission is mediated by the dynamin-related protein 1 (DRP1). DRP1 is recruited to the outer mitochondrial membrane via its receptor proteins, such as FIS1 and MFF, where it assembles into spirals to wrap around mitochondria and splits the membrane through constriction (van der Bliek, Sedensky, and Morgan 2017). Mitochondrial fission is mainly mediated by altered GTPase activity of DRP1 via post-translational modifications (Oliver and Reddy 2019; Giacomello et al. 2020). Mitochondrial fusion is also facilitated by dynamin family proteins. Whereas outer membrane fusion is

mediated by the mitofusins MFN1 and MFN2 (FZO-1 in *C. elegans*), inner membrane fusion is mediated by OPA1 (EAT-3 in *C. elegans*). Mitochondrial fusion is regulated by the overall fusion machinery levels (i.e., transcription and degradation) or post-translational modifications (Oliver and Reddy 2019; Giacomello et al. 2020).

The mitochondrial unfolded protein response (UPR^mt) is an adaptive transcriptional response elicited by various forms of mitochondrial dysfunction, such as defects in mitochondrial protein import, the impairment of oxidative phosphorylation, and the perturbation of mitochondrial proteostasis (Shpilka and Haynes 2018). In *C. elegans,* the bZIP transcription factor ATFS-1 (activating transcription factor associated with stress-1), a mammalian ATF-5 ortholog, is primarily responsible for mediating the UPR^mt transcriptional response in the nucleus (Haynes et al. 2010). Although ATFS-1 possesses both a mitochondrial targeting sequence (MTS) and a nuclear localization sequence, ATFS-1 is normally targeted to the mitochondria and undergoes degradation. However, when its mitochondrial import is reduced or blocked due to mitochondrial dysfunction, ATFS-1 is transported to the nucleus, where it directly activates the transcription of over 500 genes involved in mitochondrial quality control and cellular metabolism to restore mitochondrial proteostasis (Melber and Haynes 2018; Nargund et al. 2015). In addition to ATFS-1, the homeobox transcription factor DVE-1, along with its ubiquitin-like coactivator UBL-1 is also required for UPR^mt induction (Haynes et al. 2007). Recent studies have shown that chromatin remodeling and epigenetic regulation are also critical for UPR^mt transcriptional regulation (Tian et al. 2016; Merkwirth et al. 2016).

C. elegans is well suited to the study of the genetic basis of alcoholic striated muscle disease. In addition to its genetic amenability, *C. elegans* body wall muscles are structurally analogous to mammalian striated muscles, and their structure and subcellular organelles can be easily

observed through the transparent bodies of live animals. The mitochondria in body wall muscles are regularly organized along the myofiber in an easily discernable fashion, and the mitochondrial fission and fusion machineries are conserved. Furthermore, the processes involved in cellular signaling, stress responses, and cell death, which are considered major targets of alcohol toxicity pathways, are evolutionarily conserved and well characterized.

In this report, we show that *C. elegans* recapitulates key aspects of alcoholic myopathy; alcohol exposure causes mitochondrial fragmentation, induces oxidative stress and unfolded protein responses, and reduces muscle size and strength. Furthermore, our genetic analysis showed that the toxic effects of alcohol on *C. elegans* muscle result mainly from mitochondrial dysfunction. Remarkably, we found that the modulation of mitochondrial physiology by activation of the mitochondrial unfolded protein response (UPR^{mt}) is protective against alcohol-mediated muscle dysfunction.

Materials and Methods

Worm strains and maintenance. All *C. elegans* strains were cultured at 20 °C on NGM (nematode growth medium) plates seeded with *E. coli* OP50. The following strains were used in this study: N2, SJ4100 (*zcIs13*[*hsp-6p*::GFP]), SJ4005 (*zcIs4*[*hsp-4p*::GFP]), CL2070 (*dvIs70*[*hsp-16.2p*::GFP + *rol-6 (su1006)*]), CL2166 (*dvIs19*[*gst-4p*::GFP::NLS]) (Link and Johnson 2002; Oh and Kim 2013), SJ4197(*zcIs39*[*dve-1p*::*dev-1*::GFP], CF2124(*muIs139*[*dod-11p*::RFP(NLS) + *rol-6(su1006)*]), the infection reporter strain AU133 (*agIs17*[*irg-1p*::GFP + *myo-2p*::mCherry]) (Estes et al. 2010), the infection reporter strain AY101 (*acIs101*[*irg-5p*::GFP + *rol-6(su1006)*]) (Bolz, Tenor, and Aballay 2010), the xenobiotic detoxification reporter strain CY573 (*bvIs5*[*cyp-35B1p*::GFP + *gcy-7p*::GFP]) (Iser et al. 2011), the hypertonic stress reporter

strain VP198 (*kbIs5*[*gpdh-1p*::GFP + *rol-6(su1006)*]) (Lamitina 2006), the proteasome stress

reporter strain GR2183 (*mgIs72*[*rpt-3p::GFP* + *dyp-5*(+)] (Lehrbach and Ruvkun 2016), the

hypoxia reporter strain DMS640 (*nIs470* [*cysl-2p*::GFP + *myo-2p*::mCherry] (Ma et al. 2012),

EU2917(*drp-1*(*or194[GFP::drp-1]*) (Lowry et al. 2015), *drp-1(tm1108)*, *fzo-1(tm1133)*, *mff-*

1(tm2955), *mff-2(tm3041)*, *fis-1(tm1867)*, *fis-2(gk414)*, *dct-1(tm376)*, *pdr-1(gk448)*, *pink-*

1(tm1799), *ced-3(n717)*, *ced-9(n2812)*;*ced-3(n717)*, *atfs-1(gk3094lf)*, and *atfs-1(et15gf)*. The

transgenic strains were constructed using standard DNA microinjection methods. The following

transgenes were generated in our lab: *cimIs46*[*myo-3*::GFP], *cimIs42*[*twk-28p*::*atp-9*::GFP],

cimIs40[*myo-3p*::*tomm-20*(mts)::FusionRed], and *cimEx102*[*atfs-1p*::*atfs-1*::GFP].

Ethanol treatment. As described previously (Oh and Kim 2019), the NGM agar plates used for

all of the ethanol treatment experiments were dried without lids for 25 min in a 60 °C incubator.

This drying process ensures rapid ethanol absorption into the agar, and this process usually

reduces the agar to 85-90% of its original volume. After the plates were cooled to room

temperature, OP50 *E. coli* were seeded in the center of the plate and were allowed to grow

overnight. The next day, the desired amount of ethanol (300 mM), which yielded an internal

ethanol concentration of approximately 30 mM (Alaimo et al. 2012; Scott et al. 2017), was

applied to the NGM plates while avoiding direct contact with the bacteria. The plates were then

sealed with parafilm and left at room temperature for equilibration for at least one hour. The

desired number of animals at the L4 stage were placed on the plate, which was cultured for 24

hours in a 20 °C incubator.

Burrowing assay. The burrowing assay was performed as described by Lesanpezeshki et al.,

with some modifications (Lesanpezeshki et al. 2019). Briefly, we placed fifteen age-matched (24

hours post L4) naïve or ethanol-exposed animals at the bottom center of a 12-well plate. We then

added 2 ml of 26% (w/w) Pluronic F-127 solution and waited for 5 min for it to transition from liquid to gel at room temperature. Two microliters of isoamyl alcohol (1:200 dilution in 70% ethanol) were spotted on the top surface, and then twenty microliters of OP50 bacterial culture was added to the dried isoamyl alcohol spot. The animals that successfully burrowed to the top to swim in the bacterial culture solution were counted every fifteen minutes and removed. Triplicate assays for each genotype and treatment were concurrently performed for 90 min.

Thrashing assay. Fifteen animals were placed in 1 ml of M9 buffer on a 35 mm unseeded NGM plate with care to minimize the co-transfer of the OP50 bacteria. The worms were allowed to rest for 5 min to become acclimated to the liquid environment. A video was recorded for 30 seconds using Image Pro 10 (Media Cybernetics Inc., Rockville, MD, USA). By replaying the video at a slower frame rate, the number of thrashings of individual worms was counted manually. Worms that remained in the field view for the entire 30 seconds were counted, and the genotype of the worms was blinded to the person who performed the counting. One thrash was counted when the head or tail of the worm swung back.

Measurement of fluorescent reporter expression. Worms were mounted with 6 mM levamisole in M9 buffer on a 2% agarose pad. Images were captured using a 10x objective on a Zeiss Axio Observer Z1 microscope and Metamorph 7.8 (Molecular Devices Co., San Jose, CA, USA). Using Metamorph, the outlines of the worms were manually drawn, and the integrated pixel intensity was obtained. The background intensity, which was obtained from a neighboring region, was subtracted from the intensity of the sample.

Mitochondrial morphology analysis. Worms were mounted on 2% agarose pads using 6 mM levamisole in M9 solution. Images were captured using a 63x objective on a Zeiss Axio Observer Z1 microscope (Zeiss Microscopy, Jena, Germany). First, the categorical score scale was

established, and by comparing them to the established standard images, each muscle cell was given a score.

High pressure freeze electron microscopy (HPF-EM). Samples were prepared using high-pressure freeze fixation (Weimer 2006). Thirty young adult worms that were cultured in the absence (control) or presence of ethanol were flash-frozen under high pressure (Leica SPF HPM 100, Leica, Germany). Frozen specimens then underwent freeze substitution (Leica Reichert AFS) during which samples were held at -90°C for 107 hr in 0.1% tannic acid and 2% OsO_4 in anhydrous acetone. The temperature was then increased at 5°C/hr to -20°C, kept at -20°C for 14 hr, and increased by 10°C/hr to 20°C. After fixation, samples were infiltrated with 50% Epon/acetone for 4 hr, 90% Epon/acetone for 18 hr, and 100% Epon for 5 hr. Finally, samples were embedded in Epon and incubated for 48 hr at 65°C. Worms were orientated with the ventral axis facing the diamond knife, and ultrathin (70 nm) longitudinal sections were cut using a Leica Ultracut 6 and collected on formvar-covered, carbon-coated copper grids (FCF2010-Cu, EMS, Hatfield, PA, USA). Post-staining was performed using 2.5% aqueous uranyl acetate for 4 min, followed by Reynolds lead citrate for 2 min. Images were acquired using a JEOL JEM-1220 transmission electron microscope (JEOL Inc., Peabody, MA, USA) operating at 80 kV using a Gatan digital camera (Gatan Inc., Pleasanton, CA, USA) at a magnification of 6k. Images were collected from the ventral body muscle belly containing mitochondria. Image acquisition and analysis using NIH ImageJ/Fiji software were performed blinded for experimental condition (control vs EtOH-treated wildtype worms).

Quantitative real-time PCR

L4 stage worms were plated on either control or ethanol-treated plates for 20 to 24 hours. Worms were collected, washed with M9 buffer, and stored in DNA/RNA shield solution (Zymo

Research, Irvine, CA, USA) at -80°C overnight. Total RNA was isolated using Quick-RNA Microprep kit (Zymo Research, Irvine, CA, USA) following the manufacturer's instruction. 0.5 g RNA was used to produce cDNA using iScript cDNA kit in a final volume of 20 l (Bio-Rad Laboratories, Hercules, CA, USA). 200 nM of each primer and 0.5 l cDNA reaction mixture was used for quantitative real-time PCR using Power SYBR GREEN master mix (ThermoFisher Scientific, Waltham, MA, USA) and ABI 7500 instrument (ThermoFisher Scientific, Waltham, MA, USA). The following primers were used:

drp-1 Forward: GAAGACGGTCAAATGGAACAC

drp-1 Reverse: GCACGGCATCGAAGTCTGT

fzo-1 Forward: GTGCTGCCGATAATGAACCAC

fzo-1 Reverse: TTCCCGCTGTTCAGAACTAAC

cdc-42 Forward: CTGCTGGACAGGAAGATTACG

cdc-42 Reverse: CTCGGACATTCTCGAATGAAG

These primer pairs have been validated in a published study (Kim et al. 2018). Four biological RNA samples and three technical PCR reactions were included in the analysis.

Western blot analysis

Collected worm pellets were frozen in -80 °C for overnight. The pellets were lysed by sonication in lysis buffer (2% SDS, 100 mM NaCl, 10 % glycerol, 50 mM Tris HCl, pH6.8). The lysate was cleared by centrifugation for 10 min at 20,000g at 4 °C. Protein amount was quantified using Pierce BCA protein assay kit (ThermoFisher Scientific, Waltham, MA, USA). 40 g of total protein was mixed with SDS gel loading buffer including -mercaptoethanol and heated for 5 min at 95 °C. The samples were run on 7.5 % polyacrylamide gel and transferred to PVDF membrane (Bio-Rad Laboratories, Hercules, CA, USA). Western blot was performed using anti-

177

GFP antibody (#2956 Cell Signaling Technology, Danvers, MA, USA) and anti- -tubulin (AA4.3 Developmental Studies Hybridoma Bank, Iowa City, IA, USA).

Statistical analysis. All graphing and statistical analyses were performed using Prism 7 (GraphPad Software, San Diego, CA, USA). The sample numbers represent the biological replicates. Sample sizes were chosen based on previous reports on similar studies. None of the samples or animals are excluded from data analysis. Sample randomization was not used in this study. All of the data analyses, except thrashing assay, are not blinded.

Results

Ethanol causes muscle dysfunction in *C. elegans*

To understand the toxic effects of ethanol on muscle function, we exposed *C. elegans* for 24 hours to a low dose of ethanol, which has a mild acute effect on locomotion, and then measured its movement in a liquid medium. While naïve control animals cultured in the absence of ethanol showed vigorous thrashing behavior, ethanol-exposed animals exhibited a significant reduction in the frequency of thrashing (Fig. 1A, Supplemental Video S1). This impaired thrashing did not result from neural depression caused by ethanol, since animals resistant to the intoxicating effects of ethanol still showed an impairment in thrashing (Supplemental Fig. S1). The mobility of *C. elegans* in a natural habitat mainly consists of movements in the three-dimensional space. To better simulate natural locomotion, we performed a modified burrow assay (Lesanpezeshki et al. 2019), in which naïve control and ethanol-exposed animals were allowed to migrate across a solidified Pluronic F-127 gel layer from the bottom of a 12-well plate to an olfactory attractant on the surface. This assay has been shown to effectively detect even a slight deficit in neuromuscular function (Lesanpezeshki et al. 2019). We found that compared to naïve animals,

the ethanol-exposed animals had difficulties in reaching the surface (Fig. 1B). In humans, alcoholic skeletal myopathy leads to muscle fiber atrophy along with muscle weakness (Kimball and Lang 2018). We thus compared the sizes of the striated body wall muscle cells in naïve and ethanol-exposed animals. Ethanol-exposed animals indeed had smaller muscle cells than naïve animals (Fig. 1C and D). Furthermore, recovery after ethanol exposure on a regular culture plate for 4 hours did not reduce the deficit in muscle size, indicating that muscle damage caused by ethanol exposure was not an acute, temporary effect. This reduction in muscle size could be due to reduced feeding. However, 24 hours of exposure to ethanol at this dose had no impact on the rate of pharyngeal pumping, indicating that a reduction in food intake caused by ethanol exposure is unlikely to cause a reduction in muscle function and size (Fig. 1 E).

Ethanol induces mitochondrial and ER stress responses in *C. elegans*.

To explore how ethanol exposure causes deficits in muscle function, we first determined which stress responses were induced in *C. elegans* after ethanol exposure using previously established reporter strains. All of the tested strains are listed in the Materials and Methods. In these strains, the promoter sequences of a variety of stress response genes are fused to fluorescent protein coding sequences, and an elevation in fluorescent protein expression is indicative of the induction of the stress response. As previously reported (Alaimo et al. 2012), the robust induction of the alcohol dehydrogenase gene reporter *sodh-1* was observed (Supplemental Fig. S2). We found that 24 hours of exposure to ethanol increased the expression of the ER (*hsp-4p*::GFP) and mitochondrial UPR (*hsp-6p*::GFP) reporters but did not appreciably affect the expression of the cytosolic stress reporter *hsp-16.2p*::GFP (Fig. 2A). In addition, we observed that the expression of the oxidative stress reporter *gst-4p::*GFP was induced by ethanol exposure

(Fig. 2B). These results together indicate that ethanol induces the expression of genes that are involved in alcohol detoxification, similar to that observed in mammals.

Ethanol causes mitochondrial fragmentation in *C. elegans* muscles.

The observed stress response profile suggests that mitochondrial dysfunction might underlie ethanol-induced cellular stress, since mitochondrial dysfunction is known to cause oxidative stress and UPR^{mt}, which indirectly leads to UPR^{ER} (Sebastian et al. 2012; Lebeau et al. 2018). Mitochondrial function is intimately linked to the dynamic regulation of its architecture; mitochondria undergo fusion and fission, and the balance of these two processes determines the mitochondrial architecture. Various cellular stressors alter mitochondrial function, and changes in mitochondrial structure enable the cell to restore mitochondrial homeostasis (Eisner, Picard, and Hajnoczky 2018). Therefore, we examined whether ethanol exposure would alter the mitochondrial architecture in muscle.

To assess the mitochondrial networks in striated body-wall muscle, we generated an integrated transgenic line that expresses a fusion protein on the outer mitochondrial membrane consisting of the mitochondrial targeting sequence of TOMM-20 and FusionRed (*tomm-20*::FusionRed) under the control of the muscle-specific *myo-3* promoter. We observed that animals exposed to ethanol for 24 hours showed swollen mitochondria, fragmented mitochondrial networks, or the complete disruption of mitochondrial networks in striated body-wall muscle (Fig. 3A). We further investigated whether ethanol-mediated mitochondrial fragmentation is observed in wild-type muscle using transmission electron microscopy. Blinded EM experiments also demonstrated that muscle cells of ethanol-exposed animals exhibited

fragmented and round mitochondria while muscle cells of control animals showed linear elongated mitochondrial network (Fig. 3B). Mitochondrial fragmentation can result from either increased fission or decreased fusion. Therefore, we reasoned that if a reduction in fusion was responsible for ethanol-mediated mitochondrial fragmentation, significant mitochondrial fragmentation in fission-defective animals would be expected, but if increased fission was the major cause of fragmentation, then fragmentation would be alleviated in fission-defective animals. In *C. elegans,* mitochondrial fission is mediated by DRP-1 and its receptors FIS-1/FIS-2 and MFF-1/MFF-2 (Shen et al. 2014; Labrousse et al. 1999) (Fig. 3C). First, we tested whether muscle mitochondria undergo fragmentation in ethanol-exposed *drp-1(tm1108)*-null mutant animals. Although it was not feasible to quantify the degree of fragmentation due to the highly connected mitochondrial network in *drp-1* mutant animals, ethanol did not change the mitochondrial architecture in the *drp-1* mutant, demonstrating that DRP-1 is necessary for ethanol-induced mitochondrial fragmentation (Fig. 3D). Consistent with previous observations (Shen et al. 2014), naïve control *fis-1(tm1867);fis-2(gk414)* double-mutant animals showed a normal mitochondrial network structure. When *fis-1;fis-2* animals were cultured in the presence of ethanol for 24 hours, they showed relatively mild mitochondrial fragmentation when compared to that observed in wild-type animals (Supplemental Fig. S3A). We also examined *mff-1(tm2955);mff-2(tm3041)* double-mutant animals for ethanol-mediated changes in mitochondrial architecture. Naïve control *mff-1;mff-2* mutant animals exhibited an increase in interconnected mitochondrial networks (Fig. 3C and 3D), consistent with the fact that MFF proteins are the major receptors for DRP-1. Ethanol-exposed *mff-1;mff-2* mutant animals did not show any appreciable fragmentation and maintained interconnected mitochondrial networks similarly to control animals. In *C. elegans* mitochondrial fusion is mediated by FZO-1, the

ortholog of human mitofusin 1 (MFN1) and mitofusin 2 (MFN2). Previous studies noted that

mitochondrial fission and fusion dynamics can also be altered by transcriptional regulation of

fission and fusion machinery (Mai et al. 2010; Cartoni et al. 2005). Particularly, mitochondrial

fusion machinery is known to be downregulated by stressors, including ethanol (Eisner, Lenaers,

and Hajnoczky 2014). Therefore, we determined whether ethanol exposure for 24 hours changes

the levels of *drp-1* and *fzo-1* mRNAs. We found that ethanol exposure did not change either

mRNA level significantly (Supplemental Fig S3B), excluding the possibility that ethanol

exposure alters the transcription of *drp-1* and *fzo-1* genes. We also determined the level of DRP-

1 protein in a genome-edited GFP::*drp-1* strain by Western blot analysis, and did not observe any

change after ethanol exposure (Supplemental Fig S3C). Together, these results indicate that

ethanol-induced mitochondrial fragmentation is primarily mediated by increased mitochondrial

fission likely through post-translational regulation of DRP-1.

We also determined whether mitophagy plays a role in ethanol-induced mitochondrial

fragmentation (Supplemental Fig. S4A). Mitochondrial fragmentation can be a process that

separates damaged mitochondria from heathy mitochondrial networks that ultimately results in

mitophagy (Palikaras, Lionaki, and Tavernarakis 2015). Thus, a deficit in mitophagy may block

ethanol-induced mitochondrial fragmentation. However, even though the number of

mitochondria was considerably increased in the mitophagy mutant animals, mitochondria still

underwent ethanol-induced fragmentation. Cell death mediators, such as CED-9 and CED-3, are

known to influence mitochondrial fission and fusion (Tan et al. 2008; Lu, Rolland, and Conradt

2011), but the mutant animals also exhibited alcohol-induced mitochondrial fragmentation at a

level comparable to that observed in wild-type counterparts (Supplemental Fig. S4B). Together,

these results indicate that genes that mediate mitophagy and cell death are not involved in ethanol-induced mitochondrial fragmentation.

Excessive mitochondrial fragmentation leads to the induction of UPR^mt.

Because long-term ethanol exposure in *C. elegans* causes both mitochondrial stress responses and fragmentation, we explored whether each had any effect on the other. Therefore, we measured the levels of UPR^mt in *drp-1* and *fzo-1* mutant animals, which have defects in mitochondrial fission and fusion, respectively. Both *drp-1* and *fzo-1* mutant animals exhibited higher levels of UPR^mt reporter expression than the wild type control (Fig. 4A). These results showed that perturbation of the mitochondrial structure by a defect in either fusion or fission elicits mitochondrial stress. After ethanol exposure, reporter expression was further increased in *drp-1* mutant animals that had highly connected mitochondria but not in *fzo-1* mutants that had highly fragmented mitochondria (Fig. 4A). We also observed that the expression of the oxidative stress response gene reporter *gst-4p::GFP* behaved similarly to that of the UPR^mt reporter (Fig. 4B). Together, these results suggest that disruption of normal mitochondrial networks causes UPR^mt and oxidative stress, and that mitochondrial fragmentation contributes to ethanol-induced UPR^mt and oxidative stress response activation.

Activated UPR^mt counteracts ethanol-induced muscle dysfunction.

ATFS-1 is a master regulator of UPR^mt, and its nuclear localization is an indicator of mitochondrial dysfunction (Nargund et al. 2012). We determined whether ethanol exposure increases the nuclear localization of ATFS-1 using a GFP-tagged ATFS-1 transgene. When the transgenic animals were cultured in the absence of ethanol, ATFS-1 was barely detectable due to

efficient degradation under normal conditions (Fig. 5A), as previously reported (Nargund et al. 2012). After 24 hours of ethanol exposure, ATFS-1 was found in the nuclei, albeit at a low level (Fig. 5A), which was similar to a previous report (Nargund et al. 2012). In addition to ATFS-1, we examined a coregulator of UPR^{mt}, DVE-1, which translocates into the nucleus upon mitochondrial stress (Haynes et al. 2007), and found that ethanol exposure increases the nuclear localization of DVE-1 (Fig. 5B). These results indicate that ethanol-induced UPR^{mt} is mediated by ATFS-1 and DVE-1.

We hypothesized that the activation of UPR^{mt} is a homeotic mechanism that is activated to cope with ethanol toxicity; therefore, UPR^{mt} is protective, at least in the short term, against ethanol toxicity. Thus, we compared the muscle function of wild type, *atfs-1*(*lf, loss-of-function*), and *atfs-1*(*et15gf*, *gain-of-function*) animals using thrashing and burrowing assays (Fig. 6, Supplemental Video S1). Under control conditions, neither *atfs-1(lf)* or *atfs-1(et15gf)* mutant animals were significantly different from wild-type animals in terms of thrashing frequency and burrowing ability (Fig. 6). After exposure to ethanol for 24 hours, both the wild-type and *atfs-1(lf)* mutant animals showed diminished thrashing and burrowing. By contrast, ethanol-exposed *atfs-1(et15gf)* mutant animals showed strikingly robust thrashing and burrowing comparable to that of their naïve control counterparts, demonstrating that *atfs-1(et15gf)* mutant animals maintained muscle function after ethanol exposure (Fig. 6, Supplemental Video S1). Together, these results indicate that perpetual UPR^{mt} activation protects animals from muscle weakness caused by ethanol toxicity.

Discussions

Chronic alcohol abuse leads to skeletal myopathy and cardiomyopathy in humans. It is also well known that striated muscles in alcoholic patients show abnormalities in their mitochondrial structures, and defects in myofibril contractility, and metabolic reprogramming (Kimball and Lang 2018). In this study, we employed two methods to measure muscle function: thrashing and burrowing assays. Unlike locomotion on a standard nematode culture dish, these two assays utilize environments that are more energetically challenging, and therefore, the functional capacity of muscles can be readily examined. Using these two assays, we demonstrated that ethanol-exposed animals exhibited similar functional deficits in muscles as those seen in alcohol-induced skeletal myopathy.

It has been noted that stress response pathways are activated in alcoholic myopathy (Fernandez-Sola et al. 2007; Simon, Jolley, and Molina 2017). The availability of various reporter strains to probe the activation of specific stress response pathways allowed us to demonstrate that ethanol exposure induces mitochondrial stress, ER stress, and oxidative stress responses. This response profile suggests that the primary target of ethanol may be the mitochondria. It is known that mitochondrial stress can lead to ER stress (Sebastian et al. 2012; Lebeau et al. 2018), and mitochondria are a major player in the oxidative stress pathway. Mitochondrial dysfunction can also explain the functional deficits in muscles, since mitochondria are the primary source of energy production.

Mitochondrial architecture is closely linked to mitochondrial function; highly connected mitochondria are more efficient energy producers, and fragmented mitochondria are inefficient at oxidative phosphorylation. We discovered that ethanol exposure leads to mitochondrial fragmentation in *C. elegans*. Such ethanol-induced mitochondrial fragmentation was observed in human and rodent cardiomyocytes and skeletal muscles (Sudarikova Yu, Bakeeva, and

Tsiplenkova 1997; Urbano-Marquez and Fernandez-Sola 2004; Eisner, Lenaers, and Hajnoczky 2014; Eisner et al. 2017). Mitochondrial fragmentation can result from the excessive fission or deficient fusion of mitochondria. Mutations in the mitochondrial fission factor genes *mff-1/2* inhibited ethanol-induced mitochondrial fragmentation efficiently, while mutations in *fis-1/2* led to partial inhibition. FIS-1/2 have been known as fission factors, but recently, they have been shown to increase mitochondrial fragmentation by inhibiting fusion rather than by activating the fission process directly (Yu et al. 2019). This may explain our observation that the *fis-1/2* mutation was less effective in preventing ethanol-induced mitochondrial fragmentation than the *mff-1/2* mutation, which is likely to facilitate fission directly. This further supports the notion that increased fission contributes to ethanol-induced mitochondrial fragmentation more than the reduction of fusion, although we cannot completely rule out the possibility that mitochondrial fusion is also affected by ethanol.

We observed that the expression of *hsp-6p*::GFP was elevated in both *drp-1* and *fzo-1* mutant animals, but the expression level was further increased by ethanol exposure only in *drp-1* mutant animals. Although we and others have shown that the outer mitochondrial membrane of *drp-1* mutant animals is highly connected, it has been reported that the mitochondrial matrix appears to be compartmentalized (Kanazawa et al. 2008), suggesting that there might be a mechanism to partially segregate the inner mitochondrial membrane without DRP-1 to maintain normal mitochondrial function to some degree. This may explain the lower level of *hsp-6p*::GFP induction in *drp-1* mutant animals than in *fzo-1* mutant animals, in which mitochondria are completely fragmented and lose their normal function. In *drp-1* mutant animals, ethanol cannot induce the fragmentation of the outer mitochondrial membrane. However, considering that ethanol further enhances *hsp-6p*::GFP expression in *drp-1* mutant animals, it is possible that

ethanol exposure may target the inner mitochondrial membrane for fission in the absence of DRP-1.

We showed that perpetual UPR^mt activation mediated by constitutively active ATFS-1 protects against alcohol-induced muscle dysfunction. Paradoxically, our data also indicated that ethanol exposure induces UPR^mt through ATFS-1 activation. This raises a question: why would the muscle function of ethanol-exposed animals decline even though ethanol activated a protective UPR^mt response? One possibility is that while the ability of ethanol to induce UPR^mt via ATFS-1 is not robust enough to protect against alcohol-mediated muscle weakness, constitutive activation of ATFS-1 via a gain-of-function mutation is sufficiently robust for such protection. Alternatively, UPR^mt induction prior to ethanol exposure may be necessary to prevent cellular damage.

A simple mechanistic explanation for the protection against alcohol-mediated muscle dysfunction in *atfs-1(et15gf)* animals is that they produce high levels of ATP due to increased mitochondrial biogenesis. However, published data showed that ATFS-1 does not increase ATP production (Nargund et al. 2015). ATFS-1 represses the transcription of genes encoding oxidative phosphorylation components and TCA cycle enzymes but increases the transcription of glycolytic enzyme genes, thus maintaining overall ATP production. Furthermore, ATFS-1 regulates the biosynthesis of certain lipid species (Liu et al. 2014; Oks et al. 2018). In addition to this global metabolic adaption, ATFS-1 promotes oxidative phosphorylation complex assembly and an increase in protective mitochondrial chaperones and proteases, which is designed to improve the health of the mitochondrial proteome (Melber and Haynes 2018; Berendzen et al. 2016). Importantly, long-term UPR^mt is beneficial in protecting against certain types of stresses or infections (Rauthan et al. 2013; Pellegrino et al. 2014; Kaufman and Crowder 2015; Oks et al.

2018; Liu et al. 2014), but it is potentially harmful against others (Bennett et al. 2014; Lamech and Haynes 2015). Intriguingly, the skeletal muscles of chronic alcohol users were reported to exhibit a reduction in aerobic metabolism and an increase in anaerobic metabolism (Haida et al. 1998). This may be explained by our finding of the ethanol-mediated activation of UPR^{mt}, which led to metabolic adaptation. Based on this information, we speculate that UPR^{mt} induced by ATFS-1 activation is directly involved in protection against alcohol-mediated muscle dysfunction. Interestingly, although we do not know if UPR^{mt} influences alcohol-induced tissue damage, several studies in mammals have indeed shown that UPR^{mt} upregulation is protective against certain types of stress-induced organ damage (Gariani et al. 2016; Smyrnias et al. 2019; Wang, Lim, et al. 2019). Studies in both *C. elegans* and mammals showed that UPR^{mt} promotes mitochondrial protein homeostasis, increases mitochondrial protein import, confers innate immunity, and reorganizes metabolic enzymes (Melber and Haynes 2018; Fiorese et al. 2016; Much et al. 2016; Quiros et al. 2017). Based on these studies, we speculate that our findings in *C. elegans* are applicable in mammalian systems; UPR^{mt} has beneficial effects on muscle function of chronic alcohol users and helps to cope with alcohol-mediated muscle damage. Taken together, we propose that mitochondrial dysfunction and consequent UPR^{mt} activation may modulate many of the pathologies associated with alcoholic myopathy, and further understanding of UPR^{mt} in alcoholic myopathy may lead to better therapeutic interventions.

Acknowledgements

188

Author Contributions

KO and HK designed and performed research, analyzed the data and wrote the manuscript. SS and JR performed research, analyzed the data and contributed to writing.

References

1.   Souza-Smith, F. M., Lang, C. H., Nagy, L. E., Bailey, S. M., Parsons, L. H., and Murray, G. J. (2016) Physiological processes underlying organ injury in alcohol abuse. *American journal of physiology. Endocrinology and metabolism* **311**, E605-619

2.   Urbano-Marquez, A., Estruch, R., Navarro-Lopez, F., Grau, J. M., Mont, L., and Rubin, E. (1989) The effects of alcoholism on skeletal and cardiac muscle. *N Engl J Med* **320**, 409-415

3.   Kimball, S. R., and Lang, C. H. (2018) Mechanisms Underlying Muscle Protein Imbalance Induced by Alcohol. *Annu Rev Nutr* **38**, 197-217

4.   Preedy, V. R., Salisbury, J. R., and Peters, T. J. (1994) Alcoholic muscle disease: features and mechanisms. *J Pathol* **173**, 309-315

5.   Eisner, V., Picard, M., and Hajnoczky, G. (2018) Mitochondrial dynamics in adaptive and maladaptive cellular stress responses. *Nat Cell Biol* **20**, 755-765

6.   van der Bliek, A. M., Sedensky, M. M., and Morgan, P. G. (2017) Cell Biology of the Mitochondrion. *Genetics* **207**, 843-871

7.   Oliver, D. M. A., and Reddy, P. H. (2019) Molecular Basis of Alzheimer's Disease: Focus on Mitochondria. *J Alzheimers Dis* **72**, S95-S116

8.   Giacomello, M., Pyakurel, A., Glytsou, C., and Scorrano, L. (2020) The cell biology of mitochondrial membrane dynamics. *Nature reviews. Molecular cell biology*

9.   Shpilka, T., and Haynes, C. M. (2018) The mitochondrial UPR: mechanisms, physiological functions and implications in ageing. *Nature reviews. Molecular cell biology* **19**, 109-120

10. Haynes, C. M., Yang, Y., Blais, S. P., Neubert, T. A., and Ron, D. (2010) The matrix peptide exporter HAF-1 signals a mitochondrial UPR by activating the transcription factor ZC376.7 in C. elegans. *Mol Cell* **37**, 529-540

11. Melber, A., and Haynes, C. M. (2018) UPR(mt) regulation and output: a stress response mediated by mitochondrial-nuclear communication. *Cell research* **28**, 281-295

12. Nargund, A. M., Fiorese, C. J., Pellegrino, M. W., Deng, P., and Haynes, C. M. (2015) Mitochondrial and nuclear accumulation of the transcription factor ATFS-1 promotes OXPHOS recovery during the UPR(mt). *Mol Cell* **58**, 123-133

13. Haynes, C. M., Petrova, K., Benedetti, C., Yang, Y., and Ron, D. (2007) ClpP mediates activation of a mitochondrial unfolded protein response in C. elegans. *Developmental cell* **13**, 467-480

14. Tian, Y., Garcia, G., Bian, Q., Steffen, K. K., Joe, L., Wolff, S., Meyer, B. J., and Dillin, A. (2016) Mitochondrial Stress Induces Chromatin Reorganization to Promote Longevity and UPR(mt). *Cell* **165**, 1197-1208

15. Merkwirth, C., Jovaisaite, V., Durieux, J., Matilainen, O., Jordan, S. D., Quiros, P. M., Steffen, K. K., Williams, E. G., Mouchiroud, L., Tronnes, S. U., Murillo, V., Wolff, S. C., Shaw, R. J., Auwerx, J., and Dillin, A. (2016) Two Conserved Histone Demethylases Regulate Mitochondrial Stress-Induced Longevity. *Cell* **165**, 1209-1223

16. Link, C. D., and Johnson, C. J. (2002) Reporter transgenes for study of oxidant stress in Caenorhabditis elegans. *Methods in enzymology* **353**, 497-505

17. Oh, K. H., and Kim, H. (2013) Reduced IGF signaling prevents muscle cell death in a Caenorhabditis elegans model of muscular dystrophy. *Proceedings of National Academy of Science U S A* **110**, 19024-19029

18.   Estes, K. A., Dunbar, T. L., Powell, J. R., Ausubel, F. M., and Troemel, E. R. (2010) bZIP transcription factor zip-2 mediates an early response to Pseudomonas aeruginosa infection in Caenorhabditis elegans. *Proceedings of National Academy of Science U S A* **107**, 2153-2158

19.   Bolz, D. D., Tenor, J. L., and Aballay, A. (2010) A conserved PMK-1/p38 MAPK is required in caenorhabditis elegans tissue-specific immune response to Yersinia pestis infection. *Journal of Biological Chemistry* **285**, 10832-10840

20.   Iser, W. B., Wilson, M. A., Wood, W. H., 3rd, Becker, K., and Wolkow, C. A. (2011) Co-regulation of the DAF-16 target gene, cyp-35B1/dod-13, by HSF-1 in C. elegans dauer larvae and daf-2 insulin pathway mutants. *PLoS ONE* **6**, e17369

21.   Lamitina, T. (2006) Functional genomic approaches in C. elegans. *Methods in molecular biology* **351**, 127-138

22.   Lehrbach, N. J., and Ruvkun, G. (2016) Proteasome dysfunction triggers activation of SKN-1A/Nrf1 by the aspartic protease DDI-1. *Elife* **5**

23.   Ma, D. K., Vozdek, R., Bhatla, N., and Horvitz, H. R. (2012) CYSL-1 interacts with the O2-sensing hydroxylase EGL-9 to promote H2S-modulated hypoxia-induced behavioral plasticity in C. elegans. *Neuron* **73**, 925-940

24.   Lowry, J., Yochem, J., Chuang, C. H., Sugioka, K., Connolly, A. A., and Bowerman, B. (2015) High-Throughput Cloning of Temperature-Sensitive Caenorhabditis elegans Mutants with Adult Syncytial Germline Membrane Architecture Defects. *G3 (Bethesda)* **5**, 2241-2255

25.   Oh, K. H., and Kim, H. (2019) BK channel clustering is required for normal behavioral alcohol sensitivity in C. elegans. *Scientific reports* **9**, 10224

26.   Alaimo, J. T., Davis, S. J., Song, S. S., Burnette, C. R., Grotewiel, M., Shelton, K. L., Pierce-Shimomura, J. T., Davies, A. G., and Bettinger, J. C. (2012) Ethanol metabolism and osmolarity modify behavioral responses to ethanol in C. elegans. *Alcoholism, clinical and experimental research* **36**, 1840-1850

27.   Scott, L. L., Davis, S. J., Yen, R. C., Ordemann, G. J., Nordquist, S. K., Bannai, D., and Pierce, J. T. (2017) Behavioral Deficits Following Withdrawal from Chronic Ethanol Are Influenced by SLO Channel Function in Caenorhabditis elegans. *Genetics* **206**, 1445-1458

28.   Lesanpezeshki, L., Hewitt, J. E., Laranjeiro, R., Antebi, A., Driscoll, M., Szewczyk, N. J., Blawzdziewicz, J., Lacerda, C. M. R., and Vanapalli, S. A. (2019) Pluronic gel-based burrowing assay for rapid assessment of neuromuscular health in C. elegans. *Scientific reports* **9**, 15246

29.   Weimer, R. M. (2006) Preservation of C. elegans tissue via high-pressure freezing and freeze-substitution for ultrastructural analysis and immunocytochemistry. *Methods in molecular biology* **351**, 203-221

30.   Kim, H., Perentis, R. J., Caldwell, G. A., and Caldwell, K. A. (2018) Gene-by-environment interactions that disrupt mitochondrial homeostasis cause neurodegeneration in C. elegans Parkinson's models. *Cell Death Dis* **9**, 555

31.   Sebastian, D., Hernandez-Alvarez, M. I., Segales, J., Sorianello, E., Munoz, J. P., Sala, D., Waget, A., Liesa, M., Paz, J. C., Gopalacharyulu, P., Oresic, M., Pich, S., Burcelin, R., Palacin, M., and Zorzano, A. (2012) Mitofusin 2 (Mfn2) links mitochondrial and endoplasmic reticulum function with insulin signaling and is essential for normal glucose homeostasis. *Proceedings of National Academy of Science U S A* **109**, 5523-5528

32. Lebeau, J., Saunders, J. M., Moraes, V. W. R., Madhavan, A., Madrazo, N., Anthony, M. C., and Wiseman, R. L. (2018) The PERK Arm of the Unfolded Protein Response Regulates Mitochondrial Morphology during Acute Endoplasmic Reticulum Stress. *Cell reports* **22**, 2827-2836

33. Shen, Q., Yamano, K., Head, B. P., Kawajiri, S., Cheung, J. T., Wang, C., Cho, J. H., Hattori, N., Youle, R. J., and van der Bliek, A. M. (2014) Mutations in Fis1 disrupt orderly disposal of defective mitochondria. *Molecular biology of the cell* **25**, 145-159

34. Labrousse, A. M., Zappaterra, M. D., Rube, D. A., and van der Bliek, A. M. (1999) C. elegans dynamin-related protein DRP-1 controls severing of the mitochondrial outer membrane. *Mol Cell* **4**, 815-826

35. Mai, S., Klinkenberg, M., Auburger, G., Bereiter-Hahn, J., and Jendrach, M. (2010) Decreased expression of Drp1 and Fis1 mediates mitochondrial elongation in senescent cells and enhances resistance to oxidative stress through PINK1. *J Cell Sci* **123**, 917-926

36. Cartoni, R., Leger, B., Hock, M. B., Praz, M., Crettenand, A., Pich, S., Ziltener, J. L., Luthi, F., Deriaz, O., Zorzano, A., Gobelet, C., Kralli, A., and Russell, A. P. (2005) Mitofusins 1/2 and ERRalpha expression are increased in human skeletal muscle after physical exercise. *The Journal of physiology* **567**, 349-358

37. Eisner, V., Lenaers, G., and Hajnoczky, G. (2014) Mitochondrial fusion is frequent in skeletal muscle and supports excitation-contraction coupling. *J Cell Biol* **205**, 179-195

38. Palikaras, K., Lionaki, E., and Tavernarakis, N. (2015) Coordination of mitophagy and mitochondrial biogenesis during ageing in C. elegans. *Nature* **521**, 525-528

39. Tan, F. J., Husain, M., Manlandro, C. M., Koppenol, M., Fire, A. Z., and Hill, R. B. (2008) CED-9 and mitochondrial homeostasis in C. elegans muscle. *J Cell Sci* **121**, 3373-3382

40. Lu, Y., Rolland, S. G., and Conradt, B. (2011) A molecular switch that governs mitochondrial fusion and fission mediated by the BCL2-like protein CED-9 of Caenorhabditis elegans. *Proceedings of National Academy of Science U S A* **108**, E813-822

41. Nargund, A. M., Pellegrino, M. W., Fiorese, C. J., Baker, B. M., and Haynes, C. M. (2012) Mitochondrial import efficiency of ATFS-1 regulates mitochondrial UPR activation. *Science* **337**, 587-590

42. Fernandez-Sola, J., Preedy, V. R., Lang, C. H., Gonzalez-Reimers, E., Arno, M., Lin, J. C., Wiseman, H., Zhou, S., Emery, P. W., Nakahara, T., Hashimoto, K., Hirano, M., Santolaria-Fernandez, F., Gonzalez-Hernandez, T., Fatjo, F., Sacanella, E., Estruch, R., Nicolas, J. M., and Urbano-Marquez, A. (2007) Molecular and cellular events in alcohol-induced muscle disease. *Alcoholism, clinical and experimental research* **31**, 1953-1962

43. Simon, L., Jolley, S. E., and Molina, P. E. (2017) Alcoholic Myopathy: Pathophysiologic Mechanisms and Clinical Implications. *Alcohol Res* **38**, 207-217

44. Sudarikova Yu, V., Bakeeva, L. E., and Tsiplenkova, V. G. (1997) Ultrastructure of mitochondrial reticulum of human cardiomyocytes in alcohol cardiomyopathy. *Biochemistry (Mosc)* **62**, 989-1002

45. Urbano-Marquez, A., and Fernandez-Sola, J. (2004) Effects of alcohol on skeletal and cardiac muscle. *Muscle Nerve* **30**, 689-707

46.   Eisner, V., Cupo, R. R., Gao, E., Csordas, G., Slovinsky, W. S., Paillard, M., Cheng, L., Ibetti, J., Chen, S. R., Chuprun, J. K., Hoek, J. B., Koch, W. J., and Hajnoczky, G. (2017) Mitochondrial fusion dynamics is robust in the heart and depends on calcium oscillations and contractile activity. *Proceedings of National Academy of Science U S A* **114**, E859-E868

47.   Yu, R., Jin, S. B., Lendahl, U., Nister, M., and Zhao, J. (2019) Human Fis1 regulates mitochondrial dynamics through inhibition of the fusion machinery. *EMBO J* **38**

48.   Kanazawa, T., Zappaterra, M. D., Hasegawa, A., Wright, A. P., Newman-Smith, E. D., Buttle, K. F., McDonald, K., Mannella, C. A., and van der Bliek, A. M. (2008) The C. elegans Opa1 homologue EAT-3 is essential for resistance to free radicals. *PLoS Genetics* **4**, e1000022

49.   Liu, Y., Samuel, B. S., Breen, P. C., and Ruvkun, G. (2014) Caenorhabditis elegans pathways that surveil and defend mitochondria. *Nature* **508**, 406-410

50.   Oks, O., Lewin, S., Goncalves, I. L., and Sapir, A. (2018) The UPR(mt) Protects Caenorhabditis elegans from Mitochondrial Dysfunction by Upregulating Specific Enzymes of the Mevalonate Pathway. *Genetics* **209**, 457-473

51.   Berendzen, K. M., Durieux, J., Shao, L. W., Tian, Y., Kim, H. E., Wolff, S., Liu, Y., and Dillin, A. (2016) Neuroendocrine Coordination of Mitochondrial Stress Signaling and Proteostasis. *Cell* **166**, 1553-1563 e1510

52.   Rauthan, M., Ranji, P., Aguilera Pradenas, N., Pitot, C., and Pilon, M. (2013) The mitochondrial unfolded protein response activator ATFS-1 protects cells from inhibition of the mevalonate pathway. *Proceedings of National Academy of Science U S A* **110**, 5981-5986

53.   Pellegrino, M. W., Nargund, A. M., Kirienko, N. V., Gillis, R., Fiorese, C. J., and Haynes, C. M. (2014) Mitochondrial UPR-regulated innate immunity provides resistance to pathogen infection. *Nature* **516**, 414-417

54.   Kaufman, D. M., and Crowder, C. M. (2015) Mitochondrial Proteostatic Collapse Leads to Hypoxic Injury. *Curr Biol* **25**, 2171-2176

55.   Bennett, C. F., Vander Wende, H., Simko, M., Klum, S., Barfield, S., Choi, H., Pineda, V. V., and Kaeberlein, M. (2014) Activation of the mitochondrial unfolded protein response does not predict longevity in Caenorhabditis elegans. *Nature communications* **5**, 3483

56.   Lamech, L. T., and Haynes, C. M. (2015) The unpredictability of prolonged activation of stress response pathways. *J Cell Biol* **209**, 781-787

57.   Haida, M., Yazaki, K., Kurita, D., and Shinohara, Y. (1998) Mitochondrial dysfunction of human muscle in chronic alcoholism detected by using 31P-magnetic resonance spectroscopy and near-infrared light absorption. *Alcoholism, clinical and experimental research* **22**, 108S-110S

58.   Gariani, K., Menzies, K. J., Ryu, D., Wegner, C. J., Wang, X., Ropelle, E. R., Moullan, N., Zhang, H., Perino, A., Lemos, V., Kim, B., Park, Y. K., Piersigilli, A., Pham, T. X., Yang, Y., Ku, C. S., Koo, S. I., Fomitchova, A., Canto, C., Schoonjans, K., Sauve, A. A., Lee, J. Y., and Auwerx, J. (2016) Eliciting the mitochondrial unfolded protein response by nicotinamide adenine dinucleotide repletion reverses fatty liver disease in mice. *Hepatology* **63**, 1190-1204

59.   Smyrnias, I., Gray, S. P., Okonko, D. O., Sawyer, G., Zoccarato, A., Catibog, N., Lopez, B., Gonzalez, A., Ravassa, S., Diez, J., and Shah, A. M. (2019) Cardioprotective Effect of

the Mitochondrial Unfolded Protein Response During Chronic Pressure Overload. *J Am Coll Cardiol* **73**, 1795-1806

60.   Wang, Y. T., Lim, Y., McCall, M. N., Huang, K. T., Haynes, C. M., Nehrke, K., and Brookes, P. S. (2019) Cardioprotection by the mitochondrial unfolded protein response requires ATF5. *American journal of physiology. Heart and circulatory physiology* **317**, H472-H478

61.   Fiorese, C. J., Schulz, A. M., Lin, Y. F., Rosin, N., Pellegrino, M. W., and Haynes, C. M. (2016) The Transcription Factor ATF5 Mediates a Mammalian Mitochondrial UPR. *Curr Biol* **26**, 2037-2043

62.   Much, C., Auchynnikava, T., Pavlinic, D., Buness, A., Rappsilber, J., Benes, V., Allshire, R., and O'Carroll, D. (2016) Endogenous Mouse Dicer Is an Exclusively Cytoplasmic Protein. *PLoS Genetics* **12**, e1006095

63.   Quiros, P. M., Prado, M. A., Zamboni, N., D'Amico, D., Williams, R. W., Finley, D., Gygi, S. P., and Auwerx, J. (2017) Multi-omics analysis identifies ATF4 as a key regulator of the mitochondrial stress response in mammals. *J Cell Biol* **216**, 2027-2045

Figure legends

Fig. 1. Long-term ethanol exposure causes muscle dysfunction. *(A)* Ethanol-exposed animals exhibit a reduction in the thrashing frequency in a liquid environment compared to control animals. ****$p < 0.0001$, unpaired t-test. *(B)* Ethanol-exposed animals exhibit a significant delay in burrowing across 26% Pluronic F-127 gel. Triplicate measurements of 15 animals, **$p < 0.005$, ****$p < 0.0001$, two-way ANOVA, Sidak's post hoc analysis. *(C, D)* Ethanol-exposed animals persistently showed smaller muscle sizes than paired control animals even after 4 hours of recovery. Scale bar, 10 μm. Myosin fibers were visualized using transgenic animals expressing *myo-3*::GFP (*cimIs46*). L4 stage animals were cultured in the absence (control 0 h) or presence (recovery 0 h) of ethanol for 24 hours, and half of them were allowed to recover on NGM plates in the absence of ethanol for an additional 4 hours. The borders of muscle cells are marked by arrowheads (mean ± SEM, t-test, **$p < 0.01$). *(E)* The pharyngeal pumping rate remained the same in control and ethanol-exposed animals. Ten L4-stage animals were cultured in the absence (control) or presence of ethanol, and then their pharyngeal pumping rate was measured. $p = 0.9$, t-test

Fig. 2. Chronic ethanol exposure induces the expression of stress response genes. *(A)* Mitochondrial and ER but not cytosolic stress responses were induced after 24 hours of ethanol exposure. *hsp-6p*::GFP, *hsp-4p*::GFP, and *hsp-16.2p*::GFP were used as reporters for UPR^{mt}, UPR^{ER}, and UPR^{cyto}, respectively. In control animals, *hsp-6* and *hsp-4* were minimally expressed in some tissues. In ethanol-exposed animals, *hsp-6* and *hsp-4* were expressed throughout the entire body, including in body wall muscle. mean ± SEM, t-test, ****$p < 0.0001$ *(B)* Ethanol

exposure induced oxidative stress. *gst-4p*::GFP was induced after 24 hours of ethanol exposure. The white asterisks denote body wall muscle cells. Mean ± SEM, t-test, ****$p < 0.0001$

Fig. 3. Ethanol-exposed animals exhibit muscle mitochondrial fragmentation in a fission machinery-dependent manner. *(A)* Muscle mitochondrial networks underwent fragmentation when *cimIs40*[*myo-3p::tomm-20(1-68)::*FusionRed] animals were exposed to ethanol for 24 hours. 1: normal linear networks; 2: moderately fragmented; 3: severely fragmented but arranged in a linear fashion; 4: completely fragmented with no discernable linear position. Scale bar: 10 μm, $p < 0.0001$, Mann-Whitney test. The numbers above the bar graph are the sample numbers. *(B)* Transmission electron microscopy in striated body wall muscles of wild-type control (upper three panels) and 24 hr ethanol-exposed animals (lower three panels). Scale bar, 2 μm. *(C)* Schematic drawing of the DRP-1 and DRP-1 receptors MFF-1/2 and FIS-1/2. *(D)* Mitochondrial networks in control and ethanol-exposed *drp-1* and *mff-1,2* (*mff-1;mff-2*) double-mutant animals. Scale bar, 10 μm. *(E)* Quantification of mitochondrial networks in wild-type and *mff-1,2* double mutant animals. ****$p < 0.0001$, Kruskal-Wallis test, Dunn's post-hoc analysis. The numbers above the bar graph are the sample numbers.

Fig. 4. Alcohol-induced mitochondrial fragmentation contributes to UPR^mt and the oxidative stress response. *(A)* UPR^mt (*hsp-6p*::GFP) was upregulated in both *drp-1* and *fzo-1* mutants, but UPR^mt in *fzo-1* mutant animals was not further increased by ethanol exposure. mean ± SEM ****$p < 0.0001$, ***$p < 0.001$, t-test. *(B)* The oxidative stress response (*gst-4p*::GFP) was upregulated by ethanol exposure in wild-type and *drp-1* mutant animals but not in *fzo-1* mutant

animals with hyperfragmented mitochondria. mean ± SEM ****$p < 0.0001$, ***$p < 0.0008$, ns = 0.867, one-way ANOVA, Sidak's post-hoc analysis.

Fig. 5. Ethanol activates transcription factors involved in the induction of the UPR^{mt}. *(A)* Ethanol exposure for 24 hours mobilizes ATFS-1::GFP to cell nuclei in the intestine. The dotted circles denote intestinal cell nuclei. *(B)* Nuclear DVE-1, which is required for the induction of *hsp-6* upon mitochondrial stress in addition to ATFS-1, is also increased upon ethanol exposure. The SJ4197 strain (*zcIs39[dve-1p::dve-1::gfp]*) was used. The number of DVE-1-positive nuclei was counted, excluding those in the head region, where DVE-1::GFP is constitutively present in nuclei. Mean ± SEM ****$p < 0.0001$, t-test.

Fig. 6. Constitutive activation of ATFS-1 protects against ethanol-mediated muscle weakness. *(A)* The thrashing assay after 24 hours of ethanol exposure showed that *atfs-1(gf, gain-of-function)* mutant animals but not wild-type or *atfs-1(lf, loss-of-function)* animals showed normal thrashing. Mean ± SEM ****$p < 0.0001$, 2-way ANOVA, Tukey's post hoc analysis. *(B)* Age-matched wild-type, *atfs-1(gf),* and *atfs-1(lf)* animals exhibited normal burrowing ability when grown under normal conditions. *(C)* After 24 hours of ethanol exposure, *atfs-1(gf)* animals but not wild-type or *atfs-1(lf)* animals exhibited normal burrowing ability. Triplicate measurements of 15 animals, mean ± SEM **$p < 0.01$, ***$p < 0.001$, ****$p < 0.0001$, 2-way ANOVA, Tukey's post hoc analysis.

Figure 1

Figure 2

A

hsp-4p::GFP

$p < 0.0001$
****

hsp-6p::GFP

$p < 0.0001$
****

B

gst-4p::GFP

**** $p < 0.0001$
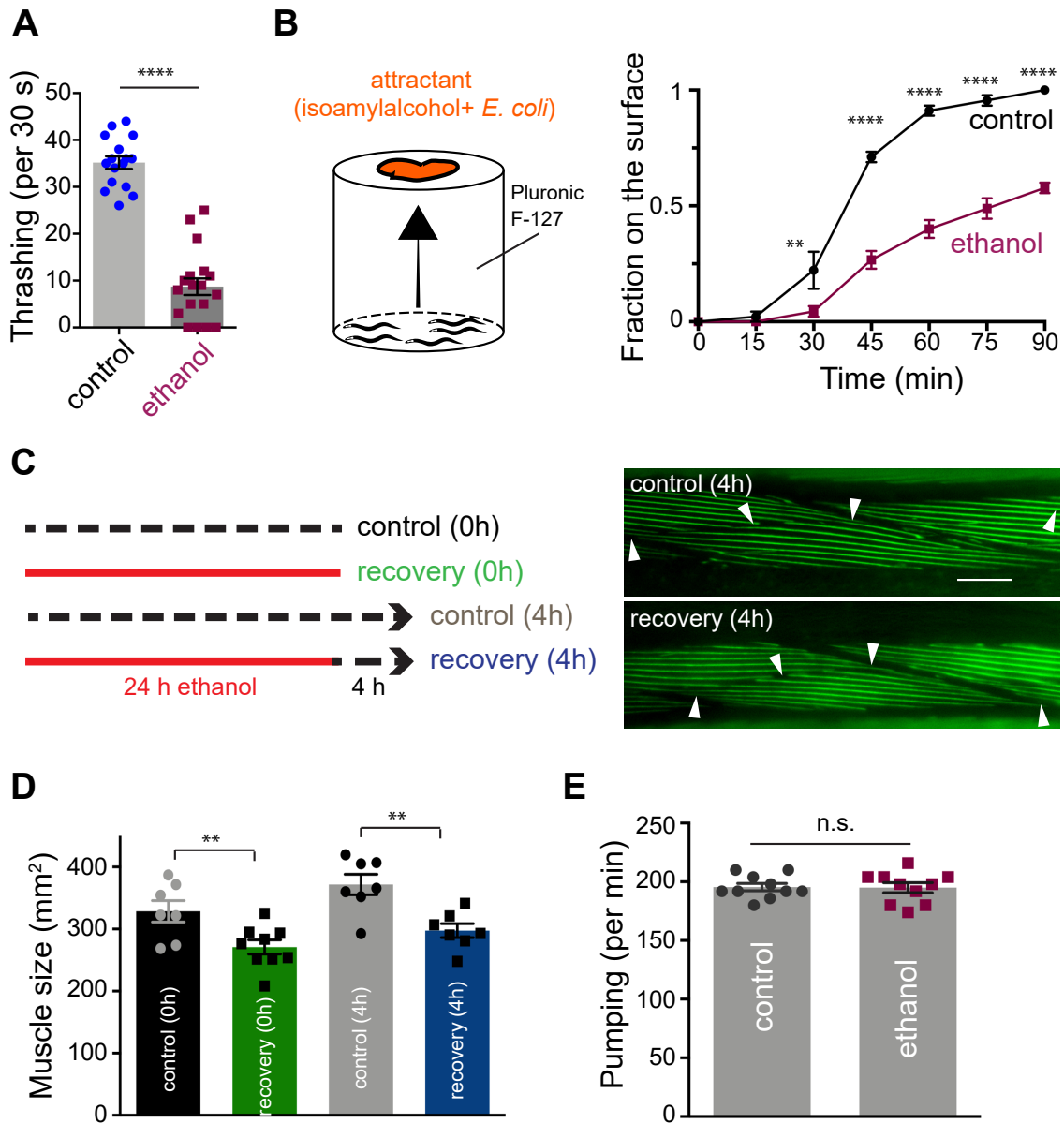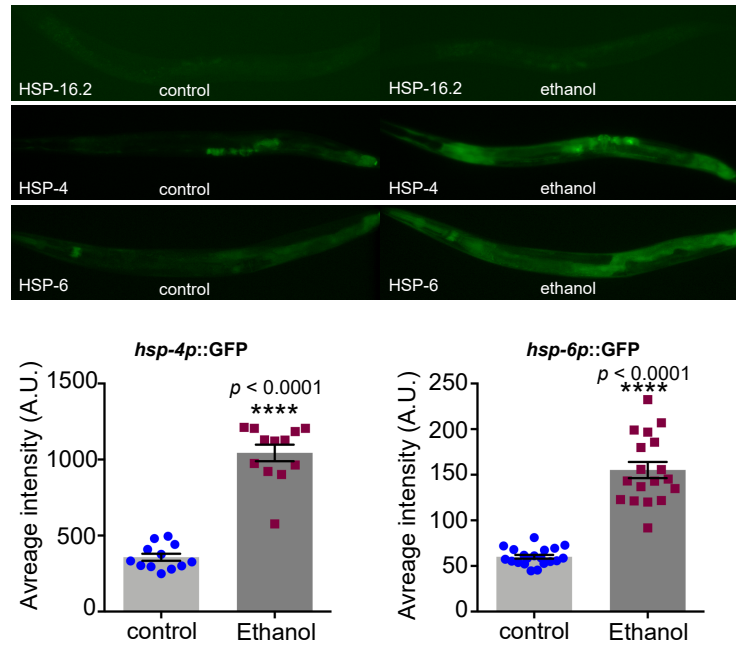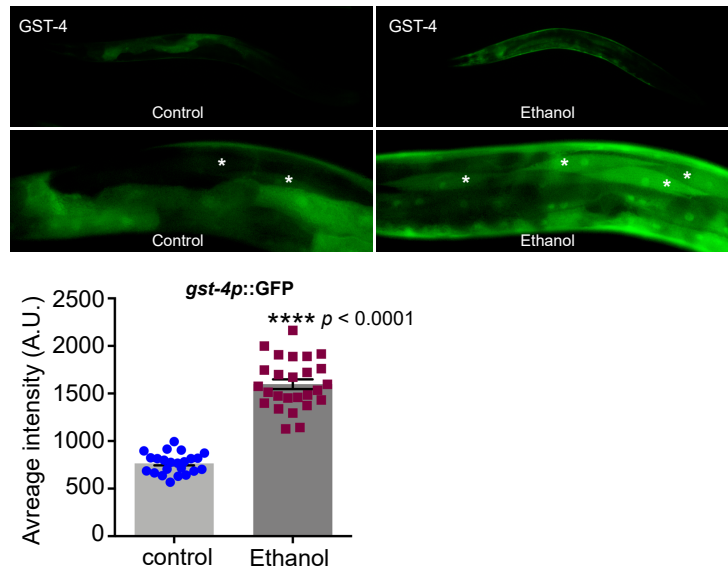
Figure 3

Figure 4

Figure 5

A *atfs-1::GFP*

B *dve-1::GFP*

Figure 6

A

slo-1(eg142)

****

B

sodh-1p::NLS::RFP

Control

EtOH
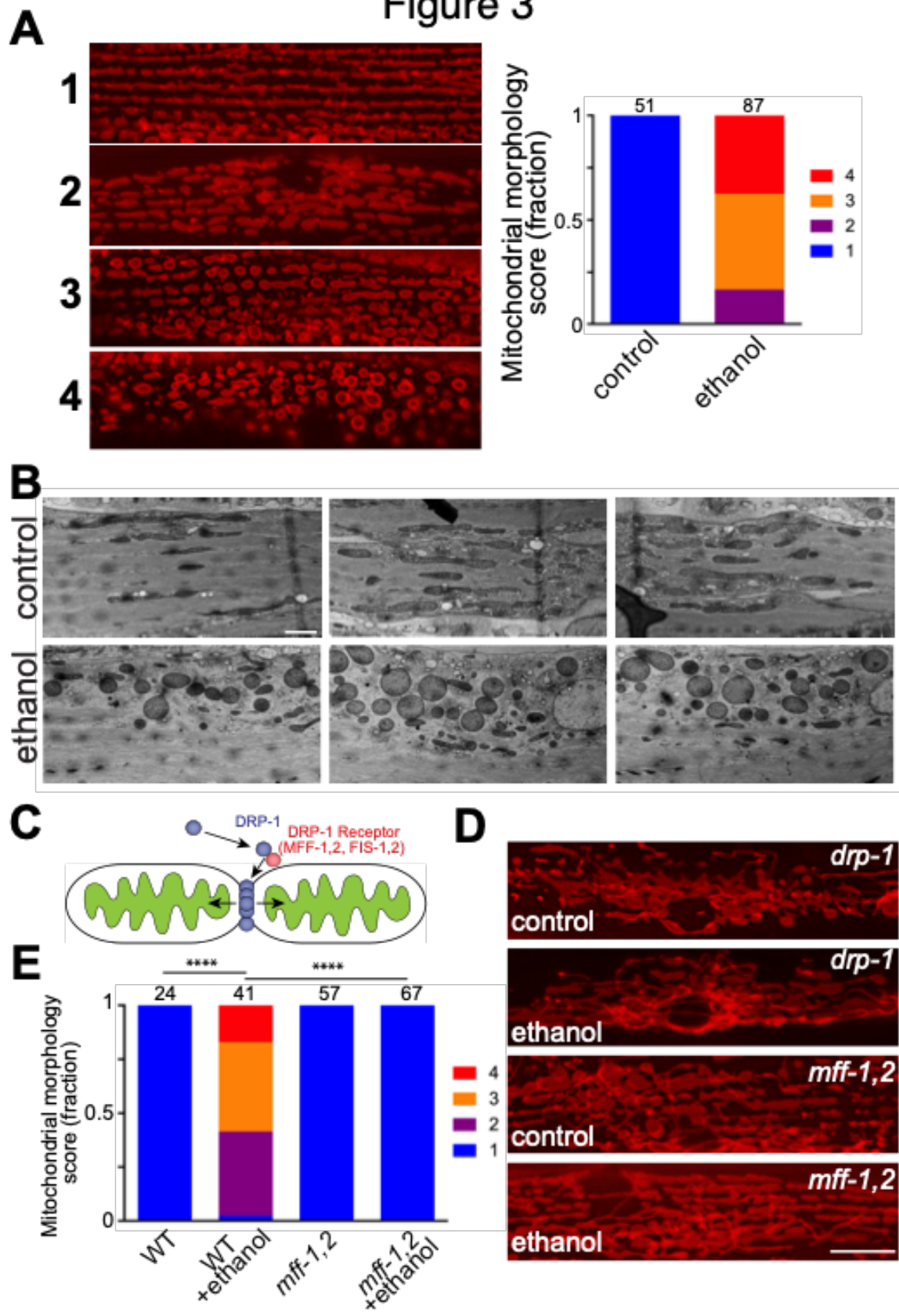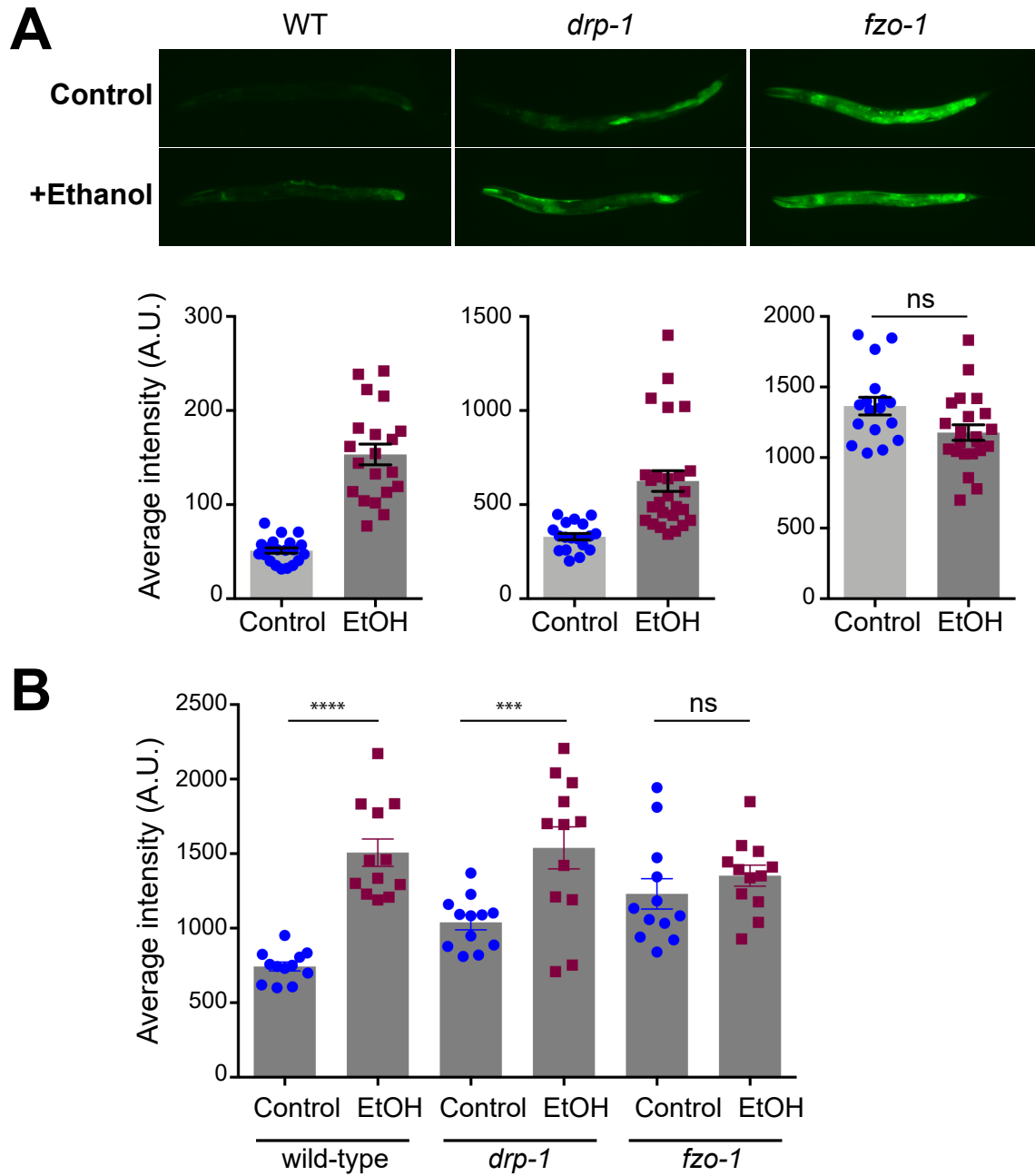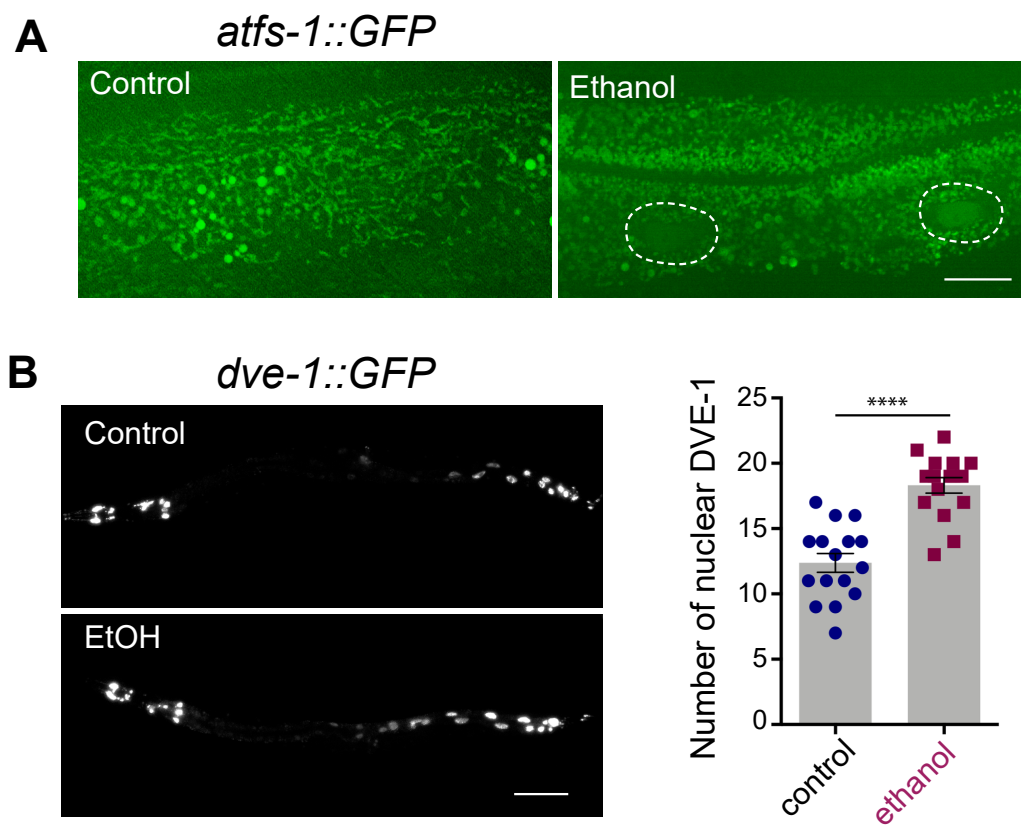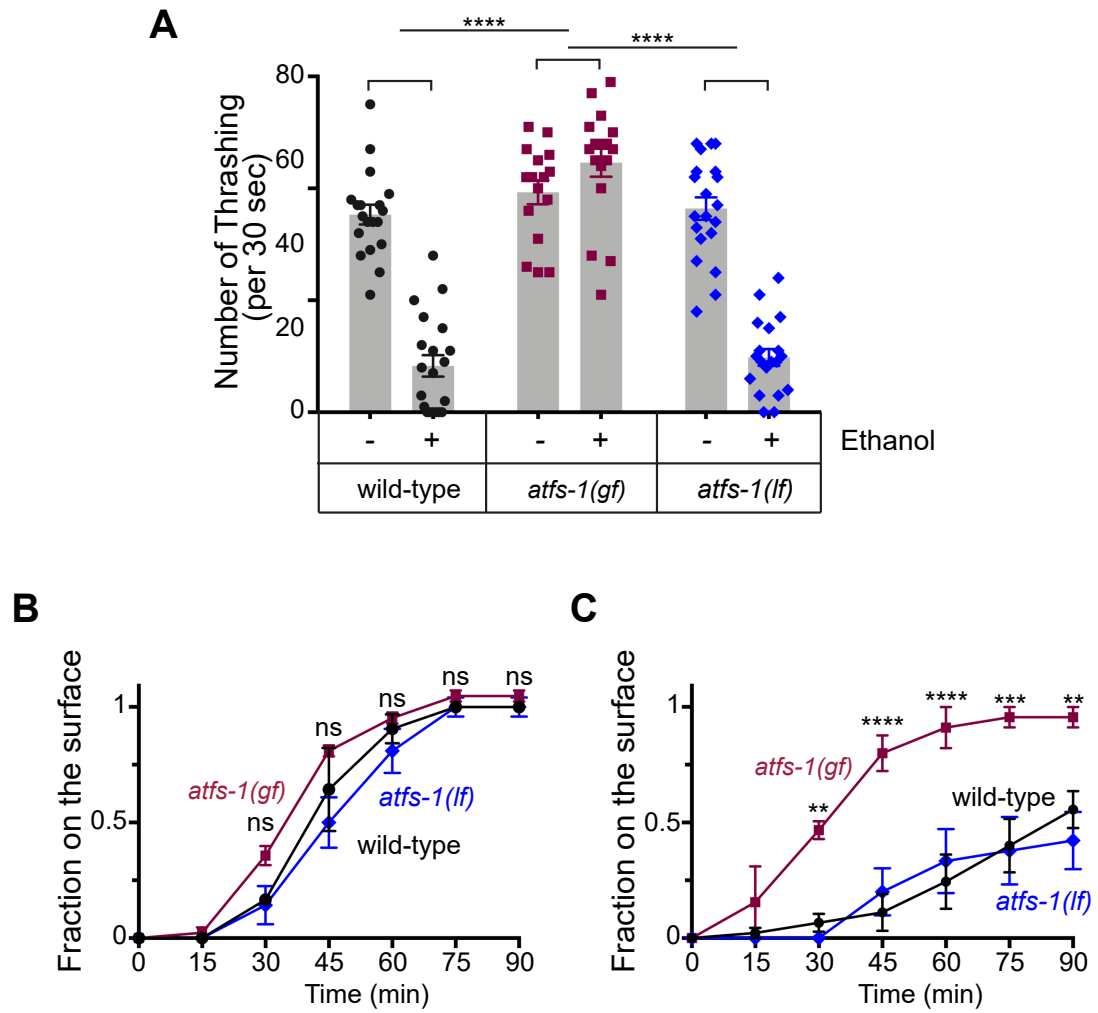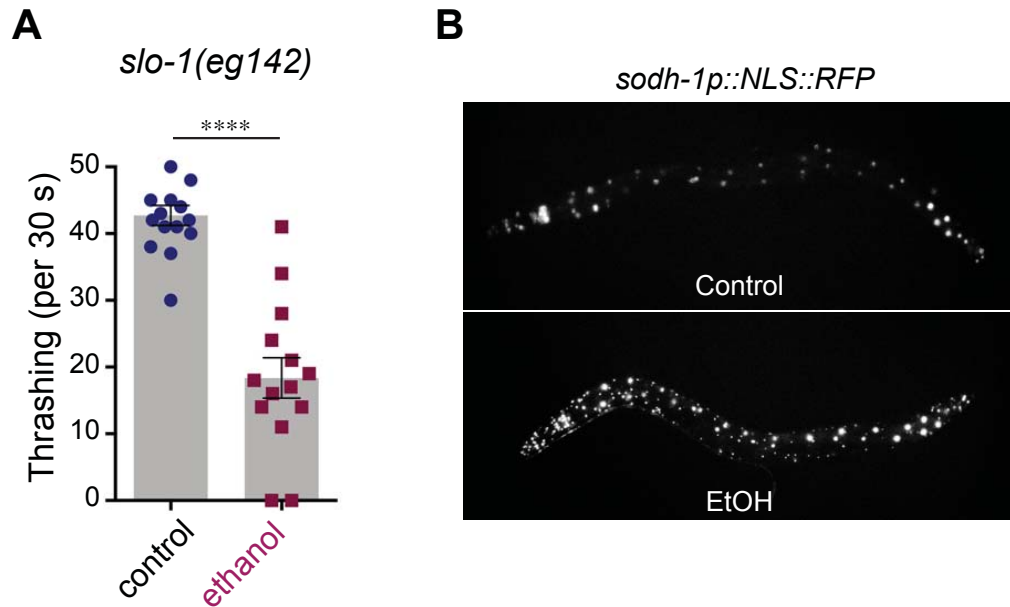
Supplemental Fig. S1. Ethanol induces stress responses independent of acute alcohol tolerance. *(A)* Animals resistant to the intoxicating effects of ethanol still show an impairment in thrashing. *slo-1(eg142)* mutant animals were exposed to ethanol for 24 hours. Mean ± SEM ****$p <$ 0.0001, t-test. *(B)* Ethanol strongly induced the expression of the alcohol dehydrogenase *sodh-1*. The CF2124 strain (*muIs139 [dod-11p::RFP(NLS) + rol-6(su1006)]*) was exposed to ethanol in the L4 stage for 24 hours.

A

fis-1;fis-2

control

+Ethanol

B

C

anti-GFP

anti-tubulin

N2   control   +ethanol

1   1.03
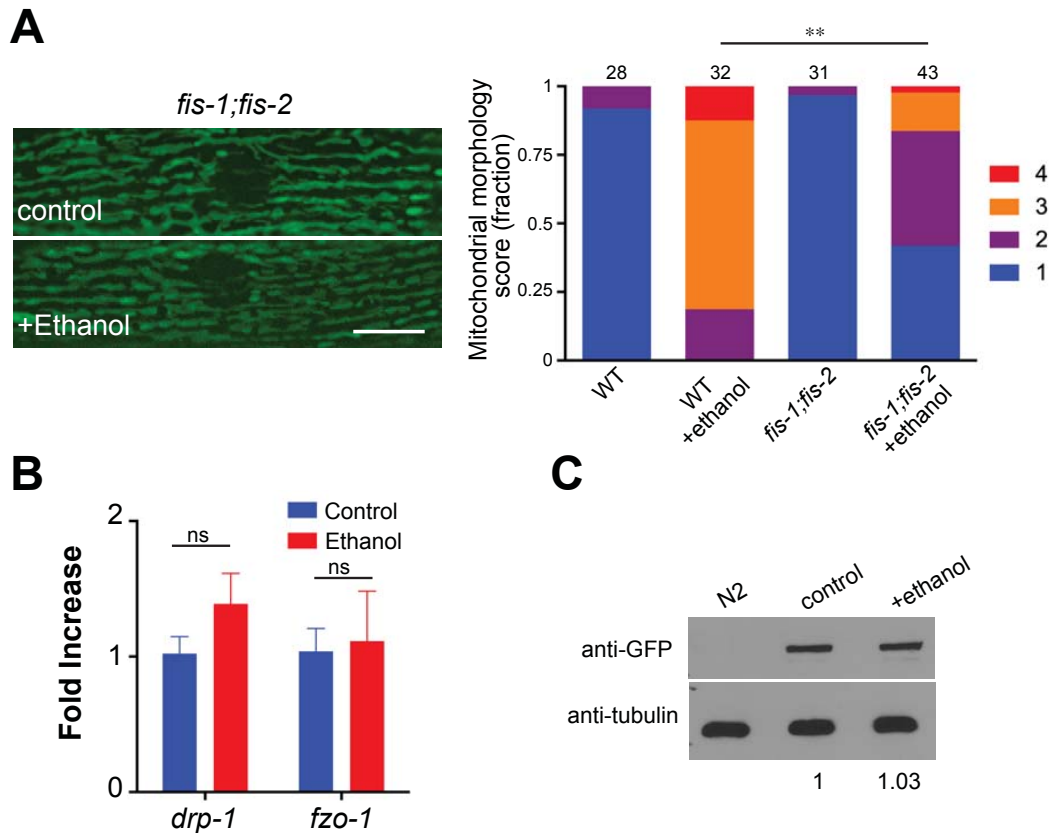
Supplemental Fig. S2. Mutations in genes that mediate mitophagy and cell death do not alter ethanol-induced mitochondrial fragmentation. *(A)* Mitochondrial networks in control and ethanol-exposed wild- type and *fis-1;fis-2* double-mutant animals. Mitochondrial networks were assessed in a *cimIs42*[*twk-28p*::*atp-9*::GFP] background. Scale bar, 10 μm. **$p < 0.01$, Kruskal - Wallis test, Dunn's post hoc analysis. The numbers above the bar graph are the sample numbers. *(B)* The levels of *drp-1* and *fzo-1* mRNA were not different between control and ethanol-exposed wild-type animals. The data for qRT-PCR were normalized with *cdc-42*, a house keeping gene. Four biological replicates. Mean ± SEM, ns: not significant, unpaired t-test. *(C)* Western blot analysis with genome-edited strain EU2917 (*drp-1(or194[GFP::drp-1]).* N2: wild type animals that do not express GFP. GFP signals were normalized against -tubulin. The control sample was set to 1. Western blot was repeated three times with three biological samples. The relative level of ethanol-treated sample was $1.03 ± 0.05$ (Mean ± SEM), n= 3.
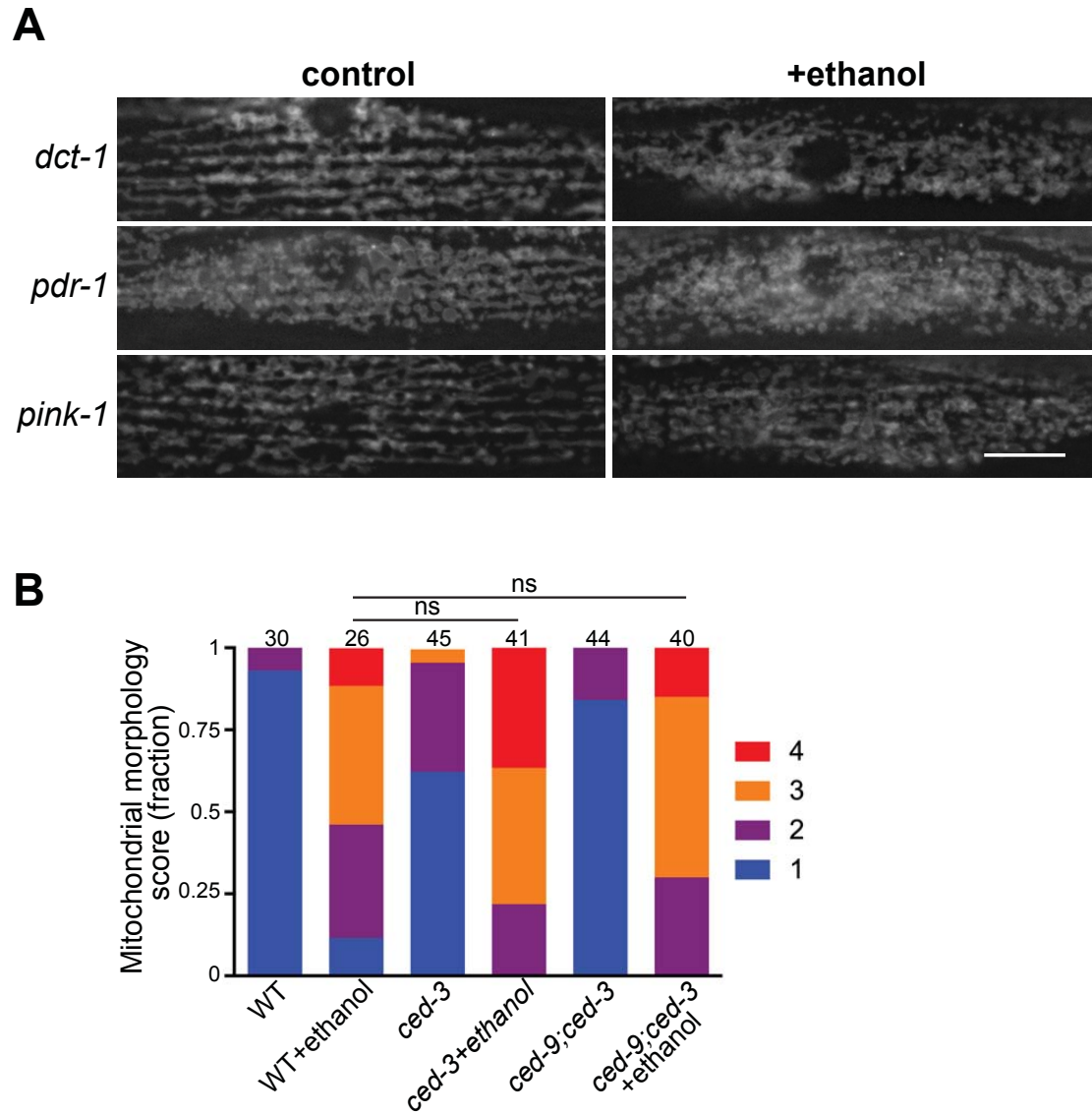
Supplemental Fig. S3. *(A)* Mitochondrial networks in control and ethanol-exposed *dct-1, pdr-1,* and *pink-1* mutant animals. These mutants exhibited dense mitochondrial networks, which hindered accurate quantification. Scale bar, 10 μm. *(B)* Mitochondrial networks in control and ethanol-exposed wild-type, *ced-3*, and *ced-9;ced-3* mutant animals. The numbers above the bar graph are the sample numbers. ns: not significant.

Copyright license for reproduction in dissertation

JOHN WILEY AND SONS LICENSE
TERMS AND CONDITIONS

Oct 05, 2020

This Agreement between Seema Sheoran ("You") and John Wiley and Sons ("John Wiley and Sons") consists of your license details and the terms and conditions provided by John Wiley and Sons and Copyright Clearance Center.

License Number	4922840427962
License date	Oct 05, 2020
Licensed Content Publisher	John Wiley and Sons
Licensed Content Publication	THE FASEB JOURNAL
Licensed Content Title	Alcohol induces mitochondrial fragmentation and stress responses to maintain normal muscle function in Caenorhabditis elegans
Licensed Content Author	Hongkyun Kim, Janet E. Richmond, Seema Sheoran, et al
Licensed Content Date	Apr 15, 2020
Licensed Content Volume	34
Licensed Content Issue	6
Licensed Content Pages	13
Type of use	Dissertation/Thesis
Requestor type	Author of this Wiley article
Format	Electronic
Portion	Full article
Will you be translating?	No

Title	Ultrastructural analysis of proteins implicated in synaptic vesicle docking and priming in C. elegans
Institution name	University of Illinois at Chicago
Expected presentation date	Nov 2020
Requestor Location	Seema Sheoran 950 S Halsted St. SEL 4311 CHICAGO, IL 60607 United States Attn: Seema Sheoran
Publisher Tax ID	EU826007151
Total	0.00 USD
Terms and Conditions	

TERMS AND CONDITIONS

to any maximum distribution number specified in the license. The first instance of republication or reuse granted by this license must be completed within two years of the date of the grant of this license (although copies prepared before the end date may be distributed thereafter). The Wiley Materials shall not be used in any other manner or for any other purpose, beyond what is granted in the license. Permission is granted subject to an appropriate acknowledgement given to the author, title of the material/book/journal and the publisher. You shall also duplicate the copyright notice that appears in the Wiley publication in your use of the Wiley Material. Permission is also granted on the understanding that nowhere in the text is a previously published source acknowledged for all or part of this Wiley Material. Any third party content is expressly excluded from this permission.

- With respect to the Wiley Materials, all rights are reserved. Except as expressly granted by the terms of the license, no part of the Wiley Materials may be copied, modified, adapted (except for minor reformatting required by the new Publication), translated, reproduced, transferred or distributed, in any form or by any means, and no derivative works may be made based on the Wiley Materials without the prior permission of the respective copyright owner.**For STM Signatory Publishers clearing permission under the terms of the [STM Permissions Guidelines](#) only, the terms of the license are extended to include subsequent editions and for editions in other languages, provided such editions are for the work as a whole in situ and does not involve the separate exploitation of the permitted figures or extracts,** You may not alter, remove or suppress in any manner any copyright, trademark or other notices displayed by the Wiley Materials. You may not license, rent, sell, loan, lease, pledge, offer as security, transfer or assign the Wiley Materials on a stand-alone basis, or any of the rights granted to you hereunder to any other person.

- The Wiley Materials and all of the intellectual property rights therein shall at all times remain the exclusive property of John Wiley & Sons Inc, the Wiley Companies, or their respective licensors, and your interest therein is only that of having possession of and the right to reproduce the Wiley Materials pursuant to Section 2 herein during the continuance of this Agreement. You agree that you own no right, title or interest in or to the Wiley Materials or any of the intellectual property rights therein. You shall have no rights hereunder other than the license as provided for above in Section 2. No right, license or interest to any trademark, trade

name, service mark or other branding ("Marks") of WILEY or its licensors is granted hereunder, and you agree that you shall not assert any such right, license or interest with respect thereto

- NEITHER WILEY NOR ITS LICENSORS MAKES ANY WARRANTY OR REPRESENTATION OF ANY KIND TO YOU OR ANY THIRD PARTY, EXPRESS, IMPLIED OR STATUTORY, WITH RESPECT TO THE MATERIALS OR THE ACCURACY OF ANY INFORMATION CONTAINED IN THE MATERIALS, INCLUDING, WITHOUT LIMITATION, ANY IMPLIED WARRANTY OF MERCHANTABILITY, ACCURACY, SATISFACTORY QUALITY, FITNESS FOR A PARTICULAR PURPOSE, USABILITY, INTEGRATION OR NON-INFRINGEMENT AND ALL SUCH WARRANTIES ARE HEREBY EXCLUDED BY WILEY AND ITS LICENSORS AND WAIVED BY YOU.

- WILEY shall have the right to terminate this Agreement immediately upon breach of this Agreement by you.

- You shall indemnify, defend and hold harmless WILEY, its Licensors and their respective directors, officers, agents and employees, from and against any actual or threatened claims, demands, causes of action or proceedings arising from any breach of this Agreement by you.

- IN NO EVENT SHALL WILEY OR ITS LICENSORS BE LIABLE TO YOU OR ANY OTHER PARTY OR ANY OTHER PERSON OR ENTITY FOR ANY SPECIAL, CONSEQUENTIAL, INCIDENTAL, INDIRECT, EXEMPLARY OR PUNITIVE DAMAGES, HOWEVER CAUSED, ARISING OUT OF OR IN CONNECTION WITH THE DOWNLOADING, PROVISIONING, VIEWING OR USE OF THE MATERIALS REGARDLESS OF THE FORM OF ACTION, WHETHER FOR BREACH OF CONTRACT, BREACH OF WARRANTY, TORT, NEGLIGENCE, INFRINGEMENT OR OTHERWISE (INCLUDING, WITHOUT LIMITATION, DAMAGES BASED ON LOSS OF PROFITS, DATA, FILES, USE, BUSINESS OPPORTUNITY OR CLAIMS OF THIRD PARTIES), AND WHETHER OR NOT THE PARTY HAS BEEN ADVISED OF THE POSSIBILITY OF SUCH DAMAGES. THIS LIMITATION SHALL APPLY NOTWITHSTANDING ANY FAILURE OF ESSENTIAL PURPOSE OF ANY LIMITED REMEDY PROVIDED HEREIN.

- Should any provision of this Agreement be held by a court of competent jurisdiction to be illegal, invalid, or unenforceable, that provision shall be deemed amended to achieve as nearly as possible the same economic effect as the original provision, and the legality, validity and enforceability of the remaining provisions of this Agreement shall not be affected or impaired thereby.

- The failure of either party to enforce any term or condition of this Agreement shall not constitute a waiver of either party's right to enforce each and every term and condition of this Agreement. No breach under this agreement shall be deemed waived or excused by either party unless such waiver or consent is in writing signed by the party granting such waiver or consent. The waiver by or consent of a party to a breach of any provision of this Agreement shall not operate or be construed as a waiver of or consent to any other or subsequent breach by such other party.

- This Agreement may not be assigned (including by operation of law or otherwise) by you without WILEY's prior written consent.

- Any fee required for this permission shall be non-refundable after thirty (30) days from receipt by the CCC.

- These terms and conditions together with CCC's Billing and Payment terms and conditions (which are incorporated herein) form the entire agreement between you and WILEY concerning this licensing transaction and (in the absence of fraud) supersedes all prior agreements and representations of the parties, oral or written. This Agreement may not be amended except in writing signed by both parties. This Agreement shall be binding upon and inure to the benefit of the parties' successors, legal representatives, and authorized assigns.

- In the event of any conflict between your obligations established by these terms and conditions and those established by CCC's Billing and Payment terms and conditions, these terms and conditions shall prevail.

- WILEY expressly reserves all rights not specifically granted in the combination of (i) the license details provided by you and accepted in the course of this licensing transaction, (ii) these terms and conditions and (iii) CCC's Billing and Payment terms and conditions.

- This Agreement will be void if the Type of Use, Format, Circulation, or Requestor Type was misrepresented during the licensing process.

- This Agreement shall be governed by and construed in accordance with the laws of the State of New York, USA, without regards to such state's conflict of law rules. Any legal action, suit or proceeding arising out of or relating to these Terms and Conditions or the breach thereof shall be instituted in a court of competent jurisdiction in New York County in the State of New York in the United States of America and each party hereby consents and submits to the personal jurisdiction of such court, waives any objection to venue in such court and consents to service of process by registered or certified mail, return receipt requested, at the last known address of such party.

WILEY OPEN ACCESS TERMS AND CONDITIONS

Wiley Publishes Open Access Articles in fully Open Access Journals and in Subscription journals offering Online Open. Although most of the fully Open Access journals publish open access articles under the terms of the Creative Commons Attribution (CC BY) License only, the subscription journals and a few of the Open Access Journals offer a choice of Creative Commons Licenses. The license type is clearly identified on the article.

The Creative Commons Attribution License

The [Creative Commons Attribution License (CC-BY)](#) allows users to copy, distribute and transmit an article, adapt the article and make commercial use of the article. The CC-BY license permits commercial and non-

Creative Commons Attribution Non-Commercial License

The [Creative Commons Attribution Non-Commercial (CC-BY-NC)License](#) permits use, distribution and reproduction in any medium, provided the original work is properly cited and is not used for commercial purposes.(see below)

Creative Commons Attribution-Non-Commercial-NoDerivs License

The [Creative Commons Attribution Non-Commercial-NoDerivs License](#) (CC-BY-NC-ND) permits use, distribution and reproduction in any medium,

provided the original work is properly cited, is not used for commercial purposes and no modifications or adaptations are made. (see below)

Use by commercial "for-profit" organizations

Use of Wiley Open Access articles for commercial, promotional, or marketing purposes requires further explicit permission from Wiley and will be subject to a fee.

Further details can be found on Wiley Online Library http://olabout.wiley.com/WileyCDA/Section/id-410895.html

Other Terms and Conditions:

v1.10 Last updated September 2015

Questions? customercare@copyright.com or +1-855-239-3415 (toll free in the US) or +1-978-646-2777.

APPENDIX B

Molecular mechanism underlying the activation of KPC-1 in context of PVD dendritic self-avoidance

Introduction

Specific branching pattern of dendrites is essential for a neuron to receive inputs only from its specific receptive field, which in turn ensures the proper functioning of a neuron in its neuronal circuit. Although the structure of dendritic arbors is a key feature in neuronal connectivity and its function, the mechanism underlying dendritic branching is not fully understood.

In mammals, disruption of transcription factor CREST (for calcium-responsive transactivator) and signaling pathways such as CaMKII-NeuroD and Sema3A profoundly impair generation and maintenance of dendrite (Aizawa et al. 2004; Gaudilliere et al. 2004; Morita et al. 2006). Studies in *Drosophila* have identified transcription factors, receptor–ligand interactions, various signaling pathways, local translational machinery, cytoskeletal elements, Golgi outposts and endosomes as regulators of dendritic branching (Jan and Jan 2010). In *C.elegans,* a multi-protein receptor ligand complex has been shown to be indispensable for dendritic patterning (Fig. 1). Epidermis-ligands SAX-7 (Sensory AXon guidance) and MNR-1 (MeNoRin, dendritic branching protein); and a ligand secreted by the body wall muscles LECT-2 (LEukocyte cell-derived ChemoTaxin 2), bind to the DMA-1 transmembrane receptor present on the PVD sensory neuron and guide the dendritic arborization in a spatial manner (Diaz-Balzac et al. 2016; Dong et al. 2013; Liu and Shen 2011; Salzberg, Diaz-Balzac, et al. 2013; Zou et al. 2016).
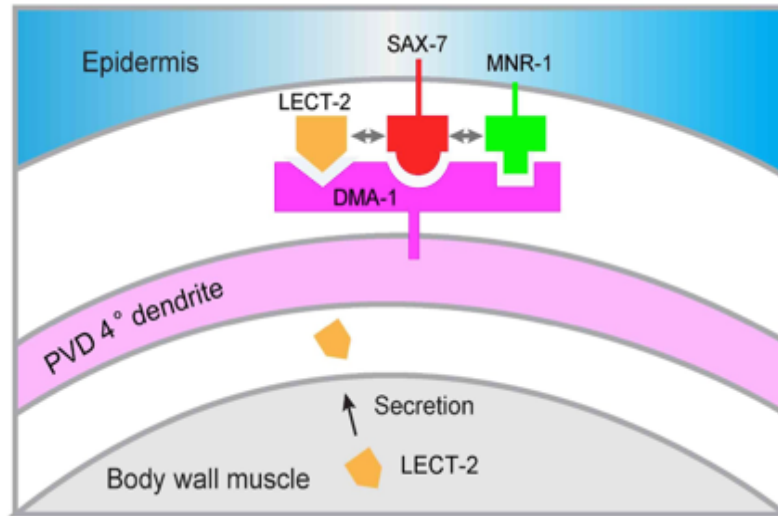
Figure 1. A diagram showing DMA-1 receptor and its ligands SAX-7, MNR-1, and LECT-2. Image reproduced from [Zou et al., 2016. eLife 2016;5:e18345. Fig. 10C]

Studies since the 1980s have revealed two important dendrite organization principles: self-avoidance and tiling (Grueber and Sagasti 2010; Kramer and Kuwada 1983). Self-avoidance is the phenomenon in which dendrites arising from the same soma avoid each other. Tiling, by contrast, refers to the ability of dendrites arising from different somas to co-exist. Self-avoidance ensures non-redundant coverage of dendritic territories and hence ensures functional appropriate coverage of neuronal inputs. In 2007, parallel studies identified the role of *Dscam* (Down syndrome cell-adhesion molecule) in controlling dendritic self- avoidance in *Drosophila* da sensory neurons (Hattori et al. 2007; Hughes et al. 2007; Matthews et al. 2007; Millard et al. 2007; Soba et al. 2007). *Dscam* encodes a large number of cell-surface proteins of the Immunoglobulin superfamily. Interaction between identical isoforms of *Dscam* result in self recognition and hence repulsion between sister dendrites. Similarly, homophilic interactions between Procadherin isoforms in vertebrates generate repulsive cues between dendrites from the same neuron (Lefebvre et al. 2012). Recently, a study identified the role of a proprotein convertase KPC-1 in dendritic self-avoidance in *C. elegans* (Dong et al. 2016).

KPC-1 (Kex-2 Proprotein Convertase family), a *C.elegans* Furin homolog, is a member of the paired basic amino acid cleaving enzyme (PACE) family of proprotein convertases. Mammalian furin is activated by the proteolytic cleavage of its N-terminal Pro domain by its own catalytic domain (Thomas 2002). Similarly, KPC-1 also needs to cleave its Pro domain to be fully activated. Previous studies have shown that KPC-1 is required for dendritic branching as KPC-1 loss-of-function mutants show severe loss of higher order dendrites in PVD sensory neuron (Salzberg, Ramirez-Suarez, and Bulow 2014; Schroeder et al. 2013). In a genetic
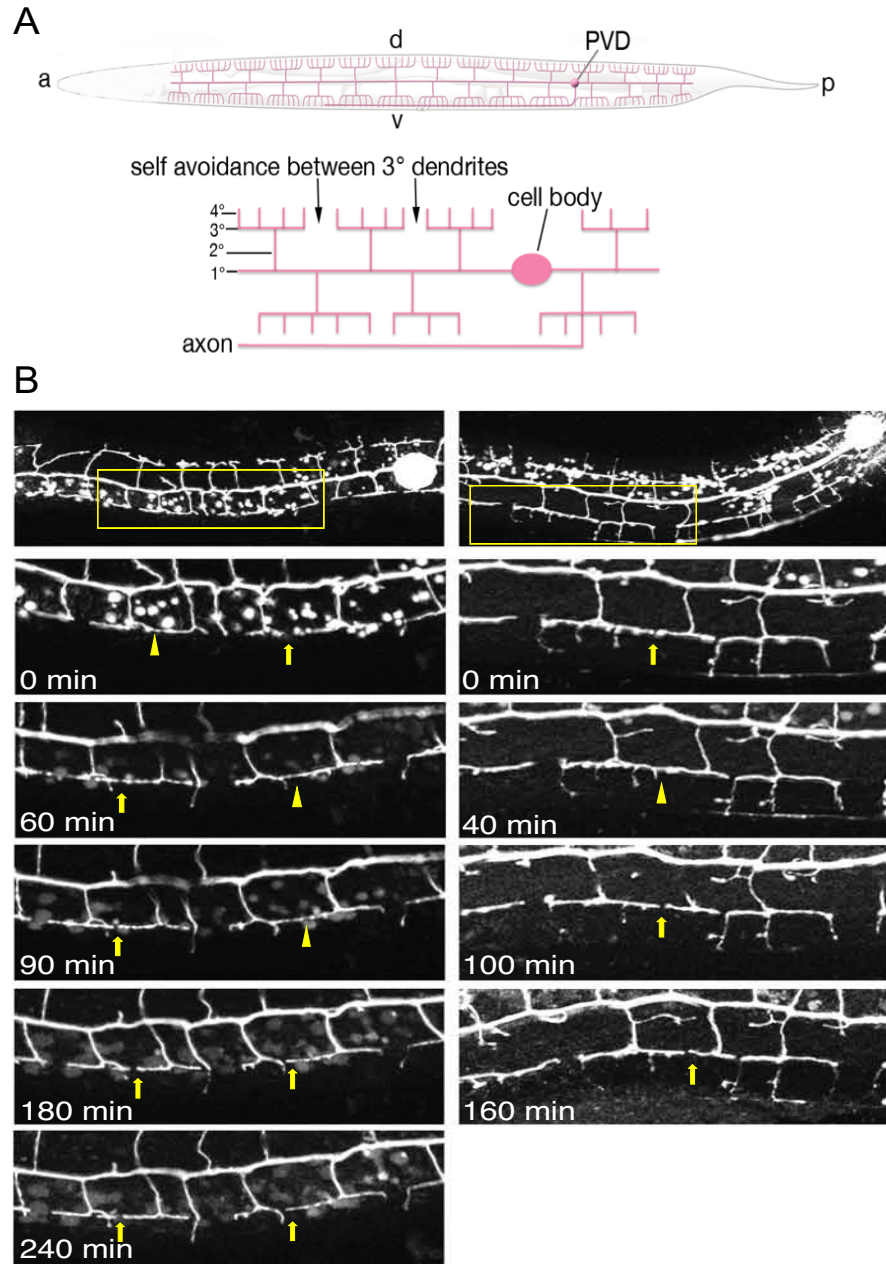
Figure 2. **Overexpression of KPC-1 does not inhibit initial contact between the 3° dendrites.**

(A) Diagrams showing the coverage of PVD dendrites in an animal and organization of dendrites (adapted from WormAtlas). a: anterior, p: posterior, d: dorsal, v: ventral. (B) Representative images of two animals with overexpressed KPC-1.

screen for mutants with PVD dendrite self-avoidance defects, Chang lab identified another allele of *kpc-1*, *xr58*, which resulted in an amino acid substitution P440S in its catalytic domain that likely affected its protease function[Dong et al. 2016]. *kpc-1(xr58)* mutants show a severe self-avoidance defect between the sister dendrites. Overexpression of *kpc-1* results in self-avoidance between the 3° dendrites. My time lapse imaging data shows that when KPC-1 is overexpressed in the PVD neuron, the 3° dendrites first make contact and later show self- avoidance, similar to wild type (Fig. 2). This shows that the overexpression of KPC-1 does not inhibit the initial contact between the 3° dendrites, instead it promotes self-avoidance after the 3° dendrites contact each other.

In addition to the self-avoidance defect, *kpc-1(xr58)* mutants show an increase in the number of the 3° dendrites whereas known dendrite patterning molecular components such as *dma-1*, *sax-7* and *mnr-1* mutants show reduced number of the 3° dendrites (Fig. 3). This suggests that KPC-1 inhibits SAX-7, MNR-1 or DMA-1. If this is true, *kpc-1* mutation will cause upregulation of the tripartite complex and mutation in *sax-7*, *mnr-1,* or *dma-1* will be able to suppress it. Indeed, my double mutant analysis shows that mutations in the *sax-7*, *mnr-1,* or *dma-1* suppress *kpc-1(xr58)* phenotype (Fig. 3). In addition, *kpc-1(xr58)* mutants show a striking self-avoidance defect in the higher order dendrites of the PVD sensory neuron. A recent study showed that KPC-1 downregulates the DMA-1 receptor on PVD dendrites by targeting it to late endosomes. Down regulation of DMA-1 receptor by KPC-1 allows dendrites to move away from their SAX-7/MNR-1 ligand rich intermediate targets in order to complete dendritic arborization. But, the detailed mechanism-of-action underlying the KPC-1 mediated dendritic self-avoidance is yet to be identified.
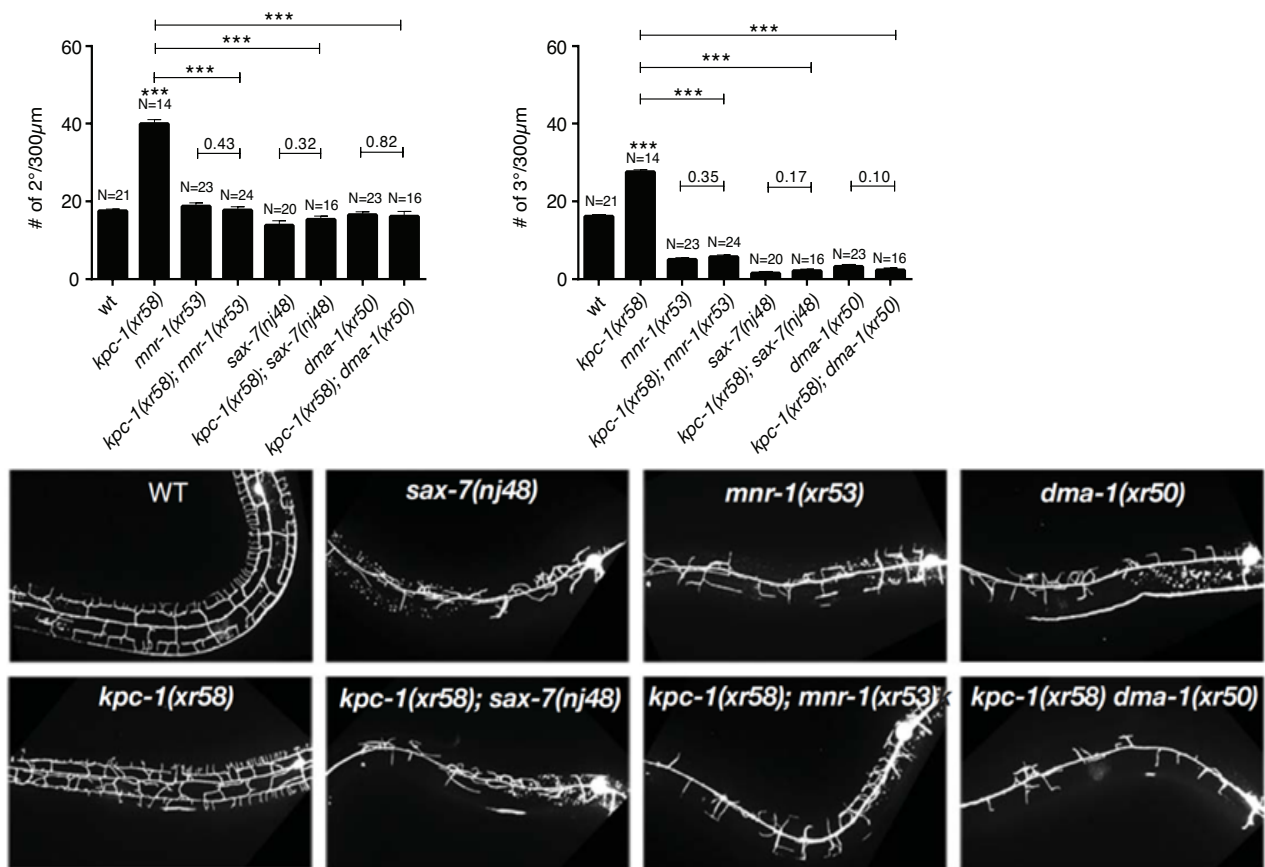
Figure 3. **Mutations in the sax-7, mnr-1, and dma-1 suppress kpc-1(xr58) dendritic phenotype.** Graphs show the average number of 2° and 3° dendrites measured along the 30 um of the 1° dendrite. Representative images of respective genotypes are shown under the graphs.

Significance of Spatio-Temporal Regulation of Neuronal Branching and Connectivity

The human nervous system is composed of 10^{12} neurons that form 10^{15} connections. These numbers signify a daunting task for the human brain to achieve proper neuronal patterning. Dendrites needs to achieve their stereotypic morphology in order to receive input from their designated receptive fields. In addition, axons have to follow a defined trajectory in order to form the connection with its designated target. This complexity of the human brain makes it more interesting to identify the specific molecules and mechanisms involved in regulating precise neuronal connectivity.

Since the pioneering work of Ramon Y Cajal, beginning in late 1800s, morphology of neurons is one of the main criteria in identifying distinct neurons. During development, a neuron undergoes different stages of neuronal branching and achieves its final morphology with the help of cues expressed at different developmental stages and in different cells. Attainment of neuron type specific connectivity in turn leads to establishment of appropriate activity patterns within the neuronal network. As the geometry of neuronal arbors critically influences neuronal properties, stringent spatio-temporal regulation of neuronal branching and connectivity is critical. However, much remains to be understood regarding the mechanism underlying the spatio-temporal regulation of neuronal branching and connectivity.

C. elegans as a model organism to study Neuronal Branching

C. elegans has emerged as an apt model system to study neuronal branching due to various reasons. It has a simple nervous system composed of 302 neurons with a nearly complete map of all axons and synapses. This reduces the challenges faced in other model systems with a complex nervous system. Optical transparency of *C. elegans* allows visualization of florescent

reporters *in vivo*. In addition, availability of fluorescent reporters for each of the 302 neurons allows visualization of neurons at a single cell resolution. Short life cycle of *C. elegans* allows faster generation of worms with different genetic backgrounds and relatively quicker acquisition of data. It is a tractable genetic model system to identify, characterize and investigate the interaction of genes involved in biological processes. Due to its short life cycle, large scale genetic screens for identifying genes involved in neuronal branching can be carried out in a short period of time. Genetic screens are indispensable tools in worms, as they allow for unbiased identification of genes involved in particular aspects of development. Moreover, *C. elegans* was the first multicellular organism to have the complete genome sequenced and this resulted in several databases and resources that are currently available online for the scientific community. There are a significant number of proteins that are evolutionary conserved between this nematode and humans. 83% of *C. elegans* proteins have been found to have homologs in humans. Therefore, there is a high possibility that what is identified in worms will be applicable to humans.

Results

1.1.   *Forward genetic screen to identify the mutants that suppress the self- avoidance defect in*

        kpc-1(xr58) mutants.

       I carried out a forward genetic screen in *kpc-1(xr58)* mutants showing self-avoidance defects in the PVD sensory neuron dendrites. PVD polymodal neuron has highly branched and organized dendrite structures with the self-avoidance and tiling characteristics (Oren-Suissa et al. 2010; Sulston and Horvitz 1977; White et al. 1986) (Fig. 2A). *C. elegans* have two PVD neurons (PVDL and PVDR), on each side of the adult animal. PVD dendrites have a stereotypic dendritic arbor that covers two thirds of the entire animal body. The PVD cell body is post embryonically

225

generated during the larval stage 2 (L2) and sends out primary (1°) dendrite in anterior-posterior directions. During the larval stage 2 (L2) to larval stage 3 (L3), secondary (2°) dendrites branch out from the primary dendrite and grow along the dorsal ventral axis. Upon reaching the border of the outer body wall muscles, secondary dendrites form tertiary (3°) dendrites orthogonally to themselves. Finally, during the L3 to L4 stage, quaternary (4°) dendrites branch out from the tertiary dendrites along the dorso-ventral axis to complete the architecture of the menorah-like structures. In adult animals, 3° dendrites from neighboring menorah point towards each other but do not touch. Through time lapse imaging it has been shown that PVD dendrites form non-overlapping structures by contact dependent self-avoidance (Smith et al. 2010). During the L3 stage 3° dendrites grow toward each other and form contact. Upon contact, 3° dendrites start to retract and hence a gap is formed between the sister tertiary dendrites which is maintained in the mature PVD dendrite arbor (Fig. 2A). In *kpc-1(xr58)* mutants, the contact dependent self-avoidance is lost and 3° dendrites do not retract after contact. During the genetic screen, I looked for the mutants that show suppression of the self-avoidance defect in *kpc-1(xr58)* mutants.

I screened 3150 genomes and identified a suppressor of *kpc-1(xr58)* named *sup-4(xr64)*. More than 90% of *kpc-1(xr58); sup-4(xr64)* animals show a PVD phenotype similar to wild type with self-avoidance between sister dendrites (Fig. 4). Further, I analyzed the self-avoidance index for the wild type, *kpc-1(xr58)* and *kpc-1(xr58); sup-4(xr64)* mutants. Self- avoidance index is defined as the number of gaps between the sister tertiary dendrites of PVD neuron divided by the total number of gaps and contacts between the tertiary dendrites [Self avoidance index = number of gaps/ (number of gaps + number of contacts)]. For the wild type animals, self-avoidance index is 0.985 whereas in case of *kpc-1(xr58)* mutants, due to more number of contacts between the tertiary dendrites this value is decreased to 0.288. But, *sup-4(xr64)*

226

mutation in the *kpc-1(xr58)* mutant background rescues the self-avoidance index to 0.708, similar to wild type.

As the genetic screen was carried out in the *kpc-1(xr58)* background, the identified *sup-4(xr64)* is also in a *kpc-1(xr58)* background. Therefore, my next step was to remove the *kpc-1(xr58)* mutation to identify the PVD phenotype of *sup-4(xr64)* mutant alone. Using genetic crosses, I identified that although the penetrance is only 15%, *sup-4(xr64)* mutants have an abnormal PVD phenotype. This includes a primary dendrite guidance defect, reduction in the number of secondary and higher order dendrites in the region distal to the PVD cell body and a shorter primary dendrite (Fig. 4).

I further outcrossed the *sup-4(xr64)* mutant six times to get rid of any background mutation caused by EMS mutagenesis. In order to confirm that the *sup-4(xr64)* mutation indeed suppresses the *kpc-1(xr58)* self-avoidance defect, I reconstituted the *kpc-1(xr58); sup-4(xr64)* double mutant from *kpc-1(xr58)* and *sup-4(xr64)* single mutants. The reconstituted *kpc-1(xr58); sup-4(xr64)* double mutant shows suppression of self-avoidance defect similar to the *kpc-1(xr58); sup-4(xr64)* that was originally identified through the genetic screen.

A recent study has shown that KPC-1 downregulates the DMA-1 receptor (Dong et al. 2016). DMA-1 receptor is a crucial component of the ligand-receptor complex that is critical for PVD dendritic branching (Liu and Shen 2011). Loss of DMA-1 results in a decrease in the number of higher order PVD dendrites, whereas overexpression of DMA-1 results in an increase in number of PVD dendrites and a self- avoidance defect similar to *kpc-1(xr58)* mutants. Also, *kpc-1(xr58)* mutants show upregulated DMA-1 levels in the PVD neuron (Dong et al. 2016). One
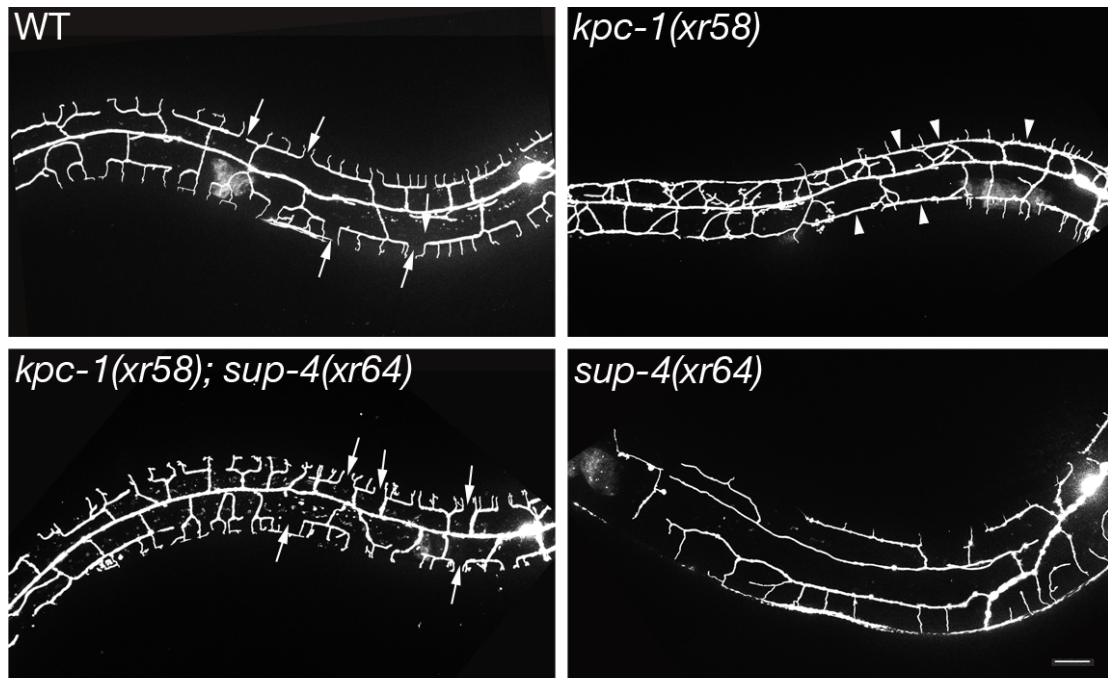
Figure 4. *sup-4(xr64)* **mutation suppresses self-avoidance defect in** *kpc-1(xr58)* **mutants.** Representative images of PVD dendrite phenotype in wild type (WT), *kpc-1(xr58)*, *kpc-1(xr58); sup-4(xr64)* and *sup-4(xr64)* mutants. Arrows: self-avoidance (gaps) between 3° dendrites. Arrowheads: self-avoidance defect (contact) between 3° dendrites. Scale bar: 20μm.

of the possibilities is that *sup-4(xr64)* mutation is in the *dma-1* gene that brings downs the DMA-1 receptor levels to wild type and hence suppresses the self-avoidance defect in the *kpc-1(xr58); sup-4(xr64)* mutants. My sequencing result has ruled out this possibility as it shows no mutation in the *dma-1* coding region in the *sup-4(xr64)* mutant.

I had planned to use SNP (Single Nucleotide Polymorphism) based whole genome sequencing (WGS) to identify the mutation in *sup-4(xr64)*. This strategy involves crossing the *sup-4(xr64)* mutant with a polymorphic strain, cloning out F2s with the mutant phenotype, pooling of the progenies of F2 animals, isolating DNA and sending it out for whole genome sequencing (Doitsidou et al. 2010). The density of polymorphic SNP markers is decreased in the mutation bearing DNA region and this enables the identification of the mutation in the WGS data. I have prepared the *sup-4(xr64)* genomic DNA for sending it out for SNP based WGS.

1.2. *Placing sup-4 in a molecular pathway*

PVD dendrites arborize precisely between epidermis and muscle tissues. This precise arborization is regulated by a specific receptor-ligand complex. This complex includes the DMA-1 transmembrane receptor present on the PVD dendrites and ligands such as SAX-7, MNR-1 and LECT-2 present/secreted by epidermis and muscles respectively (Salzberg, Diaz-Balzac, et al. 2013; Zou et al. 2016). DMA-1 receptor is only activated when LECT-2, SAX-7 and MNR-1 are all present. This kind of combinatorial receptor-ligand interaction results in the precise targeting and patterning of PVD dendrites. In order to examine the genetic interaction between *sup-4* and the four essential molecular components i.e. *dma-1*, *sax-7*, *mnr-1* and *lect-2*, I built and analyzed the PVD phenotype in *sup-4; dma-1, sup-4; sax-7, sup-4; mnr-1*, and *sup-4; lect-2* double mutants. In contrast to *sup-4(xr58)* mutant which has atleast a few intact menorahs

near the PVD cell body, *dma-1/sax-7/mnr-1/lect-2* single mutants completely lack menorah structures and show trapping of higher order dendrites near the primary dendrite (Fig. 5). If SUP-4 is indeed acting through the DMA-1 receptor and SAX-7/MNR-1/LECT-2 ligand complex, then the absence of any of these components would result in a double mutant phenotype that is indistinguishable from *dma-1/sax-7/mnr-1/lect-2* single mutants. My data correlates with the expected outcome (Fig. 5). All of the double mutants show PVD phenotype similar to the *dma-1/sax-7/mnr-1/lect-2* single mutants.
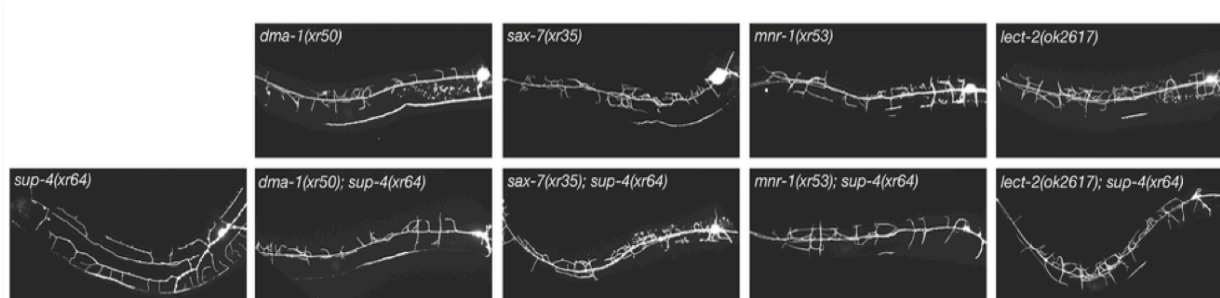
Figure 5. SUP-4 acts through the DMA-1 receptor and SAX-7/MNR-1/LECT-2 ligand complex. Representative images of the PVD dendrites in single mutants: *dma-1(xr50)*, *sax-7(xr35)*, *mnr-1(xr53)*, *lect-2(ok2617)*, *sup-4(xr64)* and double mutants *dma-1(xr50); sup-4(xr64)*, *sax-7(xr35); sup-4(xr64)*, *mnr-1(xr53); sup-4(xr64)* and *lect-2(ok2617); sup-4(xr64)*.

References

1.   Aizawa, H., et al., *Dendrite development regulated by CREST, a calcium-regulated transcriptional activator.* Science, 2004. **303**(5655): p. 197-202.

2.   Gaudilliere, B., et al., *A CaMKII-NeuroD signaling pathway specifies dendritic morphogenesis.* Neuron, 2004. **41**(2): p. 229-41.

3.   Morita, A., et al., *Regulation of dendritic branching and spine maturation by semaphorin3A-Fyn signaling.* J Neurosci, 2006. **26**(11): p. 2971-80.

4.   Jan, Y.N. and L.Y. Jan, *Branching out: mechanisms of dendritic arborization.* Nat Rev Neurosci, 2010. **11**(5): p. 316-28.

5.   Diaz-Balzac, C.A., et al., *Muscle- and Skin-Derived Cues Jointly Orchestrate Patterning of Somatosensory Dendrites.* Curr Biol, 2016. **26**(17): p. 2379-87.

6.   Dong, X., et al., *An extracellular adhesion molecule complex patterns dendritic branching and morphogenesis.* Cell, 2013. **155**(2): p. 296-307.

7.   Liu, O.W. and K. Shen, *The transmembrane LRR protein DMA-1 promotes dendrite branching and growth in C. elegans.* Nat Neurosci, 2011. **15**(1): p. 57-63.

8.   Salzberg, Y., et al., *Skin-derived cues control arborization of sensory dendrites in Caenorhabditis elegans.* Cell, 2013. **155**(2): p. 308-20.

9.   Zou, W., et al., *A multi-protein receptor-ligand complex underlies combinatorial dendrite guidance choices in C. elegans.* Elife, 2016. **5**.

10.   Grueber, W.B. and A. Sagasti, *Self-avoidance and tiling: Mechanisms of dendrite and axon spacing.* Cold Spring Harb Perspect Biol, 2010. **2**(9): p. a001750.

11.   Kramer, A.P. and J.Y. Kuwada, *Formation of the receptive fields of leech mechanosensory neurons during embryonic development.* J Neurosci, 1983. **3**(12): p. 2474-86.

12.   Hattori, D., et al., *Dscam diversity is essential for neuronal wiring and self-recognition.* Nature, 2007. **449**(7159): p. 223-7.

13.   Hughes, M.E., et al., *Homophilic Dscam interactions control complex dendrite morphogenesis.* Neuron, 2007. **54**(3): p. 417-27.

14.   Matthews, B.J., et al., *Dendrite self-avoidance is controlled by Dscam.* Cell, 2007. **129**(3): p. 593-604.

15. Millard, S.S., et al., *Dscam2 mediates axonal tiling in the Drosophila visual system.* Nature, 2007. **447**(7145): p. 720-4.

16. Soba, P., et al., *Drosophila sensory neurons require Dscam for dendritic self-avoidance and proper dendritic field organization.* Neuron, 2007. **54**(3): p. 403-16.

17. Lefebvre, J.L., et al., *Protocadherins mediate dendritic self-avoidance in the mammalian nervous system.* Nature, 2012. **488**(7412): p. 517-21.

18. Dong, X., et al., *Precise regulation of the guidance receptor DMA-1 by KPC-1/Furin instructs dendritic branching decisions.* Elife, 2016. **5**.

19. Thomas, G., *Furin at the cutting edge: from protein traffic to embryogenesis and disease.* Nat Rev Mol Cell Biol, 2002. **3**(10): p. 753-66.

20. Salzberg, Y., N.J. Ramirez-Suarez, and H.E. Bulow, *The proprotein convertase KPC-1/furin controls branching and self-avoidance of sensory dendrites in Caenorhabditis elegans.* PLoS Genet, 2014. **10**(9): p. e1004657.

21. Schroeder, N.E., et al., *Dauer-specific dendrite arborization in C. elegans is regulated by KPC-1/Furin.* Curr Biol, 2013. **23**(16): p. 1527-35.

22. Oren-Suissa, M., et al., *The fusogen EFF-1 controls sculpting of mechanosensory dendrites.* Science, 2010. **328**(5983): p. 1285-8.

23. Sulston, J.E. and H.R. Horvitz, *Post-embryonic cell lineages of the nematode, Caenorhabditis elegans.* Dev Biol, 1977. **56**(1): p. 110-56.

24. White, J.G., et al., *The structure of the nervous system of the nematode Caenorhabditis elegans.* Philos Trans R Soc Lond B Biol Sci, 1986. **314**(1165): p. 1-340.

25. Smith, C.J., et al., *Time-lapse imaging and cell-specific expression profiling reveal dynamic branching and molecular determinants of a multi-dendritic nociceptor in C. elegans.* Dev Biol, 2010. **345**(1): p. 18-33.

26. Doitsidou, M., et al., *C. elegans mutant identification with a one-step whole-genome-sequencing and SNP mapping strategy.* PLoS One, 2010. **5**(11): p. e15435.

Fig. 1.1

Requestor Location

Publisher Tax ID   98-0397604

Fig 1.3.

This Agreement between Seema Sheoran ("You") and John Wiley and Sons ("John Wiley and Sons") consists of your license details and the terms and conditions provided by John Wiley and Sons and Copyright Clearance Center.

License Number	4942341162981
License date	Nov 05, 2020
Licensed Content Publisher	John Wiley and Sons
Licensed Content Publication	Developmental Dynamics
Licensed Content Title	"CRASH"ing with the worm: Insights into L1CAM functions and mechanisms
Licensed Content Author	Shan Zhou, Lihsia Chen
Licensed Content Date	Mar 11, 2010
Licensed Content Volume	239
Licensed Content Issue	5
Licensed Content Pages	12
Type of use	Dissertation/Thesis
Requestor type	University/Academic
Format	Electronic
Portion	Figure/table

Number of figures/tables	1
Will you be translating?	No
Title	Ultrastructural analysis of proteins implicated in synaptic vesicle docking and priming in C. elegans
Institution name	University of Illinois at Chicago
Expected presentation date	Nov 2020
Portions	Figure 4

Fig. 2A.4

This Agreement between Seema Sheoran ("You") and John Wiley and Sons ("John Wiley and Sons") consists of your license details and the terms and conditions provided by John Wiley and Sons and Copyright Clearance Center.

License Number	4942351003487
License date	Nov 05, 2020
Licensed Content Publisher	John Wiley and Sons
Licensed Content Publication	The EMBO Journal
Licensed Content Title	Modular architecture of Munc13/calmodulin complexes: dual regulation by Ca2 and possible function in short-term synaptic plasticity
Licensed Content Author	Christian Griesinger, Teresa Carlomagno, Olaf Jahn, et al
Licensed Content Date	Dec 10, 2009
Licensed Content Volume	29
Licensed Content Issue	3

Licensed Content Pages	12
Type of use	Dissertation/Thesis
Requestor type	University/Academic
Format	Electronic
Portion	Figure/table
Number of figures/tables	1
Will you be translating?	No
Title	Ultrastructural analysis of proteins implicated in synaptic vesicle docking and priming in C. elegans
Institution name	University of Illinois at Chicago
Expected presentation date	Nov 2020
Portions	Figure 4A

CITED LITERATURE

Aizawa, H., S. C. Hu, K. Bobb, K. Balakrishnan, G. Ince, I. Gurevich, M. Cowan, and A. Ghosh. 2004. 'Dendrite development regulated by CREST, a calcium-regulated transcriptional activator', *Science*, 303: 197-202.

Alaimo, J. T., S. J. Davis, S. S. Song, C. R. Burnette, M. Grotewiel, K. L. Shelton, J. T. Pierce-Shimomura, A. G. Davies, and J. C. Bettinger. 2012. 'Ethanol metabolism and osmolarity modify behavioral responses to ethanol in C. elegans', *Alcohol Clin Exp Res*, 36: 1840-50.

Andrews-Zwilling, Y. S., H. Kawabe, K. Reim, F. Varoqueaux, and N. Brose. 2006. 'Binding to Rab3A-interacting molecule RIM regulates the presynaptic recruitment of Munc13-1 and ubMunc13-2', *J Biol Chem*, 281: 19720-31.

Aravamudan, B., T. Fergestad, W. S. Davis, C. K. Rodesch, and K. Broadie. 1999. 'Drosophila UNC-13 is essential for synaptic transmission', *Nat Neurosci*, 2: 965-71.

Atwood, H. L., and S. Karunanithi. 2002. 'Diversification of synaptic strength: presynaptic elements', *Nat Rev Neurosci*, 3: 497-516.

Augustin, I., A. Betz, C. Herrmann, T. Jo, and N. Brose. 1999a. 'Differential expression of two novel Munc13 proteins in rat brain', *Biochem J*, 337 (Pt 3): 363-71.

———. 1999b. 'Differential expression of two novel Munc13 proteins in rat brain', *Biochem J*, 337 (Pt 3): 363-71.

Augustin, I., S. Korte, M. Rickmann, H. A. Kretzschmar, T. C. Südhof, J. W. Herms, and N. Brose. 2001. 'The cerebellum-specific Munc13 isoform Munc13-3 regulates cerebellar synaptic transmission and motor learning in mice', *J Neurosci*, 21: 10-7.

Augustin, I., C. Rosenmund, T. C. Südhof, and N. Brose. 1999. 'Munc13-1 is essential for fusion competence of glutamatergic synaptic vesicles', *Nature*, 400: 457-61.

Aurelio, O., D. H. Hall, and O. Hobert. 2002. 'Immunoglobulin-domain proteins required for maintenance of ventral nerve cord organization', *Science*, 295: 686-90.

Babu, Y. S., C. E. Bugg, and W. J. Cook. 1988. 'Structure of calmodulin refined at 2.2 A resolution', *J Mol Biol*, 204: 191-204.

Basu, J., A. Betz, N. Brose, and C. Rosenmund. 2007. 'Munc13-1 C1 domain activation lowers the energy barrier for synaptic vesicle fusion', *J Neurosci*, 27: 1200-10.

Basu, J., N. Shen, I. Dulubova, J. Lu, R. Guan, O. Guryev, N. V. Grishin, C. Rosenmund, and J. Rizo. 2005. 'A minimal domain responsible for Munc13 activity', *Nat Struct Mol Biol*, 12: 1017-8.

Bechara, A., H. Nawabi, F. Moret, A. Yaron, E. Weaver, M. Bozon, K. Abouzid, J. L. Guan, M. Tessier-Lavigne, V. Lemmon, and V. Castellani. 2008. 'FAK-MAPK-dependent adhesion disassembly downstream of L1 contributes to semaphorin3A-induced collapse', *Embo j*, 27: 1549-62.

Bénard, C., N. Tjoe, T. Boulin, J. Recio, and O. Hobert. 2009. 'The small, secreted immunoglobulin protein ZIG-3 maintains axon position in Caenorhabditis elegans', *Genetics*, 183: 917-27.

Bénard, C. Y., A. Boyanov, D. H. Hall, and O. Hobert. 2006. 'DIG-1, a novel giant protein, non-autonomously mediates maintenance of nervous system architecture', *Development*, 133: 3329-40.

Bennett, C. F., H. Vander Wende, M. Simko, S. Klum, S. Barfield, H. Choi, V. V. Pineda, and M. Kaeberlein. 2014. 'Activation of the mitochondrial unfolded protein response does not predict longevity in Caenorhabditis elegans', *Nat Commun*, 5: 3483.

Berendzen, K. M., J. Durieux, L. W. Shao, Y. Tian, H. E. Kim, S. Wolff, Y. Liu, and A. Dillin. 2016. 'Neuroendocrine Coordination of Mitochondrial Stress Signaling and Proteostasis', *Cell*, 166: 1553-63 e10.

Betz, A., U. Ashery, M. Rickmann, I. Augustin, E. Neher, T. C. Südhof, J. Rettig, and N. Brose. 1998. 'Munc13-1 is a presynaptic phorbol ester receptor that enhances neurotransmitter release', *Neuron*, 21: 123-36.

Betz, A., M. Okamoto, F. Benseler, and N. Brose. 1997. 'Direct interaction of the rat unc-13 homologue Munc13-1 with the N terminus of syntaxin', *J Biol Chem*, 272: 2520-6.

Betz, A., P. Thakur, H. J. Junge, U. Ashery, J. S. Rhee, V. Scheuss, C. Rosenmund, J. Rettig, and N. Brose. 2001. 'Functional interaction of the active zone proteins Munc13-1 and RIM1 in synaptic vesicle priming', *Neuron*, 30: 183-96.

Böhme, M. A., C. Beis, S. Reddy-Alla, E. Reynolds, M. M. Mampell, A. T. Grasskamp, J. Lützkendorf, D. D. Bergeron, J. H. Driller, H. Babikir, F. Göttfert, I. M. Robinson, C. J. O'Kane, S. W. Hell, M. C. Wahl, U. Stelzl, B. Loll, A. M. Walter, and S. J. Sigrist. 2016. 'Active zone scaffolds differentially accumulate Unc13 isoforms to tune Ca(2+) channel-vesicle coupling', *Nat Neurosci*, 19: 1311-20.

Bolz, D. D., J. L. Tenor, and A. Aballay. 2010. 'A conserved PMK-1/p38 MAPK is required in caenorhabditis elegans tissue-specific immune response to Yersinia pestis infection', *J Biol Chem*, 285: 10832-40.

Brenner, S. 1974. 'The genetics of Caenorhabditis elegans', *Genetics*, 77: 71-94.

Breustedt, J., A. Gundlfinger, F. Varoqueaux, K. Reim, N. Brose, and D. Schmitz. 2010. 'Munc13-2 differentially affects hippocampal synaptic transmission and plasticity', *Cereb Cortex*, 20: 1109-20.

Broadie, K., A. Prokop, H. J. Bellen, C. J. O'Kane, K. L. Schulze, and S. T. Sweeney. 1995. 'Syntaxin and synaptobrevin function downstream of vesicle docking in Drosophila', *Neuron*, 15: 663-73.

Bröcker, C., A. Kuhlee, C. Gatsogiannis, H. J. Balderhaar, C. Hönscher, S. Engelbrecht-Vandré, C. Ungermann, and S. Raunser. 2012. 'Molecular architecture of the multisubunit homotypic fusion and vacuole protein sorting (HOPS) tethering complex', *Proc Natl Acad Sci U S A*, 109: 1991-6.

Brockmann, M. M., F. Zarebidaki, M. Camacho, M. K. Grauel, T. Trimbuch, T. C. Südhof, and C. Rosenmund. 2020. 'A Trio of Active Zone Proteins Comprised of RIM-BPs, RIMs, and Munc13s Governs Neurotransmitter Release', *Cell Rep*, 32: 107960.

Brose, N., K. Hofmann, Y. Hata, and T. C. Sudhof. 1995. 'Mammalian homologues of Caenorhabditis elegans unc-13 gene define novel family of C2-domain proteins', *J Biol Chem*, 270: 25273-80.

Bülow, H. E., T. Boulin, and O. Hobert. 2004. 'Differential functions of the C. elegans FGF receptor in axon outgrowth and maintenance of axon position', *Neuron*, 42: 367-74.

Burdina, A. O., S. M. Klosterman, L. Shtessel, S. Ahmed, and J. E. Richmond. 2011. 'In vivo analysis of conserved C. elegans tomosyn domains', *PLoS One*, 6: e26185.

Calloway, N., G. Gouzer, M. Xue, and T. A. Ryan. 2015. 'The active-zone protein Munc13 controls the use-dependence of presynaptic voltage-gated calcium channels', *Elife*, 4.

Camacho, M., J. Basu, T. Trimbuch, S. Chang, C. Pulido-Lozano, S. S. Chang, I. Duluvova, M. Abo-Rady, J. Rizo, and C. Rosenmund. 2017a. 'Heterodimerization of Munc13 C2A domain with RIM regulates synaptic vesicle docking and priming', *Nat Commun*, 8: 15293.

———. 2017b. 'Heterodimerization of Munc13 C(2)A domain with RIM regulates synaptic vesicle docking and priming', *Nat Commun*, 8: 15293.

Caplan, S., L. M. Hartnell, R. C. Aguilar, N. Naslavsky, and J. S. Bonifacino. 2001. 'Human Vam6p promotes lysosome clustering and fusion in vivo', *J Cell Biol*, 154: 109-22.

Cartoni, R., B. Leger, M. B. Hock, M. Praz, A. Crettenand, S. Pich, J. L. Ziltener, F. Luthi, O. Deriaz, A. Zorzano, C. Gobelet, A. Kralli, and A. P. Russell. 2005. 'Mitofusins 1/2 and ERRalpha expression are increased in human skeletal muscle after physical exercise', *J Physiol*, 567: 349-58.

Castellani, V., J. Falk, and G. Rougon. 2004. 'Semaphorin3A-induced receptor endocytosis during axon guidance responses is mediated by L1 CAM', *Mol Cell Neurosci*, 26: 89-100.

Chapman, E. R., and A. F. Davis. 1998. 'Direct interaction of a Ca2+-binding loop of synaptotagmin with lipid bilayers', *J Biol Chem*, 273: 13995-4001.

Chapman, E. R., R. C. Desai, A. F. Davis, and C. K. Tornehl. 1998. 'Delineation of the oligomerization, AP-2 binding, and synprint binding region of the C2B domain of synaptotagmin', *J Biol Chem*, 273: 32966-72.

Chen, L., B. Ong, and V. Bennett. 2001. 'LAD-1, the Caenorhabditis elegans L1CAM homologue, participates in embryonic and gonadal morphogenesis and is a substrate for fibroblast growth factor receptor pathway-dependent phosphotyrosine-based signaling', *J Cell Biol*, 154: 841-55.

Chen, L., and S. Zhou. 2010. '"CRASH"ing with the worm: insights into L1CAM functions and mechanisms', *Dev Dyn*, 239: 1490-501.

Chen, Z., B. Cooper, S. Kalla, F. Varoqueaux, and S. M. Young, Jr. 2013. 'The Munc13 proteins differentially regulate readily releasable pool dynamics and calcium-dependent recovery at a central synapse', *J Neurosci*, 33: 8336-51.

Cherra, S. J., 3rd, and Y. Jin. 2015. 'Advances in synapse formation: forging connections in the worm', *Wiley Interdiscip Rev Dev Biol*, 4: 85-97.

Chou, H. T., D. Dukovski, M. G. Chambers, K. M. Reinisch, and T. Walz. 2016. 'CATCHR, HOPS and CORVET tethering complexes share a similar architecture', *Nat Struct Mol Biol*, 23: 761-3.

Coleman, B., I. Topalidou, and M. Ailion. 2018. 'Modulation of Gq-Rho Signaling by the ERK MAPK Pathway Controls Locomotion in Caenorhabditis elegans', *Genetics*, 209: 523-35.

Coppola, T., S. Magnin-Luthi, V. Perret-Menoud, S. Gattesco, G. Schiavo, and R. Regazzi. 2001. 'Direct interaction of the Rab3 effector RIM with Ca2+ channels, SNAP-25, and synaptotagmin', *J Biol Chem*, 276: 32756-62.

Das, J., S. Xu, S. Pany, A. Guillory, V. Shah, and G. W. Roman. 2013. 'The pre-synaptic Munc13-1 binds alcohol and modulates alcohol self-administration in Drosophila', *J Neurochem*, 126: 715-26.

Davis, J. Q., and V. Bennett. 1994. 'Ankyrin binding activity shared by the neurofascin/L1/NrCAM family of nervous system cell adhesion molecules', *J Biol Chem*, 269: 27163-6.

Deng, L., P. S. Kaeser, W. Xu, and T. C. Südhof. 2011. 'RIM proteins activate vesicle priming by reversing autoinhibitory homodimerization of Munc13', *Neuron*, 69: 317-31.

Diaz-Balzac, C. A., M. Rahman, M. I. Lazaro-Pena, L. A. Martin Hernandez, Y. Salzberg, C. Aguirre-Chen, Z. Kaprielian, and H. E. Bulow. 2016. 'Muscle- and Skin-Derived Cues Jointly Orchestrate Patterning of Somatosensory Dendrites', *Curr Biol*, 26: 2379-87.

Dimova, K., H. Kawabe, A. Betz, N. Brose, and O. Jahn. 2006. 'Characterization of the Munc13-calmodulin interaction by photoaffinity labeling', *Biochim Biophys Acta*, 1763: 1256-65.

Doitsidou, M., R. J. Poole, S. Sarin, H. Bigelow, and O. Hobert. 2010. 'C. elegans mutant identification with a one-step whole-genome-sequencing and SNP mapping strategy', *PLoS One*, 5: e15435.

Dong, X., H. Chiu, Y. J. Park, W. Zou, Y. Zou, E. Ozkan, C. Chang, and K. Shen. 2016. 'Precise regulation of the guidance receptor DMA-1 by KPC-1/Furin instructs dendritic branching decisions', *Elife*, 5.

Dong, X., O. W. Liu, A. S. Howell, and K. Shen. 2013. 'An extracellular adhesion molecule complex patterns dendritic branching and morphogenesis', *Cell*, 155: 296-307.

Dulubova, I., X. Lou, J. Lu, I. Huryeva, A. Alam, R. Schneggenburger, T. C. Südhof, and J. Rizo. 2005. 'A Munc13/RIM/Rab3 tripartite complex: from priming to plasticity?', *Embo j*, 24: 2839-50.

Dulubova, I., S. Sugita, S. Hill, M. Hosaka, I. Fernandez, T. C. Südhof, and J. Rizo. 1999. 'A conformational switch in syntaxin during exocytosis: role of munc18', *Embo j*, 18: 4372-82.

Egawa, J., S. Hoya, Y. Watanabe, A. Nunokawa, M. Shibuya, M. Ikeda, E. Inoue, S. Okuda, K. Kondo, T. Saito, N. Kaneko, T. Muratake, H. Igeta, N. Iwata, and T. Someya. 2016. 'Rare UNC13B variations and risk of schizophrenia: Whole-exome sequencing in a multiplex family and follow-up resequencing and a case-control study', *Am J Med Genet B Neuropsychiatr Genet*, 171: 797-805.

Eisner, V., R. R. Cupo, E. Gao, G. Csordas, W. S. Slovinsky, M. Paillard, L. Cheng, J. Ibetti, S. R. Chen, J. K. Chuprun, J. B. Hoek, W. J. Koch, and G. Hajnoczky. 2017. 'Mitochondrial fusion dynamics is robust in the heart and depends on calcium oscillations and contractile activity', *Proc Natl Acad Sci U S A*, 114: E859-E68.

Eisner, V., G. Lenaers, and G. Hajnoczky. 2014. 'Mitochondrial fusion is frequent in skeletal muscle and supports excitation-contraction coupling', *J Cell Biol*, 205: 179-95.

Eisner, V., M. Picard, and G. Hajnoczky. 2018. 'Mitochondrial dynamics in adaptive and maladaptive cellular stress responses', *Nat Cell Biol*, 20: 755-65.

Elbaz-Alon, Y., E. Rosenfeld-Gur, V. Shinder, A. H. Futerman, T. Geiger, and M. Schuldiner. 2014. 'A dynamic interface between vacuoles and mitochondria in yeast', *Dev Cell*, 30: 95-102.

Engel, A. G., D. Selcen, X. M. Shen, M. Milone, and C. M. Harper. 2016. 'Loss of MUNC13-1 function causes microcephaly, cortical hyperexcitability, and fatal myasthenia', *Neurol Genet*, 2: e105.

Estes, K. A., T. L. Dunbar, J. R. Powell, F. M. Ausubel, and E. R. Troemel. 2010. 'bZIP transcription factor zip-2 mediates an early response to Pseudomonas aeruginosa infection in Caenorhabditis elegans', *Proc Natl Acad Sci U S A*, 107: 2153-8.

Fernandes, A. C., V. Uytterhoeven, S. Kuenen, Y. C. Wang, J. R. Slabbaert, J. Swerts, J. Kasprowicz, S. Aerts, and P. Verstreken. 2014. 'Reduced synaptic vesicle protein degradation at lysosomes curbs TBC1D24/sky-induced neurodegeneration', *J Cell Biol*, 207: 453-62.

Fernández, R. M., R. Núñez-Torres, L. García-Díaz, J. C. de Agustín, G. Antiñolo, and S. Borrego. 2012. 'Association of X-linked hydrocephalus and Hirschsprung disease: report of a new patient with a mutation in the L1CAM gene', *Am J Med Genet A*, 158a: 816-20.

Fernandez-Sola, J., V. R. Preedy, C. H. Lang, E. Gonzalez-Reimers, M. Arno, J. C. Lin, H. Wiseman, S. Zhou, P. W. Emery, T. Nakahara, K. Hashimoto, M. Hirano, F. Santolaria-Fernandez, T. Gonzalez-Hernandez, F. Fatjo, E. Sacanella, R. Estruch, J. M. Nicolas, and A. Urbano-Marquez. 2007. 'Molecular and cellular events in alcohol-induced muscle disease', *Alcohol Clin Exp Res*, 31: 1953-62.

Fiorese, C. J., A. M. Schulz, Y. F. Lin, N. Rosin, M. W. Pellegrino, and C. M. Haynes. 2016. 'The Transcription Factor ATF5 Mediates a Mammalian Mitochondrial UPR', *Curr Biol*, 26: 2037-43.

Fransen, E., V. Lemmon, G. Van Camp, L. Vits, P. Coucke, and P. J. Willems. 1995. 'CRASH syndrome: clinical spectrum of corpus callosum hypoplasia, retardation, adducted thumbs, spastic paraparesis and hydrocephalus due to mutations in one single gene, L1', *Eur J Hum Genet*, 3: 273-84.

Frints, S. G., P. Marynen, D. Hartmann, J. P. Fryns, J. Steyaert, M. Schachner, B. Rolf, K. Craessaerts, A. Snellinx, K. Hollanders, R. D'Hooge, P. P. De Deyn, and G. Froyen. 2003. 'CALL interrupted in a patient with non-specific mental retardation: gene dosage-dependent alteration of murine brain development and behavior', *Hum Mol Genet*, 12: 1463-74.

Frokjaer-Jensen, C., M. W. Davis, M. Sarov, J. Taylor, S. Flibotte, M. LaBella, A. Pozniakovsky, D. G. Moerman, and E. M. Jorgensen. 2014. 'Random and targeted transgene insertion in Caenorhabditis elegans using a modified Mos1 transposon', *Nat Methods*, 11: 529-34.

Fromer, M., A. J. Pocklington, D. H. Kavanagh, H. J. Williams, S. Dwyer, P. Gormley, L. Georgieva, E. Rees, P. Palta, D. M. Ruderfer, N. Carrera, I. Humphreys, J. S. Johnson, P. Roussos, D. D. Barker, E. Banks, V. Milanova, S. G. Grant, E. Hannon, S. A. Rose, K. Chambert, M. Mahajan, E. M. Scolnick, J. L. Moran, G. Kirov, A. Palotie, S. A. McCarroll, P. Holmans, P. Sklar, M. J. Owen, S. M. Purcell, and M. C. O'Donovan. 2014. 'De novo mutations in schizophrenia implicate synaptic networks', *Nature*, 506: 179-84.

Garg, S., M. Sharma, C. Ung, A. Tuli, D. C. Barral, D. L. Hava, N. Veerapen, G. S. Besra, N. Hacohen, and M. B. Brenner. 2011. 'Lysosomal trafficking, antigen presentation, and microbial killing are controlled by the Arf-like GTPase Arl8b', *Immunity*, 35: 182-93.

Gariani, K., K. J. Menzies, D. Ryu, C. J. Wegner, X. Wang, E. R. Ropelle, N. Moullan, H. Zhang, A. Perino, V. Lemos, B. Kim, Y. K. Park, A. Piersigilli, T. X. Pham, Y. Yang, C. S. Ku, S. I. Koo, A. Fomitchova, C. Canto, K. Schoonjans, A. A. Sauve, J. Y. Lee, and J. Auwerx. 2016. 'Eliciting the mitochondrial unfolded protein response by nicotinamide adenine dinucleotide repletion reverses fatty liver disease in mice', *Hepatology*, 63: 1190-204.

Gaudilliere, B., Y. Konishi, N. de la Iglesia, Gl Yao, and A. Bonni. 2004. 'A CaMKII-NeuroD signaling pathway specifies dendritic morphogenesis', *Neuron*, 41: 229-41.

Gerber, S. H., J. C. Rah, S. W. Min, X. Liu, H. de Wit, I. Dulubova, A. C. Meyer, J. Rizo, M. Arancillo, R. E. Hammer, M. Verhage, C. Rosenmund, and T. C. Sudhof. 2008. 'Conformational switch of syntaxin-1 controls synaptic vesicle fusion', *Science*, 321: 1507-10.

Giacomello, M., A. Pyakurel, C. Glytsou, and L. Scorrano. 2020. 'The cell biology of mitochondrial membrane dynamics', *Nat Rev Mol Cell Biol*.

González Montoro, A., K. Auffarth, C. Hönscher, M. Bohnert, T. Becker, B. Warscheid, F. Reggiori, M. van der Laan, F. Fröhlich, and C. Ungermann. 2018. 'Vps39 Interacts with Tom40 to Establish One of Two Functionally Distinct Vacuole-Mitochondria Contact Sites', *Dev Cell*, 45: 621-36.e7.

Gracheva, E. O., A. O. Burdina, A. M. Holgado, M. Berthelot-Grosjean, B. D. Ackley, G. Hadwiger, M. L. Nonet, R. M. Weimer, and J. E. Richmond. 2006. 'Tomosyn inhibits synaptic vesicle priming in Caenorhabditis elegans', *PLoS Biol*, 4: e261.

Gracheva, E. O., A. O. Burdina, D. Touroutine, M. Berthelot-Grosjean, H. Parekh, and J. E. Richmond. 2007. 'Tomosyn negatively regulates both synaptic transmitter and neuropeptide release at the C. elegans neuromuscular junction', *J Physiol*, 585: 705-9.

Gracheva, E. O., G. Hadwiger, M. L. Nonet, and J. E. Richmond. 2008. 'Direct interactions between C. elegans RAB-3 and Rim provide a mechanism to target vesicles to the presynaptic density', *Neurosci Lett*, 444: 137-42.

Gracheva, E. O., E. B. Maryon, M. Berthelot-Grosjean, and J. E. Richmond. 2010. 'Differential Regulation of Synaptic Vesicle Tethering and Docking by UNC-18 and TOM-1', *Front Synaptic Neurosci*, 2: 141.

Grueber, W. B., and A. Sagasti. 2010. 'Self-avoidance and tiling: Mechanisms of dendrite and axon spacing', *Cold Spring Harb Perspect Biol*, 2: a001750.

Haida, M., K. Yazaki, D. Kurita, and Y. Shinohara. 1998. 'Mitochondrial dysfunction of human muscle in chronic alcoholism detected by using 31P-magnetic resonance spectroscopy and near-infrared light absorption', *Alcohol Clin Exp Res*, 22: 108S-10S.

Hallam, S. J., A. Goncharov, J. McEwen, R. Baran, and Y. Jin. 2002. 'SYD-1, a presynaptic protein with PDZ, C2 and rhoGAP-like domains, specifies axon identity in C. elegans', *Nat Neurosci*, 5: 1137-46.

Hammarlund, M., M. T. Palfreyman, S. Watanabe, S. Olsen, and E. M. Jorgensen. 2007. 'Open syntaxin docks synaptic vesicles', *PLoS Biol*, 5: e198.

Hanson, P. I., R. Roth, H. Morisaki, R. Jahn, and J. E. Heuser. 1997. 'Structure and conformational changes in NSF and its membrane receptor complexes visualized by quick-freeze/deep-etch electron microscopy', *Cell*, 90: 523-35.

Hattori, D., E. Demir, H. W. Kim, E. Viragh, S. L. Zipursky, and B. J. Dickson. 2007. 'Dscam diversity is essential for neuronal wiring and self-recognition', *Nature*, 449: 223-7.

Haynes, C. M., K. Petrova, C. Benedetti, Y. Yang, and D. Ron. 2007. 'ClpP mediates activation of a mitochondrial unfolded protein response in C. elegans', *Dev Cell*, 13: 467-80.

Haynes, C. M., Y. Yang, S. P. Blais, T. A. Neubert, and D. Ron. 2010. 'The matrix peptide exporter HAF-1 signals a mitochondrial UPR by activating the transcription factor ZC376.7 in C. elegans', *Mol Cell*, 37: 529-40.

Hönscher, C., M. Mari, K. Auffarth, M. Bohnert, J. Griffith, W. Geerts, M. van der Laan, M. Cabrera, F. Reggiori, and C. Ungermann. 2014. 'Cellular metabolism regulates contact sites between vacuoles and mitochondria', *Dev Cell*, 30: 86-94.

Hortsch, M., K. Nagaraj, and R. Mualla. 2014. 'The L1 family of cell adhesion molecules: a sickening number of mutations and protein functions', *Adv Neurobiol*, 8: 195-229.

Hosono, R., T. Sassa, and S. Kuno. 1987. 'Mutations affecting acetylcholine levels in the nematode Caenorhabditis elegans', *J Neurochem*, 49: 1820-3.

Hu, Z., X. J. Tong, and J. M. Kaplan. 2013. 'UNC-13L, UNC-13S, and Tomosyn form a protein code for fast and slow neurotransmitter release in Caenorhabditis elegans', *Elife*, 2: e00967.

Hu, Z., A. B. Vashlishan-Murray, and J. M. Kaplan. 2015. 'NLP-12 engages different UNC-13 proteins to potentiate tonic and evoked release', *J Neurosci*, 35: 1038-42.

Hughes, M. E., R. Bortnick, A. Tsubouchi, P. Baumer, M. Kondo, T. Uemura, and D. Schmucker. 2007. 'Homophilic Dscam interactions control complex dendrite morphogenesis', *Neuron*, 54: 417-27.

Imig, C., S. W. Min, S. Krinner, M. Arancillo, C. Rosenmund, T. C. Südhof, J. Rhee, N. Brose, and B. H. Cooper. 2014. 'The morphological and molecular nature of synaptic vesicle priming at presynaptic active zones', *Neuron*, 84: 416-31.

Iser, W. B., M. A. Wilson, W. H. Wood, 3rd, K. Becker, and C. A. Wolkow. 2011. 'Co-regulation of the DAF-16 target gene, cyp-35B1/dod-13, by HSF-1 in C. elegans dauer larvae and daf-2 insulin pathway mutants', *PLoS One*, 6: e17369.

Jahn, R., and D. Fasshauer. 2012. 'Molecular machines governing exocytosis of synaptic vesicles', *Nature*, 490: 201-7.

Jan, Y. N., and L. Y. Jan. 2010. 'Branching out: mechanisms of dendritic arborization', *Nat Rev Neurosci*, 11: 316-28.

Jiang, P., T. Nishimura, Y. Sakamaki, E. Itakura, T. Hatta, T. Natsume, and N. Mizushima. 2014. 'The HOPS complex mediates autophagosome-lysosome fusion through interaction with syntaxin 17', *Mol Biol Cell*, 25: 1327-37.

Junge, H. J., J. S. Rhee, O. Jahn, F. Varoqueaux, J. Spiess, M. N. Waxham, C. Rosenmund, and N. Brose. 2004. 'Calmodulin and Munc13 form a Ca2+ sensor/effector complex that controls short-term synaptic plasticity', *Cell*, 118: 389-401.

Kage-Nakadai, E., R. Imae, Y. Suehiro, S. Yoshina, S. Hori, and S. Mitani. 2014. 'A conditional knockout toolkit for Caenorhabditis elegans based on the Cre/loxP recombination', *PLoS One*, 9: e114680.

Kajiho, H., Y. Kajiho, E. Frittoli, S. Confalonieri, G. Bertalot, G. Viale, P. P. Di Fiore, A. Oldani, M. Garre, G. V. Beznoussenko, A. Palamidessi, M. Vecchi, P. Chavrier, F. Perez, and G. Scita. 2016. 'RAB2A controls MT1-MMP endocytic and E-cadherin polarized Golgi trafficking to promote invasive breast cancer programs', *EMBO Rep*, 17: 1061-80.

Kanazawa, T., M. D. Zappaterra, A. Hasegawa, A. P. Wright, E. D. Newman-Smith, K. F. Buttle, K. McDonald, C. A. Mannella, and A. M. van der Bliek. 2008. 'The C. elegans Opa1 homologue EAT-3 is essential for resistance to free radicals', *PLoS Genet*, 4: e1000022.

Kaufman, D. M., and C. M. Crowder. 2015. 'Mitochondrial Proteostatic Collapse Leads to Hypoxic Injury', *Curr Biol*, 25: 2171-6.

Kawabe, H., M. Mitkovski, P. S. Kaeser, J. Hirrlinger, F. Opazo, D. Nestvogel, S. Kalla, A. Fejtova, S. E. Verrier, S. R. Bungers, B. H. Cooper, F. Varoqueaux, Y. Wang, R. B. Nehring, E. D.

Gundelfinger, C. Rosenmund, S. O. Rizzoli, T. C. Südhof, J. S. Rhee, and N. Brose. 2017. 'ELKS1 localizes the synaptic vesicle priming protein bMunc13-2 to a specific subset of active zones', *J Cell Biol*, 216: 1143-61.

Kazanietz, M. G., N. E. Lewin, J. D. Bruns, and P. M. Blumberg. 1995. 'Characterization of the cysteine-rich region of the Caenorhabditis elegans protein Unc-13 as a high affinity phorbol ester receptor. Analysis of ligand-binding interactions, lipid cofactor requirements, and inhibitor sensitivity', *J Biol Chem*, 270: 10777-83.

Kim, B. Y., Y. Sahara, A. Yamamoto, E. Kominami, S. Kohsaka, and C. Akazawa. 2006. 'The interaction of mammalian Class C Vps with nSec-1/Munc18-a and syntaxin 1A regulates pre-synaptic release', *Biochem Biophys Res Commun*, 350: 691-7.

Kim, H., R. J. Perentis, G. A. Caldwell, and K. A. Caldwell. 2018. 'Gene-by-environment interactions that disrupt mitochondrial homeostasis cause neurodegeneration in C. elegans Parkinson's models', *Cell Death Dis*, 9: 555.

Kimball, S. R., and C. H. Lang. 2018. 'Mechanisms Underlying Muscle Protein Imbalance Induced by Alcohol', *Annu Rev Nutr*, 38: 197-217.

Koch, H., K. Hofmann, and N. Brose. 2000. 'Definition of Munc13-homology-domains and characterization of a novel ubiquitously expressed Munc13 isoform', *Biochem J*, 349: 247-53.

Kohn, R. E., J. S. Duerr, J. R. McManus, A. Duke, T. L. Rakow, H. Maruyama, G. Moulder, I. N. Maruyama, R. J. Barstead, and J. B. Rand. 2000. 'Expression of multiple UNC-13 proteins in the Caenorhabditis elegans nervous system', *Mol Biol Cell*, 11: 3441-52.

Koushika, S. P., J. E. Richmond, G. Hadwiger, R. M. Weimer, E. M. Jorgensen, and M. L. Nonet. 2001. 'A post-docking role for active zone protein Rim', *Nat Neurosci*, 4: 997-1005.

Kramer, A. P., and J. Y. Kuwada. 1983. 'Formation of the receptive fields of leech mechanosensory neurons during embryonic development', *J Neurosci*, 3: 2474-86.

Kulahin, N., S. Li, A. Hinsby, V. Kiselyov, V. Berezin, and E. Bock. 2008. 'Fibronectin type III (FN3) modules of the neuronal cell adhesion molecule L1 interact directly with the fibroblast growth factor (FGF) receptor', *Mol Cell Neurosci*, 37: 528-36.

Kusch, V., G. Bornschein, D. Loreth, J. Bank, J. Jordan, D. Baur, M. Watanabe, A. Kulik, M. Heckmann, J. Eilers, and H. Schmidt. 2018. 'Munc13-3 Is Required for the Developmental Localization of Ca(2+) Channels to Active Zones and the Nanopositioning of Ca(v)2.1 Near Release Sensors', *Cell Rep*, 22: 1965-73.

Labrousse, A. M., M. D. Zappaterra, D. A. Rube, and A. M. van der Bliek. 1999. 'C. elegans dynamin-related protein DRP-1 controls severing of the mitochondrial outer membrane', *Mol Cell*, 4: 815-26.

Lackner, M. R., K. Kornfeld, L. M. Miller, H. R. Horvitz, and S. K. Kim. 1994. 'A MAP kinase homolog, mpk-1, is involved in ras-mediated induction of vulval cell fates in Caenorhabditis elegans', *Genes Dev*, 8: 160-73.

Lackner, M. R., S. J. Nurrish, and J. M. Kaplan. 1999. 'Facilitation of synaptic transmission by EGL-30 Gqalpha and EGL-8 PLCbeta: DAG binding to UNC-13 is required to stimulate acetylcholine release', *Neuron*, 24: 335-46.

Lai, Y., U. B. Choi, J. Leitz, H. J. Rhee, C. Lee, B. Altas, M. Zhao, R. A. Pfuetzner, A. L. Wang, N. Brose, J. Rhee, and A. T. Brunger. 2017. 'Molecular Mechanisms of Synaptic Vesicle Priming by Munc13 and Munc18', *Neuron*, 95: 591-607.e10.

Lamech, L. T., and C. M. Haynes. 2015. 'The unpredictability of prolonged activation of stress response pathways', *J Cell Biol*, 209: 781-7.

Lamitina, T. 2006. 'Functional genomic approaches in C. elegans', *Methods Mol Biol*, 351: 127-38.

'large-scale screening for targeted knockouts in the Caenorhabditis elegans genome'. 2012. *G3 (Bethesda)*, 2: 1415-25.

Lebeau, J., J. M. Saunders, V. W. R. Moraes, A. Madhavan, N. Madrazo, M. C. Anthony, and R. L. Wiseman. 2018. 'The PERK Arm of the Unfolded Protein Response Regulates Mitochondrial Morphology during Acute Endoplasmic Reticulum Stress', *Cell Rep*, 22: 2827-36.

Lefebvre, J. L., D. Kostadinov, W. V. Chen, T. Maniatis, and J. R. Sanes. 2012. 'Protocadherins mediate dendritic self-avoidance in the mammalian nervous system', *Nature*, 488: 517-21.

Lehrbach, N. J., and G. Ruvkun. 2016. 'Proteasome dysfunction triggers activation of SKN-1A/Nrf1 by the aspartic protease DDI-1', *eLife*, 5.

Lesanpezeshki, L., J. E. Hewitt, R. Laranjeiro, A. Antebi, M. Driscoll, N. J. Szewczyk, J. Blawzdziewicz, C. M. R. Lacerda, and S. A. Vanapalli. 2019. 'Pluronic gel-based burrowing assay for rapid assessment of neuromuscular health in C. elegans', *Sci Rep*, 9: 15246.

Li, L., H. Liu, Q. Hall, W. Wang, Y. Yu, J. M. Kaplan, and Z. Hu. 2019a. 'A Hyperactive Form of unc-13 Enhances Ca(2+) Sensitivity and Synaptic Vesicle Release Probability in C. elegans', *Cell Rep*, 28: 2979-95.e4.

———. 2019b. 'A Hyperactive Form of unc-13 Enhances Ca(2+) Sensitivity and Synaptic Vesicle Release Probability in C. elegans', *Cell Rep*, 28: 2979-95 e4.

Li, L., O. H. Shin, J. S. Rhee, D. Arac, J. C. Rah, J. Rizo, T. Sudhof, and C. Rosenmund. 2006. 'Phosphatidylinositol phosphates as co-activators of Ca2+ binding to C2 domains of synaptotagmin 1', *J Biol Chem*, 281: 15845-52.

Link, C. D., and C. J. Johnson. 2002. 'Reporter transgenes for study of oxidant stress in Caenorhabditis elegans', *Methods Enzymol*, 353: 497-505.

Lipstein, N., T. Sakaba, B. H. Cooper, K. H. Lin, N. Strenzke, U. Ashery, J. S. Rhee, H. Taschenberger, E. Neher, and N. Brose. 2013. 'Dynamic control of synaptic vesicle replenishment and short-term plasticity by Ca(2+)-calmodulin-Munc13-1 signaling', *Neuron*, 79: 82-96.

Lipstein, N., N. M. Verhoeven-Duif, F. E. Michelassi, N. Calloway, P. M. van Hasselt, K. Pienkowska, G. van Haaften, M. M. van Haelst, R. van Empelen, I. Cuppen, H. C. van Teeseling, A. M. Evelein, J. A. Vorstman, S. Thoms, O. Jahn, K. J. Duran, G. R. Monroe, T. A. Ryan, H. Taschenberger, J. S. Dittman, J. S. Rhee, G. Visser, J. J. Jans, and N. Brose. 2017. 'Synaptic UNC13A protein variant causes increased neurotransmission and dyskinetic movement disorder', *J Clin Invest*, 127: 1005-18.

Liu, H., L. Li, D. Nedelcu, Q. Hall, L. Zhou, W. Wang, Y. Yu, J. M. Kaplan, and Z. Hu. 2019. 'Heterodimerization of UNC-13/RIM regulates synaptic vesicle release probability but not priming in C. elegans', *Elife*, 8.

Liu, O. W., and K. Shen. 2011. 'The transmembrane LRR protein DMA-1 promotes dendrite branching and growth in C. elegans', *Nat Neurosci*, 15: 57-63.

Liu, X., A. B. Seven, M. Camacho, V. Esser, J. Xu, T. Trimbuch, B. Quade, L. Su, C. Ma, C. Rosenmund, and J. Rizo. 2016. 'Functional synergy between the Munc13 C-terminal C1 and C2 domains', *Elife*, 5.

Liu, Y., B. S. Samuel, P. C. Breen, and G. Ruvkun. 2014. 'Caenorhabditis elegans pathways that surveil and defend mitochondria', *Nature*, 508: 406-10.

Lou, X., N. Korogod, N. Brose, and R. Schneggenburger. 2008. 'Phorbol esters modulate spontaneous and Ca2+-evoked transmitter release via acting on both Munc13 and protein kinase C', *J Neurosci*, 28: 8257-67.

Lowry, J., J. Yochem, C. H. Chuang, K. Sugioka, A. A. Connolly, and B. Bowerman. 2015. 'High-Throughput Cloning of Temperature-Sensitive Caenorhabditis elegans Mutants with Adult Syncytial Germline Membrane Architecture Defects', *G3 (Bethesda)*, 5: 2241-55.

Lu, J., M. Machius, I. Dulubova, H. Dai, T. C. Südhof, D. R. Tomchick, and J. Rizo. 2006. 'Structural basis for a Munc13-1 homodimer to Munc13-1/RIM heterodimer switch', *PLoS Biol*, 4: e192.

Lu, Y., S. G. Rolland, and B. Conradt. 2011. 'A molecular switch that governs mitochondrial fusion and fission mediated by the BCL2-like protein CED-9 of Caenorhabditis elegans', *Proc Natl Acad Sci U S A*, 108: E813-22.

Lürick, A., D. Kümmel, and C. Ungermann. 2018. 'Multisubunit tethers in membrane fusion', *Curr Biol*, 28: R417-r20.

Lustig, M., G. Zanazzi, T. Sakurai, C. Blanco, S. R. Levinson, S. Lambert, M. Grumet, and J. L. Salzer. 2001. 'Nr-CAM and neurofascin interactions regulate ankyrin G and sodium channel clustering at the node of Ranvier', *Curr Biol*, 11: 1864-9.

Ma, C., W. Li, Y. Xu, and J. Rizo. 2011. 'Munc13 mediates the transition from the closed syntaxin-Munc18 complex to the SNARE complex', *Nat Struct Mol Biol*, 18: 542-9.

Ma, D. K., R. Vozdek, N. Bhatla, and H. R. Horvitz. 2012. 'CYSL-1 interacts with the O2-sensing hydroxylase EGL-9 to promote H2S-modulated hypoxia-induced behavioral plasticity in C. elegans', *Neuron*, 73: 925-40.

Madison, J. M., S. Nurrish, and J. M. Kaplan. 2005. 'UNC-13 interaction with syntaxin is required for synaptic transmission', *Curr Biol*, 15: 2236-42.

Magdziarek, M., A. A. Bolembach, K. P. Stepien, B. Quade, X. Liu, and J. Rizo. 2020. 'Re-examining how Munc13-1 facilitates opening of syntaxin-1', *Protein Sci*, 29: 1440-58.

Mai, S., M. Klinkenberg, G. Auburger, J. Bereiter-Hahn, and M. Jendrach. 2010. 'Decreased expression of Drp1 and Fis1 mediates mitochondrial elongation in senescent cells and enhances resistance to oxidative stress through PINK1', *J Cell Sci*, 123: 917-26.

Margittai, M., D. Fasshauer, R. Jahn, and R. Langen. 2003. 'The Habc domain and the SNARE core complex are connected by a highly flexible linker', *Biochemistry*, 42: 4009-14.

Marui, T., I. Funatogawa, S. Koishi, K. Yamamoto, H. Matsumoto, O. Hashimoto, E. Nanba, H. Nishida, T. Sugiyama, K. Kasai, K. Watanabe, Y. Kano, T. Sasaki, and N. Kato. 2009. 'Association of the neuronal cell adhesion molecule (NRCAM) gene variants with autism', *Int J Neuropsychopharmacol*, 12: 1-10.

Maruyama, I. N., and S. Brenner. 1991. 'A phorbol ester/diacylglycerol-binding protein encoded by the unc-13 gene of Caenorhabditis elegans', *Proc Natl Acad Sci U S A*, 88: 5729-33.

Matthews, B. J., M. E. Kim, J. J. Flanagan, D. Hattori, J. C. Clemens, S. L. Zipursky, and W. B. Grueber. 2007. 'Dendrite self-avoidance is controlled by Dscam', *Cell*, 129: 593-604.

McEwan, D. G., D. Popovic, A. Gubas, S. Terawaki, H. Suzuki, D. Stadel, F. P. Coxon, D. Miranda de Stegmann, S. Bhogaraju, K. Maddi, A. Kirchof, E. Gatti, M. H. Helfrich, S. Wakatsuki, C. Behrends, P. Pierre, and I. Dikic. 2015. 'PLEKHM1 regulates autophagosome-lysosome fusion through HOPS complex and LC3/GABARAP proteins', *Mol Cell*, 57: 39-54.

Melber, A., and C. M. Haynes. 2018. 'UPR(mt) regulation and output: a stress response mediated by mitochondrial-nuclear communication', *Cell Res*, 28: 281-95.

Merkwirth, C., V. Jovaisaite, J. Durieux, O. Matilainen, S. D. Jordan, P. M. Quiros, K. K. Steffen, E. G. Williams, L. Mouchiroud, S. U. Tronnes, V. Murillo, S. C. Wolff, R. J. Shaw, J. Auwerx, and A. Dillin. 2016. 'Two Conserved Histone Demethylases Regulate Mitochondrial Stress-Induced Longevity', *Cell*, 165: 1209-23.

Messler, S., S. Kropp, V. Episkopou, A. Felici, J. Würthner, R. Lemke, M. Jerabek-Willemsen, R. Willecke, S. Scheu, K. Pfeffer, and J. U. Wurthner. 2011. 'The TGF-β signaling modulators TRAP1/TGFBRAP1 and VPS39/Vam6/TLP are essential for early embryonic development', *Immunobiology*, 216: 343-50.

Michelassi, F., H. Liu, Z. Hu, and J. S. Dittman. 2017a. 'A C1-C2 Module in Munc13 Inhibits Calcium-Dependent Neurotransmitter Release', *Neuron*, 95: 577-90 e5.

———. 2017b. 'A C1-C2 Module in Munc13 Inhibits Calcium-Dependent Neurotransmitter Release', *Neuron*, 95: 577-90.e5.

Millard, S. S., J. J. Flanagan, K. S. Pappu, W. Wu, and S. L. Zipursky. 2007. 'Dscam2 mediates axonal tiling in the Drosophila visual system', *Nature*, 447: 720-4.

Miller, K. G., A. Alfonso, M. Nguyen, J. A. Crowell, C. D. Johnson, and J. B. Rand. 1996. 'A genetic selection for Caenorhabditis elegans synaptic transmission mutants', *Proc Natl Acad Sci U S A*, 93: 12593-8.

Misura, K. M., R. H. Scheller, and W. I. Weis. 2000. 'Three-dimensional structure of the neuronal-Sec1-syntaxin 1a complex', *Nature*, 404: 355-62.

Moerman, D. G., and R. J. Barstead. 2008. 'Towards a mutation in every gene in Caenorhabditis elegans', *Brief Funct Genomic Proteomic*, 7: 195-204.

Morita, A., N. Yamashita, Y. Sasaki, Y. Uchida, O. Nakajima, F. Nakamura, T. Yagi, M. Taniguchi, H. Usui, R. Katoh-Semba, K. Takei, and Y. Goshima. 2006. 'Regulation of dendritic branching and spine maturation by semaphorin3A-Fyn signaling', *J Neurosci*, 26: 2971-80.

Much, C., T. Auchynnikava, D. Pavlinic, A. Buness, J. Rappsilber, V. Benes, R. Allshire, and D. O'Carroll. 2016. 'Endogenous Mouse Dicer Is an Exclusively Cytoplasmic Protein', *PLoS Genet*, 12: e1006095.

Narayanappa, M., H. W. Liu, L. Li, F. Michelassi, Z. T. Hu, and J. Dittman. 2020. 'The C2C-MCT Domain of Munc13 is Essential for Priming Synaptic Vesicles', *Biophysical Journal*, 118: 401a-01a.

Nargund, A. M., C. J. Fiorese, M. W. Pellegrino, P. Deng, and C. M. Haynes. 2015. 'Mitochondrial and nuclear accumulation of the transcription factor ATFS-1 promotes OXPHOS recovery during the UPR(mt)', *Mol Cell*, 58: 123-33.

Nargund, A. M., M. W. Pellegrino, C. J. Fiorese, B. M. Baker, and C. M. Haynes. 2012. 'Mitochondrial import efficiency of ATFS-1 regulates mitochondrial UPR activation', *Science*, 337: 587-90.

Nguyen, M., A. Alfonso, C. D. Johnson, and J. B. Rand. 1995. 'Caenorhabditis elegans mutants resistant to inhibitors of acetylcholinesterase', *Genetics*, 140: 527-35.

Nickerson, D. P., C. L. Brett, and A. J. Merz. 2009. 'Vps-C complexes: gatekeepers of endolysosomal traffic', *Curr Opin Cell Biol*, 21: 543-51.

Nonet, M. L., O. Saifee, H. Zhao, J. B. Rand, and L. Wei. 1998. 'Synaptic transmission deficits in Caenorhabditis elegans synaptobrevin mutants', *J Neurosci*, 18: 70-80.

Nonet, M. L., J. E. Staunton, M. P. Kilgard, T. Fergestad, E. Hartwieg, H. R. Horvitz, E. M. Jorgensen, and B. J. Meyer. 1997. 'Caenorhabditis elegans rab-3 mutant synapses exhibit impaired function and are partially depleted of vesicles', *J Neurosci*, 17: 8061-73.

Norris, A. D., H. M. Kim, M. P. Colaiacovo, and J. A. Calarco. 2015. 'Efficient Genome Editing in Caenorhabditis elegans with a Toolkit of Dual-Marker Selection Cassettes', *Genetics*, 201: 449-58.

Oh, K. H., and H. Kim. 2013. 'Reduced IGF signaling prevents muscle cell death in a Caenorhabditis elegans model of muscular dystrophy', *Proc Natl Acad Sci U S A*, 110: 19024-9.

———. 2019. 'BK channel clustering is required for normal behavioral alcohol sensitivity in C. elegans', *Sci Rep*, 9: 10224.

Oks, O., S. Lewin, I. L. Goncalves, and A. Sapir. 2018. 'The UPR(mt) Protects Caenorhabditis elegans from Mitochondrial Dysfunction by Upregulating Specific Enzymes of the Mevalonate Pathway', *Genetics*, 209: 457-73.

Oliver, D. M. A., and P. H. Reddy. 2019. 'Molecular Basis of Alzheimer's Disease: Focus on Mitochondria', *J Alzheimers Dis*, 72: S95-S116.

Opperman, K., M. Moseley-Alldredge, J. Yochem, L. Bell, T. Kanayinkal, and L. Chen. 2015. 'A novel nondevelopmental role of the sax-7/L1CAM cell adhesion molecule in synaptic regulation in Caenorhabditis elegans', *Genetics*, 199: 497-509.

Oren-Suissa, M., D. H. Hall, M. Treinin, G. Shemer, and B. Podbilewicz. 2010. 'The fusogen EFF-1 controls sculpting of mechanosensory dendrites', *Science*, 328: 1285-8.

Palfreyman, M. T., and E. M. Jorgensen. 2017. 'Unc13 Aligns SNAREs and Superprimes Synaptic Vesicles', *Neuron*, 95: 473-75.

Palikaras, K., E. Lionaki, and N. Tavernarakis. 2015. 'Coordination of mitophagy and mitochondrial biogenesis during ageing in C. elegans', *Nature*, 521: 525-8.

Patel, M. R., E. K. Lehrman, V. Y. Poon, J. G. Crump, M. Zhen, C. I. Bargmann, and K. Shen. 2006. 'Hierarchical assembly of presynaptic components in defined C. elegans synapses', *Nat Neurosci*, 9: 1488-98.

Pellegrino, M. W., A. M. Nargund, N. V. Kirienko, R. Gillis, C. J. Fiorese, and C. M. Haynes. 2014. 'Mitochondrial UPR-regulated innate immunity provides resistance to pathogen infection', *Nature*, 516: 414-7.

Plemel, R. L., B. T. Lobingier, C. L. Brett, C. G. Angers, D. P. Nickerson, A. Paulsel, D. Sprague, and A. J. Merz. 2011. 'Subunit organization and Rab interactions of Vps-C protein complexes that control endolysosomal membrane traffic', *Mol Biol Cell*, 22: 1353-63.

Pocock, R., C. Y. Bénard, L. Shapiro, and O. Hobert. 2008. 'Functional dissection of the C. elegans cell adhesion molecule SAX-7, a homologue of human L1', *Mol Cell Neurosci*, 37: 56-68.

Poirier, M. A., W. Xiao, J. C. Macosko, C. Chan, Y. K. Shin, and M. K. Bennett. 1998. 'The synaptic SNARE complex is a parallel four-stranded helical bundle', *Nat Struct Biol*, 5: 765-9.

Preedy, V. R., J. R. Salisbury, and T. J. Peters. 1994. 'Alcoholic muscle disease: features and mechanisms', *J Pathol*, 173: 309-15.

Purcell, S. M., J. L. Moran, M. Fromer, D. Ruderfer, N. Solovieff, P. Roussos, C. O'Dushlaine, K. Chambert, S. E. Bergen, A. Kähler, L. Duncan, E. Stahl, G. Genovese, E. Fernández, M. O. Collins, N. H. Komiyama, J. S. Choudhary, P. K. Magnusson, E. Banks, K. Shakir, K. Garimella, T. Fennell, M. DePristo, S. G. Grant, S. J. Haggarty, S. Gabriel, E. M. Scolnick, E. S. Lander, C. M. Hultman, P. F. Sullivan, S. A. McCarroll, and P. Sklar. 2014. 'A polygenic burden of rare disruptive mutations in schizophrenia', *Nature*, 506: 185-90.

Quade, B., M. Camacho, X. Zhao, M. Orlando, T. Trimbuch, J. Xu, W. Li, D. Nicastro, C. Rosenmund, and J. Rizo. 2019. 'Membrane bridging by Munc13-1 is crucial for neurotransmitter release', *Elife*, 8.

Quiros, P. M., M. A. Prado, N. Zamboni, D. D'Amico, R. W. Williams, D. Finley, S. P. Gygi, and J. Auwerx. 2017. 'Multi-omics analysis identifies ATF4 as a key regulator of the mitochondrial stress response in mammals', *J Cell Biol*, 216: 2027-45.

Rauthan, M., P. Ranji, N. Aguilera Pradenas, C. Pitot, and M. Pilon. 2013. 'The mitochondrial unfolded protein response activator ATFS-1 protects cells from inhibition of the mevalonate pathway', *Proc Natl Acad Sci U S A*, 110: 5981-6.

Raymond, C. K., I. Howald-Stevenson, C. A. Vater, and T. H. Stevens. 1992. 'Morphological classification of the yeast vacuolar protein sorting mutants: evidence for a prevacuolar compartment in class E vps mutants', *Mol Biol Cell*, 3: 1389-402.

Rhee, J. S., A. Betz, S. Pyott, K. Reim, F. Varoqueaux, I. Augustin, D. Hesse, T. C. Südhof, M. Takahashi, C. Rosenmund, and N. Brose. 2002. 'Beta phorbol ester- and diacylglycerol-induced augmentation of transmitter release is mediated by Munc13s and not by PKCs', *Cell*, 108: 121-33.

Rhee, J. S., L. Y. Li, O. H. Shin, J. C. Rah, J. Rizo, T. C. Sudhof, and C. Rosenmund. 2005. 'Augmenting neurotransmitter release by enhancing the apparent Ca2+ affinity of synaptotagmin 1', *Proc Natl Acad Sci U S A*, 102: 18664-9.

Richmond, J. 2005. 'Synaptic function', *WormBook*: 1-14.

———. 2009. 'Dissecting and recording from the C. Elegans neuromuscular junction', *J Vis Exp*.

Richmond, J. E., and K. S. Broadie. 2002. 'The synaptic vesicle cycle: exocytosis and endocytosis in Drosophila and C. elegans', *Curr Opin Neurobiol*, 12: 499-507.

Richmond, J. E., W. S. Davis, and E. M. Jorgensen. 1999. 'UNC-13 is required for synaptic vesicle fusion in C. elegans', *Nat Neurosci*, 2: 959-64.

Richmond, J. E., R. M. Weimer, and E. M. Jorgensen. 2001. 'An open form of syntaxin bypasses the requirement for UNC-13 in vesicle priming', *Nature*, 412: 338-41.

Rink, J., E. Ghigo, Y. Kalaidzidis, and M. Zerial. 2005. 'Rab conversion as a mechanism of progression from early to late endosomes', *Cell*, 122: 735-49.

Rizo, J., and T. C. Südhof. 1998. 'C2-domains, structure and function of a universal Ca2+-binding domain', *J Biol Chem*, 273: 15879-82.

Rodríguez-Castañeda, F., M. Maestre-Martínez, N. Coudevylle, K. Dimova, H. Junge, N. Lipstein, D. Lee, S. Becker, N. Brose, O. Jahn, T. Carlomagno, and C. Griesinger. 2010. 'Modular architecture of Munc13/calmodulin complexes: dual regulation by Ca2+ and possible function in short-term synaptic plasticity', *Embo j*, 29: 680-91.

Rosenmund, C., A. Sigler, I. Augustin, K. Reim, N. Brose, and J. S. Rhee. 2002. 'Differential control of vesicle priming and short-term plasticity by Munc13 isoforms', *Neuron*, 33: 411-24.

Rosenmund, C., and C. F. Stevens. 1996. 'Definition of the readily releasable pool of vesicles at hippocampal synapses', *Neuron*, 16: 1197-207.

Rossner, S. 2004. 'New players in old amyloid precursor protein-processing pathways', *Int J Dev Neurosci*, 22: 467-74.

Rostaing, P., R. M. Weimer, E. M. Jorgensen, A. Triller, and J. L. Bessereau. 2004. 'Preservation of immunoreactivity and fine structure of adult C. elegans tissues using high-pressure freezing', *J Histochem Cytochem*, 52: 1-12.

Sakurai, K., O. Migita, M. Toru, and T. Arinami. 2002. 'An association between a missense polymorphism in the close homologue of L1 (CHL1, CALL) gene and schizophrenia', *Mol Psychiatry*, 7: 412-5.

Sakurai, T. 2012. 'The role of NrCAM in neural development and disorders--beyond a simple glue in the brain', *Mol Cell Neurosci*, 49: 351-63.

Salzberg, Y., C. A. Diaz-Balzac, N. J. Ramirez-Suarez, M. Attreed, E. Tecle, M. Desbois, Z. Kaprielian, and H. E. Bulow. 2013. 'Skin-derived cues control arborization of sensory dendrites in Caenorhabditis elegans', *Cell*, 155: 308-20.

Salzberg, Y., C. A. Díaz-Balzac, N. J. Ramirez-Suarez, M. Attreed, E. Tecle, M. Desbois, Z. Kaprielian, and H. E. Bülow. 2013. 'Skin-derived cues control arborization of sensory dendrites in Caenorhabditis elegans', *Cell*, 155: 308-20.

Salzberg, Y., N. J. Ramirez-Suarez, and H. E. Bulow. 2014. 'The proprotein convertase KPC-1/furin controls branching and self-avoidance of sensory dendrites in Caenorhabditis elegans', *PLoS Genet*, 10: e1004657.

Sasakura, H., H. Inada, A. Kuhara, E. Fusaoka, D. Takemoto, K. Takeuchi, and I. Mori. 2005. 'Maintenance of neuronal positions in organized ganglia by SAX-7, a Caenorhabditis elegans homologue of L1', *Embo j*, 24: 1477-88.

Sato, T. K., P. Rehling, M. R. Peterson, and S. D. Emr. 2000. 'Class C Vps protein complex regulates vacuolar SNARE pairing and is required for vesicle docking/fusion', *Mol Cell*, 6: 661-71.

Schaefer, A. M., G. D. Hadwiger, and M. L. Nonet. 2000. 'rpm-1, a conserved neuronal gene that regulates targeting and synaptogenesis in C. elegans', *Neuron*, 26: 345-56.

Schaefer, A. W., H. Kamiguchi, E. V. Wong, C. M. Beach, G. Landreth, and V. Lemmon. 1999. 'Activation of the MAPK signal cascade by the neural cell adhesion molecule L1 requires L1 internalization', *J Biol Chem*, 274: 37965-73.

Schmid, R. S., W. M. Pruitt, and P. F. Maness. 2000. 'A MAP kinase-signaling pathway mediates neurite outgrowth on L1 and requires Src-dependent endocytosis', *J Neurosci*, 20: 4177-88.

Schoch, S., P. E. Castillo, T. Jo, K. Mukherjee, M. Geppert, Y. Wang, F. Schmitz, R. C. Malenka, and T. C. Südhof. 2002. 'RIM1alpha forms a protein scaffold for regulating neurotransmitter release at the active zone', *Nature*, 415: 321-6.

Schonthaler, H. B., V. C. Fleisch, O. Biehlmaier, Y. Makhankov, O. Rinner, R. Bahadori, R. Geisler, H. Schwarz, S. C. Neuhauss, and R. Dahm. 2008. 'The zebrafish mutant lbk/vam6

resembles human multisystemic disorders caused by aberrant trafficking of endosomal vesicles', *Development*, 135: 387-99.

Schroeder, N. E., R. J. Androwski, A. Rashid, H. Lee, J. Lee, and M. M. Barr. 2013. 'Dauer-specific dendrite arborization in C. elegans is regulated by KPC-1/Furin', *Curr Biol*, 23: 1527-35.

Scott, L. L., S. J. Davis, R. C. Yen, G. J. Ordemann, S. K. Nordquist, D. Bannai, and J. T. Pierce. 2017. 'Behavioral Deficits Following Withdrawal from Chronic Ethanol Are Influenced by SLO Channel Function in Caenorhabditis elegans', *Genetics*, 206: 1445-58.

Sebastian, D., M. I. Hernandez-Alvarez, J. Segales, E. Sorianello, J. P. Munoz, D. Sala, A. Waget, M. Liesa, J. C. Paz, P. Gopalacharyulu, M. Oresic, S. Pich, R. Burcelin, M. Palacin, and A. Zorzano. 2012. 'Mitofusin 2 (Mfn2) links mitochondrial and endoplasmic reticulum function with insulin signaling and is essential for normal glucose homeostasis', *Proc Natl Acad Sci U S A*, 109: 5523-8.

Shen, N., O. Guryev, and J. Rizo. 2005. 'Intramolecular occlusion of the diacylglycerol-binding site in the C1 domain of munc13-1', *Biochemistry*, 44: 1089-96.

Shen, Q., K. Yamano, B. P. Head, S. Kawajiri, J. T. Cheung, C. Wang, J. H. Cho, N. Hattori, R. J. Youle, and A. M. van der Bliek. 2014. 'Mutations in Fis1 disrupt orderly disposal of defective mitochondria', *Mol Biol Cell*, 25: 145-59.

Sheng, Z. H., C. T. Yokoyama, and W. A. Catterall. 1997. 'Interaction of the synprint site of N-type Ca2+ channels with the C2B domain of synaptotagmin I', *Proc Natl Acad Sci U S A*, 94: 5405-10.

Shin, O. H., J. Lu, J. S. Rhee, D. R. Tomchick, Z. P. Pang, S. M. Wojcik, M. Camacho-Perez, N. Brose, M. Machius, J. Rizo, C. Rosenmund, and T. C. Sudhof. 2010. 'Munc13 C2B domain is an activity-dependent Ca2+ regulator of synaptic exocytosis', *Nat Struct Mol Biol*, 17: 280-8.

Shin, O. H., J. Lu, J. S. Rhee, D. R. Tomchick, Z. P. Pang, S. M. Wojcik, M. Camacho-Perez, N. Brose, M. Machius, J. Rizo, C. Rosenmund, and T. C. Südhof. 2010. 'Munc13 C2B domain is an activity-dependent Ca2+ regulator of synaptic exocytosis', *Nat Struct Mol Biol*, 17: 280-8.

Shpilka, T., and C. M. Haynes. 2018. 'The mitochondrial UPR: mechanisms, physiological functions and implications in ageing', *Nat Rev Mol Cell Biol*, 19: 109-20.

Shu, T., H. Jin, J. E. Rothman, and Y. Zhang. 2020. 'Munc13-1 MUN domain and Munc18-1 cooperatively chaperone SNARE assembly through a tetrameric complex', *Proc Natl Acad Sci U S A*, 117: 1036-41.

Simon, L., S. E. Jolley, and P. E. Molina. 2017. 'Alcoholic Myopathy: Pathophysiologic Mechanisms and Clinical Implications', *Alcohol Res*, 38: 207-17.

Smaga, I., K. Wydra, M. Frankowska, F. Fumagalli, M. Sanak, and M. Filip. 2020. 'Cocaine Self-Administration and Abstinence Modulate NMDA Receptor Subunits and Active Zone Proteins in the Rat Nucleus Accumbens', *Molecules*, 25.

Smith, C. J., J. D. Watson, W. C. Spencer, T. O'Brien, B. Cha, A. Albeg, M. Treinin, and D. M. Miller, 3rd. 2010. 'Time-lapse imaging and cell-specific expression profiling reveal dynamic branching and molecular determinants of a multi-dendritic nociceptor in C. elegans', *Dev Biol*, 345: 18-33.

Smith, J. E., and T. S. Reese. 1980. 'Use of aldehyde fixatives to determine the rate of synaptic transmitter release', *J Exp Biol*, 89: 19-29.

Smyrnias, I., S. P. Gray, D. O. Okonko, G. Sawyer, A. Zoccarato, N. Catibog, B. Lopez, A. Gonzalez, S. Ravassa, J. Diez, and A. M. Shah. 2019. 'Cardioprotective Effect of the Mitochondrial Unfolded Protein Response During Chronic Pressure Overload', *J Am Coll Cardiol*, 73: 1795-806.

Soba, P., S. Zhu, K. Emoto, S. Younger, S. J. Yang, H. H. Yu, T. Lee, L. Y. Jan, and Y. N. Jan. 2007. 'Drosophila sensory neurons require Dscam for dendritic self-avoidance and proper dendritic field organization', *Neuron*, 54: 403-16.

Söllner, T., M. K. Bennett, S. W. Whiteheart, R. H. Scheller, and J. E. Rothman. 1993. 'A protein assembly-disassembly pathway in vitro that may correspond to sequential steps of synaptic vesicle docking, activation, and fusion', *Cell*, 75: 409-18.

Song, Y., M. Ailenberg, and M. Silverman. 1998. 'Cloning of a novel gene in the human kidney homologous to rat munc13s: its potential role in diabetic nephropathy', *Kidney Int*, 53: 1689-95.

Souza-Smith, F. M., C. H. Lang, L. E. Nagy, S. M. Bailey, L. H. Parsons, and G. J. Murray. 2016. 'Physiological processes underlying organ injury in alcohol abuse', *Am J Physiol Endocrinol Metab*, 311: E605-19.

Stevens, D. R., Z. X. Wu, U. Matti, H. J. Junge, C. Schirra, U. Becherer, S. M. Wojcik, N. Brose, and J. Rettig. 2005. 'Identification of the minimal protein domain required for priming activity of Munc13-1', *Curr Biol*, 15: 2243-8.

Sudarikova Yu, V., L. E. Bakeeva, and V. G. Tsiplenkova. 1997. 'Ultrastructure of mitochondrial reticulum of human cardiomyocytes in alcohol cardiomyopathy', *Biochemistry (Mosc)*, 62: 989-1002.

Sudhof, T. C., and J. Rizo. 2011. 'Synaptic vesicle exocytosis', *Cold Spring Harb Perspect Biol*, 3.

Sulston, J. E., and H. R. Horvitz. 1977. 'Post-embryonic cell lineages of the nematode, Caenorhabditis elegans', *Dev Biol*, 56: 110-56.

Sutton, R. B., D. Fasshauer, R. Jahn, and A. T. Brunger. 1998. 'Crystal structure of a SNARE complex involved in synaptic exocytosis at 2.4 A resolution', *Nature*, 395: 347-53.

Takáts, S., K. Pircs, P. Nagy, Á Varga, M. Kárpáti, K. Hegedűs, H. Kramer, A. L. Kovács, M. Sass, and G. Juhász. 2014. 'Interaction of the HOPS complex with Syntaxin 17 mediates autophagosome clearance in Drosophila', *Mol Biol Cell*, 25: 1338-54.

Tan, F. J., M. Husain, C. M. Manlandro, M. Koppenol, A. Z. Fire, and R. B. Hill. 2008. 'CED-9 and mitochondrial homeostasis in C. elegans muscle', *J Cell Sci*, 121: 3373-82.

Thomas, G. 2002. 'Furin at the cutting edge: from protein traffic to embryogenesis and disease', *Nat Rev Mol Cell Biol*, 3: 753-66.

Tian, Y., G. Garcia, Q. Bian, K. K. Steffen, L. Joe, S. Wolff, B. J. Meyer, and A. Dillin. 2016. 'Mitochondrial Stress Induces Chromatin Reorganization to Promote Longevity and UPR(mt)', *Cell*, 165: 1197-208.

Topalidou, I., P. A. Chen, K. Cooper, S. Watanabe, E. M. Jorgensen, and M. Ailion. 2017. 'The NCA-1 and NCA-2 Ion Channels Function Downstream of G(q) and Rho To Regulate Locomotion in Caenorhabditis elegans', *Genetics*, 206: 265-82.

Urbano-Marquez, A., R. Estruch, F. Navarro-Lopez, J. M. Grau, L. Mont, and E. Rubin. 1989. 'The effects of alcoholism on skeletal and cardiac muscle', *N Engl J Med*, 320: 409-15.

Urbano-Marquez, A., and J. Fernandez-Sola. 2004. 'Effects of alcohol on skeletal and cardiac muscle', *Muscle Nerve*, 30: 689-707.

van der Beek, J., C. Jonker, R. van der Welle, N. Liv, and J. Klumperman. 2019. 'CORVET, CHEVI and HOPS - multisubunit tethers of the endo-lysosomal system in health and disease', *J Cell Sci*, 132.

van der Bliek, A. M., M. M. Sedensky, and P. G. Morgan. 2017. 'Cell Biology of the Mitochondrion', *Genetics*, 207: 843-71.

Varoqueaux, F., A. Sigler, J. S. Rhee, N. Brose, C. Enk, K. Reim, and C. Rosenmund. 2002. 'Total arrest of spontaneous and evoked synaptic transmission but normal synaptogenesis in the absence of Munc13-mediated vesicle priming', *Proc Natl Acad Sci U S A*, 99: 9037-42.

Vida, T. A., G. Huyer, and S. D. Emr. 1993. 'Yeast vacuolar proenzymes are sorted in the late Golgi complex and transported to the vacuole via a prevacuolar endosome-like compartment', *J Cell Biol*, 121: 1245-56.

Wada, Y., Y. Ohsumi, and Y. Anraku. 1992. 'Genes for directing vacuolar morphogenesis in Saccharomyces cerevisiae. I. Isolation and characterization of two classes of vam mutants', *J Biol Chem*, 267: 18665-70.

Wang, S., U. B. Choi, J. Gong, X. Yang, Y. Li, A. L. Wang, X. Yang, A. T. Brunger, and C. Ma. 2017. 'Conformational change of syntaxin linker region induced by Munc13s initiates SNARE complex formation in synaptic exocytosis', *Embo j*, 36: 816-29.

Wang, S., Y. Li, J. Gong, S. Ye, X. Yang, R. Zhang, and C. Ma. 2019. 'Munc18 and Munc13 serve as a functional template to orchestrate neuronal SNARE complex assembly', *Nat Commun*, 10: 69.

Wang, X., J. Gong, L. Zhu, S. Wang, X. Yang, Y. Xu, X. Yang, and C. Ma. 2020. 'Munc13 activates the Munc18-1/syntaxin-1 complex and enables Munc18-1 to prime SNARE assembly', *Embo j*, 39: e103631.

Wang, X., J. Kweon, S. Larson, and L. Chen. 2005. 'A role for the C. elegans L1CAM homologue lad-1/sax-7 in maintaining tissue attachment', *Dev Biol*, 284: 273-91.

Wang, X., W. Zhang, T. Cheever, V. Schwarz, K. Opperman, H. Hutter, D. Koepp, and L. Chen. 2008. 'The C. elegans L1CAM homologue LAD-2 functions as a coreceptor in MAB-20/Sema2 mediated axon guidance', *J Cell Biol*, 180: 233-46.

Wang, Y. T., Y. Lim, M. N. McCall, K. T. Huang, C. M. Haynes, K. Nehrke, and P. S. Brookes. 2019. 'Cardioprotection by the mitochondrial unfolded protein response requires ATF5', *Am J Physiol Heart Circ Physiol*, 317: H472-H78.

Weimer, R. M. 2006. 'Preservation of C. elegans tissue via high-pressure freezing and freeze-substitution for ultrastructural analysis and immunocytochemistry', *Methods Mol Biol*, 351: 203-21.

Weimer, R. M., E. O. Gracheva, O. Meyrignac, K. G. Miller, J. E. Richmond, and J. L. Bessereau. 2006. 'UNC-13 and UNC-10/rim localize synaptic vesicles to specific membrane domains', *J Neurosci*, 26: 8040-7.

White, J. G., E. Southgate, J. N. Thomson, and S. Brenner. 1986. 'The structure of the nervous system of the nematode Caenorhabditis elegans', *Philos Trans R Soc Lond B Biol Sci*, 314: 1-340.

Xu, J., M. Camacho, Y. Xu, V. Esser, X. Liu, T. Trimbuch, Y. Z. Pan, C. Ma, D. R. Tomchick, C. Rosenmund, and J. Rizo. 2017a. 'Mechanistic insights into neurotransmitter release and presynaptic plasticity from the crystal structure of Munc13-1 C1C2BMUN', *Elife*, 6.

———. 2017b. 'Mechanistic insights into neurotransmitter release and presynaptic plasticity from the crystal structure of Munc13-1 C(1)C(2)BMUN', *Elife*, 6.

Xu, S., S. Pany, K. Benny, K. Tarique, O. Al-Hatem, K. Gajewski, J. L. Leasure, J. Das, and G. Roman. 2018. 'Ethanol Regulates Presynaptic Activity and Sedation through Presynaptic Unc13 Proteins in Drosophila', *eNeuro*, 5.

Xu, X. Z., P. D. Wes, H. Chen, H. S. Li, M. Yu, S. Morgan, Y. Liu, and C. Montell. 1998. 'Retinal targets for calmodulin include proteins implicated in synaptic transmission', *J Biol Chem*, 273: 31297-307.

Yang, X., S. Wang, Y. Sheng, M. Zhang, W. Zou, L. Wu, L. Kang, J. Rizo, R. Zhang, T. Xu, and C. Ma. 2015. 'Syntaxin opening by the MUN domain underlies the function of Munc13 in synaptic-vesicle priming', *Nat Struct Mol Biol*, 22: 547-54.

Yang, Y., and N. Calakos. 2011. 'Munc13-1 is required for presynaptic long-term potentiation', *J Neurosci*, 31: 12053-7.

You, Y., and J. Das. 2020. 'Effect of ethanol on Munc13-1 C1 in Membrane: A Molecular Dynamics Simulation Study', *Alcohol Clin Exp Res*.

Yu, R., S. B. Jin, U. Lendahl, M. Nister, and J. Zhao. 2019. 'Human Fis1 regulates mitochondrial dynamics through inhibition of the fusion machinery', *Embo J*, 38.

Zallen, J. A., S. A. Kirch, and C. I. Bargmann. 1999. 'Genes required for axon pathfinding and extension in the C. elegans nerve ring', *Development*, 126: 3679-92.

Zhen, M., X. Huang, B. Bamber, and Y. Jin. 2000. 'Regulation of presynaptic terminal organization by C. elegans RPM-1, a putative guanine nucleotide exchanger with a RING-H2 finger domain', *Neuron*, 26: 331-43.

Zhou, S., K. Opperman, X. Wang, and L. Chen. 2008. 'unc-44 Ankyrin and stn-2 gamma-syntrophin regulate sax-7 L1CAM function in maintaining neuronal positioning in Caenorhabditis elegans', *Genetics*, 180: 1429-43.

Zhu, T., X. Liang, X. M. Wang, and K. Shen. 2017. 'Dynein and EFF-1 control dendrite morphology by regulating the localization pattern of SAX-7 in epidermal cells', *J Cell Sci*, 130: 4063-71.

Zou, W., A. Shen, X. Dong, M. Tugizova, Y. K. Xiang, and K. Shen. 2016. 'A multi-protein receptor-ligand complex underlies combinatorial dendrite guidance choices in C. elegans', *Elife*, 5.

Zucker, R. S., D.M. Kullman, P.S. Kaesar. 2014. Release of neurotransmitters. From molecules to networks (third edition). 443-488.

SEEMA SHEORAN

Department of Biological Sciences, University of Illinois at Chicago

EDUCATION

University of Illinois at Chicago   *Chicago, IL*

PhD , Biological Sciences, GPA 3.6/4.0   2014-Present

- DAAD scholarship for short-term research in Germany

- Chancellor's Student Service and Leadership Award

- 4 Travel Awards, presented my research at scientific conferences

National Center for Biological Sciences (TIFR)   *Bangalore, India*

MS, Life Sciences   2013

- Research Fellowship (2010-13), Govt. of India, awarded to <1% of nationwide applicants

- Best Poster Presentation Award, International Society of Developmental Neuroscience

University of Delhi   *Delhi, India*

BS (Honors), Biomedical Sciences   2010

- Academic Excellence Award, in top 5% of my class

- D.C. Arora fellowship for meritorious students, awarded to only 1 student per department

- Finalist, Science aptitude contest for undergraduates from ~90 colleges

PUBLICATIONS

- **Sheoran, S**, Krout, M, Hu, Z, Richmond, JE. Munc13 and its multiple domains (Review). *In preparation.*

- Moseley-Alldredge, M, **Sheoran, S**, Yoo, H, O'Keefe, C, Richmond JE, Chen L. SAX-7/L1CAM and MPK-1/Erk promote coordinated locomotion. *In preparation*.

- Liu, H, Li, L, **Sheoran, S**, Yu, Y, Richmond, JE, Hu, Z. UNC-13 regulates the heterogeneity of release probability at the *C. elegans* neuromuscular junction. *Under review*.

- Kulkarni, SS, Sabharwal, V, **Sheoran, S**, Basu, A, Matsumoto, K, Hisamoto, N, Ghosh-Roy, A, and Koushika, SP. In regenerating neurons UNC-16/JIP3 negatively regulates actin & microtubule dynamics differentially dependent on DLK-1. *Under review.*
- Oh, KH, **Sheoran, S**, Richmond, JE, Kim, H. Alcohol induces mitochondrial fragmentation and stress responses to maintain normal muscle function in *Caenorhabditis elegans*. *The FASEB Journal*. 2020; 34: 8204– 8216.

POSTER PRESENTATIONS

- Haowen Liu, Lei Li, Yi Yu, Seema Sheoran, Janet Richmond, Zhitao Hu. A dual role for the UNC-13 M domain in Ca2+ triggered neurotransmitter release. Laboratory of Integrative Neuroscience Symposium 2020, UIC.
- Haowen Liu, Lei Li, Yi Yu, Seema Sheoran, Janet Richmond, Zhitao Hu. A dual role for the UNC-13 M domain in Ca2+ triggered neurotransmitter release. Society for Neuroscience Annual Meeting 2019, Chicago.
- Melinda Moseley-Alldredge, Seema Sheoran, Hayoung Yoo, Calvin O'Keefe, Janet Richmond, Lihsia Chen. SAX-7 and MPK-1/Erk promote coordinated locomotion in *C. elegans. CeNeuro* 2018, Madison.
- Melinda Moseley-Alldredge, Seema Sheoran, Hayoung Yoo, Calvin O'Keefe, Janet Richmond, Lihsia Chen. SAX-7 and MPK-1/Erk promote coordinated locomotion in *C. elegans.* Society for Neuroscience 2018, San Diego.

TEACHING

- Neuroscience I (BIOS484)
- Neuroscience II (BIOS 485)
- Animal Physiology (BIOS 240)
- Cell Biology Laboratory (BIOS 223)
- Cellular Neurobiology Laboratory (BIOS 489)